Critical Analysis of Simulated Thermomechanical Processing of Aluminium Can Body Stock

A dissertation presented for the degree of Master of Science in Engineering in the Faculty of Engineering and the Built Environment, University of Cape Town

Student: Chase Kennedy Hyde

Supervisors: Prof. R.D. Knusten & Dr. S.L. George

Centre for Materials Engineering, Mechanical Engineering Department

Date: March 2015

Abstract

Hot Plane Strain Compression (PSC) testing is a thermomechanical testing method used to simulate the deformation condition of industrial rolling. Thermomechanical processing (TMP) factors such as the amount of strain, strain rate and temperature all influence the microstructural evolution. The geometry of the PSC test sample and anvil are important factors in order to achieve the plane strain condition and acceptable strain distribution within deformed sample. Geometrical factors such as the breadth ratio (B_R) relates the the samples breadth (b) to anvils face width (w) and this ratio has a significant effect on the breadth spread of the sample. The height ratio (H_R) relates w to the samples height (h) and this ratio has a significant effect on the strain distribution. Two different geometric PSC testing configurations were investigated for this study, the one configuration had less favourable geometric ratios with a B_R of 3 and a H_R of 1 and the other configuration had more favourable ratios, with the B_R of 4.62 and the H_R of 1.3.

This investigation is to evaluate the feasibility of a newly installed TMP machinery, the Gleeble 3800, to simulate the hot finishing rolling conditions by the use of hot PSC tests for the production of the can body stock (CBS) aluminium alloy AA3104. Single hot PSC tests were carried out at temperatures of 300, 350 and 400 °C at strain rates of 10, 30 and 100 sec^{-1} and multi-pass hot PSC tests were carried out to simulate the different rolling passes experienced on the hot finishing rolling mill of the production of the aluminium alloy AA3104. The strain rate, temperature control, flow stress and microstructural flow were investigate to establish whether PSC testing is feasible on the Gleeble 3800.

The Gleeble 3800 proved to be a reliable, credible and repeatable PSC testing machine for both geometric testing configurations within its boundaries. The less favourable geometric testing condition ($B_R = 3$ and $H_R = 1$) achieved better thermal gradient control of the sample in comparison to the more geometric favourable configuration ($B_R = 4.62$ and $= H_R = 1.3$). The geometric favourable configuration achieved consistently small yet significant higher accurate flow stress values for each hot PSC testing conditions. The multi-pass hot PSC tests that simulated the three pass hot finishing rolling conditions was not successfully achieved, and only two multi-pass hot PSC tests can be performed consecutively due to the limited amount of material that can be deformed within a laboratory environment.

Acknowledgements

I would like to give thanks to the following people during my time as a masters student at the CME:

- To my supervisors Prof. Knusten and Dr. George for their guidance, advice and unlimited knowledge.
- To the people at Hulamin, Francois Vlok and Michael Shirran for allowing this project to happen and by providing crucial information about Hulamin's inner workings to help me understand my project.
- To the good people at TSC, Ricky Ricks and Paul Evans for their very useful help and insight into their work and mine.
- To Glen Newins and his skilled team at the mechanical workshop at UCT who were always willing to help.
- To the staff at the CME for keeping the centre running at tip top condition and for helping me with the things I couldn't do.
- To my fellow CME students whom I could discuss and bounce ideas off.
- To Rae Dalton for pulling through for me at the end when things were looking bleak.
- To my parents who have always supported me and also for having the patience for letting me finish my masters research project.

Declaration

I, Chase Kennedy Hyde, know the meaning of plagiarism and declare that all the work in this document, save for that which is properly acknowledged, is my own.

Signature: Signed by candidate

Signature removed

Date: 26/05/2015

Contents

List of Tables

List of Figures

Chapter 1

Introduction

1.1 Subject of Investigation

The subject of this investigation is the thermomechanical processing (TMP) procedure required to simulate industrial rolling in an laboratory environment, through the use of hot plane strain compression (PSC) testing. The investigation focuses on the rolling conditions of the hot finishing rolling mill at Hulamin Limited, with particular emphasis on the aluminium alloy AA3104 that is used for the beverage-can body stock (CBS).

1.2 Motivation and Background

The beverage-can sector is a massive global industry, producing an estimated 280 billion cans per year, with the largest markets in the United States and Europe [1]. Beverage cans over the past few decades have proven as a resilient packaging option for carbonated soft drinks, alcoholic beverages, vegetable and fruit juices, iced teas and energy drinks. Worldwide, beverage-can production continues to grow annually by approximately 3% [2]. In Sub-Saharan Africa, however, the beverage-can market has shown slow initial development, though it has strong future prospects [3]. Forecasts suggest continual growth over the next few years due to increased local income, improvement of infrastructure and economic growth on the African continent. For the worldwide market, the full-aluminium can constitutes 75% of the market, while the other 25% consists of the tin-plated steel beverage can [1].

1.2.1 South African Beverage Can

The beverage-can manufacturer for South African and Sub-Saharan Africa is Bevcan, a subsidiary of the packaging company Nampak Limited. The beverage cans produced in South Africa are typically hybrid-type cans that utilise a tin-plated steel body with an aluminium lid. This traditional type of can is now being upgraded, as South Africa follows the global trend of producing full-aluminium beverage cans. The full-aluminium can was introduced into the South African market mid-2013 [4]. Several factors make the shift towards the full-aluminium beverage can an attractive option. Firstly, the aluminium can is more cost effective than the tin-plated steel can. This is mainly due to aluminium being a more stable commodity than steel, which has volatile price fluctuations. Transportation costs are also reduced owing to aluminium being approximately 60% lighter than steel. The move is therefore economically logical. Aluminium cans are also lightweight and corrosion resistant: their excellent barrier protection allows for rapid cooling and extends the shelf life of the product. Another favourable aspect of the aluminium beverage can, especially in light of growing environmental concerns, is that it can be recycled indefinitely. It is also an easier product to recycle, since it is composed of only one class of material: the tin-plated steel can found in the South African market is composed of a mixture of materials, making the recycling process more complicated and more resource intensive. The Collect-a-Can initiative for beverage-can recycling in South Africa has a large following. In terms of recycling, South Africa currently has a recovery rate of 72% and is projected to meet the United Nations' target of 75% by 2015 [5]. Collect-a-Can aims to achieve a recovery rate of 100% within the next 20 years. These targets become more attainable with the aluminium can on the South African market, given to the natural intrinsic value of aluminium. The informal can-collecting industry is expected to grow, as collectors try to earn a living or supplement income by selling collected aluminium, and growth in this sector would increase recovery rates dramatically. In order to aid in the recycling of the aluminium beverage cans, Hulamin Limited has invested R300 million into a recycling facility, creating a closed loop for the life cycle of the aluminium beverage can [6].

Upgrades of the older steel-can production lines to make way for the faster, more advanced aluminium lines were implemented to satisfy the growing customer demand. Nampak first upgraded one of its production lines at its largest factory at Springs in June 2013. This upgraded line can produce up to 3 000 cans-per-minute, compared to the 1 600 cans-per-minute rate of the older tin-plated steel can line [7]. As of June 2014, the Springs plant has fully converted all of its production lines, with additional upgrades planned for plants in Cape Town, Rosslyn (Pretoria) and Angola [7]. These line upgrades will significantly increase the demand for aluminium CBS. Hulamin Limited plans to meet the demand for aluminium CBS by producing locally manufactured CBS.

1.2.2 Can Body Stock

Hulamin Limited is South Africa's aluminium producer of semi-finished products, producing primary extruded and rolled products. Currently Hulamin produces the can end stock (CES) for beverage cans produced by Bevcan. Due to Bevcan's recent transition to the production of full-aluminium cans, Hulamin is now producing aluminium CBS as well. According to Hulamin's Integrated Annual Report [8], the aluminium can production lines implemented by Bevcan will increase the demand for CBS to 10 000 tons per annum. Hulamin has signed a pilot contact with Bevcan to demonstrate that CBS can be locally produced: under the terms of the contact, Hulamin is providing 15 000 tons of CBS by the end of 2015. Hulamin has carried out can-production trials on Hulamin-produced CBS in Europe, the Middle East and South Africa with pleasing results.

The performance of the Hulamin-produced AA3104 CBS during the canning operation relies chiefly on the production-process conditions imposed on this alloy during rolling. The aluminium AA3104 CBS endures extremely demanding production-process conditions, and stringent specifications regarding the alloy's surface quality and mechanical properties need to be met to ensure the customers' satisfaction. Hulamin uses a single-stand hot reversing mill as shown in Figure 2.1. The worldwide norm during the hot finishing step of the production of aluminium CBS is to use tandem mill configuration (Figure 2.2) for rolling passes. This rolling technique used by Hulamin, however, creates a challenge when trying to control rolling conditions, such as the variation of interpass times between rolling steps. Unlike the tandem mill, where the interpass time is fixed for each section of the rolling plate, a reversing mill has different interpass times, with the plate coiled and uncoiled for each pass. These different interpass times also affect the temperature at which the plate is rolled, especially for the leading and tail edges of the plate. Temperature, in turn, has an effect on the microstructure of the material, especially on the crystallographic texture orientation of the grains formed during the hot rolling conditions. Having the correct balance of crystallographic textures in the final product results in minimal earring on the drawn can.

In order to analyse the effects of rolling, industrial trials can be implemented, but they are expensive and time consuming. They also interrupt rolling schedules, since they cause rolling downtime. Replicating off-line hot rolling conditions via small-scale laboratory tests is therefore advantageous.

1.3 Aims and Objectives

The two core objectives of this study are:

1. To evaluate the feasibility of simulating the Hulamin hot finishing rolling conditions for aluminium AA3104 CBS within a small-scale laboratory, by performing hot plane strain compression (PSC) testing with the Gleeble 3800 thermomechanical processing facility at the University of Cape Town (UCT). This objective is dealt with in Chapters 4-7.

2. To investigate the microstructural flow during the multi-pass hot PSC rolling simulations. This objective is dealt with in Chapter 8.

The above core objectives will be achieved through the following sub-aims:

- To determine the fundamental mechanism of hot PSC testing on the Gleeble 3800, and to gauge the capabilities of the Gleeble 3800 in terms of the temperature, strain, strain rate and material flow stress.

- To determine the impact that the lubricating condition between the PSC sample and the anvil has on the material and on results, as well as which lubricant provides the most suitable conditions for achieving legitimate results.

- To determine whether the anvil-to-sample optimised geometries provide more favourable results than the standard testing geometry, as well as which geometric configuration best suits hot PSC testing on the Gleeble 3800 thermomechanical machine.

- To validate the hot PSC testing of the AA3104 on the Gleeble 3800 through a comparative study with the available literature, considering the temperature, strain, strain rate, material flow stress and determined constitutive equation of the AA3104.

- To determine whether a multi-pass hot PSC simulation test can be used to successfully carry out the three hot finishing rolling pass schedules at Hulamin.

- To determine the effect that different sample-to-anvil geometries have on the microstructural flow of the hot PSC sample and whether the geometrically optimised testing condition provides more favourable results.

1.4 Limitations and Scope of Project

This project is chiefly concerned with the hot PSC of aluminium alloy AA3104 produced by Hulamin. The TMP testing matrix was designed from the conditions that are achieved on the hot finishing rolling mill at Hulamin's rolling plant. This means that high strain rate conditions at hot finishing rolling temperatures are considered, while PSC at room temperature or lower temperatures with lower strain rates are excluded. Only two different types of PSC geometric configurations are studied due to the limited time and material available; however, these two configurations display differences that are large enough to draw conclusions from. Due to the limited amount of AA3104 aluminium alloy available and the limited information provided of the rolling schedules, the rolling simulations are only simulated from one specific rolling schedule and different rolling conditions are not investigated. Further research into the crystallographic orientation of the PSC samples could be carried out, using X-ray diffraction or electron backscatter diffraction (EBSD). This research is, however, beyond the scope of the present study due to the time constraints imposed on the researcher.

1.5 Experimental Approach

In order to achieve its objectives, this experiment takes the following approach:

- Initially hot PSC tests are performed on the Gleeble 3800 with a range of temperatures and strain rates, based on the conditions of the hot finishing mill at the Hulamin rolling plant. The initial hot PSC tests are used to gauge the capabilities of the Gleeble 3800 as well as to differentiate the different types of lubricants that are used at the interface between the anvil and the sample.
- Hot ring compression tests are conducted to investigate the effect of lubricants on the material during different high temperature and strain rate conditions.
- A comprehensive set of hot PSC tests are carried out on the Gleeble 3800 with the same range of temperature and strain rates as the initial hot PSC tests. For these hot PSC tests, two different anvil-to-sample geometries are investigated. One is the standard manufacturers' recommended geometry, which is the less geometrically favourable configuration for PSC testing, and the other is a modified testing configuration that allows for a more geometrically favourable configuration.
- Leading edge rolling simulated multi-pass hot PSC tests of the AA3104 CBS are conducted on the Gleeble 3800 for one, two and three simulated passes.

- Polarized light optical microscopy (PLOM) is carried out on the industrially rolled AA3104 CBS as well as the single hot PSC deformation tests and on the hot PSC samples that have been subjected to multi-pass simulated PSC tests.

Chapter 2

Literature Review

2.1 Aluminium Alloy AA3104

The material under investigation in this report is the aluminium alloy AA3104, which is used for the production of CBS. This aluminium alloy is a 3XXX-series non-heat treatable alloy that is characterised by its major element, manganese (Mn). Table 2.1 shows the elemental makeup in weight percent for the tabulated items. The 3XXX-series alloys provide low to medium strength depending on the amount of work hardening, formability and high corrosion-resistant properties. Manganese raises the recrystallisation temperature and also improves the uniformity of dispersion hardening [9]. This aids with the control of the recovery and recrystallisation of the material as well as with the final grain size and texture in the annealed sheet [10]. The coarse constituent particles and small dispersions are formed with the lower soluble elements of iron and silicon; these constituent particles serve as nucleation sites for recrystallisation. The small dispersions also act as obstacles against grain boundary migration [10]. Moreover, magnesium is a notable alloying element that has a similar composition amount to that of manganese within the aluminium alloy AA3104. Magnesium supplements manganese by offering further solid-solution strengthening and dispersion formation, thus resulting in further improvements in strength and work-hardening rates [11].

Table 2.1: Aluminium alloy AA3104 chemical composition (wt%) [12].

AA3104	Si	Fe	Cu	Mn	Mg	Zn	Ti	Al
	0.6	0.8	0.05-0.05	0.8-1.4	0.8-1.3	0.25	0.1	Rem.

For non-heat treatable aluminium alloys, a tempering designation system is used to describe the specific treatments performed on the alloy, and these treatments influence the characteristics of the final product. The designation system consists of letters followed by one or more numbers. For the aluminium alloy AA3104, the temper designation is H19.

The letter after the alloying classification describes the basic tempering condition of the alloy, where the letter 'H' signals that the alloy is under the strain-hardening condition. The first number after the letter determines the specific combination of basic operations: in this case the number '1' shows that this alloy has only been strain-hardened, with no stabilising or annealing treatment employed. The second number determines the degree of strain hardening used on the alloy, with the number '9' indicating that this alloy is under a special hard condition for a specific application [13]. In terms of its basic mechanical properties, AA3104-H19 has a modulus of elasticity of 69.0 GPa, a tensile strength of 260 MPa and an ultimate tensile strength of 290 MPa [14].

2.1.1 Production of Aluminium Alloy AA3104 at Hulamin Limited

The aluminium alloy AA3104 investigated here is manufactured by Hulamin Limited. During production, the material goes through a series of processes in order to achieve the final dimensions required for the final product, including the desired mechanical and microstructural features. First, Hulamin melts primary pig and rolling ingots from local smelters, which consists of approximately one third of recycled process scrap from the plant. The metal is also treated, filtered and re-alloyed according to the alloys specification as shown in Table 2.1. The melting furnace reaches temperatures from 660-700 °C. The molten metal is then transferred to a holding furnace that allows impurities to settle out. Once settled, the molten metal is skimmed and cleaned to remove further impurities. The molten metal is then transferred to water-cooled moulds in order to solidify, and a 16 t, 600 mm-thick direct chill (DC) cast ingot is formed. The DC cast ingot is scalped to remove surface oxides and transferred to furnaces ranging from 550-600 °C for a duration between 4 and 8 hours. This process, known as homogenisation, achieves a consistent microstructure throughout the ingot [15]. After the homogenous heat treatment, the ingot is ready for TMP by means of hot rolling. The rolling process involves plastically deforming the metal between two rolls. Rolling allows for high throughput as well as good process control of the product. The high temperature from the homogenisation process allows the ingot to be at a high enough temperature to undergo hot rolling.

Hot rolling at the Hulamin rolling plant undergoes a two-step process. The first process consists of multiple passes through the hot roughing mill, which is also known as a 4-high breakdown mill as shown in Figure 2.1a. This first process of hot rolling reduces the ingots thickness by about 95% to ±20 mm, while the length increases 24 times to a length of ±140 m. This product is known as transfer bar. The leading and tail ends of the transfer bar are sheared on the run-out table while the transfer bar is en route to the hot finishing mill. The second hot rolling process is know as the hot finishing step and is carried out on a 4-high hot reversing mill with coilers and decoilers on either side on the mill, as shown in Figure

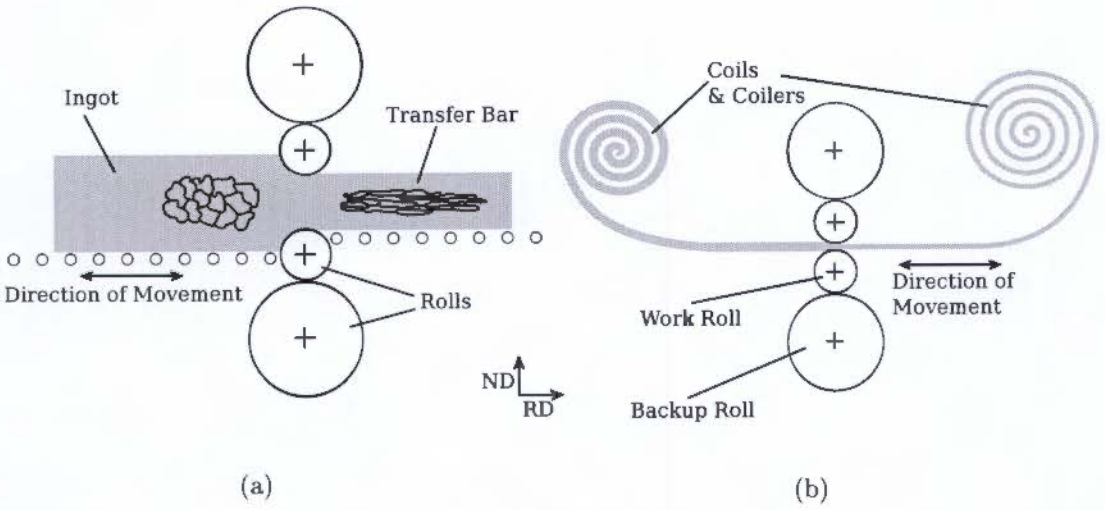

Figure 2.1: Schematic of the hot rolling process encountered at Hulamin rolling plant, the hot (a) roughing process and the hot (b) finishing rolling process.

2.1b. This process is a critical step in the production of CBS, as high tolerances are needed and temperature, rolling speed, rolling force, tension, strain, strain rate and interpass time are all carefully set and monitored. Careful control is needed during this process in order to achieve advantageous microstructural characteristics for the stringent requirement of CBS. Microstructural evolution during hot rolling is further discussed in Section 2.2.4. The hot finishing process at Hulamin operates within a temperature range of 350-280 °C, with the final product gauge of 2 mm. Once the final pass has been completed the sheet is coiled and removed from the hot line and allowed to cool to ambient temperatures for preparation for the cold rolling operations.

The cold rolling process starts at ambient temperatures; at this point the CBS gains a significant amount of work hardening due to the multiplication of dislocations and the general increase in internal energy state within the material. During the cold rolling operation, very tight tolerances for the gauge of the sheet can be achieved, as well as a good surface finish. CBS temperatures are also raised, to within a range of 100-140 °C [15], from the adiabatic heating and friction of the rolls during the deformation process. The cold rolling process is a single process in which multiple passes are carried out in series. The CBS is uncoiled, rolled on tandem mills (Figure 2.2) and then coiled up again after the multiple consecutive passes are performed. For the CBS produced at Hulamin, the cold rolling process undergoes a 3-pass schedule to a final gauge of 0.26 mm. In order to regulate the mechanical properties of the CBS, a short tempering heat treatment is adopted after the cold rolling. It involves a bake at 200 °C for 20 minutes.

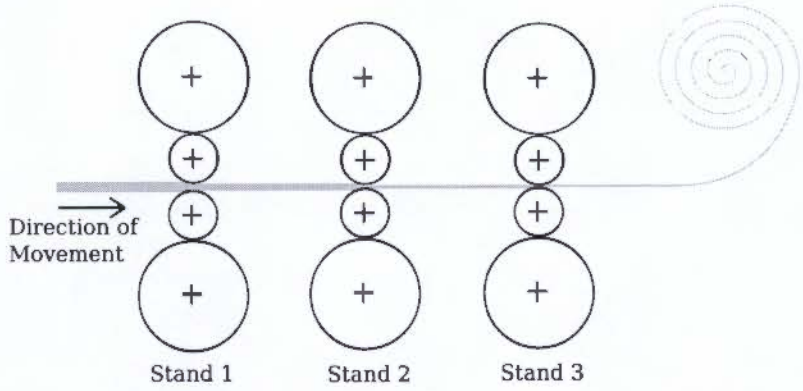

Figure 2.2: Tandem rolling process with 3 stands of rolling mills in a row.

2.2 Factors Influencing the Microstructure of Aluminium During Processing

The microstructure of a material determines how the material behaves under loading conditions and environments. The industrial process of a product is therefore critical in determining the mechanical characteristics of the end product, with production processes directly effecting the microstructure of the end product. TMP uses an understanding of metallurgy to achieve the most favourable microstructure during the production of a material, in order to gain the optimal mechanical performance for the material's use.

2.2.1 Deformed Structure

During the plastic deformation of a metal, such as the rolling of aluminium, a number of changes occur within the microstructure. The internal free energy of the metal is raised during the deformation process [16]. The small amount of the energy ($\pm 1\%$) used for the deformation process is stored within the microstructure by dislocation multiplication, interfaces and vacancies. Plastic deformation by rolling causes the grains to elongate within the material (see Figure 2.1a) and this causes a large increase in the total grain boundary area (that is, an increase in internally stored energy). Additional structures are also formed within the grain by the accumulation of dislocations. The sum of the stored energy from these defects creates a thermodynamically unstable system, and this unstable state is the driving force for the microstructural changes that occur during the TMP of the material. Microstructural changes will occur when the material is subjected to an annealing condition, i.e. a high enough temperature for the thermally active diffusion of atoms through the release of internal energy. The mechanisms of annealing allow for these defects to be either removed or arranged into configurations in order to achieve a lower internal energy state. There are three stages of annealing: recovery, recrystallisation and

grain growth [17]. The catalyst for the annealing mechanism is the reduction in internal stored energy, which has a softening or restorative effect on the material. Further discussion on the restorative effect on aluminium is discussed in the following sections.

2.2.2 Annealing Process

The annealing process is a restorative process for a thermodynamically unstable material. It achieves a state of greater equilibrium through the diffusion of atoms within the material. At room temperature, this is an extremely slow process; however, the release of internal energy is accelerated by subjecting the material to heat and raising the material's temperature. The annealing process causes an increase in ductility, softens the material, relieves the internal stresses, refines the structure and improves the cold working properties. The two main mechanisms of the annealing process are recovery and recrystallisation. Recovery is a precedent to recrystallisation. These two mechanisms are competing processes driven by the stored energy from the deformed state [16]. Once recrystallisation has occurred, further recovery cannot occur and thus the extent of recovery depends on the ease of the recrystallisation process within the structure. The extent of recovery is largely dependant on the material's stacking fault energy (γ_{SFE}). The γ_{SFE} of the material governs whether dislocations can dissociate readily or not. The γ_{SFE} value for aluminium is considered to be high, with a value of approximately 170 $mJ.m^{-2}$. As a result, aluminium predominantly undergoes recovery, with recrystallisation not as easily achieved.

Recovery

A deformed microstructure has a high dislocation density, due to the dislocations interacting and multiplying with one another and raising the internal energy of the material. Recovery is the initial restorative step during the annealing processes. The main mechanism is based largely on the annihilation of point defects and the rearrangement of dislocations into subgrains. This dual process is schematised in Figure 2.3. The high dislocation density state (Figure 2.3a) undergoes recovery to form a recovered state (Figure 2.3b). Subgrains are formed by the rearrangement of dislocations to form low-angle grain boundaries. The grains maintain their shape and the microstructural changes occur on a small scale, not visible by optical microscopy [17]. Evidence of the changes can be obtained via X-ray diffraction and the electron microscope, which show subgrains arranging into networks of dislocations at the subgrain boundary and forming cellular configurations [9]. Further recovery allows for these subgrains to gradually increase in size and produce boundaries that are essential free from dislocation tangles [18]. Physical mechanical

measurement is the easiest way to measure the extent of recovery achieved within a material as it shows a decrease in the strength of the material. Most of the aluminium alloys behave in a similar fashion to one another with regard to recovery, although the response varies according to the composition of the alloy.

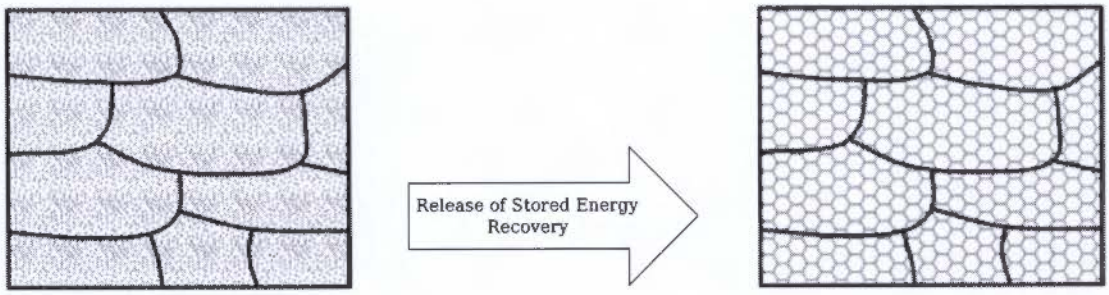

(a) (b)

Figure 2.3: Recovery process from a (a) deformed state to a (b) recovered structured by the development of subgrains through annihilation and the rearrangement of dislocations [16].

During the annihilation and rearrangement phase of recovery, dislocations glide, climb and cross slip. These mechanism are ultimately determined by the γ_{SFE} of the material, based on its composition [16]. For materials with low γ_{SFE}, such as copper, brass and stainless steels, dislocation climb is difficult to achieve and therefore little recovery occurs before the onset of recrystallisation. By contrast, metals such as aluminium have high γ_{SFE}, making dislocation climb easily and rapidly achieved. A significant amount of recovery can therefore be achieved before the recrystallisation process.

Recrystallisation

The recrystallisation of material involves the nucleation, formation, appearance and initial growth of a resolvable new strain-free grain structure [18]. Nucleation sites for recrystallisation preferentially occur in areas of high disorientation at the interfacial boundaries. Other nucleation areas can form from the mobility and growth of selected sub-grains that fall into high-angled grain boundaries. Figure 2.4 schematically demonstrates recrystallisation. The process can be seen microscopically, including the formation of new grains and their respective nucleated positions. The recrystallisation temperature can be defined as the temperature at which the microstructure will be 50% recrystallised in 30 minutes [17]. Generally, the recrystallisation temperature is within a range of between half and one third of the absolute melting temperature of the metal. Factors such as the metal's purity, prior work and grain size affect recrystallisation kinetics. Impurities that are present as a second-phase retard the grain boundary movement, raising the recrystallisation temperature of the material.

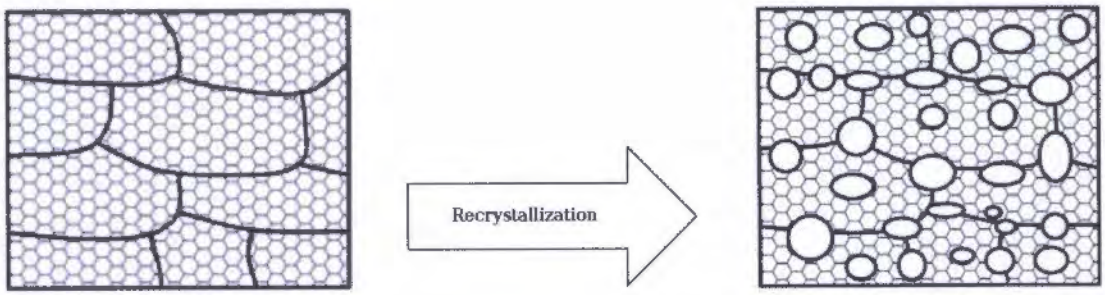

Figure 2.4: A (a) recovered structure undergoes (b) recrystallisation by the initiation and nucleation of grains to form new strain free grains [16].

Grain growth occurs from a recrystallised structure. The process proceeds with the gradual elimination of small grains at the expense of other recrystallised grains. This elimination is achieved by reducing the energy associated with grain boundaries. Larger equiaxed grains are formed, as can be seen in Figure 2.5 of the 99.00 wt% purity aluminium alloy AA1200. Over longer periods, these grains will grow to a greater extent by consuming other grains. New recrystallised grains also form a preferred orientation, which is dependent on the mechanical properties of the material, particularly the anisotropy of the material.

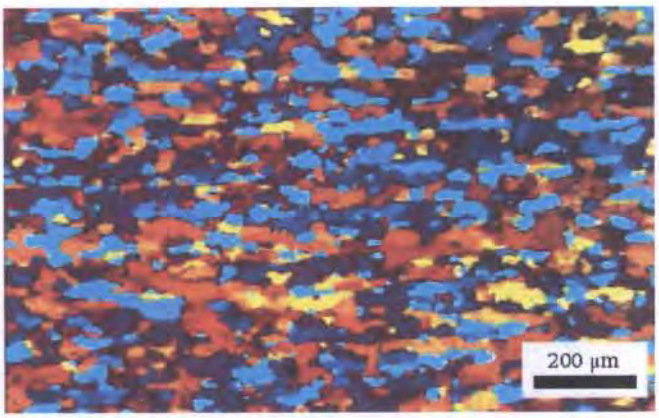

Figure 2.5: Aluminium alloy AA1200 (Al 99.00wt%) that has undergone recrystallisation under the condition of 400°C for 30 minutes [19].

2.2.3 Texture

For cubic metals, deformation occurs primarily by either slip or twinning. Slip occurs as a result of the dislocation glide of either an edge or screw dislocation within the activated slip plane. Deformation by slip is more common than deformation by twinning. However, twinning can easily occur under certain conditions, when there are not enough slip systems to accommodate deformation, and it is more predominant with materials that have a low γ_{SFE}. The most significant property governing the deformation mechanism is the value of

the γ_{SFE}, which determines the rate of dislocation climb and cross slip [16]. For face-centred cubic (FCC) materials, with a medium to high γ_{SFE}, such as aluminium, deformation by slip is the preferred mechanism. In metals with low γ_{SFE}, the dislocations dissociate to form stacking faults, and deformation by twinning occurs. The plastic deformation of FCC aluminium occurs by crystallographic slip predominately on the {111} planes and in the <110> direction [20].

During the plastic deformation of metals, especially during the rolling process, the orientation of individual grains within a metal will change relative to the direction of the applied stress. Consequently, deformation occurs on the most favourably orientated slip system [16]. The rotation of the grains during the deformation process towards a preferred crystallographic orientation is known as texture. The crystallographic texture within the metal has a strong influence on its mechanical properties, causing anisotropic behaviour. A strong textural component in a material will result in the strong directionality of that material, while a less randomly distributed texture will not bring about the same effect. The deformation textures of FCC metals are determined primarily by their γ_{SFE}. Deformed textures also affect the recrystallisation kinetics, with nucleation occurring preferentially within specific regions of particular orientations. This dynamic results in recrystallisation textures, which have their own preferred orientation and which, in turn, have a significant effect on the material's behaviour. The resulting texture of the material is highly influential during the forming processes, specifically during cupping and deep drawing.

2.2.4 Evolution of Microstructure During Hot Working

In the processing of a material under hot working conditions, the workability of the material is an important factor. The workability of a material can be identified by the ease with which the material can be formed while remaining defect-free. The working loads achievable during the forming process are reliant on the plastic flow of the material. The factors that determine the plastic flow of a material are the deformation temperature, the amount of strain and the strain rate at which the material is being deformed/formed. By varying one of these factors, it is possible to quantify annealing and deformation as functions of TMP. The strain rate and temperature can be described by a single parameter known as the Zener-Holloman (Z) parameter [21]. Z is also known as the temperature-compensated strain rate and is described by the equation:

$$Z = \dot{\varepsilon} \exp\left(\frac{Q}{RT}\right) \tag{2.1}$$

where $\dot{\varepsilon}$ is the strain rate, Q is the activation of energy, R is the universal gas constant and T is the deformation temperature (measured in °K). Z is a critical factor, considering

the bulk hot working conditions and the development of the microstructure during TMP. Understanding the microstructural development and how it relates to Z during TMP is essential for achieving the desirable microstructure within the final product.

Dynamic Softening

The pivotal mechanisms during TMP are dynamic recovery (DRV) and dynamic recrystallisation (DRX). The dynamic restorative mechanism occurs during the deformation process, in contrast with static restorative phenomena, as discussed in Section 2.2.2. There are many features that are common to the static process, but the simultaneous operation of deformation and softening leads to differences [16]. Due to the high γ_{SFE} associated with aluminium and its alloys such as AA3104, dynamic recovery dominates the dynamic softening mechanism [22]. During hot bulk deformation, work hardening occurs initially due to the interactions and multiplication of dislocations. The dislocation density increases and so too does the internal stored energy, which in turn increases the driving force for DRV. Recovery ensues, including some annihilation of dislocations, and low-angled subgrains are formed. This recovery process, coupled with the creation of dislocations from the work hardening, results in the occurrence of two competing processes. At certain levels of strain, the rate of work hardening and recovery achieves a dynamic equilibrium due to the constant generation and annihilation of dislocations and thus a steady dislocation density is maintained [16]. This process of hot deformation can be depicted by the shape of the flow stress curve, as seen in Figure 2.6 for the deformation of Al–5%Mg. The shape of the flow stress curve here is a typical response that aluminium alloys undergo during TMP. Figure 2.6 clearly shows the initial work hardening of the material until it reaches a critical strain, with the stress steady during the rest of the deformation. Under some conditions, especially under high strain rates and large strains, the curve in flow stress can decrease, as the temperature of the specimen rises during deformation due to the additional heat generated by adiabatic heating during the work of deformation [16]. The mechanical response from hot working as depicted by stress strain curves provides a reflection of the microstructure of the material.

There are two schools of thought with regard to the evolution of the microstructure during dynamic softening of aluminium. The debate over whether aluminium undergoes continuous dynamic recrystallisation (CDRX) or DRV has been topical for the last three decades. One school of thought, mentioned above, holds that for materials with high γ_{SFE}, such as aluminium, DRX does not readily occur, and that DRV is instead the preferential mode. The formation of cells of subgrains acts as a series of sinks for the mobile dislocations from the ease of climb. These cellular subgrains are continually formed and destroyed during TMP and, as a result, the material contains equiaxed subgrains within the primary elongated

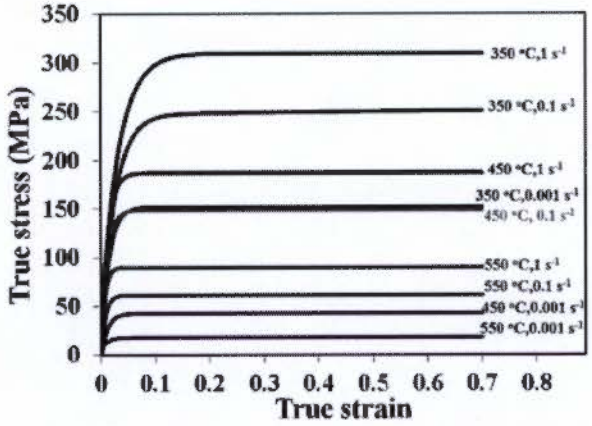

Figure 2.6: Flow stress curve of Al–5%Mg deformed at various temperatures and strain rates [23].

grains [22]. The other school of thought is in favour of CDRX. Due to the high efficiency of the dynamic recovery process, new grains are not formed by classical nucleation. They are developed by the progressive transformation of subgrains into new grains within the deformed grain by the accumulation of dislocations, which then allows for an increase in misorientation of the boundaries between grains. This results in the formation of high-angle boundaries [24]. These theories can be summarised by Figure 2.7, which shows a schematic of DRV (Figure 2.7a) and CCRX (Figure 2.7b) occurring during hot working.

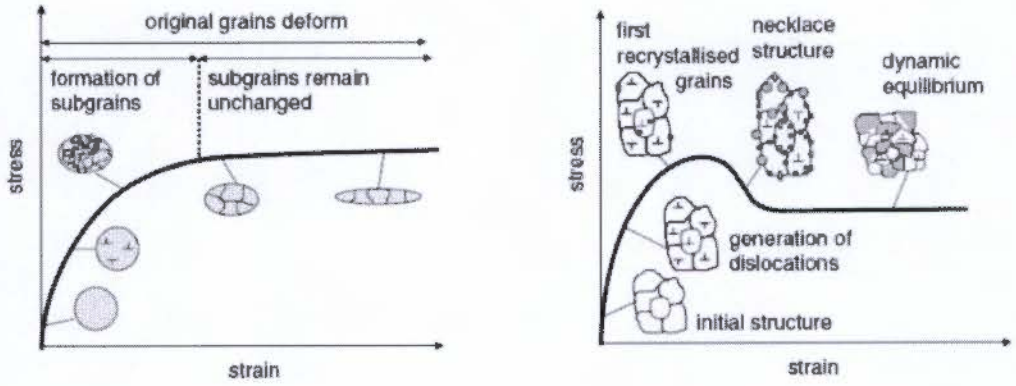

(a) (b)

Figure 2.7: Evolution of the microstructure undergoing (a) dynamic recovery and (b) continuous dynamic recrystallisation during hot deformation [24].

2.2.5 Hot Rolling of Can Body Stock

The production of the CBS at the Hulamin rolling plant has been described in Section 2.1.1. This investigation is focused on the hot finishing procedure, as the microstructural changes occurring during this particular process have a large influence on the final properties and performance of CBS. There are two circumstances in which a change of the microstructure during the hot finishing rolling process is expected: during the actual act of deformation

by the rolling action and during the time between rolling actions, know as the interpass time. Deformation by rolling occurs in a fraction of a second, while the interpass time can range from a couple of seconds to a couple of minutes, depending on the rolling schedule and type of rolling mill. During both of these processes, restoration processes occur. During the interpass times, static recovery, recrystallisation and grain growth, as mentioned in Section 2.2.2, can occur. During the rolling action DRV and/or DRX can occur and these restorative effects are dependant on the Z, which is well documented by Jonas et al. [25].

The deformation texture arising during the rolling of aluminium CBS produces gradual crystallographic rotation of the deformed grain into specific orientations with respect to the surface of the material and the direction in which the material is being worked. In a rolled sheet, the major textures formed are described in Table 2.2. The relative strength of these textures gives rise to the anisotropic behaviour of the CBS during the deep-drawing operation through the formation of ears, where more exaggerated ears result from a higher percentage of individual texture components responsible for particular earing locations. Earing denotes the undulations that appear on top of a drawn cup as highlighted in Figure 2.8.

Table 2.2: Major texture component found rolled aluminium CBS [16].

Texture	Name	Earing positions rel. to RD
{100}<001>	Cube	4 ears at 0/90°
{110}<001>	Goss	2 ears 0/180°
{110}<112>	Brass	4 ears 45°
{112}<111>	Copper	4 ears 45°
{123}<412>	S (~R)	4 ears 45°

The textures associated with rolling and deformation are Brass, Copper and S textures, resulting in ears along 45° to the rolling direction (RD). When the CBS undergoes recrystallisation (dynamic or static), the new grains frequently develop in orientations that differ to that of the principle components of the deformed textures [18]. These restorative textures have a strong tendency to form new grains with a cube {100} plane parallel to the surface of the sheet and a cube edge parallel to the rolling direction. In contrast to the rolling textures, 4 ears are produced at the 0° and 90° positions around the drawn cup. These are called cube and goss textures.

Figure 2.8 shows the different ears formed on the cup from the drawing operation, which is the first production step in the production of beverage cans. The rolling direction depicted in Figure 2.8 runs from left to right across the page. The ideal situation is to produce a can that has virtually no ears, or to minimise the amount of earing produced. The desirable texture produced from the hot finishing rolling condition requires a strong cube texture to be formed from recrystallisation. The cube texture during rolling does not disappear; its intensity is only diminished by the formation of the rolling textures. The cube texture is found to be preserved within cube bands in the hot rolled microstructure [16] and this is

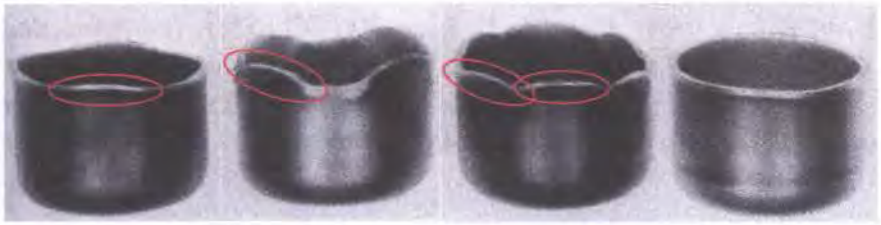

(a) (b) (c) (d)

Figure 2.8: Different ears produced in drawn aluminium cups showing (a) 90° earing, (b) 45° earing, (c) mixed 90° and 45° earing and (d) no earing with respect to the rolling direction [18].

further confirmed by work of Daaland and Nes [26], which showed that cube-orientated grains survive during large heavy reductions without rotating towards the rolling textures. These surviving cube grains serve as nucleation sites for the generation of secondary cube textures, formed by recrystallisation during the hot rolling procedure, and thus result in a strong final cube texture. The subsequent cold rolling will reduce the strength of the newly formed cube texture as competing rolling textures form during deformation. The aim is to 'balance' the volume fraction of the texture components, in order to achieve a mixed texture distribution and ultimately minimise the earing produced in the final CBS. The aforementioned texture evolution is represented by the schematic in Figure 2.9, which illustrates the progression of the textures produced during the production of CBS.

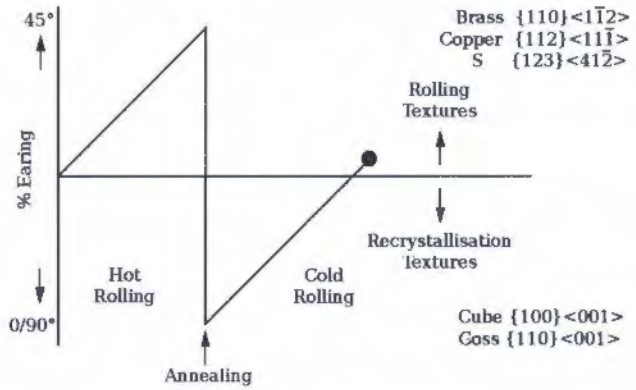

Figure 2.9: Progressive development of textures and earing during the hot and cold rolling stages of aluminium CBS [20].

2.3 Plane Strain Compression Testing

2.3.1 Introduction

PSC testing is the deformation of a rectangular test sample across its breadth by the use of a pair of narrow anvils having longer length than the testing sample's breadth. This causes a narrow rectangular deformation band across the sample. Figure 2.10 is a schematic

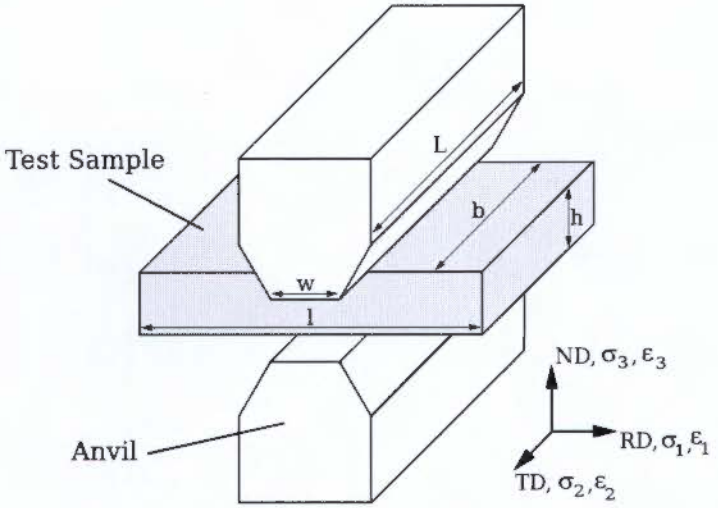

Figure 2.10: Plane strain compression schematic showing the anvil and test sample in relation to the orientation, as well as important varies associated with the testing procedure.

representing the typical PSC testing configuration and layout. The plane strain condition is the displacement of the material which is limited to two planes, as shown in Figure 2.10 the plane strain condition is occurring in the principle planes 1 and 3. For this investigation, the normal direction (ND) and the rolling direction (RD) and lie on the principle planes 1 and 3, respectively, shown by Figure 2.10. PSC testing was originally developed to simulate the rolling of plate or strip, as the imposed rolling deformation closely relates to the plane strain condition [27]. Hot PSC testing has be adopted and is one of the most commonly used tests for the generation of flow stress data for the use in the simulation of TMP of materials. This type of testing is useful for testing conditions that required high strains, where axisymmetric compression test is unsuitable owing to the strain limitation that results from barrelling under high strains. In addition, PSC testing is attractive due to the compression of a relatively large volume of material, thus allowing for suitable microstructural investigations [28].

The PSC testing was first suggested by Orowan [27] in 1943 with the modification of a existing compression test so that it could simulate material flow experienced during rolling by impeding the lateral spread along the breadth of the sample, occurring along the transverse direction (TD). However, it was Ford [29] who successfully implemented the testing technique determining the cold rolling loads from testing copper and carbon steels. Ford recognised that the friction along the breadth of the anvil helped restrict the movement of the material flow in the TD, and thus achieving a condition which is close to the plane strain condition. Ford also investigated that the initial tooling and testing sample geometries play significant roles which govern the deformation characteristics of the material.

2.3.2 Strain Distribution

During the deformation of a PSC sample, the flow of the material within the region between the two anvils is governed by the prevailing slip-line field. A slip-line field is a two dimensional vector diagram that shows the directions of maximum shear, identified with the direction of slip at any point along the line [30]. These slip-line fields resolve, causing a network of slip-lines. Figure 2.11 is the first slip-line field conducted by Hill et al. [31] and shows the slip-line field of a rectangular block between two perfectly rough parallel anvils. The four corner points, at the interface of the material and anvils, in the ND and RD plane is where the plastic zones will initiate.

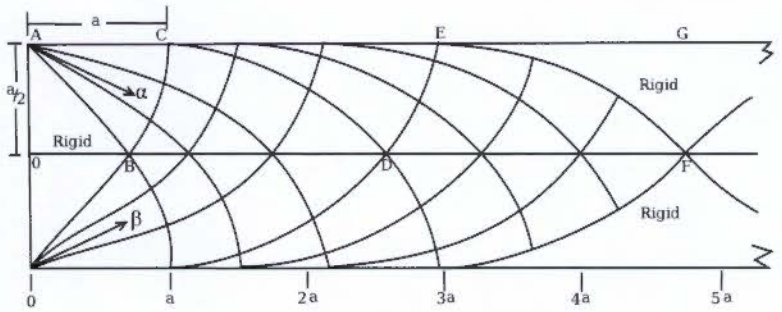

Figure 2.11: Slip-line field for a PSC that has perfectly rough surface interface [31].

The straight lines are drawn from these corners to meet the centre line at 45° and these lines represent the boundary between the rigid and plastic regions during compression. Other slip-lines intersect orthogonally and meet the anvils normally or tangentially. Each line is associated with another, in so much that each is equal in magnitude and opposite in direction, in order to maintain rotational equilibrium. Slip-line field theory has also been used by Green [32] to describe solutions for a smooth surface of the anvils. These two studies both found that the slip-line fields and the pressure on the anvils are sensitive to geometries of the samples height (h) and anvils face width (w). Therefore the geometry of the anvil and sample height are important for the determination of the flow stress and the strain distribution of the material. Figure 2.12 is the solution of slip-line fields under the condition of a frictionless surface, this is the most basic solution of the slip-line fields. The slip-lines consist of a series of straight lines, intersecting at mid-thickness of the sample and meeting the anvil surface at 45°, thus creating a slip-line field of crosses. The different $\frac{w}{h}$ ratios clearly show that a greater number of 'crosses' are formed with a higher $\frac{w}{h}$ ratio. During a PSC test, the $\frac{w}{h}$ ratio increases, thus creating more 'crosses' within the material, depending on the amount of deformation. The actual slip-lines or plastic flow of the material during a test can be described as a mixture between the slip-line field solutions as demonstrated in Figure 2.11 and those in Figure 2.12.

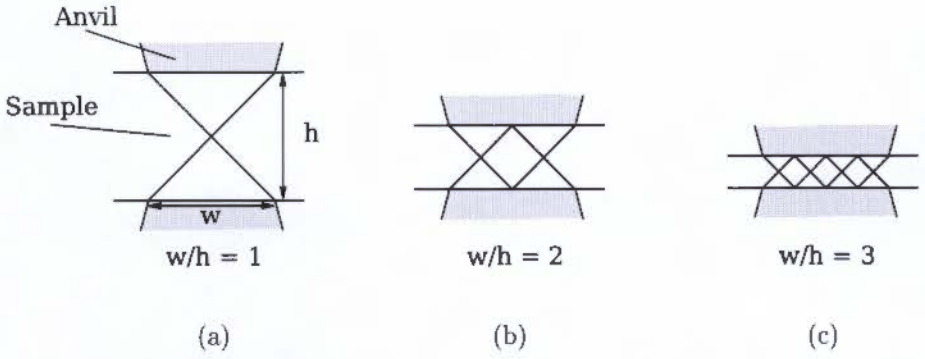

Figure 2.12: Slip-lines fields for a PSC test that has a frictionless interface.

2.3.3 Geometric Dimensions Considerations

The use of the slip-line field theory has proved to provide fairly good representation of the strain distribution within the test sample under going PSC tests [33, 19, 34, 32, 31]. However, the slip-line theory has limitations, as it does not take into consideration of effects of temperature, strain rate and the materials' sensitivity to strain. In practice, these factors have an effect on the strain distribution and thus, the flow stress during the deformation process. The heterogeneity of the deformation of commercial purity aluminium and Al-1Mg-1Mn alloys has been studied by Beynon and Sellars [33], where hot PSC tests were performed at a temperature of 300 °C and room temperature. In order to track the strain distribution within the material, the test samples were halved along the longitudinal direction (along the ND and RD plane at $\frac{1}{2}$b). A square grid was hand scribed on the sectioned face and then clamped back together prior to the heating and deformation. The analysis of the distortion of the grid provides information regarding the local strain and the overall strain distribution of the material under PSC testing. Different initial heights of the sample (h) were chosen, thus allowing for different initial $\frac{w}{h}$ ratios to be tested. From Beynon and Sellars [33] work, it was determined that strain distribution occurred as localised bands of strain and these strain bands corresponded to those predicted by the slip-line field theory [31, 32]. Beynon and Sellars [33] also concluded that the prior strain history had no effect on the distribution of strain under PSC conditions and that a more homogenous strain distribution is achievable with tests that have a larger $\frac{w}{h}$ ratio of the samples. It was further proposed that the inhomogeneous strain distribution gave raise to the differences in flow stress for specimens of different $\frac{w}{h}$ ratios. This is a result of the materials sensitivity to the flow stress at the localised increases in strain rate, which led to variations in the work hardening of the material. However, these effects on the flow stress of the material can become less significant under testing conditions where a larger initial $\frac{w}{h}$ ratio is utilised.

2.3.4 Finite Element Modelling

With the advances in numerical simulations, modelling of hot PSC testing has been possible. Substantial finite element (FE) analysis work by Mirza and Sellars [35, 36, 37] has produced analysis information using the ABAQUS software. The models allow for heat conduction within the specimen, the heat generated within the specimen, as well as the heat transfer from the specimen to the anvils. Mirza and Sellars [35] first carried out two dimensional FE modelling in the ND and RD plane, with perfect plane strain conditions. Commercial AISI 316L stainless steel and aluminium alloy 5052 were tested and modelled. The PSC flow stress tests were carried out experimentally. The results were then used to validate the FE models for flow stress, which is in good agreement with the experimental results. The effects of sample geometry ($\frac{w}{h}$ ratio only), local deformation within material, the material of the sample, slip-lines, fiction and strain rate were simulated. It was concluded that the local strain response during a PSC test was independent of the material and the strain rate. The results from the FE model therefore can be applied to generic PSC tests. The interface friction between the sample and the anvil demonstrated that the deformation is very sensitive to the friction condition. This was also true for the initial samples' $\frac{w}{h}$ ratio. The average strain within the finite elements of 10% of the highest and lowest values, have shown strong dependance on both the $\frac{w}{h}$ ratio and the friction condition. From a microstructural point of view these regions of elements are of importance. This shows that values of a low $\frac{w}{h}$ ratio results in large strain rate gradients within the activated slip-lines.

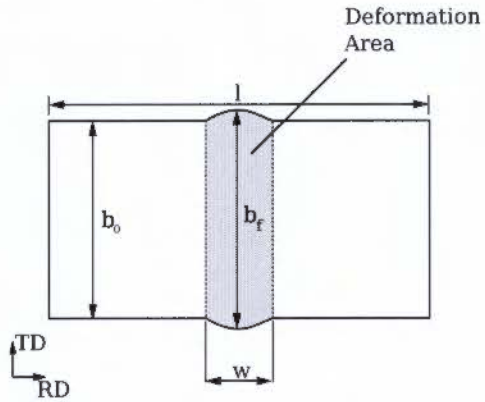

Figure 2.13: Schematic of a deformed PSC sample, showing the deformation area as well as the breadth spreading (b_f).

During the deformation of a PSC test, there is a certain amount of lateral spread of the test sample. The lateral spread, or the breadth spreading (b_f), is depicted in Figure 2.13. The greater breadth spread experienced, the less the deformation condition meets the requirements for plane strain. It is therefore important to keep the breadth spread to a minimum while performing a PSC test. The initial work by Ford [29] demonstrated that the breadth (b) should be 5 - 10 times larger than the anvil face width (w). Understanding which conditions cause the breadth spreading can aid in the optimisation of the testing.

Further FE analysis by Mirza and Sellars [36] used three dimensional modelling to study the effect of friction, strain rate and geometric dimensions affecting the breadth spread of a sample during a hot PSC test for commercial AISI 316L stainless steel and aluminium alloy 5052. Similar to the previous study [35], results showed that the effect of the strain rate and material was insensitive to the breadth spread during a PSC deformation. The significant sample geometric ratio for this investigation was the $\frac{b}{w}$ ratio and the effect on the breadth spread. It was found that for the initial ratio of $\frac{b}{w}$ <5, the breadth spread increased exponentially with continued compression of the sample. This agrees well with the experimental findings of Ford [29]. This indicates to achieve a deformation where the conditions resemble those of plane strain, the initial breadth (b_0) should be as large as possible. This is true, however, practically this could cause an issue when testing, as it creates a much higher load for the PSC testing machine and, thus the machine load capacity could be reached. The FE simulated tests also revealed that the breadth spread during PSC tests is sensitive to frictional conditions. It was determined that there is a systematic trend towards a reduction in spread with an increase in friction value (μ), as shown in Figure 2.14.

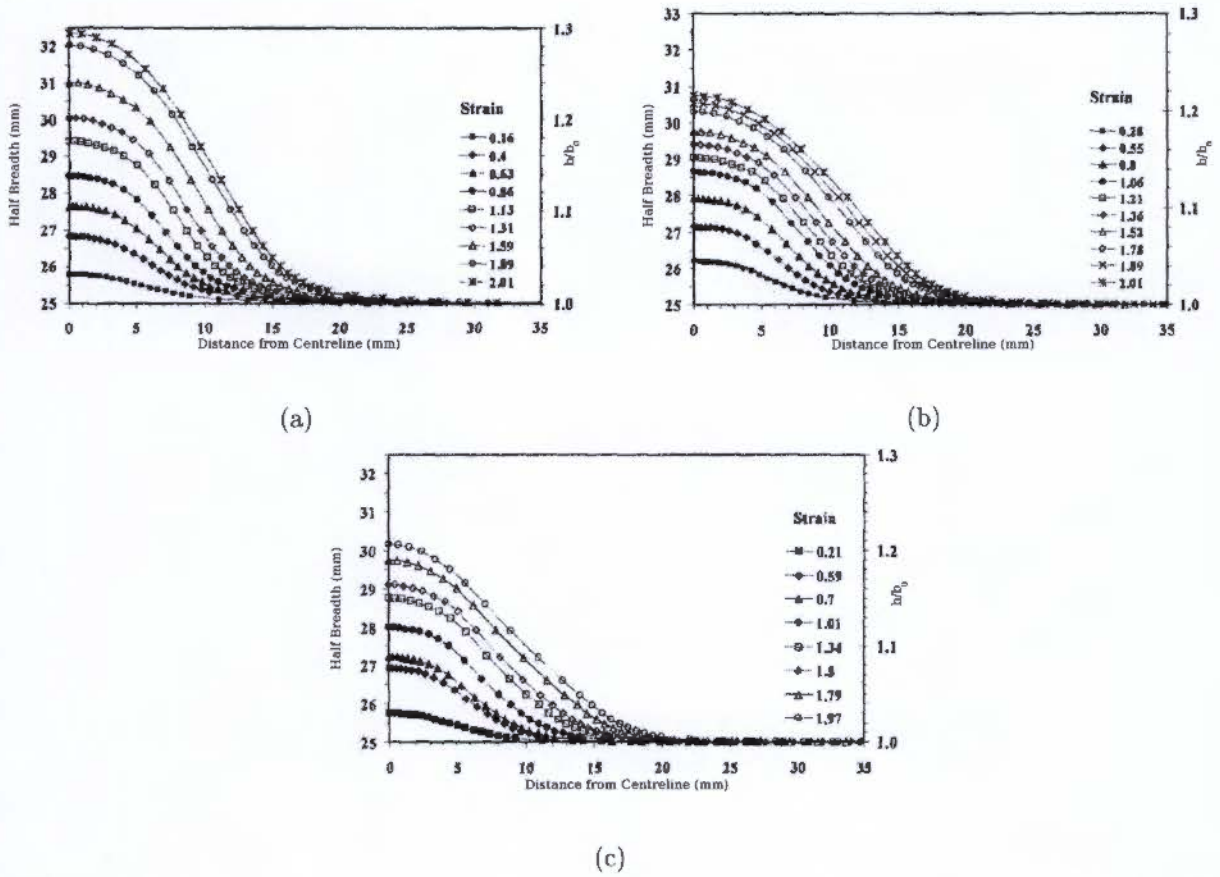

Figure 2.14: The effect of different frictional conditions where (a) μ = 0.0; (b) μ = 0.1; (c) μ = 0.3 have on the spreading of a sample with b_0= 50mm and h = 10 mm [36].

2.3.5 Asymmetric Deformation

Asymmetric deformation of the testing sample in hot PSC tests can be a common event. Achieving perfect symmetry during a compression is difficult. Asymmetric deformation in hot PSC tests can be from a variety of conditions, such as [37]:

i. Non-uniform temperature within the sample, either across the sample breadth or height.

ii. Temperature difference between the sample and anvil.

iii. Misalignment of the anvils.

iv. Difference of contact conditions at the two sample and anvil interfaces.

Any of these above mentioned conditions or combinations thereof can give rise to a distorted sample with either a 'U' shape or a 'Z' shape, as shown in Figure 2.15. The 'Z' shape is the mostly common occurring asymmetric PSC deformed sample. Continued FE modelling by Mirza and Sellars [37] investigated the effects of asymmetric deformation by modelling temperature gradients through the thickness and across the breadth of the sample, as well as the temperatures between the anvil and sample. The maximum temperature gradient modelled for conditions (i) and (ii) was set as ±20 °C for a sample with b = 20 mm and h = 10 mm. It was determined that the temperature gradients of ±20 °C had only negligible effects on the deformation and flow stress results, without causing any significant asymmetric deformation of the sample. Misalignment of the anvils was also modelled with an anvil offset of 1 mm in the RD direction, causing a 'Z' shaped (Figure 2.15b) sample, with highly asymmetrical strain distribution within the material. This asymmetry, caused all the strain to occur in one set of slip-line fields. This also resulted in lateral force on the anvil as well as the sample. However, despite the asymmetric deformation caused by the misalignment of the anvils the computed axial load vs. strain plot was indistinguishable to the a symmetrical test, thus, resulting in an identical stress-strain curve. Further work by Lacey [38] has also been confirmed this experimentally.

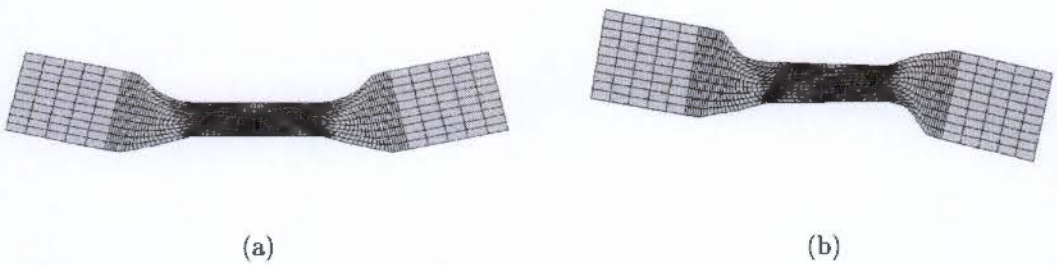

(a) (b)

Figure 2.15: Different distorted samples from a FE simulated asymmetric PSC test to form either a (a) 'U' or (b) 'Z' shape depending on the testing condition [37].

Different contact conditions between the anvil and sample are highly probable occurrence during PSC due to the actual frictional effects not constant during the deformation practice. Mirza and Sellars [37] continued to model asymmetry from different contact conditions at the anvil and sample interface. It was modelled for different uniform frictional conditions at the two interfaces as well as for non-uniform conditions across the width of the anvil. For the frictional conditions that had a uniform but different condition at the anvil-sample interface of each side of the sample, a 'U' shaped (Figure 2.15a) sample was formed with the 'U' shape forming towards the interface with the highest friction. A larger frictional difference at the interfaces will cause a more severely deformed 'U' shaped sample. Another frictional condition was modelled with a varying frictional condition from a high value on the one side of the anvil to a low value of the other side across the anvil width at the anvil-sample interface. The same condition was applied to the other sample-anvil interface, however the variation of friction was acting in the opposite direction. Results from these frictional effects caused asymmetrical deformation of a 'Z' type sample. Results from the derived flow stress curves did not have considerable effects compared to symmetrically deformed samples. However, only in extreme cases is there a small reduction in the derived flow stress curves. It was further concluded that the effect causing asymmetrical deformation in practice is largely due to non-uniform lubrication at the anvil-sample interface.

From the afore mentioned FE modelling, it must be noted that the effects of asymmetrical deformation on microstructural analysis has not been directly investigated. Recrystallisation kinetics and recrystallised grain size are sensitive to the local distributions of strain, strain rate and temperature and this will lead to asymmetry in the microstructure. This has implications for the quantitative metallographic analysis of the sample. However, from the computational observations, the overall plastic strain across the centre of the sample height is relatively small for symmetrical and asymmetrical PSC deformations. Thus, it is suggested that some care should be taken for metallographic interpretation of asymmetrically deformed samples that are not within the centre of the samples heights. Asymmetrical PSC samples tested at UCT Centre for Materials Engineering (CME) has been studied by Duckham and Knutsen [39, 40]. These PSC tests were carried out at room temperature on a modified servo-hydraulic (ESH) universal testing machine. Microstructural analysis of aluminium alloys Al-Mg and Al-1Mg-1Mn was performed by observing the flow patterns and grain morphology using optical microscopy. Bulk texture analysis was also implemented using X-ray diffraction of only the mid section of the deformed samples. During the deformation, anvil lateral displacement of 1.5% was observed for some deformations, causing asymmetric PSC tests. Under the same conditions that caused asymmetrical samples, symmetrical PSC tests were also encountered and it was therefore believed that the varying frictional conditions was the cause of the asymmetric deformation and the lateral offset of the anvils. Figure 2.16 shows the deformation to a logarithmic strain of 2.1 for a symmetrical test (Figure 2.16a)

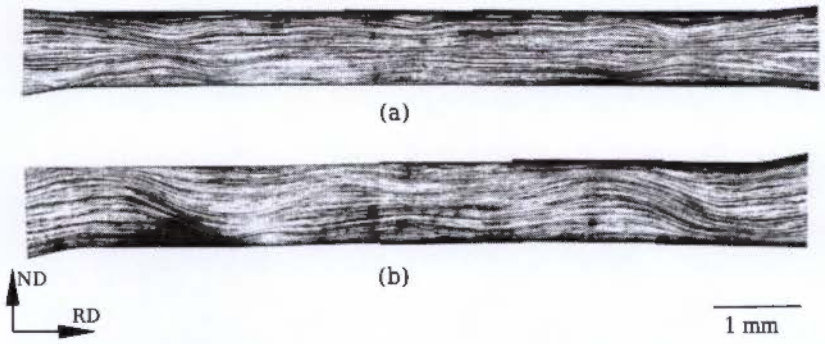

Figure 2.16: Optical micrographs of the ND and RD plane of two PSC deformed Al-1Mg samples to a strain of 2.1 for (a) symmetric deformation and (b) asymmetric deformation [39].

and an asymmetric test (Figure 2.16b) of the Al-1Mg sample. The final $\frac{w}{h}$ ratio of the test was a high value (≈ 10), and thus this followed a fairly uniform strain distribution for the symmetrical test, as shown by slip-line field theory. In comparison, the asymmetric test shows an inhomogeneous strain distribution and the sections of uniform strain is limited.

Duckham and Knusten found that, even with largely different flow pattern within the two deformed samples, the comparison of texture of the symmetric and asymmetric conditions for both deformed and recrystallized microstructures demonstrated that there was no significant influence of the asymmetric flow on the texture evolution when only the mid section of the sample is investigated. This agrees with what Mirza and Sellars [37] suggested from their FE modelling for asymmetric and symmetrically deformed samples.

2.3.6 Breadth Spread Calculation

Interpretations and calculations needed for PSC testing has been compiled by Silk and van der Winden [28] and a guideline for PSC testing has also been complied by the National Physical Laboratory (NPL) in the United Kingdom by Loveday et al. [41]. The breadth spreading occurring from a PSC test changes the deformation condition away from the ideal plane strain condition. The severity of the spreading depends on geometric optimisation, as mentioned in Section 2.3.4, and limiting the breadth spreading results in acceptable plane strain conditions. The amount by which the breadth spreads is therefore important during a deformation, due to the changing contact surface area between the sample and anvil. Therefore this must be taken into consideration when determining the flow stress for the deformation. An instantaneous breadth (b_{inst}) value during the deformation needs to be recorded, however the instantaneous breadth cannot be measured during PSC test. Therefore an empirical relationship of the instantaneous breadth can be interpolated between

the initial and final breadth. Sellars et al. [42] defined a spread coefficient, C, which is:

$$C = \frac{\left(\frac{b_f}{b_0}\right) - 1}{1 - \left(\frac{h_f}{h_0}\right)^n} \tag{2.2}$$

where b_f is the average final sample breadth, b_0 is the average initial sample breadth, h_f is the average final height of the sample, h_0 is the average initial sample height and the coefficient n is a constant. From initial PSC tests Sellars et al. determined $n = 0.5$, but further investigation with hot PSC testing of aluminium alloys by Shi et al. [43] revealed that $n = 0.18$ provided a much better fit for aluminium samples lubricated with graphite. The FE modelling by Mirza and Sellars [36] confirmed these findings. It has been suggested [41] that for other materials the optimum value of n should be determined, however if a consistent value is used the effect is small. So, therefore the instantaneous breadth (b_{inst}) is estimated as:

$$b_{inst} = b_0 \left[1 + C - C\left(\frac{h_{inst}}{h_0}\right)^n\right] \tag{2.3}$$

where h_{inst} is the instantaneous height of the sample, which is calculated from the displacement values during a PSC test.

2.3.7 Calculation of Strain

Determining the stress-strain curves for PSC tests at elevated temperatures for medium to high strain rates is useful in order to understand the materials' stress-strain characteristics for the TMP conditions. Hot PSC testing provides reliable data provided that testing conditions are optimised so that reliable flow stress data can be collected. The calculation of strain is determined by the equivalent strain ($\bar{\varepsilon}$) according to the von Mises criterion. By using the principle directions, as demonstrated in Figure 2.10, and applying the von Mises criterion, then:

$$\bar{\varepsilon} = \frac{\sqrt{2}}{3}\left[(\varepsilon_1 - \varepsilon_2)^2 + (\varepsilon_2 - \varepsilon_3)^2 + (\varepsilon_3 - \varepsilon_1)^2\right]^{\frac{1}{2}} \tag{2.4}$$

and since $\varepsilon_1 = \varepsilon_{RD}$; $\varepsilon_2 = \varepsilon_{TD}$; $\varepsilon_3 = \varepsilon_{ND}$

$$\therefore \bar{\varepsilon} = \frac{\sqrt{2}}{3}\left[(\varepsilon_{RD} - \varepsilon_{TD})^2 + (\varepsilon_{TD} - \varepsilon_{ND})^2 + (\varepsilon_{ND} - \varepsilon_{RD})^2\right]^{\frac{1}{2}} \tag{2.5}$$

where $\bar{\varepsilon}$ is the equivalent strain. ε_1, ε_2 and ε_3 are the principle strains in their respective planes. ε_{RD} is the strain in the rolling direction, ε_{TD} is the strain in the transverse direction and ε_{ND} is the strain in the normal direction. For the ideal plane strain conditions, $\varepsilon_{RD} = -\varepsilon_{ND}$ and $\varepsilon_{TD} = 0$, then:

$$\bar{\varepsilon}_{ideal} = \frac{2}{\sqrt{3}}\varepsilon_{ND} = \frac{2}{\sqrt{3}} ln \frac{h}{h_0} \tag{2.6}$$

However, as previously mentioned the breadth spreading of a PSC sample is significant, so therefore Equation 2.6 does not provide a true equivalent strain value of the deformation. This, however, can be used for quick and easy estimation calculations to determine the approximate equivalent strain. The equivalent strain can be calculated from the samples height from the displacement value of the PSC test and the instantaneous breadth value (Equation 2.3) as well as and knowing that $\varepsilon_{ND} = ln\frac{h}{h_0}$, $\varepsilon_{TD} = ln\frac{b}{b_0}$ and $\varepsilon_{RD} = -\varepsilon_{TD} - \varepsilon_{ND}$. The equivalent strain ($\bar{\varepsilon}$) is therefore:

$$\bar{\varepsilon} = \frac{2}{\sqrt{3}} \left[(\varepsilon_{TD}^2 + \epsilon_{TD}\epsilon_{ND} + \varepsilon_{ND}^2 \right]^{\frac{1}{2}} \tag{2.7}$$

It must be noted that since the ε_{TD} is related to the ε_{ND} from Equation 2.3, a term f can be defined as:

$$\bar{\varepsilon} = -f\varepsilon_{ND} \tag{2.8}$$

$$\therefore f = -\frac{\bar{\varepsilon}}{\varepsilon_{ND}} \tag{2.9}$$

For instance if a test was under ideal plane strain conditions then the term $f = \frac{2}{\sqrt{3}}$. For the calculation of the equivalent strain during a PSC test, the term f cannot be calculated 'live' by the control system. The f term can only be calculated post deformation by 'offline' analysis. Hence, a nominal term, f' is therefore employed for 'live' calculations and it it is determined as [43]:

$$f' = \frac{\frac{2}{\sqrt{3}}(b_0 - w) + w}{b_0} \tag{2.10}$$

where w is the dimension of the face width of the anvil. This f' term provides an estimation for the equivalent strain during the 'live' PSC test. By estimating the equivalent strain during a PSC test by using $f = \frac{2}{\sqrt{3}}$, this would overestimate the equivalent strain if the ideal plane strain conditions were represented. Therefore, by using the intermediate term, f', calculated by Equation 2.10, a more realistic factor is achieved. Once the PSC test has been completed, then term f can be calculated and used for further analytical purposes.

2.3.8 Friction Corrections and Calculations

Friction acting between the anvil-sample interfaces result in an increase of the load to deform the material. Therefore, corrections of the measured load is needed in order to determine the flow stress applied to the material. The deformation of the sample causes a pressure at the anvil-surface interface. The average instantaneous pressure ($\bar{p}$) experienced at the

anvil-sample is therefore:

$$\bar{p} = \frac{L}{wb} \tag{2.11}$$

where L is the applied load measured by the load cell during a deformation. The shear flow stress (k) can be deduced whether the frictional condition is sticking, sliding or a combination of the sticking and sliding friction. During the deformation, there may arise a situation where the central region of the anvil across its length is under the sticking friction condition and the regions along the anvils edge is under sliding friction. The position (z_0), where there is a change between sticking and sliding friction, is calculated as [44]:

$$z_0 = \left(\frac{h}{2\mu}\right) ln \left(\frac{1}{2\mu}\right) \tag{2.12}$$

where μ is the Coulomb friction coefficient, which is assumed as the static value during the deformation. The shear flow stress in terms of the average pressure on the anvils can be described by one of the three frictional conditions based on where the sticking and sliding friction position. Therefore:

If $2z_0 > w$, then sliding friction is occurring, and:

$$\frac{\bar{p}}{2k} = \frac{1}{bw}\left[\frac{2h^2}{\mu^2} + \frac{(b-w)h}{\mu}\right]\left[\exp\left(\frac{\mu w}{h}\right) - 1\right] - \frac{2h}{\mu b} \tag{2.13}$$

If $w > 2z_0 > 0$, then partial sticking is occurring, and:

$$\begin{aligned} \frac{\bar{p}}{2k} &= \frac{h}{\mu w}\left(\frac{1}{2\mu} - 1\right) + \frac{\frac{w}{2} - z_0}{\mu w} + \frac{\left(\frac{w}{2} - z_0\right)^2}{hw} \\ &+ \frac{1}{\mu b}\left(\frac{2z_0^2}{w} - z_0 - \frac{2hz_0}{\mu w} + \frac{h}{2\mu} - h + \frac{h^2}{w\mu^2} - \frac{2h^2}{\mu w}\right) + \frac{1}{hb}\left(z_0^2 - \frac{4z_0^3}{3w} - \frac{w^2}{12}\right) \end{aligned} \tag{2.14}$$

If $0 > 2z_0$, then sticking friction is occurring, and:

$$\frac{\bar{p}}{2k} = 1 + \frac{w}{4h} - \frac{w^2}{12hb} \tag{2.15}$$

The shear flow stress occurring within the material is now corrected with respect to type of frictional condition that is occurring within the material.

2.3.9 Calculation of Flow Stress

Similarly for the calculation of the equivalent strain, the von Mises criterion is applied for the equivalent stress. The eqnivalent flow stress ($\bar{\sigma}$) is thus:

$$\bar{\sigma} = \frac{2k}{f} \tag{2.16}$$

where $2k$ can be calculated from Equations 2.13 – 2.15 and f is determined by Eqnation 2.9. The equivalent stress can only be calculated 'offline', post deformation. In order to determine the eqnivalent stress 'live' , the nominal value f' (Equation 2.10) can be employed. Figure 2.17 shows the difference between the average instantaneous pressnre ($\bar{p}$), the shear stress (k) and the equivalent stress (σ) plotted against the equivalent strain for a low carbon steel deformed at 1000°C at a strain rate of 5 sec^{-1}. It can be noticed that each curve is adjusted following each consecutive procednre in order to resolve the corrected equivalent flow stress valne for the material being deformed.

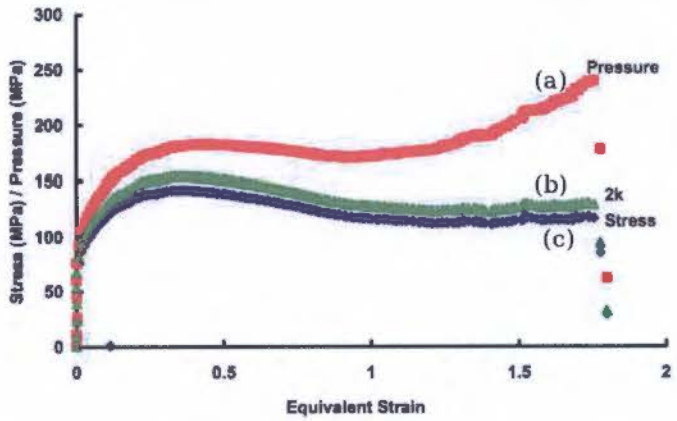

Figure 2.17: Flow stress curves of the (a) pressure on the anvil face, (b) shear stress and (c) the corrected equivalent stress for a low carbon steel that was deformed by hot PSC at 1000 °C at a strain rate of 5 sec^{-1} [41].

2.3.10 Temperature Considerations

Hot deformation occurs at lower stress values due to the ease of slip from the high deformation temperature. Additional heat is generated by plastic deformation during medium to high strain rate deformations (>1 sec^{-1}), thus resulting in thermal softening during the deformation. It is therefore important to record the temperature and temperature changes occurring during a hot PSC test. The temperature histories are recorded by a thermocouple positioned within the deformation zone, usually by inserting a thermocouple into small hole drilled into the PSC sample. For the temperature heating rate and holding conditions, it is optimal to minimise the temperature variation across the

samples breadth and height, as variations in temperature can have a considerable effect on microstructural analysis. Temperature variations recommended by the Good Practice Guide for hot PSC are described in Table 2.3 [41]. Therefore, good temperature control is essential for reliable flow stress calculations.

Table 2.3: Allowable temperature variations for hot PSC test [41].

	Test temperature, T (°C)	Temperature variation (°C)	Precision (°C)
Across sample height, h	< 600	12	±2
	$600 < T < 900$	18	±3
	> 900	24	±4
Across sample breadth, b	< 600	16	±2
	$600 < T < 900$	24	±3
	> 900	32	±4

Deformation of a sample causes heat to be generated within the sample. The size of the raise in temperature is dependent on the strain rate being imposed on the sample. An increase in adiabatic heating will occur with increasing strain rate and therefore the testing condition will not be isothermal. The adiabatic heating associated with the deformation of the sample is considered to only occur at strain rates greater than ~25 sec^{-1}. Conditions with high strain rates do not allow time for heat transfer to occur from the hot deformation zone to the colder shoulders of the sample and anvils [45], resulting in localised heating. Therefore it is important to accurately record the instantaneous temperature for each strain measurement of the sample during the PSC test. A complex thermal model has been successfully implemented by using a finite difference model by Hand et al. [45] for single or multiple deformations. A simplistic approach for determining the raise in temperature ($\triangle \bar{T}$) by adiabatic heating in the deformation zone is:

$$\triangle \bar{T} = \frac{1}{c_p \rho} \int_0^{\epsilon} \bar{p} d\varepsilon \tag{2.17}$$

where c_p is the specific heat of the material and ρ is the density of the material. From the FE analysis by Mirza and Sellars [37] a model was used to predict the the average and maximum temperature histories within the deformation zone.

Due to the heterogeneous nature of PSC testing, there are large temperature variations in deformation zone. High localised temperate regions occur within the slip-line as a result of the local formation of strain and its associated strain rate. Figure 2.18 shows the localised temperature regions that aligning with the slip-line fields in the FE analysis of AISI 316L stainless steel undergone hot PSC testing at a initial temperature of 1000 °C to a strain of 1 at a strain rate of 5 sec^{-1}. The FE analysis agrees with the early initial experimental work done by Colas and Sellars [34], where they investigated the strain and temperature distribution in hot PSC tests of AISI 316L stainless steel. The strain distributions and the corresponding

variation in local temperatures is an important fact for microstructural analysis, especially for materials that are highly sensitive to strain, strain rate and temperature, as this will have a effect on the dynamic softening mechanisms at these localised regions.

Figure 2.18: Finite element analysis of the temperature distribution in AISI 316L stainless steel that has been subjected to a hot PSC test at 1000 °C to a strain of 1 at strain rate of 5 sec^{-1} [37].

2.3.11 Constitutive Equations and Temperature Corrections

The calculation for the equivalent flow stress in Section 2.3.9 does not factor in the adiabatic heating effect, as mentioned in Section 2.3.10. Isothermal equivalent flow stress curves yield a more accurate representation of the materials' behaviour during high strain rate deformations where adiabatic heating is taking place. Constitutive equations are able to relate the flow stress of a material to the strain, strain rate and deformation temperature. Modelling the TMP of materials is useful for FE methods as well as for industrial forming applications of the material. The Zener-Holloman parameter, Z, is useful in that it combines the strain rate and the temperature and, thus Equation 2.1 plays a vital role for determining the constitutive equation. The initial development of the constitutive equation first utilises the exponential law as this provides the best fit over the data range, especially at higher stresses. Therefore [46]:

$$Z = A \exp(\beta\sigma) \tag{2.18}$$

where A and β are material constants. The exponential law can fit over a large range of Z, therefore β can be calculated by plotting $ln(Z)$ vs σ and the slope of the best fitted line will yield the β value. However, for the calculation to determine the isothermal equivalent flow stress for each PSC test, the β values must be determined for each corresponding strain value. Equation 2.18 describes the equivalent stress and its corresponding strain. β values are therefore interpolated for the corresponding strain and a best fit curve can be described by a power law $\beta = a\bar{\sigma}^b$, where a and b constants that best fit the curve. The isothermal equivalent flow stress (σ_{iso}) values can therefore be determined the from equivalent stress values, as shown by:

$$\sigma_{iso} = \bar{\sigma} + \frac{Q_{def}}{\beta R}\left(\frac{1}{T_{iso}} - \frac{1}{T_{inst}}\right) \tag{2.19}$$

where T_{iso} is the desired isothermal temperature, T_{inst} is the instantaneous temperature during the deformation.

For an equation that is valid over the entire range of stress, the hyperbolic sine relationship [47] best describes the characteristic flow stress curve that depicts the occurrence of dynamic recovery. The hyperbolic sine relationship approximates to a power law at low stresses and then to an exponential law at higher stresses. Therefore:

$$Z = A_1 \left[\sinh(\alpha\sigma)\right]^{n'} \tag{2.20}$$

where A_1, α and n' are constants. Although A_1, α and n' are constants for each specific data point, it has been shown that $\alpha = \frac{\beta}{n'}$ [47]. Therefore, it is possible to determine α in terms for each data point. By plotting $ln(Z)$ vs $ln\left[\sinh(\alpha\sigma)\right]$, then the slope of the best fit line is the n' value and the intercept is lnA_2. Thus, the constitutive equation is can be described as:

$$\sigma = \left(\frac{1}{\alpha}\right) \sinh^{-1}\left(\frac{Z}{A_2}\right)^{\frac{1}{n'}} \tag{2.21}$$

2.3.12 Inhomogeneous Deformation Corrections

The heterogeneous nature of the PSC tests relies heavily on the sample-anvil geometries, where the formation of the the slip-line field strain relies heavily on the initial $\frac{w}{h}$ ratios. Since the slip-line field strain differs for different geometric dimension, variations of the slip-line field strain and slip-line field strain rates lead to different values of flow stress. Although testing conditions allow for minimal variations of the flow stress values [41], results from FE modelling have lead to a correction procedure to negate the effects of inhomogeneous deformation for the stain and strain rate. Kowalski et al. [48] determined an expression from their FE modelling to determine the following expressions for the strain rate distribution and strain. The slip-line field strain rate is therefore [48]:

$$\frac{\dot{\varepsilon}_{SLF}}{\dot{\varepsilon}_{nom}} = 1 + \left[A_{SLF} \exp\left(-\frac{\frac{w}{h} - 1}{B_{SLF} - 1}\right)\right] \tag{2.22}$$

where $\dot{\varepsilon}_{SLF}$ is the strain rate currently in the active slip-line field and $\dot{\varepsilon}_{nom}$ is the nominal strain rate. A_{SLF} and B_{SLF} are optimised constants that have been determined as 0.8 and 5.5 respectively. The mean strain rate in the current active slip field line can be determined as [41]:

$$\epsilon_{SLF} = (s_0 - 1)\left[m.sin\left(\frac{1}{\epsilon_{nom} + n}\right)\right] + \varepsilon_{nom} \tag{2.23}$$

where m and n are optimised constants with the determined values of 0.25 and 5.5 respectively. The constant s_0 depends on the samples initial thickness. Table 2.4 describes

the value of s_0 for its respective initial heights.

Table 2.4: The value of the constant s_0 depending on the samples initial height [41].

Samples initial thickness, h_0 (mm)	Constant value s_0
10.0	1.50
5.0	1.25
2.5	1.10

Kowalski et al. [48] confirmed their findings with experimental hot PSC testing of aluminium alloy AA502 for temperatures of 300 °C and 400 °C at nominal strain rates of 0.5, 3 and 20 sec^{-1}. The optimised constants for Equations 2.22 and 2.23 are not material specific and therefore the application for determining corrected inhomogeneous flow stress-strain curves can be applied to other materials. Further corrections of flow stress curves can be applied to the coefficient of friction (μ) value, as this value is assumed constant during the PSC test. The coefficient of friction can be adjusted simplistically with respect to the amount of deformation. This is particularly useful when the change of friction is large and has a noticeable effect on the flow stress-strain curve.

2.4 Technology Strategy Consultants Experimental Review

Technology Strategy Consultants (TSC) is a consultancy firm based in the United Kingdom who provide solutions for the technology needs for manufacturing companies. TSC provides solutions for a wide variety of engineering applications, the manufacturing of aluminium is where TSC specialises. Hulamin have utilised the expertise of TSC in order to provide solutions for their aluminium alloy AA3104 intended for the production of CBS. Work by Evans and Ricks [49] from TSC have been carried out on Hulamin's aluminium alloy AA3104 by implementing single hit PSC tests. The performance and validation of this reports hot PSC testing is based from the those results. The work carried out at by Evans and Ricks was performed at the University of Sheffield on their purposely build PSC testing machine as shown in Figure 2.19.

2.4.1 Testing Conditions for AA3104

The work by Evans and Ricks for the hot PSC testing of aluminium alloy AA3104 was performed only for single hit deformations [49]. The temperature and strain rate testing matrix employed shown in Table 2.5 entailed a single deformation test per condition, totalling to 9 single hot PSC tests. The testing conditions cover a wide range of temperatures and

Table 2.5: Temperature and strain rate conditions for hot PSC tests employed by Evans and Ricks [49].

		Strain rate (sec^{-1})		
		10	30	100
Temperature (°C)	300			
	350			
	400			

strain rates that are encountered on the hot finishing rolling mill for the production of aluminium alloy AA3104, as it is described in Section 3.2. The PSC testing samples used by Evans and Ricks were machined from the near centre section of the hot rolled AA3104 slab produced by Hulamin. The dimension of the anvils and samples are included in Table 2.6 and the technical drawings of the sample is included in Appendix A. These PSC samples were deformed to a maximum strain of 1 with the heating time to reach the deformation temperature of ~120 seconds with an additional ~60 seconds holding time. Temperature was monitored with the use of a single thermocouple inserted into the small hole drilled into the mid point of the deformation zone on the side of the sample in the RD and ND plane. Once the sample was deformed at its specific temperature and strain rate condition, the sample was removed and immediately quenched in water. The total time for each test was approximately ~180 seconds.

Table 2.6: PSC anvil and sample dimensions used by Evans and Ricks[49].

Title	Symbol	Value
Anvil face width	w	15 mm
Sample length	l	60 mm
Sample breadth	b	50 mm
Sample height	h	10 mm
Breadth ratio ($\frac{b}{w}$)	B_R	5
Height ratio ($\frac{w}{h}$)	H_R	1.5

2.4.2 University of Sheffield Plane Strain Compression Testing Machine

The PSC testing machine used at the University of Sheffield is a purpose build machine by Servotest, while the basic physical principles of PSC is the same as encountered on the PSC testing machine at UCT, Gleeble 3800, there are some fundamental differences between the two machines. The main difference between the two machines is the heating system used to reached the desired testing temperature of the sample. The Servotest machine uses induction coiled heating furnaces in order to achieve the described testing temperature of the testing sample. There are three separate furnaces on the University of Sheffield's PSC testing machine as shown in Figure 2.19a-c, where the furnace shown in Figure 2.19b is where deformation takes place by a single ram that acting in the vertical direction. The Servotest

Figure 2.19: The University of Sheffield PSC testing machine.

machine also has a fully digitally controlled integrated robot arm, that inserts, positions and moves the testing sample as shown in Figure 2.19d.

2.5 Ring Compression Testing

Friction during all metal working conditions is one of the most significant variables, with effects on the deformation load, metal flow, surface quality and the internal structure of the sample during the deformation process. Many factors affect the magnitude of friction, such as the normal stresses, velocity, type of lubrication, surface quality, temperature and material properties. While friction is generally an undesirable phenomenon, it is unavoidable, therefore optimisation of the frictional effects is necessary. The study of tribology is a very important and complex sector for engineering and material science. Many number of tribological experimental tests exist and have been developed to understand friction and the effects it has. Friction can also be accounted for as the most influential factor for experimental error.

(a) (b)

Figure 2.20: Schematic representing the difference between the ID of a ring compression test for (a) low friction and (b) high friction condition [50].

The ring compression test is a popular and acceptable test that is used widely for evaluating friction effects for bulk metal forming [50]. The ring compression test was initially implemented by Kunogi [51] and then later it was improved by Male and Cockcroft [52] as a more useful method. This type of test is attractive as no direct measurement is needed for load exerted onto the sample. The ring compression test comprises a ring specimen that is plastically compressed between two flat platens in the axial direction, and the relative change of dimensions of the internal diameter (ID) and the height can be used to determine the frictional condition. For a frictionless condition, the ring would deform as if it were part of a solid disk, whereby material flows proportionately radially outwards from the centre, therefore the ID would increase by the same amount as the outside diameter (OD). For a low interfacial friction value, the OD of the ring would not increase as much as it would under the frictionless condition, because the friction restrains the expansion radially. Once a critical value is exceeded, the OD does not expand and the remainder of material flow towards the centre, thus decreasing the ID of the ring. The ID of the ring is particularly sensitive to the frictional conditions, hence the measurement of the change of the ID can describe the different frictional conditions. When the ID increases, the friction condition is considered to be low and when the ID decreases the friction condition is considered to be higher. The differences between the changes of the ID of the ring can be seen as a schematic shown in Figure 2.20.

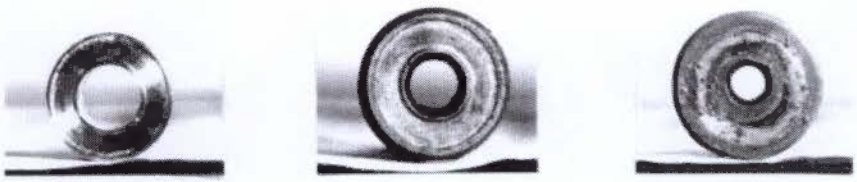

(a) (b) (c)

Figure 2.21: Typical specimens deformed by ring compression testing, where the conditions are: (a) undeformed, (b) deformed with graphite lubricant and (c) deformed with no lubricant [53].

Additional work by Avitzur [54] based on Male and Cockcroft [52] allowed a mathematical analytical approach based on the upper bound solution on the ring compression test. The outcome from this investigation developed complex curves that related the percentage change of the ID of the ring specimen vs. the percentage reduction of the height (H) of the ring specimen. These curves are known as calibration curves and are assigned to different ring specimens that have certain ring dimension geometries. The ring specimen geometries are related as the OD:ID:H, with the most common ratio as 6:3:2. The typical calibration curve for the sample ratio of 6:3:2 can be seen in Figure 2.22. The friction condition can be determined from the calibration curves through the measuring of the change to the ID and the height reduction and thus, providing a quantitative value of the friction condition. The ring compression test has limitations, as the calibration curves assume that the friction condition

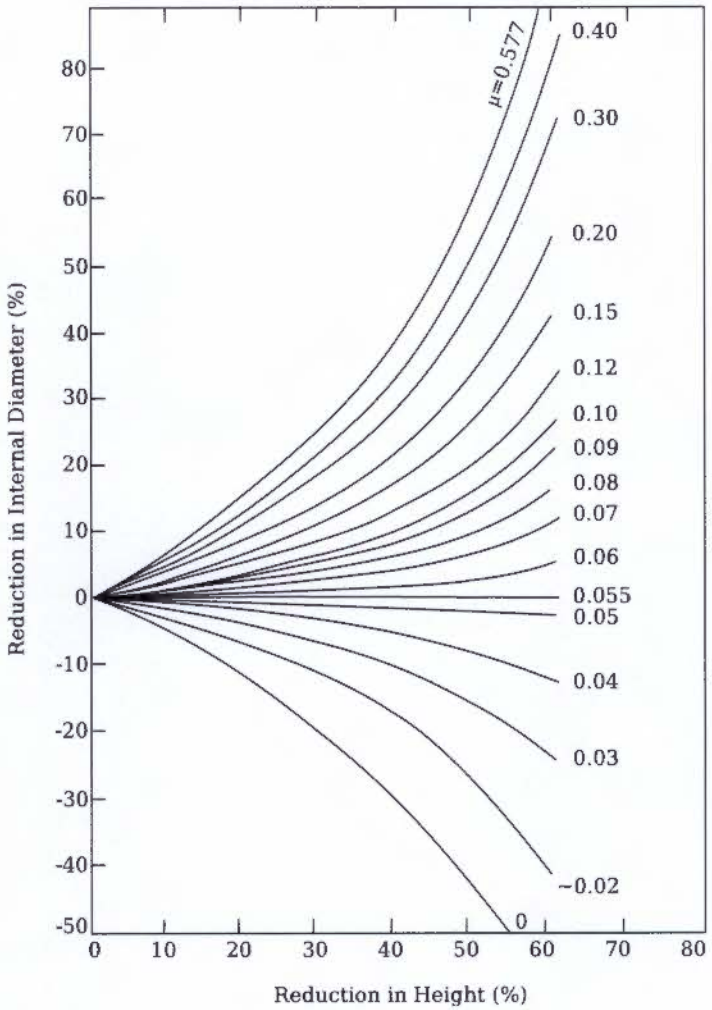

Figure 2.22: Friction calibration curves in terms of μ for the ring specimen ratio of 6:3:2 [52].

is consistent for the entire deformation and that material is not sensitive to the deformation conditions, such as factors like strain rate and work hardening rates. Work by Sofuoglu et. al [50] showed that use of generalised calibration curves is not particularly accurate as the selection of material and testing conditions have different effects and calibration curves should be material and testing condition specific in order to determine accurate friction conditions. The use of FE analysis can be used to create calibration curves for specific material and deformation conditions.

Chapter 3

Experimental Development and Procedure

This chapter describes the experimental route taken for this investigation. The testing procedure can be split into two general sections, the TMP testing conditions performed as hot PSC tests and the microstructural analysis. The hot PSC tests were initially carried out on the Gleeble 3800 in order to assess the testing performance. From the results and observations of the initial hot PSC testing and the ring compression tests; PSC testing modifications and optimisations were further carried out and analysed. After this, multi-pass hot PSC tests were performed to simulate the rolling conditions which are experienced on the hot finishing mill at Hulamin. PLOM was carried out on the TMP samples and microstructural interpretation follows for the selected samples. A flow chart summarising all of the experimental tests is included in Appendix B.

3.1 Material

The material under examination in this investigation is the aluminium alloy AA3104 provided by Hulamin in the form of a transfer bar and strip after the first and third passes on the hot finishing reversing rolling mill. The material used in this investigation is from the plant rolling trials performed by Hulamin for the development of their aluminium alloy AA3104 during the periods from September 2011 to February 2012 [15]. The material received is from trial number 4 (lot number 18/10/015A3) and the composition of trial number 4 is shown in Table 3.1. The homogenisation practice employed for this trial was to perform a soak at 560°C for four hours and followed by a cool-down to 520 °C for two hours.

The plant trials carried out at Hulamin during the period from September 2011 to

Table 3.1: Hulamin Rolled Products' aluminium alloy AA3104 material composition from plant trial number 4. [15].

Hulamin	Si	Fe	Cu	Mn	Mg	Zn	Ti	Al
AA3104	0.23	0.425	0.05-0.05	0.93	0.8-1.3	0.25	0.1	Rem.

Febrnary 2012 led to a general common observation resulting from the Erichsen cnpping tests performed by Hulamin on the alloy AA3104 after the hot finishing process that was performed with a post laboratory annealing heat treatment of 365 °C for three hours. The common observation was that across the width of the strip, a higher earing percentage at the 0°/90° positions relative to the rolling direction was found at the edges in comparison to the middle of the strip. An example of one of these findings (Trial number 5-2, lot number 28/12/180A2) is shown in Figure 3.1. The earing results for hoth of the extreme ends along the length of the strip known as the leading edge (LE) and tail edge (TE) are shown across the width of the strip for each end. The edges of the width of the strip are denoted as the driver side (DS) at the -800 position edge to the operator side (OS) at the 800 position therefore position 0 is the centre line along the strip. Higher percentage earing at 0°/90° positions can clearly be seen at the edges of DS and OS and reports by Hulamin [55] also confirm that a higher cube texture also forms at the edge of the strip. The formation of the 0°/90° earing along the width of the strip can account for the formation and strength of the cube texture formed during the laboratory annealing process; this is in agreement with the literature mentioned in Section 2.2.4.

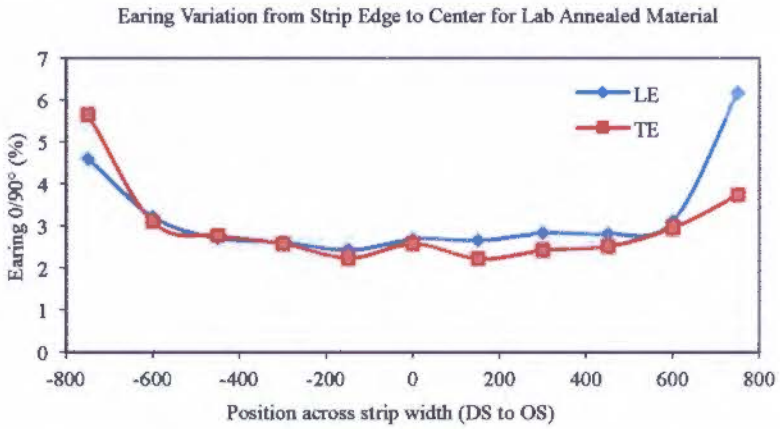

Figure 3.1: Earing variation along the strip width of the AA3104 strip after the hot finishing rolling operation [15].

3.2 Rolling Schedule of AA3104

The necessary information regarding the rolling schedule for aluminium alloy AA3104 in this investigation has been summarised in Tables 3.2–3.4. The planned entry and exit heights of

the strip, the derived reductions, strains and strip speeds are tabulated in Table 3.2. The true strain in the height direction (ND) per pass is calculated as:

$$\varepsilon_{height} = ln\left(\frac{\text{Exit height}}{\text{Entry height}}\right) \tag{3.1}$$

The negative values for the ε_{height} column describes that the strain is under compression load. The total true strain from pass 1 to pass 3 is -2.3 and the work roll diameter of the hot finishing rolling mill at Hulamin is 710 mm [55].

Table 3.2: Planned hot rolling finishing mill schedule for trial number 4 for AA3104 [15].

	Entry height (mm)	Exit height (mm)	△ Height	% Height reduction	ε_{height}	Strip speed (m/min)
Pass 1	20	9.9	10.1	50.5%	-0.70	105
Pass 2	9.9	4.8	5.1	51.5%	-0.72	270
Pass 3	4.8	2.0	2.8	58.3%	-0.88	270

From the information in Table 3.2, the strain rate for each rolling pass can be calculated. During the rolling process, two types of friction conditions occur, namely the sticking friction condition and the sliding friction condition. A practical and satisfactory calculation to determine the strain rate under the sticking friction condition can be calculated as [56]:

$$\dot{\varepsilon}_{stick} = V\left[\frac{2}{D(h_0 - h_f)}\right]^{\frac{1}{2}} ln\left(\frac{h_0}{h_f}\right) \tag{3.2}$$

where V is the peripheral speed of the work roll, D is the diameter of the work roll, h_0 and h_f are the entry and exit heights respectively for the pass. The strain rate for the sliding friction condition is calculated as [56]:

$$\dot{\varepsilon}_{slide} = \frac{V}{h_0}\left[\frac{2(h_0 - h_f)}{D}\right]^{\frac{1}{2}} \tag{3.3}$$

The strain rate of the sticking friction condition is higher than that of the strain rate under the sliding friction condition. The strain rate for both friction conditions was calculated for each pass during the hot rolling of the aluminium alloy AA3104 and is shown in Table 3.3.

Table 3.3: Strain rate calculations for each pass under the sticking and sliding friction condition.

	$\dot{\varepsilon}_{stick}$ (sec^{-1})	$\dot{\varepsilon}_{slide}$ (sec^{-1})
Pass 1	21	15
Pass 2	77	54
Pass 3	125	83

Table 3.4 describes the aim rolling temperatures on the hot rolling finishing mill and as well as the actual temperatures that were recorded during the rolling of trial number 4 using AA3104. The temperatures of the LE, middle and TE of the strip were recorded for all three

passes, and additional temperatures just for the third pass were recorded at the OS and DS for the LE, middle and TE. It can be noted that there is a thermal gradient across the width of the strip with the OS ±12°C on average hotter than the DS. This thermal gradient led to suspicion about the difference in earing behaviour as described in Figure 3.1.

Table 3.4: Aim and actual online recorded rolling temperatures for the hot finishing mill [15].

Aim temperatures (°C)		Pass 1	Pass 2	Pass 3		
		365	270	295		
Recorded on line temperature (°C)	LE	358	349	DS	OS	Thermal gradient
				262	279	11
	Middle	364	351	262	277	15
	TE	351	327	279	288	9

3.3 Gleeble 3800

The Gleeble 3800 is multipurpose thermomechanical testing machine designed and produced by Dynamic Systems Incorporated (DSI) and it was used to perform the TMP of the aluminium alloy AA3104 by PSC testing of single and multiple hits. The Gleeble 3800 was commissioned and calibrated at UCT's CME in December 2011, with the full operations occurring early in 2012. The Gleeble 3800 is a fully integrated digital closed loop control thermal and mechanical testing system [57]. The thermal system employed on the Gleeble 3800 utilises direct resistance heating in order to achieve the desired temperature testing condition of the samples in question. The temperatures measured during a test were controlled by the use of a thermocouple either welded or inserted into the testing sample. Two different modules (Figure 3.2b) can be wheeled, changed and fitted onto the Gleeble 3800 – for this investigation the Hydrawedge II module was used. When the Hydrawedge II module is attached, there are two hydromechanical rams (horizontally) operating independently and synchronously to one another: this allows for the capability to perform high speed deformations with complete independent control of both strain and strain rate [58]. The 'stroke' ram is part of the main unit on the Gleeble 3800 as shown in Figure 3.2a, and this ram is what controls the amount of strain that is needed for the deformation. The 'wedge' ram is shown in Figure 3.2b and it adjusts to achieve the desired strain rate during the deformation. This differs from other machines used for deformation testing as there is generally only one single ram that performs the deformation action. The acceleration and deceleration with the use of a single ram is noticeable, especially in high strain rate tests, and the Gleeble 3800 tries to negate this with the use of the Hydrawedge II module. The controlling tower in Figure 3.2c is where the digital control system is housed and in addition the manual controls control of the machine. Figure 3.3 shows a more detailed environment of the testing chamber, with the two rams acting in the horizontal direction as shown from left to right on the page. Due to

this investigation being one of the first uses of the Gleeble 3800 at the CME at UCT, establishing the capabilities of the machine and understanding and determining the best testing procedure were essential components of this investigation and future investigations that are to use the Gleeble 3800 thermomechanical simulation testing machine.

Figure 3.2: Gleeble 3800 thermomechanical testing machine at UCT CME.

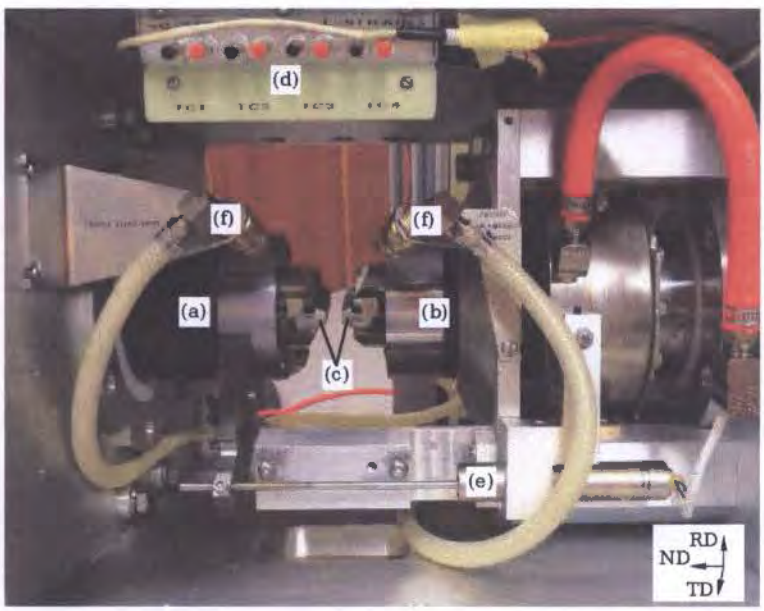

Where:
(a) Stroke ram
(b) Wedge ram
(c) PSC anvils
(d) Thermocouple posts
(e) LVDT
(f) Quenching sprays

Figure 3.3: Gleeble 3800 testing chamber with the various compouents used for PSC testing.

3.4 PSC Sample Geometry

As mentioned in the literature review the physical initial geometric dimensions of the sample and anvil have a significant effect on the PSC testing procedure and results, especially

the strain distribution within the sample and the amount of the breadth spreading of the deformed sample. The recommended geometric ratios are described in Table 3.5 according to the NPL Good Practice Guide for hot PSC tests.

Table 3.5: Recommended testing geometries for PSC testing [41].

Title	Symbol	Relationship	Preferred value	Permissible value
Breadth ratio	B_R	$B_R = \frac{b_0}{w}$	5	≥ 2
Height ratio	B_R	$B_R = \frac{w}{h_0}$	1.5	≥ 1.5
Length ratio	l_R	$l_R = \frac{l}{w}$	3	≥ 3

The dimensions of the anvil and sample geometries for PSC tests are described in Figure 2.10. The height dimensions of the sample were measured before and after the deformation with the use of a micrometer at various locations as described in Figure 3.4. The initial (h_0) and final (h_f) heights of the sample were calculated from the average of the five height readings pre- (Figure3.4a) and post-deformation (Figure 3.4b). The initial breadth value (b_0) of the sample was calculated similarly with the use of vernier callipers at the three described locations according to Figure 3.4(a). The breadth spread (b_f) value post-deformation is just the one measurement and it is measured as shown in Figure 3.4(b).

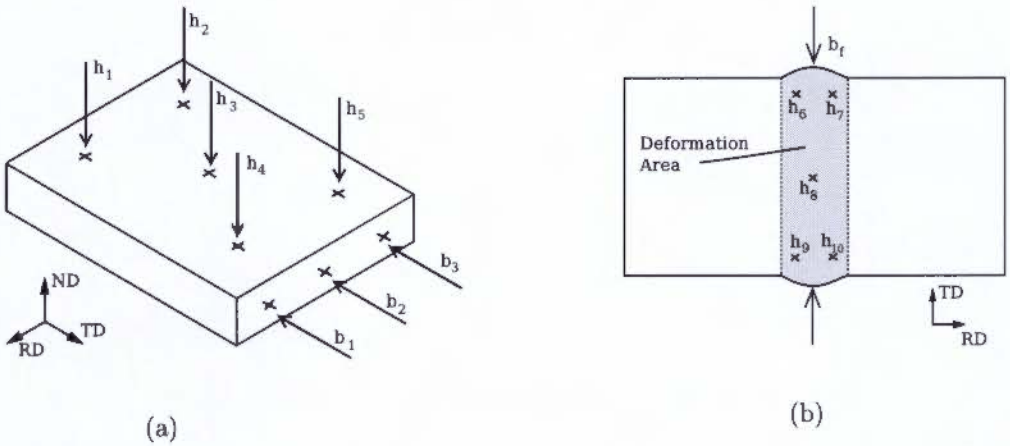

Figure 3.4: Measurement locations on the PSC sample for the breadth and height (a) before and (b) after deformation. [41].

3.5 Initial Plane Strain Compression Tests

Initial preliminary tests were carried out on the Gleeble 3800 in order to understand the basic fundamentals for hot PSC testing on the Gleeble 3800. There is no official documented standard practice for PSC testing, however the NPL in the United Kingdom has compiled a Good Practice Guide [41] to describe the best practice for hot PSC tests from strain rates of 10^{-3} to 10^{2} sec^{-1} below the solidus temperature. The basis and validation of the guide has been supported by carrying out experimental tests on AISI 316L stainless steel and

aluminium alloy AA5052 conducted at the University of Sheffield by using the Servotest PSC testing machine. This investigation has followed the Good Practice Guide as closely as possible in order to minimise the levels of uncertainty during the testing, measuring, developing and analysis processes.

3.5.1 Initial PSC Sample Preparation

In preparation for the initial PSC tests, samples were machined from the provided industrially rolled aluminium alloy AA3104. The standard sample geometric dimensions according to DSI for PSC testing are the 'large' anvil set provided with the Gleeble 3800, and these were used for the initial hot PSC tests. The standard nominal geometric dimensions recommended by the DSI for the anvil and sample are described in Table 3.6. Samples were machined to specific orientations in relation to rolled strip so that the RD measured along the l direction of the sample, the ND measured along the h direction of the sample and TD direction of the strip was measured along the b direction of the sample. The technical drawing of the recommended DSI sample is included in Appendix A. By the use of quick and easy sample machining and to preserve the amount of the transfer bar material, the initial PSC samples were machined from the provided aluminium alloy strip that had been subjected to the first pass on the hot finishing mill at Hulamin. The first pass material already had a height dimension of 9.9 mm as is shown in the rolling schedule in Table 3.2. A height value of 9.9 mm for the initial hot PSC is thought to not significantly influence the results as these tests were first used as 'dummy tests' in order to understand the implications of hot PSC testing. The samples were also given a light grinding with 1200 silicon carbide (SiC) wet sandpaper on a grinding wheel in order to remove any impurities as well as to provide a consistent surface finish. A wipe with ethanol and tissue paper was used to further clean the surfaces of the samples further.

Table 3.6: Nominal dimensions recommended by DSI for PSC testing.

Title	Symbol	Value
Anvil length	L	42 mm
Anvil face width	w	10 mm
Sample length	l	20 mm
Sample breadth	b	30 mm
Sample height	h	10 mm
Breadth ratio	B_R	3
Height ratio	H_R	1

K type (chromel and alumel) thermocouples were used to measure and monitor the temperature in the initial hot PSC tests. For these sets of initial PSC tests, either one or two thermocouples were used to monitor the sample temperature. The thermocouples were surface-welded within five wire widths apart onto the PSC sample with the voltage range

from 36-40 V. A good way to test if a quality weld has occurred between the thermocouple and sample is to test whether the thermocouple wire can hold the weight of the suspended sample. Since, only one thermocouple can be used as the control thermocouple, positioning of the control thermocouple is important. The control thermocouple was welded on the surface of deformation zone, which is at the midpoint on the side of the sample as shown in 3.5. For tests that used two thermocouples, an auxiliary thermocouple was used to provide additional temperature information at a different location on the sample. The schematic shown in Figure 3.5 describes the location in the tests that used two thermocouples.

Graphite powder was rubbed onto the contact surfaces of the samples in order to provide dry lubrication for the deformations. 'Thred Gard', a nickel-based wet lubricant, was painted uniformly across the sample's contact surface in some selected tests. Once the lubricant and thermocouples were attached to the sample, the sample was loaded into the the sample loader and the sample loader was extended. The 'stroke' ram was extended to its maximum extension and the 'wedge' ram was brought to within ±5 mm of the sample. Further information regarding the testing parameters is provided in the next section.

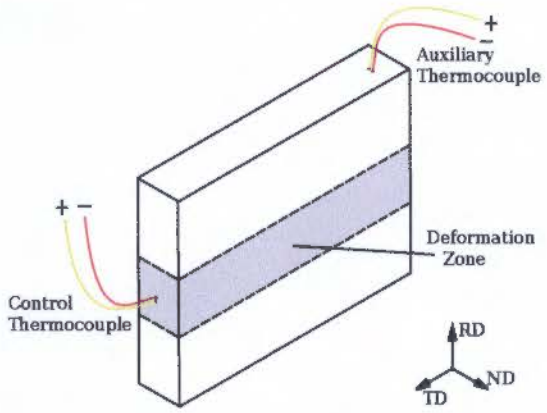

Figure 3.5: Thermocouple positions for the initial hot PSC tests.

3.5.2 Initial PSC Testing Parameters

As mentioned in Section 2.4.1 the testing parameters of this investigation are based on the work done by Evans and Ricks [49] for Hulamin, especially the temperature and strain rate conditions as these have the largest influences on the hot PSC testing results. The selected temperature and strain rate conditions listed in Table 2.5 were used in order to cover the range of temperatures and strain rates of the aluminium alloy AA3104 that were found on the hot finishing rolling mill. The three temperature conditions were 300, 350 and 400 °C and the strain rate conditions were 10, 30 and 100 sec^{-1}. A single hit deformation was performed per each temperature and strain rate condition with the use of graphite powder as the lubricant. Two additional single hit deformations were performed for the condition at the temperature

of 300 °C at a strain rate of 10 sec^{-1} and the temperature of 350 °C at a strain rate of 30 sec^{-1}. These two additional deformations were performed using the wet nickel-based lubricant. The heating rate to the deformation temperatures was set at 2 °C/sec, and a soak time at the deformation temperature for 45 seconds. Only two of the tests had a different soak time of a slightly longer time of 60 seconds. These longer soak times were first used during the tests, however it was noticed that a homogenous temperature was achieved easily enough and the longer soaking time was not necessary. After the deformation, the samples were allowed to air cool down to room temperature. Each test was performed under vacuum conditions within the testing chamber of the Gleeble 3800 by using the 'rough vacuum' setting on the Gleeble 3800 control tower. The chamber pressure for all tests was $< 2.5 \times 10^{-1}$ torr. The testing parameters were recorded for each PSC test by using the testing form included in Appendix C.

The testing parameters such as the type of deformation, the sample and anvil dimensions, strain, strain rate, deformation temperature, heating rate, soaking time and the cooling method were entered into the computer program 'Quicksim' by creating a '.qhd' and filling in the necessary information. The '.qhd' file was saved and a script language that controls the Gleeble 3800 was created from the '.qhd' file to form the langue file known as a '.gsl' (Gleeble script language). Once the testing chamber had reached a steady state vacuum under the 'rough vacuum' control, the 'play' button on the 'Quicksim' program was pressed and the 'run' button on the Gleeble control tower was turned on. Once the sample had reached a cool enough handling temperature after the deformation test, the chamber pressure was released, opened and the 'stroke' and 'wedge' rams were moved apart to enable the sample to be removed. The sample was then cleaned by removing any remnants of lubricant and the deformation dimensions were measured and recorded as illustrated by Figure 3.4b.

3.6 Ring Compression Tests

Ring compression tests were carried out to investigate the frictional effects and differences between the wet nickel-based 'Thred Gard' lubricant and the dry 0.0254 mm (0.01 in) thick graphite foil. The ring compression tests were carried out on the Gleeble 3800 thermomechanical testing machine with the Hydrawedge II module attached. The 'ISO-T' platens were used, allowing for the uniaxial compression. Typically these platens are used for hot axisymmetric compression tests with samples up to a maximum diameter size of 10mm. The ring compressions samples used for this test used they typical 6:3:2 ratio for the OD:ID:H.

3.6.1 Configuration

Liu et al. [53, 59] successfully carried out ring compression tests on the Ti-6Al-4V by using the Gleeble 1500, a previous generation of the Gleeble 3800. These tests were carried out for a glass lubricant and a graphite powder mixed with engine oil. In the work performed by Li et al., a small recess on both sides of the ring sample was machined into the sample in order to aid by keeping the wet lubricants entrapped between the sample and the anvil face. This was used to limit the squeezing out of the lubricants during the compression. The samples for this investigation were machined and turned from the aluminium alloy transfer bar AA3104 provided by Hulamin. Figure 3.6 describes the orientation of the ring compression samples with respect to the transfer bar. The dimensions of the ring compression sample have an OD of 15 mm, ID of 7.5 mm and a H of 5 mm. For the ring compression tests that used the nickel-based lubricant, a recess of 0.2 mm was machined into both sides of the sample, similar to the samples of Li et al. A normal ring compression sample was used for the tests that used the graphite foil. Drawings of both the ring compression test samples are included in Appendix A. Since a maximum sample diameter of 10mm can be used with the existing 'ISO-T' platens, a custom anvil 'end cap' was machined so that a larger sample diameter could be used to prevent the sample from flowing over the edges of the anvil 'end cap' during the deformation. The custom anvil 'end caps' were machined from Böhler K460 steel. The technical drawings of the custom end caps are included in Appendix A. The custom anvil 'end cap' was designed to limit sharp edges in order to avoid any arcing that can occur during the heating cycle of the test as charge builds up and discharges at the sharp edges.

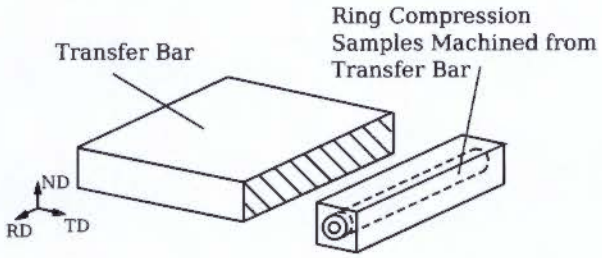

Figure 3.6: Ring compression test samples machined from the transfer bar showing the respective orientations.

3.6.2 Testing Conditions

Before any ring compression tests were carried out, the ring compression test samples were annealed at 400 °C for three hours in order to reduce the amount of anisotropy associated with industrial rolling. The temperature and strain rate testing conditions for the ring compression tests were the same as the temperature and strain rate conditions described in Table 2.5 and the initial PSC tests. It was planned that for each temperature and strain rate condition, two deformations would occur from a height reduction of between 30–60%. The

heating rate was set at 10 °C/sec, with a 15 second soak at the deformation temperature. Higher heating rates and shorter soak times, in comparison to the PSC tests, were chosen due to the samples being relatively small, and as a result of achieving a homogenous temperature easily.

3.7 Modified Plane Strain Compression Configuration

Modifications to the existing 'large' standard PSC configuration that is supplied with the Gleeble 3800 were performed in order to change the sample and anvil dimensions. These modifications were made to achieve a sample-anvil configuration that would attain a better PSC testing configuration according to the Good Practice Guide [41] as shown in Table 3.5. Owing to the limited working space available with the existing 'large' PSC platens, the nominal values for B_R and H_R were chosen as 4.62 and 1.3 respectively. These values were chosen in order to achieve the best B_R and H_R values with the current 'large' PSC platen set, a slight trade-off was needed in order to achieve the best configuration for both values, thus the optimum geometric configuration could be met. For this new modified configuration, new parts had to be made and machined. An exploded view of the one side of the modified PSC testing configuration can be seen in Appendix A. Table 3.7 describes the nominal dimensions that are were used for the modified PSC testing configuration. Two sets of the modified anvils were machined from Böhler K460 steel. A hardening heat treatment was carried out on the modified PSC anvils at 800 °C for 30 minutes, followed by oil quenching. A hardness of at least 63 HRC (Rockwell scale) was achieved during the hardening treatment of the anvils. The technical drawings and dimensions of each new machined part that represent the modified PSC configuration are included in Appendix A.

Table 3.7: Nominal dimensions for the modified PSC testing configuration.

Title	Symbol	Value
Anvil length	L	70 mm
Anvil face width	w	13 mm
Sample length	l	39 mm
Sample breadth	b	60 mm
Sample height	h	10 mm
Breadth ratio	B_R	4.62
Height ratio	H_R	1.3

3.8 Validation Plane Strain Compression Tests

The results of the initial PSC tests and the ring compression tests made it possible to establish a final procedure and a competent hot PSC practice for aluminium samples for use

on the Gleeble 3800. Appendix B displays a summary of the experimental practice that was used for following the hot PSC procedure on the aluminium AA3104 samples.

Two different sample–anvil configurations were tested in these validation hot PSC tests of the aluminium alloy AA3104. Both testing configurations followed the exact testing conditions as encountered for the initial PSC tests, except the anvil and sample dimensions were different. The standard recommended configuration proposed by the DSI as mentioned in Section 3.5.1 was the one configuration and the other was the modified PSC configuration as mentioned in Section 3.7.

3.8.1 Anvil and Sample Dimensions

The two different testing configurations in these series of tests used the exact same configuration as mentioned in Sections 3.5.1 and 3.7. However, the PSC anvils for the standard recommended configuration by the DSI were machined from Böhler K460 steel and subjected to the same hardening treatment as mentioned in Section 3.7, so that both testing configurations would have the same type of anvil hardness and material for consistent testing reasons. The technical drawings of the anvils of the standard recommended configuration by the DSI can be found in Appendix A.

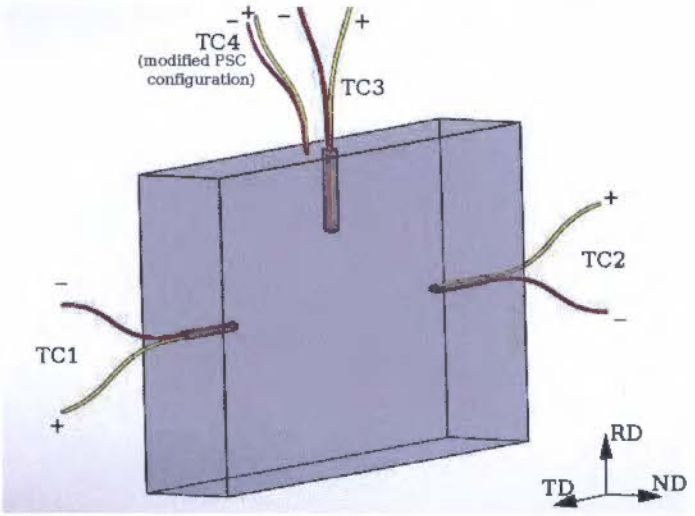

Figure 3.7: Thermocouple positioning for both types of samples used for the hot PSC tests.

The positioning and attachment of the thermocouples for these tests were operated slightly differently from the application in the previous hot PSC tests. The K-type thermocouples were inserted into 1.0 mm drilled holes, so that the inserted thermocouples would achieve a better temperature response during the deformation, as the drilled holes are a black body cavity. Inserted thermocouples also provide a more precise temperature reading due to the thermocouples being positioned within the deformation zone of the material. Figure 3.7 is a schematic showing the positions and configuration of the inserted

thermocouples. The control thermocouple, TC1, is positioned closest to the test chamber door with the thermocouple, TC2, positioned symmetrically opposite to that of TC1 at about the centre line of the ND and RD plane. TC1 and TC2 are able to measure the deformation zone temperatures within the sample and as well as to monitor the thermal gradient across the breadth of the sample. The thermocouple, TC3, measures the temperature of the sample shoulder just outside the deformation zone (±3 mm). The insertion of TC3 is to measure the temperature change within the shoulders during the deformation due to the heat transfer from the hotter deformation zone to the colder shoulders as well as to confirm the temperature of the sample. The thermocouple, TC4, was only used in the modified PSC tests. This additional thermocouple was used to monitor the temperature of the surface of the shoulders of the sample due to the larger size of the modified PSC sample. Technical drawings of both PSC testing configurations of the validation tests are included in Appendix A.

The samples used in the validation tests were machined from the transfer bar of the aluminium alloy AA3104. The samples were machined from the midsection of the transfer bar and maintained the relative rolling orientations from the industrially rolled transfer bar. Figure 3.8 is a schematic representing the sample's relative orientations and positions at the midthickness of the transfer bar.

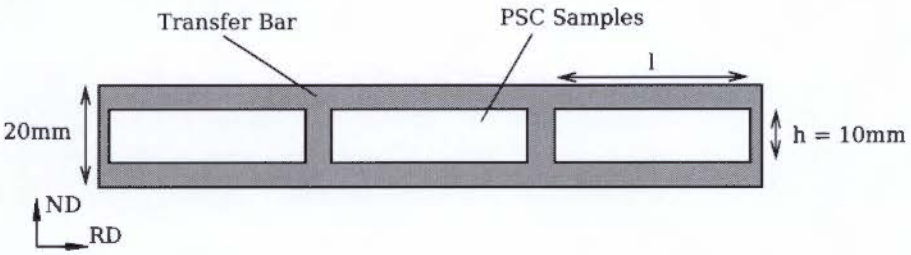

Figure 3.8: PSC samples machined from midthickness of AA3104 transfer bar.

3.8.2 Testing Conditions and Parameters

The testing conditions for both testing configurations are the exact same nominal temperature and strain condition that were used by Evans and Ricks [49] as well as in the initial PSC tests shown in the testing matrix in Table 2.5. The temperature heating rate used for all the tests was set at a fix rate of 3 °C/sec and a holding soak time at the deformation temperature of 45 seconds. The shortest test time (tests up to 300 °C) took up to 145 seconds till deformation and the longest test times (tests up to 400 °C) took up to 178 seconds, therefore no influential microstructural changes could occur over these two different time durations. The hot PSC tests were deformed to a total equivalent strain of 1.6 by a single deformation. For each temperature and strain rate testing condition, two single tests were performed for repeatability purposes. Of the two, single PSC tests at each

temperature and under each strain condition, one of the tests would undergo a forced air quench as the cooling method post deformation and the other test would undergo a water quench post deformation. The purpose of the water quench was to 'lock in' the deformed microstructure. A summary of the testing conditions is shown in Table 3.8. The lubrication chosen for all these tests was the the dry 0.0254 mm thick graphite foil. The deformation tests that utilised the modified configuration made use of an addition of tantalum foil attached across the anvil length in order to decrease the harmful temperature gradient that can occur across the breadth of larger specimens. Tantalum has a lower electrical conductivity, aiding in the decrease of the thermal gradient across the breadth of the sample. PSC tests performed by Cheng [60] on a TiAl alloyed based material also made use of tantalum foil with the use of a Gleeble thermomechanical simulator with satisfactory results.

Table 3.8: Testing conditions and parameters for the hot PSC validation tests.

Condition	Parameter	Unit
Single deformation strain	1.6	
Deformation strain rates	10, 30, 100	sec^{-1}
Deformation temperature	300, 350, 400	°C
Heating rate	3	°C/sec
Soak time	45	sec
Thermocouples	3 × K type	
Cooling method	1× Air Quench	
	1× Water Quench	
Lubrication	0.0254mm Graphite Foil	
Material	Aluminium alloy AA3104	
Samples ($b \times l \times h$)	30×20×10	mm
	60×39×10	mm
Anvil width, w	10	mm
	13	mm
Number of deformations per condition	2	
Total amount of hot PSC tests	36	

3.9 Hot Rolling Simulation Tests

3.9.1 Rolling Interpass Time Calculations

In order to simulate the rolling conditions by using PSC testing, multiple hit deformations are utilised to represent each rolling pass. The hot rolling conditions simulated for these series of tests were carried out to simulate the LE of the transfer bar prior to the hot finishing mill at Hulamin. Due to the nature of the reversing mill, variable interpass times are different from the leading and tail edge of the rolled strip. Calculated interpass times for the initial leading edge of the transfer bar can be calculated from the rolling speeds, threading, unthreading, dead time and set up times during the hot finishing industrial rolling at Hulamin. For the

three hot rolling passes experienced by the aluminium strip, the leading edge will experience the first pass the earliest, the second pass the latest and the third pass the earliest again. The pass time to roll the material for each rolling pass is calculated as shown in Table 3.9. By knowing the initial length of the transfer bar, the strip speed for each pass and the amount of strain per pass; these calculations are possible. It is safe to assume that industrial rolling is under ideal plane strain conditions, so therefore $\varepsilon_{length} = -\varepsilon_{height}$. The strip length for each pass can be calculated for each pass by knowing that true strain $\varepsilon = ln\left(\frac{l}{l_0}\right)$. The strip speed for each pass and length of material for each pass is calculated, as a result allows for the rolling time to be calculated. The dead time due to the set-up of the hot rolling finishing mill is approximately 20 seconds, while the rethreading and unthreading time for each pass is approximately 20 and 15 seconds, respectively [55].

Table 3.9: Pass time calculations on the hot finishing rolling mill at Hulamin for aluminium alloy AA3104.

	ε_{height}	ε_{length}	Strip Length (m)	Strip Speed	Time (sec)
Transfer Bar			150 [55]		
Pass 1	-0.70	0.70	302	105	86
Pass 2	-0.72	0.72	620	270	67
Pass 3	-0.88	0.88	1495	270	138

The interpass time experienced by the LE can be calculated as shown by a time breakdown as shown in Table 3.10. The interpass time between the first and the second deformation of the LE totals 188 seconds, while the interpass time between the second and third deformation is 35 seconds.

Table 3.10: Time calculations for the LE of the aluminium alloy AA3104 during the hot rolling finishing mill.

Description	Time (sec)
Dead time	20
LE deformation 1	
Pass 1	86
Threading & unthreading	35
Pass 2	67
LE deformation 2	
Threading & unthreading	35
LE deformation 3	
Pass 3	138
Threading & unthreading	35

3.9.2 Hot Rolling Simulation Tests

The deformation temperatures at which the hot rolling simulation tests for the LE were determined from the industrially measured online temperatures are shown in Table 3.4. The

nominal temperature of the first hit was set at 358 °C, 349 °C for the second and 262 °C for the third hit. The temperature profile for the full hot rolling simulation initially started at a heating rate of 3 °C/sec over 120 seconds to a temperature of 358 °C and a soak time of 45 seconds was used to allow for a homogenous temperature distribution within the sample. The sample was then subjected to its first deformation hit and allowed to cool at a rate of 0.048 °C/sec over the interpass time of 188 seconds to the second deformation hit temperature of 349 °C/sec. The sample was subjected to the second deformation hit and it was allowed to cool at a rate of 2.457 °C/sec over the interpass time of 35 seconds to the third deformation temperature of 262 °C. The sample was then subjected to the third deformation hit and a cooling rate of 1.5 °C/sec post the third deformation. Figure 3.9 illustrates a summary by graphical representation of the TMP of the LE of the aluminium alloy AA3104.

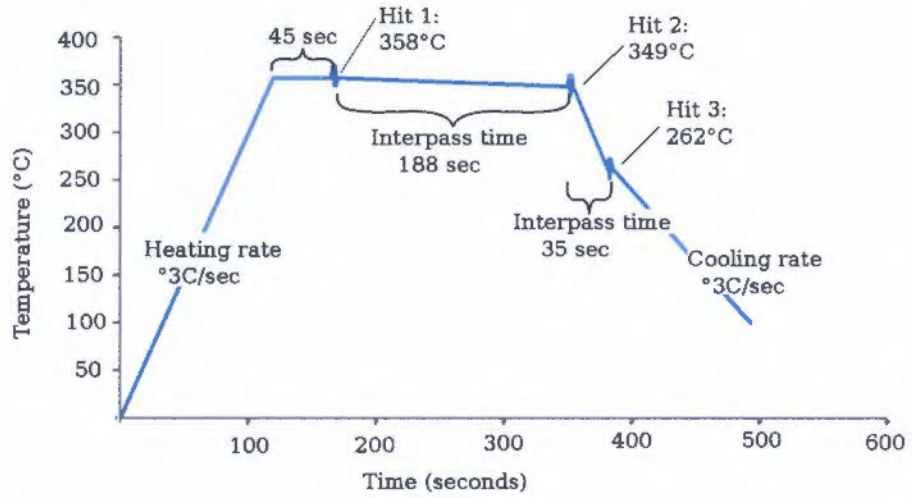

Figure 3.9: Graphical representation of the simulation of the TMP for the three passes experienced by the LE on the hot finishing rolling mill.

The deformation testing conditions of each 'hit' simulates the TMP as experienced on the hot finishing rolling mill at Hulamin for the aluminium alloy AA3104. Therefore the nominal TMP testing conditions for each simulated pass were taken from the rolling conditions experienced by the industrial rolling conditions. Table 3.11 presents the nominal mechanical and deformation temperature conditions for each hit that simulates each rolling pass. The PSC testing geometric configuration used to simulate the hot rolling conditions experienced by the LE of the aluminium alloy AA3104 is the modified testing configuration as described in Table 3.7. The PSC sample dimensions, however, for the hot rolling simulation tests are slightly different from those used for the modified PSC testing configuration as described in Section 3.8. The samples length value, l, used in these tests was set at a lesser dimension of 30 mm in order to combat the thermal gradient by reducing the total volume of material that needed to be heated. The length of the sample does not have a significant effect on the testing conditions for hot PSC testing, as long as a sufficient length is included in the deformation zone. The technical drawing of the samples

used for hot rolling simulation tests is included in Appendix A. K-type thermocouples were used once again in order to monitor, control and record the temperature of the samples during the simulation. The thermocouple arrangement of the samples used for the simulation of the rolling conditions were configured in the same way as described in Section 3.8 and Figure 3.7, however the thermocouple, TC3, was only surface-welded in its position instead of imbed the thermocouple into the material and, as a result, thermocouple TC4 was not needed.

Table 3.11: Nominal TMP conditions for each deformation that simulates the hot rolling conditions for LE of aluminium alloy AA3104.

	Strain, ε	Strain rate, $\dot{\varepsilon}$	Temperature (°C)
Hit 1	-0.70	21	358
Hit 2	-0.72	77	349
Hit 3	-0.88	125	362

Three different rolling simulation testing conditions were used when performing hot PSC testing on the Gleeble 3800 thermomechanical testing machine. Under each rolling simulation testing condition, two tests were performed for repeatability purposes, thus totalling six simulated rolling tests:

Full Rolling Simulation

This rolling simulation was carried out on PSC samples that were machined from the midthickness of the transfer bar as illustrated in Figure 3.8. The full simulated TMP for these tests was carried out by subjecting the PSC sample to all three passes that the LE of the aluminium alloy AA3104 experienced on the hot rolling finishing mill at Hulamin. The PSC sample was subjected to the TMP conditions as shown in Figure 3.9 in order to simulate the three passes experienced on the hot finishing rolling mill.

First Pass Simulation

This rolling simulation was carried out on PSC samples that were machined from the mid thickness of the transfer bar as illustrated in Figure 3.8. This simulation was to just perform the TMP of the first single pass that the LE of the aluminium alloy is subjected to on the hot finishing rolling mill at Hulamin. The PSC sample was heated at a rate of 3 °C/sec over 120 seconds time period to reach a temperature of 358 °C. A soak time of 45 seconds at a constant temperature of 358 °C was utilised in order to achieve a homogenous temperature within the sample. The sample was then subjected to the 'hit 1' deformation condition as described in Table 3.11 and allowed to cool naturally.

Second and Third Pass Simulation

This rolling simulation was carried out on PSC samples that were machined from the aluminium alloy AA3104 that had been subjected to the first pass on the hot finishing mill at Hulamin. This PSC simulation was to 'complete' the three hot rolling conditions by subjecting the PSC sample to the second and third TMP conditions that the LE of the aluminium alloy AA3104 experienced on the hot finishing rolling mill at Hulamin. This PSC sample was therefore effectively subjected to the full TMP described in Figure 3.9 in order to simulate all three passes experienced on the hot finishing rolling mill. However, the only difference was that the sample was subjected to no deformation at 'hit 1' and only the heating profile was conducted for this condition.

3.10 Polarized Light Optical Microscopy Procedure

PLOM was used in order to reveal the grain structure of the industrially rolled transfer bar as well as for the strip after the first and third hot finishing industrial rolling passes. Selected PSC samples from the validation PSC tests as well as samples from the rolling simulated PSC tests were investigated. The PSC samples that were investigated were from the DSI and modified PSC configurations that were water quenched post deformation and were subjected to the testing conditions of 300 °C at 10 sec^{-1}, 300 °C at 100 sec^{-1} and 400 °C at 100 sec^{-1}.

3.10.1 Sample Preparation

Sample preparation for the use of PLOM was sectioned on the RD and ND planes for both industrially rolled and PSC samples. The samples were extracted with the use of the abrasive cutting wheel – the type of abrasive wheel used to section the samples was the Struers 10S24 cutting wheel. During sectioning the samples were carefully clamped and cut in order to make sure that a parallel section to the RD and ND planes was obtained. PSC samples were sectioned at the midbreadth section of the sample, as the deformation in this section showed the closest resemblance to the ideal plane strain condition. Figure 3.11 is a schematic illustrating where the PLOM samples were sectioned form the PSC test samples. The DSI recommended PSC samples and the industrially rolled material were both hot mounted in resin for grinding and polishing. Hot mounting was performed by using the Stuers Labopress-3 hot mounting machine set at 150 °C at 20 kN with a seven minute heating and seven minute cooling cycle. The temperature used for hot mounting is relatively low and therefore it does not have any significant effects on the microstructure of the examined samples. The modified PSC testing samples were set in resin by using the cold mounting

method due to the samples being too long (>30 mm) for the hot mounting machine. Cold mounting per 40 mm diameter mould was made by mixing seven grams of 'Specifix' resin to one gram of 'Specifix' curing agent and allowed to set for 24 hours.

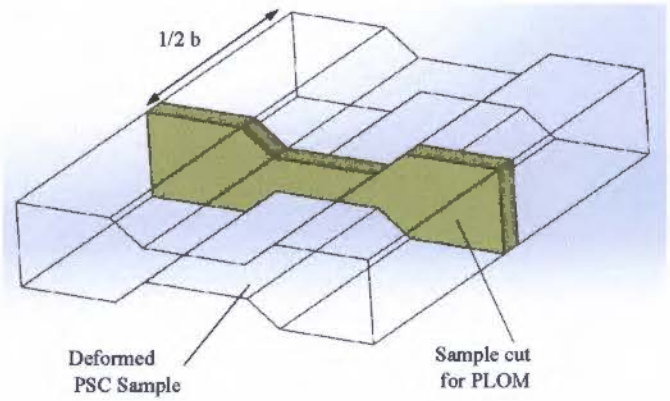

Figure 3.10: PLOM sample sectioned from PSC tests samples.

3.10.2 Grinding and Polishing

Both the cold and hot mounted samples were initially ground with 800 grit SiC water-paper on the manual grinding wheel until a smooth planar finish was obtained. The grinding and polishing process for the hot mounted samples used the Struers TegraForce-1 automatic polisher, while the cold mounted samples were ground and polished with the use of the manual grinding wheel. The polishing process, lubricant, pad and time intervals are described in Table 3.12. Two types of lubricants were used for the polishing process, the 3 μm diamond suspension was used for the initial polishing step and the OP colloidal silica suspension was used for the final polishing process in order to achieve a mirror-like surface on the samples.

Table 3.12: Grinding and polishing process for aluminium alloy AA3104.

Step	Force	Pad	Lubricant	Time (min)		Comments
				Automatic	Manual	
Grinding	10N	1200 grit SiC	Water	5	5	Even and planar?
Polishing	10N	Mol pad	3μm suspension	8	10	Scratches - repeat step
Polishing	10N	Nap pad	OP suspension	5	5	Scratches - repeat previous step
Polishing	10N	Nap pad	Water	2	2	Scratches - repeat previous step

3.10.3 Polarized Light Optical Microscopy

In order to reveal the grain structure of the aluminium alloy AA3104, PLOM was used on the Reichert MeF3A inverted microscope. Before PLOM, the samples need to be electronically anodised by using Barkers reagent. Anodising the sample deposits an Al_2O_2 anodised layer on the surface of the sample. The layer formed is anisotropic as indicated by the amount

of the anodized layer based on the different grain orientations of the surface on the sample. With the insertion of a quartz λ compensation plate into the light path a colour contrast is obtained by revealing the grains based on their orientation.

The anodising of the aluminium samples entailed creating a solution of Barkers reagent by mixing 5 ml of tetrafluoroboric acid (HBF4) with 95 ml of distilled H_2O. The electrolytic reaction reaction occurs when the anodic aluminium sample is immersed into Barkers reagent solution with an aluminium cathode. The anodising method in this investigation used two techniques to create an electric connection to the aluminium sample. The first technique used was to paint the sample with silver dag in order to create a connection from the aluminium to the positively connected tongs which grip the sample. Nail varnish was painted over the silver dag in order to insulate the silver dag from the solution as only the aluminium needed anodising. The sample was then immersed in the Barkers solution by means of tongs. The other technique used to anodise the sample was to drill a hole into the back of the sample through the resin up to the mounted sectioned aluminium. A banana plug was then snugly fitted and inserted into the drilled hole in order to create the connection to the aluminium. The sample would be immersed in the Barkers solution by holding the wire of the banana plug just so that surface of the aluminium sample would be immersed. Figure 3.11 is a schematic illustrating the two techniques used to anodise the aluminium alloy AA3104 for the preparation for PLOM. The DC power supply used to anodise the samples was set with its voltage output at 40 V. A current ranging from 0.1–0.3 A was observed during anodising. The sample was removed from the Barkers solution every 10 seconds and inspected under the microscope until the correct amount of anodisation had taken place in order to reveal the grain structure. The typical time range totalled from 30–90 seconds. Series of micrographs that covered the surface of each sample were stored and later digitally 'stitched' together with the use of software called Microsoft Image Composite Editor to reveal the overall microstructure of the sample.

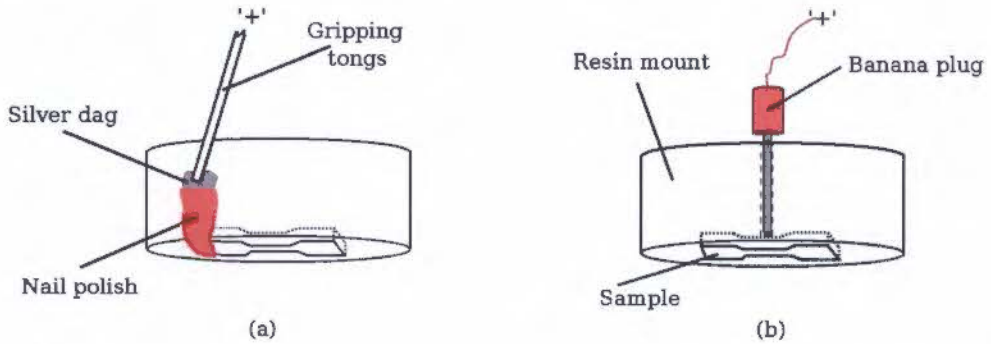

Figure 3.11: Anodising techniques used to prepare the sample for PLOM by either using (a) tongs to grip the sample or (b) by inserting a banana plug into the sample to create an electrical connection to the sectioned PSC samples.

Chapter 4

Results and Discussion of the Initial Plane Strain Compression Tests

This chapter and the subsequent chapters until Chapter 8 discuss the results that were obtained by the experimental procedure described in Chapter 5. These chapters also show the sequential development of the testing procedures during this investigation and how each collection of tests led to the advancement to the next progression of tests. This chapter specifically deals with the testing results that were determined in the initial PSC tests.

4.1 Raw Data

The raw data logged for each PSC test were the force exerted onto the sample, jaw displacement (distance between the anvil faces), thermocouple temperatures, stroke position, wedge position, power angle, programmed temperature, stress and strain. Not all the raw data values were necessarily needed for the analysis in this investigation, however, extra information provided insight into whether the PSC test was acting correctly as well as to provide additional information for troubleshooting in tests that did not run according to expected performances.

4.1.1 Typical PSC Test

The heating rate of the sample and the holding temperature at which the deformation would occur were acceptably achieved for all of the desired nominal input values in all the initial PSC tests. An example of one of the temperature profiles during the initial PSC tests is shown in Figure 4.1. This PSC test temperature profile clearly shows that the steady

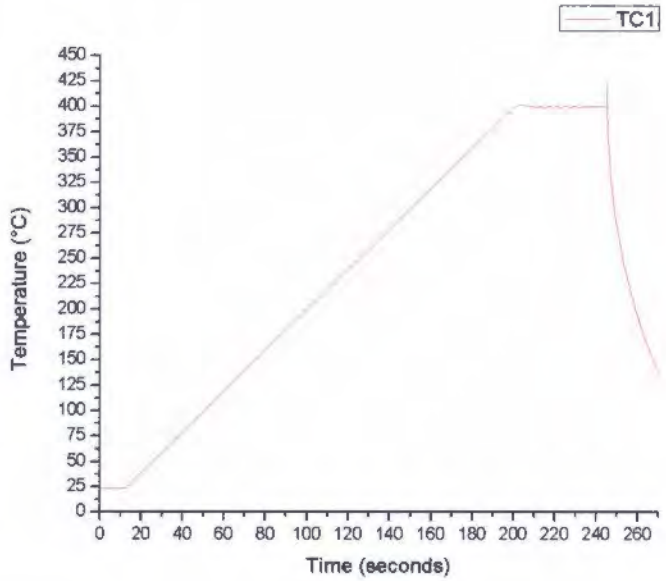

Figure 4.1: Temperature profile for the whole PSC testing cycle of the aluminium alloy AA3104 which underwent PSC at a temperature of 400°C.

heating rate of 2 °C/sec to 400 °C was accurately achieved for the holding duration of 45 seconds. The temperature spike after the holding duration indicates the deformation of the AA3104 and once the deformation had occurred, the PSC sample was cooled by the use of compressed air directed onto the PSC sample, thus creating the cooling section of the temperature profile. The area of interest of this investigation is the deformation duration of the aluminium alloy AA3104, which indicates that a higher resolution of the deformation is necessary to investigate the temperature increase during the deformation. The temperature profile of all the initial PSC tests can be viewed in Appendix D.

Graphite Powder Lubricated PSC Tests

The necessary raw data obtained from performing a PSC test were logged for each subsequent time step. The important raw data recorded in this investigation were the load value exerted onto the PSC test sample, the displacement of the jaw of the anvils and as well as the temperature of the sample during the deformation process. The default recorded data are in the format (.opj extension) of the commercial scientific graphing and data analysis software package known as OriginLab. OriginLab was used to analyse the raw data from a PSC test and the typical data response during the deformation AA3104 by a PSC test is shown in Figure 4.2 under the temperature condition of 300 °C, a strain rate of 10 sec^{-1} and to a total strain of 0.85. As shown in Figure 4.2 the load value, anvil jaw displacement and the temperature values of the thermocouples were plotted with respect to a common time axis. The typical response to a deformation was the rapid increase in load (shown by the

steep slope of the force curve) from the holding force as the jaws started to deform the PSC sample. On further deformation, the AA3104 PSC sample succumbed to yielding and a less rapid increase in force was observed by linear fashion during the remainder of the deformation. The displacement of the jaw of the anvil occurred as expected in a linear fashion. However, there was some variation of the slope of the jaw displacement in most PSC tests, but these variations were not considered significant throughout the deformation duration of these tests. During the deformation, the temperature of the material within the deformation zone increased (as indicated by TC1 in Figure 4.2) due to the adiabatic heating from the high strain rate compression of the PSC test sample. The temperature measurement of the auxiliary thermocouple (TC2) showed an insignificant rise in temperature, indicating minimal heat transfer to the shoulders of the sample. Similar types of trends as shown in Figure 4.2 were observed for all the tests that were deformed with graphite powder as the lubricant. The raw data for each individual test for the deformation are included in Appendix D.

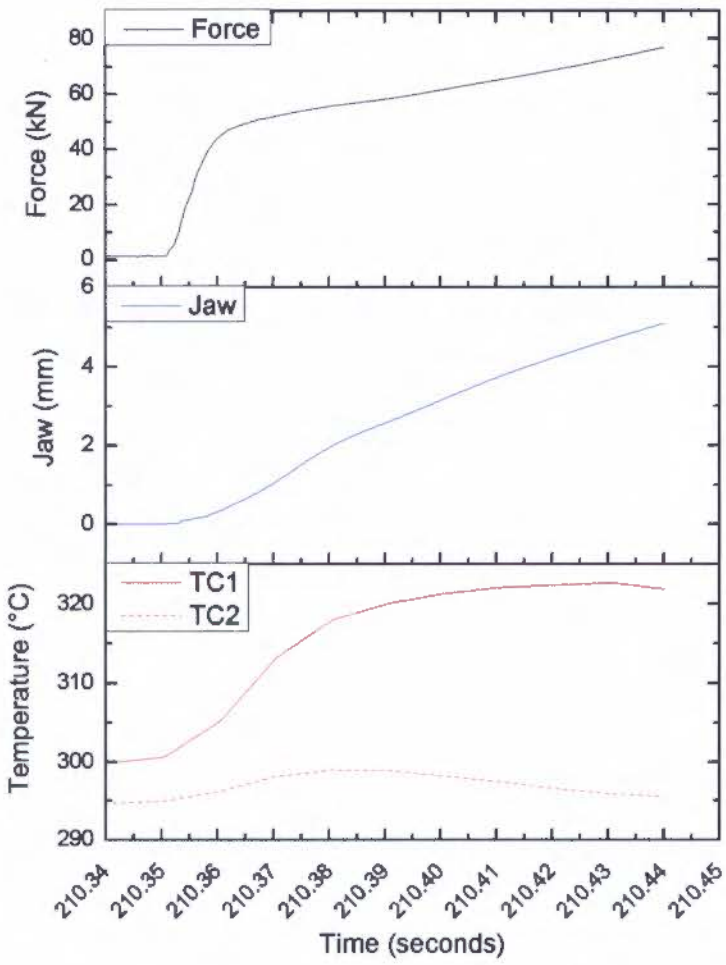

Figure 4.2: Raw deformation data of the PSC of the aluminium alloy AA3104 lubricated with graphite powder at a nominal temperature of 300 °C, strain rate of 10 sec^{-1} and to a strain of 0.85.

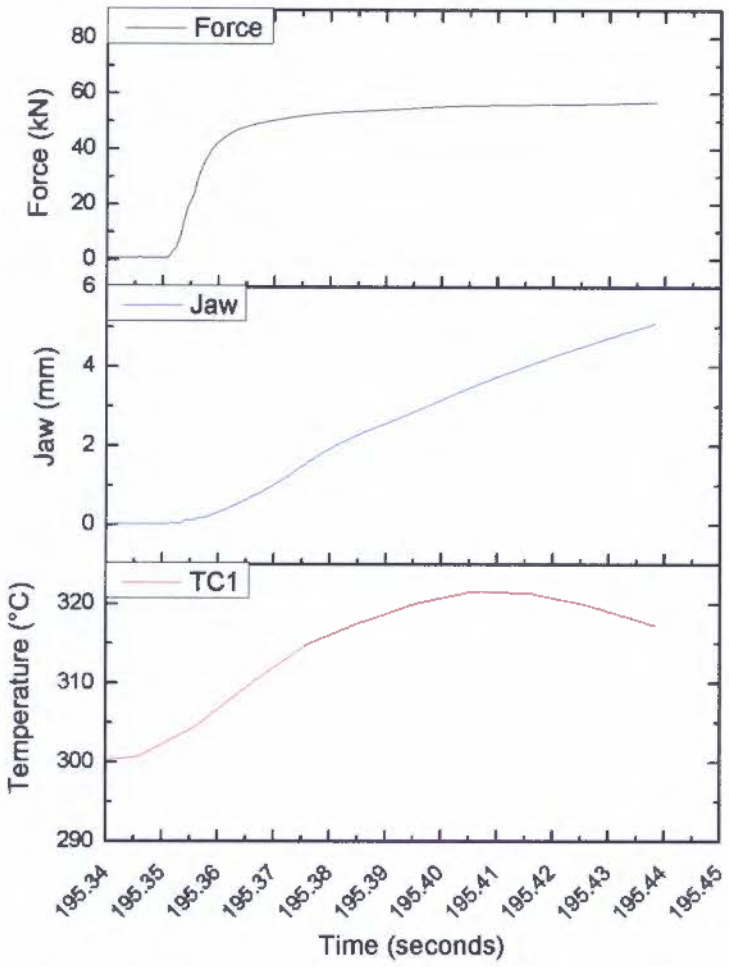

Figure 4.3: Raw deformation data of the PSC of the aluminium alloy AA3104 with the wet nickel-based lubricant at a nominal temperature of 300 °C, strain rate of 10 sec^{-1} and to a strain of 0.85.

Nickel-based Lubricated PSC Tests

Only two PSC tests were performed by using the wet nickel-based lubricant painted onto the surface of the PSC samples. For direct comparison purposes, Figure 4.3 is under the exact same testing conditions as shown in Figure 4.2, except for the use of the wet nickel-based lubricant. Very similar temperature and anvil jaw responses were experienced in both tests, providing evidence of the repeatability of the Gleeble 3800. The significant difference between these two PSC tests was the force response, especially post yielding of the material. For the tests that underwent deformations by using graphite powder as the lubricant, a continued increasing load in a linear trend was experienced on the material. However, for the PSC tests that underwent deformations by using the wet nickel-based lubricant, a far flatter curve and lower load was experienced with a slight minimal increase in load during the deformation and achieving a steady state value during further stages of the deformation. This can lead to the conclusion that the wet nickel-based lubricant provides a far superior

lubricating action in comparison to that of the graphite powder.

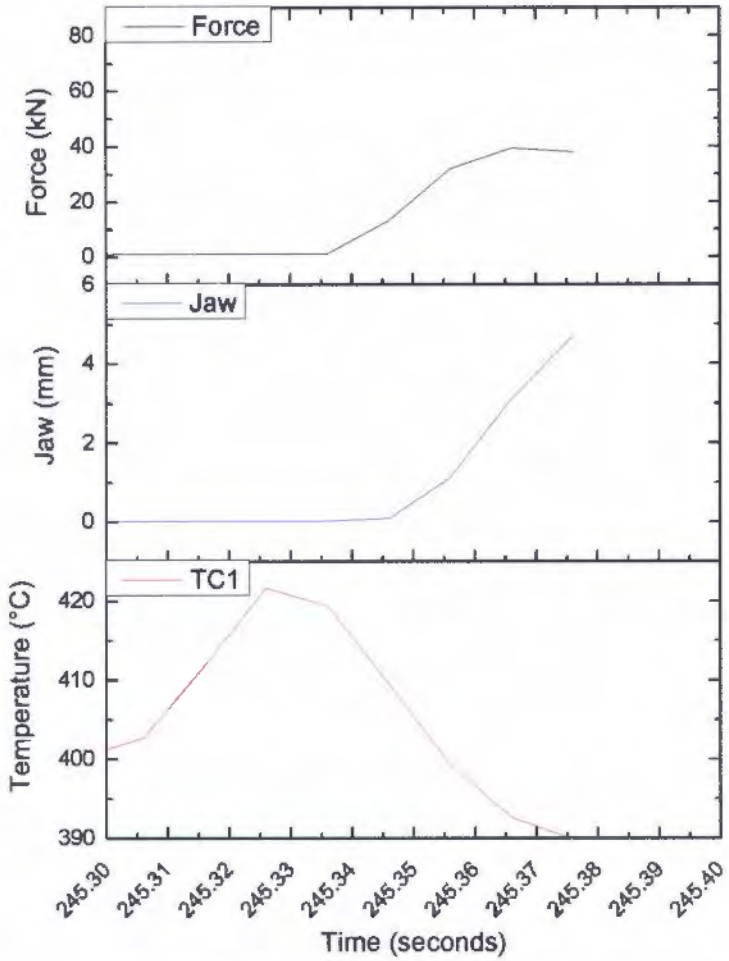

Figure 4.4: Low acquisition frequency data of a PSC test under the deformation condition of 400 °C and a strain rate of 30 sec^{-1}.

4.1.2 Issues Encountered

Due to these tests being the first PSC tests performed by using the Gleeble 3800, a steep learning curve was gained as some tests experienced less than ideal test runs. Notability, for the PSC tests under the nominal deformation conditions of 400 °C at 10 and 30 sec^{-1}, the data acquisition frequency was set too low for the strain rate. This resulted in too few data points during the deformation in order to achieve a smooth and accurate data set, thus resulting in unreliable data for those tests. The data acquisition frequency that provided an acceptable amount of data points was found to be beneficial at an acquisition rate of 1000 Hz per a strain rate of 10 sec^{-1}. Figure 4.4 is an example showing the recorded data acquisition frequency set at a value too low for the required strain rate, thus achieving a data set that does not provide clear and smooth curves during the deformation. Additionally, the

temperature increase due to the deformation is also out of synchronisation with respect to the anvil jaw and load values, thus suggesting the sample increases in temperature prior to the deformation, and this is nonsensical.

4.2 Processed Results

The raw data files for all of the tests were exported into an Excel spreadsheet format for further analysis and data processing. Since the main section of interest of this investigation was the deformation of the aluminium AA3104, isolating the data rage from the start of the deformation till the end would provide easier and more convenient data to interpret. In order to determine the exact time of the start and end of the deformation, the load with respect to time for all the tests was inspected so that the exact data points marking the start and end of the deformation could be identified . This data set for the deformation was then duplicated into another sheet for ease of access to the specific data during the deformation.

4.2.1 Data Processing Steps

Initial Calculations

The first step to process the deformation data was to determine the height of the sample (h). This was calculated by taking the difference between anvil jaw value and the initial sample height (h_0). Both these values were corrected due to the linear thermal expansion at the specific testing temperature for the sample and anvil. The linear thermal expansion coefficient of aluminium used in all tests was 25.4 mm/m °C [14]. The breadth spread coefficient (C) for each test was calculated by using Equation 2.2 with the values of b_f, b_0, h_f and h_0 corrected for the linear thermal expansion of aluminium at the specific testing condition. This then lead to the calculation of the estimate of the instantaneous breadth (b_{inst}) by utilising Equation 2.3.

Equivalent Straiu Calculatiou

Since the height values of the sample during the deformation and as well as the instantaneous breadth values were determined, the strain in the normal direction could be calculated by using the equation $\varepsilon_{ND} = ln\frac{h}{h_0}$ and similarly the strain in the transverse direction was determined with $\varepsilon_{TD} = ln\frac{b_{inst}}{b_0}$. This then allowed for the calculation of the equivalent strain value ($\bar{\varepsilon}$) for each data point by using Equation 2.5 as described in the literature review.

Friction Correction Calculation

As mentioned in the literature review, modelling the deformation data in order to account for the influence of friction is an important factor. This is due to friction impacting to a significant extent on the load and, ultimately, the equivalent stress acting on the material. In order to determine whether the frictional conditions acting on the PSC sample were sliding, partially sticking or sticking, the z_0 value was calculated by using Equation 2.12. The value of the Coulomb friction coefficient (μ) for the PSC tests that were lubricated with the graphite powder was calculated at a value of 0.1, while in the PSC tests with the wet nickel-based lubricant the chosen was 0.08. The results of the PSC tests by Evans and Ricks [49], used graphite dag as the lubricant and indicated that a value of 0.08 was the Coulomb coefficient of friction [49]. It was decided that the nickel-based lubricant would provide similar lubricating properties to those of the graphite dag, hence the value of 0.08. The value of 0.1 was decided for dry graphite powder as it would not provide as good lubricating properties as the nickel-based lubricant, hence a higher value was chosen for this set of PSC tests.

Equation 2.13 was used to calculate the $\frac{\bar{p}}{2k}$ value. The average instantaneous pressure ($\bar{p}$) was then calculated using Equation 2.11. The value of the width of the anvil (w) was corrected due to thermal expansion at the specific testing temperature by using the linear coefficient of thermal expansion for steel as 13 μm/m°C.

Equivalent Flow Stress Calculation

The previously calculated terms enabled the calculation of the equivalent flow stress ($\bar{\sigma}$) for each data point by using Equation 2.16, and the f value was calculated by using Equation 2.9. A spreadsheet for each PSC test was formulated in order to calculate the significant steps necessary to determine the equivalent stress and strain values. An example of the type of layout used for the formulation of the spreadsheet is shown in Table 4.1.

Table 4.1: Example of how each term per data set has been calculated in an Excel spreadsheet layout.

Time (seconds)	Load, L (N)	Jaw (mm)	Sample Height, h (mm)	Inst. Breadth, b_{inst} (mm)	ϵ_{ND}	ϵ_{TD}	Eq. Strain ($\bar{\epsilon}$)	Inst. Pressure, $\bar{p}$ (MPa)
raw data	raw data	raw data	h_0 - jaw	Equation 2.3	$ln\frac{h}{h_0}$	$ln\frac{b_{inst}}{b_0}$	Equation 2.5	Equation 2.11
⋮	⋮	⋮	⋮	⋮	⋮	⋮	⋮	⋮
⋮	⋮	⋮	⋮	⋮	⋮	⋮	⋮	⋮

Table Extended ...

z_0	Friction Type	$\frac{\bar{p}}{2k}$	f	Eq. Stress, $\bar{\sigma}$ (MPa)
Equation 2.12	Sliding/Partial Sticking/Sticking	Equation 2.13/2.14/2.15	Equation 2.9	Equation 2.16
⋮	⋮	⋮	⋮	⋮
⋮	⋮	⋮	⋮	⋮

4.2.2 Processed Data

The processed results facilitated the analysis of the true equivalent stress and strain values for each PSC test. All the processed results for each initial PSC test can be found in Appendix D. Further investigation could be carried out in order to determine the strain rate during the deformation. This was achieved by finding the derivative of the equivalent strain with respect to time by using the inbuilt software package on OriginLab. An example of the plot of the equivalent stress and strain rate versus the equivalent strain can be seen in Figure 4.5 under the deformation nominal conditions of 300 °C and 10 sec^{-1} for both the PSC samples that were lubricated with the graphite powder and the wet nickel-based lubricant. In all the initial PSC tests that were lubricated with graphite powder, the steady state flow stress was not established, further emphasising that the frictional effects between the sample and anvil have a significant influence on the outcome of the determination of the equivalent flow stress values. Since it is common for aluminium alloys to undergo dynamic recovery during TMP, the characteristic steady flow stress curve was not seen with the graphite powder lubricated samples. In contrast to this, in the two PSC tests that were lubricated with the wet nickel-based lubricant, the characteristic steady state flow stress curve was achieved. This clearly confirms that the type of lubricant has a significant influence on the load, and thus the equivalent stress values. This can be clearly illustrated by comparing plots of (a) and (b) in Figure 4.5, where both deformations were under the same conditions. This result, suggests that the nickel-based lubricant is the more suitable option for hot PSC testing.

The strain rate was determined by deriving the strain with respect to time, but oscillatory data following a trend were introduced into the derived data, and this was found to occur in all the initial PSC tests. In order to rectify this, smoothing of the strain rate data was performed by using the OriginLab software. The best results for smoothing the strain rate were found by using the Savitzky–Golay method with the polynomial order of 2 and with the points of window between a value of 25–60 in order to achieve a smoothed curve without skewing the results. This oscillatory data of the strain rate is also similar in fashion to that of the work by Evans and Ricks [49], where it was deemed that these effects could be due to the logging software of the data. The oscillations as shown by the strain rate for these sets of tests have a far higher magnitude in comparison to the result obtained by Evans and Ricks. Another influence on the behaviour of the strain rate oscillations could be due to noise being included in the data. With the high frequency data acquisition rates ($>$ 1000 Hz) and as well as the sensitive recording equipment, a very high resolution of data can be captured and thus by taking the first derivative of the strain the apparent noise on the strain rate is exacerbated. It can be seen by Figure 4.5 that the smoothed strain rate follows a general trend during the deformation of the PSC sample. The strain rate response during the deformation suggests that it is not influenced by the type of lubricant used during the

PSC test as Figure 4.5 illustrates.

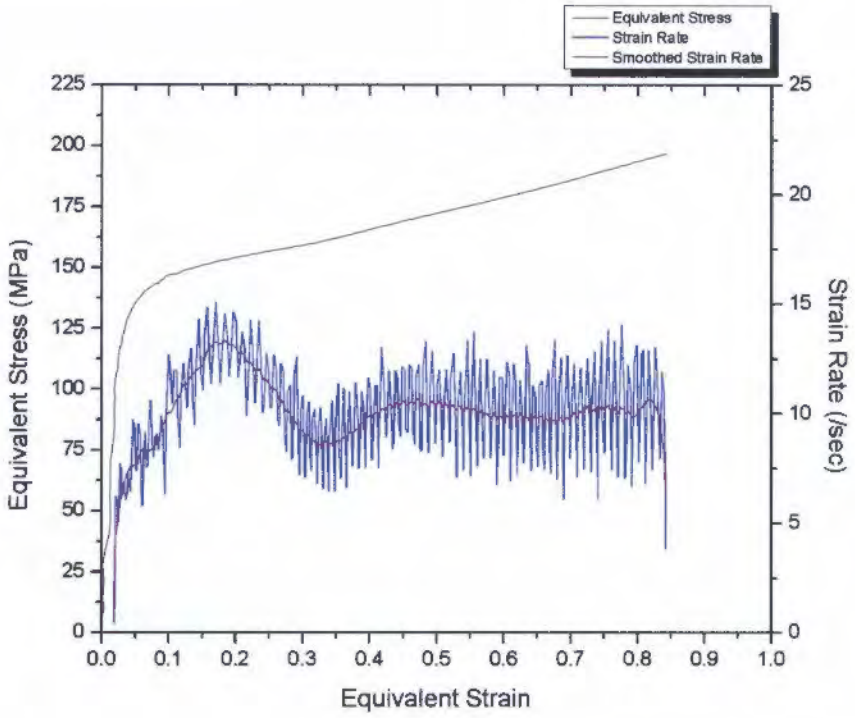

(a)

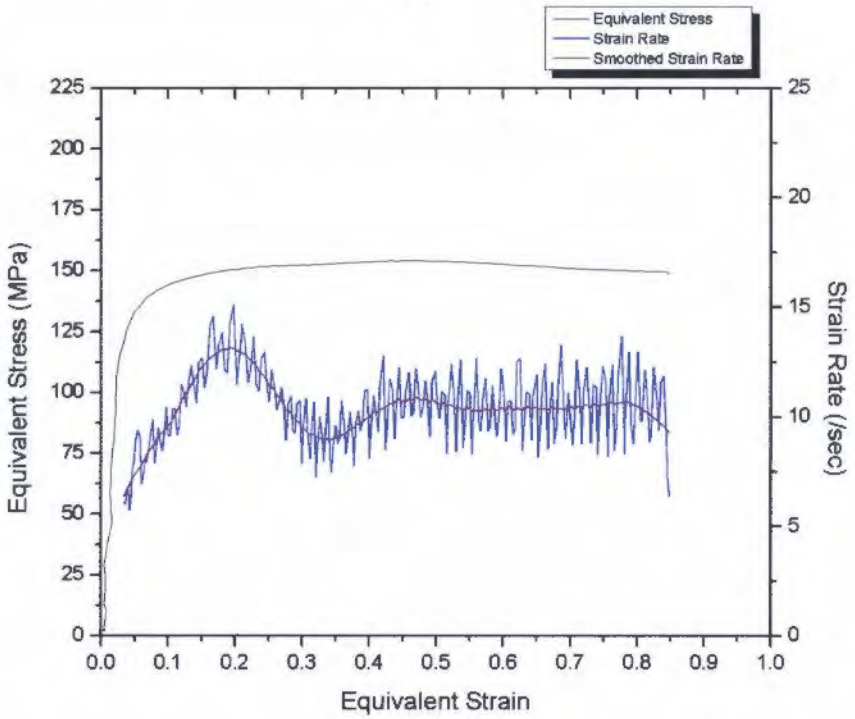

(b)

Figure 4.5: The equivalent stress and strain rate versus the equivalent strain under the deformation conditions of 300 °C and a strain rate of 10 sec^{-1} with (a) graphite powder used as a lubricant and (b) a wet nickel-based lubricant.

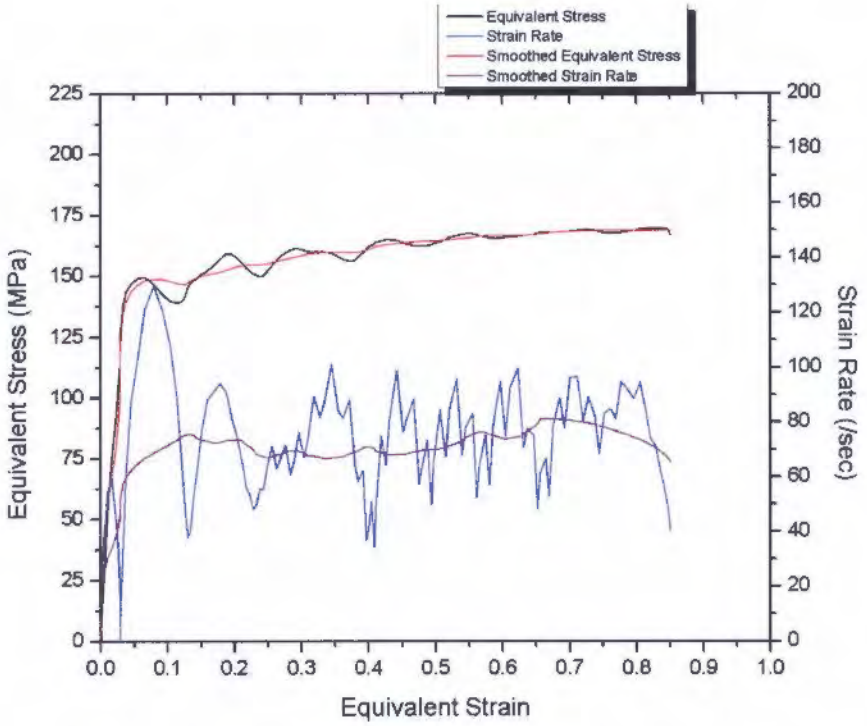

Figure 4.6: Oscillations of the equivalent stress subjected to the nominal strain rate of 100 $sec^{-1}$and a deformation temperature of 300°C.

In the PSC tests over the tested temperature range, oscillations in the load and subsequently in the equivalent stress values were noted for PSC tests that were under the nominal strain rate condition of 100 sec^{-1}. Figure 4.6 depicts the type of oscillations that are encountered at the equivalent stress values during the duration of a PSC test which is under the nominal strain rate condition of 100 sec^{-1}. These types of oscillations are different from those observed as shown by the strain rate results. Research by Roebuck et al. in conjunction with the NPL [61] have shown that load cell ringing can occur for compression tests at high strain rates, especially at strain rates of 100 sec^{-1}. Their experimental research was done over a range of materials and also concluded that additional influences such as the testing machine frame and sample vibrating at high strain rates can affect the results. Software that can reduce or remove the ringing effects has been deemed successful, however determining the point of yield has proved to be inaccurate and care must be taken when determining the yielding of the material. The best results of the smoothed equivalent stress data was carried out by using the OrginLab software and by employing the Savitzky–Golay method to the polynomial order of 4 by using the points of window within the range value of 25–60 in order to achieve the best smoothed data set.

Table 4.2: Summary of the initial PSC tests for samples that were lubricated with graphite powder.

Nominal deformation testing conditions		Experimental mean values 0.8 - 0.9 strain			Mean value full deformation
Nominal temperature (°C)	Nominal strain rate (sec^{-1})	Temperature (°C)	Strain rate (sec^{-1})	Flow stress (MPa)	Strain rate (sec^{-1})
300	10	322.1	9.73	195.2	9.79
300	30	335.5	36.4	184.6	31.0
300	100	338.6	76.1	169	68.5
350	10	355.9	10.7	151.7	10.4
350	30	373.2	44.1	148.6	33.1
350	100	367.6	86.7	163.2	71.1
400	10	-	10.2 *	104.5 *	8.00 *
400	30	391.2 *	30.7 *	103.1 *	-
400	100	419.4	79.7	118.5	71.2

* Not reliable results

4.2.3 Results Comparison

Equivalent flow stress values for the findings of Evans and Ricks [49] for the aluminium alloy AA3104 were determined from the average values of the temperature, strain rate and flow stress over the strain range of 0.8–0.9, and as a result any transient effects would have a minimal influence on the determined values. This type of method was also employed in this investigation in order to achieve comparable results. The initial PSC tests were only deformed to a total strain of 0.85, thus the mean values were calculated from 0.8 until the end of the deformation, and provided enough information needed for this part of the investigation. It must be noted that the equivalent flow stress values determined for the initial PSC tests lubricated with the graphite powder did not reach the expected steady state condition during the PSC test. This thus skews the flow stress results for the graphite powder lubricated samples as the influence of friction affected the flow stress values grossly and therefore will be ignored for the purposes of this part of the investigation. Additional useful information on the temperature and strain rate values could still be investigated as well as highlighting the effect of poorly lubricated PSC tests. The results of the initial PSC tests are summarised in Tables 4.2 and 4.3 in respect of the PSC tests that were lubricated with graphite powder and the nickel-based lubricant, respectively.

Flow Stress

From the results as shown in Tables 4.2 and 4.3 allow a direct comparison to the flow stress values of the results determined by Evans and Ricks [49] (included in Appendix E) but does not provide a fair platform for the graphite powder lubricated samples as the flow stress values determined are significantly skewed by the poor lubricating interface. In the tests that were lubricated with the wet nickel-based lubricant, an overestimate of 11.8 MPa or by

Table 4.3: Summary for the initial PSC tests for samples that are lubricated with the wet nickel-based lubricant.

Nominal deformation testing conditions		Experimental mean values 0.8 - 0.9 strain			Mean value full deformation
Nominal Temperature (°C)	Nominal Strain Rate (sec^{-1})	Temperature (°C)	Strain Rate (sec^{-1})	Flow Stress (MPa)	Strain Rate (sec^{-1})
300	10	317.8	9.95	149.6	10.2
350	30	373.3	46.9	131.6	33.5

8.6% was achieved under the PSC testing condition of 300 °C at a strain rate of 10 sec^{-1} and an overestimate of 7.8 MPa or 6.3% was achieved under the testing conditions of 350 °C at a strain rate of 30 sec^{-1}. Owing to the low number of PSC tests lubricated with the wet nickel-based lubricant, it is premature to make concrete conclusions that the wet nickel-based lubricant samples achieve similar results to those that Evans and Ricks determined. However, it can be said that the results of the PSC tests that were lubricated with the wet nickel-based lubricant do to some degree provide evidence to show that this could possibly be the case.

Strain Rate

The strain rate values of the initial PSC tests fared fairly well under the nominal testing conditions of 10 and 30 sec^{-1}, with a maximum difference from the nominal condition of 0.7 sec^{-1} in the PSC tests that were tested at a nominal strain rate of 10 sec^{-1}. The PSC tests that were under the nominal strain rate condition of 30 sec^{-1} showed that the maximum difference from the nominal condition was 16.9 sec^{-1} however by considering the mean strain rate over the whole deformation the maximum difference is reduced to a more respectable 3.5 sec^{-1}. Under the nominal strain rate testing conditions of 100 sec^{-1}, a value near 100 sec^{-1} was not achieved in any of the PSC tests. The average strain rate with its standard error was 80.8 ± 3.1 sec^{-1} for the full deformation duration. The strain rate values Evans and Ricks determined in their PSC tests under the nominal strain rate condition of 100 sec^{-1} did not easily achieve values equivalent to that of 100 sec^{-1}, however Evans and Ricks were able to achieve strain rates within the range of 83.3–97.7 sec^{-1} [49].

Temperature

The temperature measurement could be inaccurate due to the fact that the deformation of heating in tests that were subjected to the strain rates of 30 and 100 sec^{-1} were not synchronised to the start of the deformation. The increase in temperature caused by the

deformation of heating can, therefore, be directly compared to the results of Evans and Ricks [49] in the PSC tests that were subjected to the strain rate of 10 sec^{-1}. The results of the initial PSC tests at the nominal deformation temperature of 300 °C, recorded temperatures of 322.1 °C and 317.8 °C for the samples lubricated with graphite powder and the wet nickel-based lubricant, respectively. Both these tests were under the same thermomechanical testing conditions, thus resulting in a negligible difference of 4.3 °C and averaging together as 320.0 °C. The value recorded by Evans and Ricks was determined as 337 °C, thus a 17.0 °C temperature lower than that recorded by Evans and Ricks was attained. The temperature reading recorded for tests that were under the testing conditions of 350 °C and a strain rate of 10 sec^{-1} was 355.9 °C. The value recorded by Evans and Ricks under the same thermomechanical testing condition was 375 °C, thus a difference of 19.1 °C. It can be seen that a lower value in tbe temperature occurs in both testing conditions and also by a similar amount (17.0 and 19.1 °C). This could be caused by percussion-welding the thermocouples onto the surface of the sample and not inserting them into the centre of the material, as this would provide a more accurate reading of the temperature of the sample. Further thoughts on the temperature reading is that only one side of the sample is measured and therefore there is no confident way of determining the temperature of the sample on the geometrically opposite side and thus not knowing if the temperature distribution is uniform within the sample. It is also not possible to determine a thermal gradient across the sample's breadth.

4.3 Summary

Tbe initial PSC tests provided crucial information and evidence that PSC testing is viable on the Gleeble 3800 TMP machine. The testing conditions mimicked the testing conditions of the PSC tests that were performed by Evans and Ricks [49]. Three different nominal strain rate conditions of 10, 30 and 100 sec^{-1} were performed at the three different nominal temperatures of 300, 350 and 400 °C on the aluminium AA3104 CBS samples. The samples were lubricated with graphite powder in all the mentioned tests and an additional two PSC tests were performed by using a wet nickel-based lubricant at the nominal temperature and strain rate conditions of 300 °C and 10 sec^{-1} and as well as 350 °C and 30 sec^{-1}. The results show that the physical side of the TMP in the PSC tests can be achieved. However some problems encountered with respect to the quality, processing and analysis of the PSC data caused unreliable and unexpected results owing to the influence of some elements of the testing procedure on the results. The major factor that caused unfavourable testing results was the effect of friction between the surface of the anvil and sample, notably the poor lubricating conditions as a result of using graphite powder as a lubricant. Minimal or no lubricating properties were observed and caused significantly high values of the equivalent flow stress which rose as the deformation progressed, followed by an uncharacteristic flow

stress curve that is not associated with the TMP of aluminium alloys. In the PSC tests that used the wet nickel-based lubricant, the characteristic steady state flow stress condition was achieved, thereby proving that the frictional conditions under which the deformation occurs affects the flow stress value significantly. Since only two PSC tests were carried out by using the nickel-based lubricant, a full range of testing conditions was not met. However, in the PSC tests that were performed with the nickel-based lubricant, flow stress values similar to those determined by were achieved. This suggests that PSC tests on AA3104 on the Gleeble 3800 can achieve similar results to those of Evans and Ricks under the same nominal testing conditions.

Another area of interest during the initial PSC tests was the strain rate condition of 100 sec^{-1}. The nominal strain rate of 100 sec^{-1} was not successfully achieved in all the PSC tests. The highest recorded strain rate was 86.7 sec^{-1} over the strain range of 0.8–0.85 and an average strain rate of 80.8 ± 3.1 sec^{-1} was achieved for the full duration of the deformation. The Gleeble 3800 has displacement speed rating of 2000 mm/second [57], and therefore a strain rate of 100 sec^{-1} should be an achievable target. The possible reason for the lower than expected strain rate conditions can be due to not having a high enough setting for the sensitivity of the integrated control systems which control the proportional integral derivative (PID) controllers at the 'stroke' ram speed. The temperature of PSC samples achieved acceptable values at the desired nominal testing temperature. However, since only one side of the sample was measured and controlled externally it is difficult to say that the whole sample was at the specified temperature from the one reading of the thermocouple.

The initial PSC tests provided a good understanding of how the Gleeble 3800 performs under certain PSC testing conditions on the aluminium alloy AA3104 by producing some encouraging results as well as insight into other areas for improvement. A constitutive equation could not be derived based on these results, however, a practical learning experience of PSC testing was achieved. With this understanding, further improved PSC testing can be achieved in order to produce repeatable, reliable and confident results for the PSC testing of aluminium alloy AA3104.

Chapter 5

Results and Discussion of the Ring Compression Tests

5.1 Ring Compression Test Results

As revealed by the results of the initial PSC tests in Chapter 4, it was evident that the interfacial friction between the anvil and sample played a significant role on the load applied onto the PSC sample and therefore a good enough lubricant to allow for consistent sliding friction was needed. The initial PSC tests suggested that the wet nickel-based lubricant could provide this solution. However, graphite in the form of a foil could also provide acceptable lubricating conditions. Ring compression tests were performed with the nickel-based lubricant and the 0.0254 mm (0.01 in) thick graphite foil. The results of the ring compression tests for both of these lubricants are shown in Figure 5.2, and the spreadsheet of the results are also included in Appendix F. The percentage of the reduction in the internal diameter of the ring compression samples is plotted on the Y-axis, while the reduction in the height of the samples is plotted on the X-axis. This plot was then superimposed onto the calibration curve (Figure 2.22) for the ring compression sample ratio of 6:3:2.

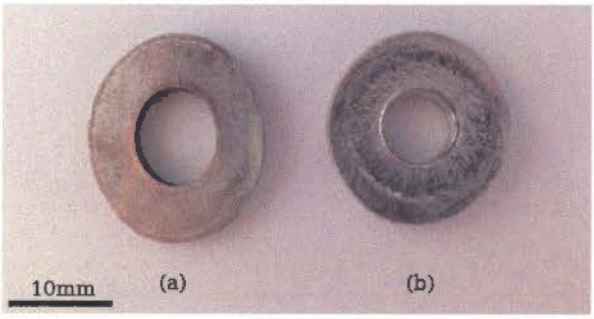

Figure 5.1: Ring compression test samples that have been deformed with the use of the (a) wet nickel-based lubricant and (b) the graphite foil.

5.1.1 Deformed Samples

Figure 5.1 illustrates the typical difference of how the two lubricants affected the deformation shape of the ring compression samples. All the samples that were lubricated with the nickel-based lubricant deformed along an elongation axis, thus representing an elliptical shape as depicted in Figure 5.1a. In all the samples that were lubricated with graphite foil the circular shape was preserved post-deformation as shown by Figure 5.1b. It was interesting that the two differently lubricated ring compression tests resulted in two differently deformed shapes. There are two reasons for the difference in the shape of the deformed samples. The one possible explanation for the irregular shape of the deformation of the wet nickel-based lubricant samples is that once deformation occurs the lubricant does not provide the same lubricating properties across the whole interface of the sample and a build-up of the lubricant can easily occur due to the application process of painting the lubricant onto the sample. This, in turn, allows for a relatively low local area of friction, hence allowing more material to flow in one particular direction. As the sample continues to deform the wet nickel-based lubricant is channelled along the axis of elongation of the sample and this continues to provide a low area of friction and therefore allows even more material to continue to flow in the same direction, hence the irregular deformation of the sample. This concept can also be carried forward to the explanation for the graphite foil lubricated samples. The graphite foil is of a consistent thickness, allowing for even coverage across the surface area of the sample. This will therefore allow consistent frictional properties across the whole area of the ring compression sample during the deformation process, which, in turn, allows for consistent radial flow of material to occur during the deformation, and the circular shape of the sample post-deformation is preserved. The other reason for the two different shapes of the ring compression samples could be due to the inherent anisotropy of the sample caused by the rolling process. Although, a heat treatment of 400 °C for 3 hours was applied to the ring compression samples to anneal the microstructure, the anisotropic effects will still be present within the material to a certain degree. The lower frictional condition experienced in the case of the nickel-based lubricant offers a lesser resistance to the anisotropic behaviour during deformation in comparison to the graphite foil. Thus, the lower coefficient of friction caused by the nickel-based lubricant reveals the anisotropic nature of the material, allowing easier flow of the material during the compression with the result that an elliptical deformed sample is formed. The internal diameter of the elliptical deformed ring compression sample was calculated by using the average measurements along the longest internal diameter and the measurement perpendicular to this measurement. This allowed for an estimation of the internal diameter of a sample that retained its circular shape post-deformation.

Another noticeable difference between the ring compression samples that were lubricated with the wet nickel-based lubricant and the graphite foil was the difference of

the surface finish of the samples. A smooth surface finish was observed in the samples that were lubricated with the wet nickel-based lubricant, while a more rough and 'orange peel' type surface finish was observed in the graphite foil samples. The smooth surface finish is evident as a result from the lower coefficient of friction in the use of the wet nickel-based lubricant.

5.1.2 Friction Calibration Curve

The results as shown in Figure 5.2 reveal two distinct groupings of data gathered during the ring compression tests which were performed with the wet nickel-based lubricant and the graphite foil. The scatter of data is too wide to provide any tangible values for the coefficient of friction under the specific conditions presented by both groupings of data representing the graphite foil and wet nickel-based lubricant. The trends derived from the different temperature and strain rate conditions can also not be determined due to the scatter of the data. The data do however provide a rough estimate of what the coefficient of friction could be for the different lubricants. The results depicted in Figure 5.2 indicate that the coefficient of friction values for graphite foil range from 0.07–0.15, while the range of values for the wet nickel-based lubricant is from ~0.02–0.045.

5.2 Summary

Ring compression tests were performed on the aluminium alloy AA3104 using two different lubricants, a wet nickel-based lubricant and graphite foil lubricant. The testing conditions for the ring compression tests were set at the same temperature and strain rate conditions that were used in the initial PSC tests in order to gain insight into the coefficient of friction for both lubricants under certain temperature and strain rate conditions. The results obtained led to the conclusion that the spread of data for both ring compression tests carried out with wet nickel-lubricant and graphite foil, respectively, was far too great in order to obtain values for the coefficient of friction under specific testing conditions. The data that can be extracted from the results can only provide a rough estimation range for the performance of the coefficient of friction of the lubricants due to the range of temperature and strain rate conditions. The coefficient of friction of the wet nickel-based lubricant ranges from ~0.02–0.045, while the coefficient of friction for the graphite foil is from 0.07–0.15. In order to provide more accurate data for the ring compression tests it is necessary to determine specific friction calibration curves for the AA3104 aluminium alloy under these ranges of testing conditions. The general friction calibration curves used in this investigation did not provide accurate enough information to determine the specific coefficient of friction under

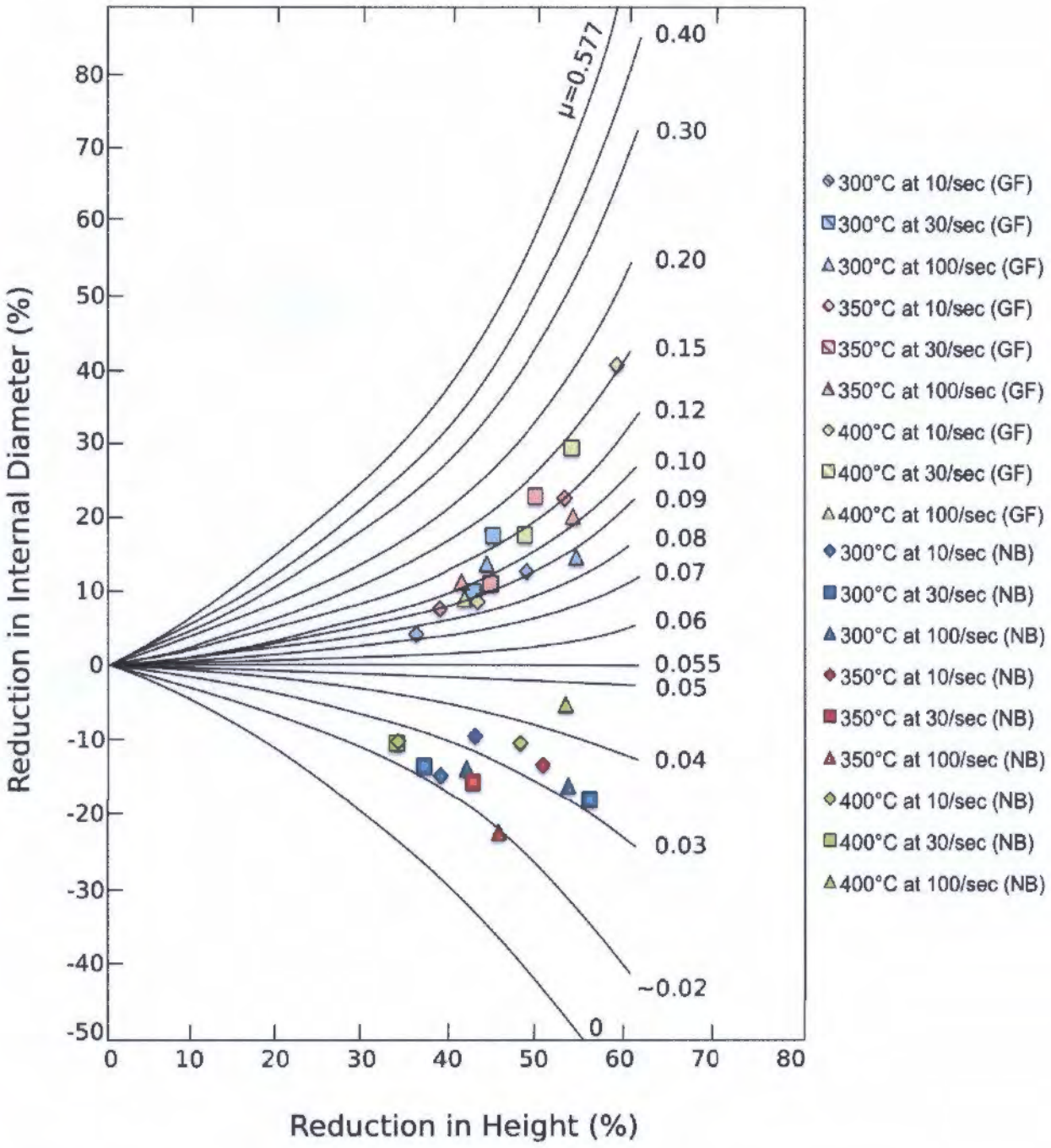

Figure 5.2: Ring compression test results by comparing the performance of the wet nickel-based lubricant (NB) and the graphite foil (GF).

certain testing conditions.

As expected, based on the results the nickel-based lubricant obtained a lower coefficient of friction in comparison to that of the graphite foil. However, ring compression tests that were carried out with the wet nickel-based lubricant produced unexpected elliptical deformed samples. The graphite foil samples preserved their circular shape, which led to uncertainty about whether the anisotropy of the rolled AA3104 or the inconsistency of the wet nickel-based lubricant had caused the unexpected elliptical deformed samples. Based on these results, the graphite foil was selected as the safer lubricant to be used for future PSC tests in remainder of this investigation. The graphite foil provides a constant thickness of the lubricant and, therefore, allows for more consistent lubricating properties during the deformation of samples. An additional advantage of graphite foil is that it is a dry lubricant and therefore no oil burns off at high temperatures in comparison to the wet nickel-based lubricant. The graphite foil allows for easier electrical conduction needed for the direct resistive heating of the Gleeble 3800. The value of the coefficient of friction for the graphite foil to be used in the remainder of the PSC tests will be a value of 0.08. This value of the coefficient of friction falls within the range of values determined during the ring compression tests. Evans and Ricks used graphite dag with the coefficient of lubrication of 0.08 [49], and thus this value falls in line with the graphite foil as these two lubricants are based on similar lubricating properties.

Chapter 6

Results and Discussion of the Validation Plane Strain Compression Tests

Based from the results and knowledge gained from the initial PSC tests and the ring compression tests, a full PSC testing procedure for two different sample to anvil geometries was carried out on the Gleeble 3800 in order to analyse and validate the performance of the Gleeble 3800.

6.1 General Observations

General physical observations made during the validation PSC tests were noted for the DSI and modified PSC testing configurations post deformation. They will be discussed below.

6.1.1 Deformed PSC Sample Shapes

The shapes of the deformed PSC samples for the DSI and modified testing configuration had some differences. The PSC samples obtained from the DSI testing configuration maintained a symmetrical shape, where most of the samples from the modified PSC testing configuration were asymmetrical in their deformed state, resulting in a 'Z' type sample. An example of the the asymmetrically deformed 'Z' type sample and the symmetrical deformed sample are illustrated by Figure 6.1 for the two different testing configurations. The asymmetrical deformation of the modified configuration sample is due to the varying frictional condition between the sample and anvil surface and thus resulting in a distorted PSC sample. Since the modified PSC sample has a larger contact surface area in relation to the DSI configured sample, the chances of a varying friction condition are highly likely. However, as mentioned in

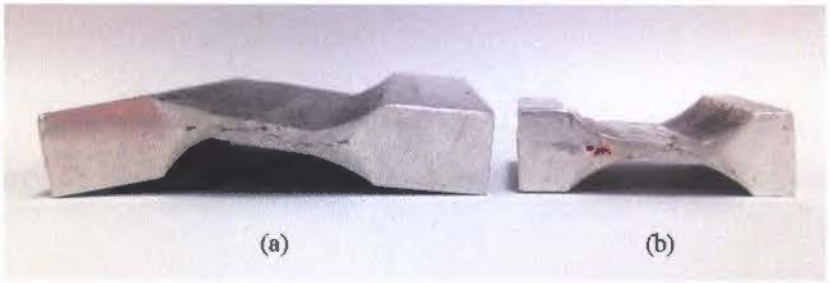

Figure 6.1: Deformed shapes of the (a) asymmetrical 'Z' type sample and the (b) symmetrical sample of the modified and DSI PSC testing configurations respectively.

the literature review, asymmetrically deformed PSC samples do not have a significant effect on the derived flow stress curves [37, 38] and if care is taken in the microstructural analysis for the bulk texture measurements, no significant effects of the asymmetrically deformed samples will influence the texture results [39].

6.1.2 Surface Finish

Another interesting observation of the PSC samples for both of the DSI and modified testing configuration is the surface finish of the deformed area of the sample. Figure 6.2 illustrates the typical surface finish that is found on the PSC samples used for both the DSI and modified testing configuration post deformation. The sample generally has the intact foil still on the sample as shown in Figure 6.2a. The surface finish of the intact foil is very smooth. However, once the graphite foil has been removed from the PSC sample, a rougher 'orange peel' type surface finish is revealed on the aluminium sample as shown in Figure 6.2b. This type of surface finish is similar to what occurred in the ring compression tests in which the samples were also lubricated with the graphite foil. The 'orange peel' type surface friction is possibly due to the continual sticking and sliding of the graphite foil on the aluminium surface during the deformation thus indenting the surface of the aluminium where there is a build-up of the graphite foil at the localised areas. The smooth side of the graphite foil indicates a sliding frictional condition between the anvil and graphite foil. The roughing of the surface of the aluminium alloy AA3104 sample does not cause any alarm for this investigation. However care should be taken if the surface of the deformed PSC sample is an important feature, especially under high magnification microscopy.

6.1.3 Breadth Spreading

The breadth spreading of the PSC sample is an important feature of PSC testing as the larger the change in the breadth of the sample during deformation, the lesser the plane strain condition is met. Hence, it is ideal to minimise the breadth spreading of the sample.

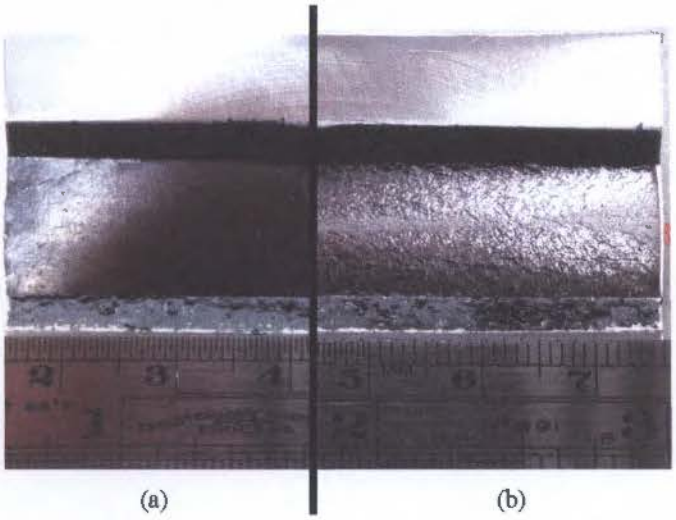

Figure 6.2: Surface finish of the deformed area of the PSC sample (a) with the graphite foil on and (b) with the graphite foil removed from the sample.

The change of the breadth of the all of PSC samples for the both of the two different PSC testing configurations was calculated as shown in Table 6.1. These results facilitated the calculation of the average value with its standard error for the the breadth spreading percentage. The average breadth spread for the DSI configuration is 12.93 ±0.29%, while the modified configuration is 5.93 ±0.13%. As expected, based on the literature review, the modified PSC testing configuration achieved a far better plane strain condition during the deformation of the aluminium alloy AA3104. In order to provide further relevance to these results, the average breadth spreading value for the two testing configurations was compared to experimental work done by Duckham [40], which was conducted on aluminium at the CME at UCT on a modified ESH universal testing machine. The comparison of these results is shown in Figure 6.3, where the percentage of the breadth spread is represented per unit strain. For the DSI configuration the B_R is 3, where the breadth spread per unit strain is 8.1%. The modified configuration breadth spread per unit strain is 3.7% with its B_R at 4.62. It can be clearly seen that the breadth spreading on the Gleeble 3800 for both of PSC testing configurations is significantly lower than the results obtained by Duckham. The data points of the PSC tests on the Gleeble 3800 as shown in Figure 6.3 suggest that a similar curve to that of Duckham's could be formed by performing additional PSC tests using different B_R values. The modified PSC testing configuration allows for more of an ideal plane strain testing condition and thus allows for a closer simulation of industrial rolling.

Table 6.1: Breadth spreading results of the DSI and modified PSC testing configurations.

Nominal testing conditions			DSI configuration				Modified configuration			
Temp. (°C)	Strain rate (sec^{-1})		Initial breadth, b_0 (mm)	Final breadth, b_f (mm)	△ Breadth (mm)	△ Breadth (%)	Initial breadth, b_0 (mm)	Final breadth, b_f (mm)	△ Breadth (mm)	△ Breadth (%)
300	10	Test1	30.00	33.84	3.84	12.80	60.00	63.84	3.84	6.40
		Test2	30.01	33.30	3.29	10.96	60.00	63.44	3.44	5.73
	30	Test1	30.00	33.96	3.96	13.20	60.00	63.14	3.14	5.23
		Test2	30.00	33.56	3.56	11.87	60.00	63.04	3.04	5.07
	100	Test1	30.00	33.26	3.26	10.87	60.00	63.16	3.16	5.27
		Test2	30.00	33.76	3.76	12.53	60.00	63.42	3.42	5.70
350	10	Test1	30.01	33.92	3.91	13.03	60.00	63.68	3.68	6.13
		Test2	30.00	33.94	3.94	13.13	60.00	63.06	3.06	5.10
	30	Test1	30.00	33.70	3.70	12.33	60.00	63.40	3.40	5.67
		Test2	30.00	33.18	4.18	13.93	60.00	63.80	3.80	6.33
	100	Test1	30.00	33.26	3.26	10.87	60.00	63.40	3.40	6.67
		Test2	30.00	33.70	3.70	12.33	60.00	63.96	3.96	6.60
400	10	Test1	30.00	34.16	4.16	13.87	60.00	63.88	3.88	6.47
		Test2	30.00	34.34	4.34	14.47	60.00	63.94	3.94	6.57
	30	Test1	30.00	34.26	4.26	14.20	60.00	63.54	3.54	5.90
		Test2	30.00	34.54	4.54	15.13	60.00	63.74	3.74	6.23
	100	Test1	30.00	34.20	4.20	14.00	60.00	64.08	3.08	6.80
		Test2	30.00	33.95	3.94	13.13	60.00	63.56	3.56	5.93

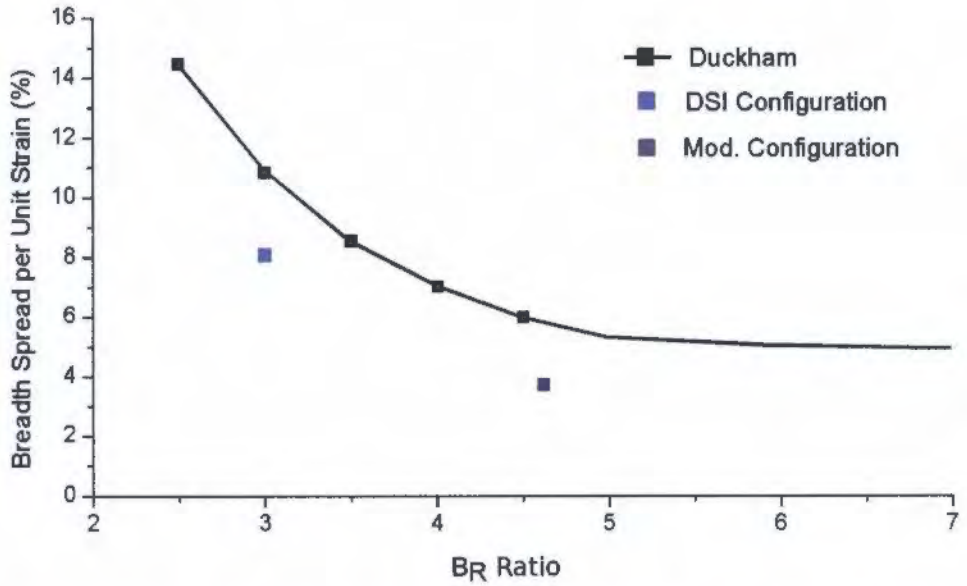

Figure 6.3: The percentage breadth spreading value represented per unit of strain as a function of the different B_R values as represented by the DSI and modified PSC testing configuration on the Gleeble 3800. These values are compared to the PSC results obtained by Duckham [40], which were performed on a modified ESH universal testing machine.

6.2 Raw Data

The necessary raw data collected for the validation PSC tests were the load, the displacement of the jaw and all the thermocouple readings with respect to time. The stroke position, wedge position, power angle, programmed temperature, stress and strain data were also collected as additional data in order to make sure that the test was running correctly and, if a mishap occurred, it could be easily troubleshooted based on the additional data collected. The necessary raw data for both of the PSC tests that involved the DSI configuration and the modified configuration can be found in Appendices G and H, respectively. The raw data during the deformation of the PSC test under the nominal testing conditions with a strain rate of 10 sec^{-1} and temperature of 300 °C for the DSI configuration and the modified configuration can be seen in Figures 6.4 and 6.5 respectively. Figures 6.4 and 6.5 depict the typical PSC responses of the DSI and modified configurations, respectively.

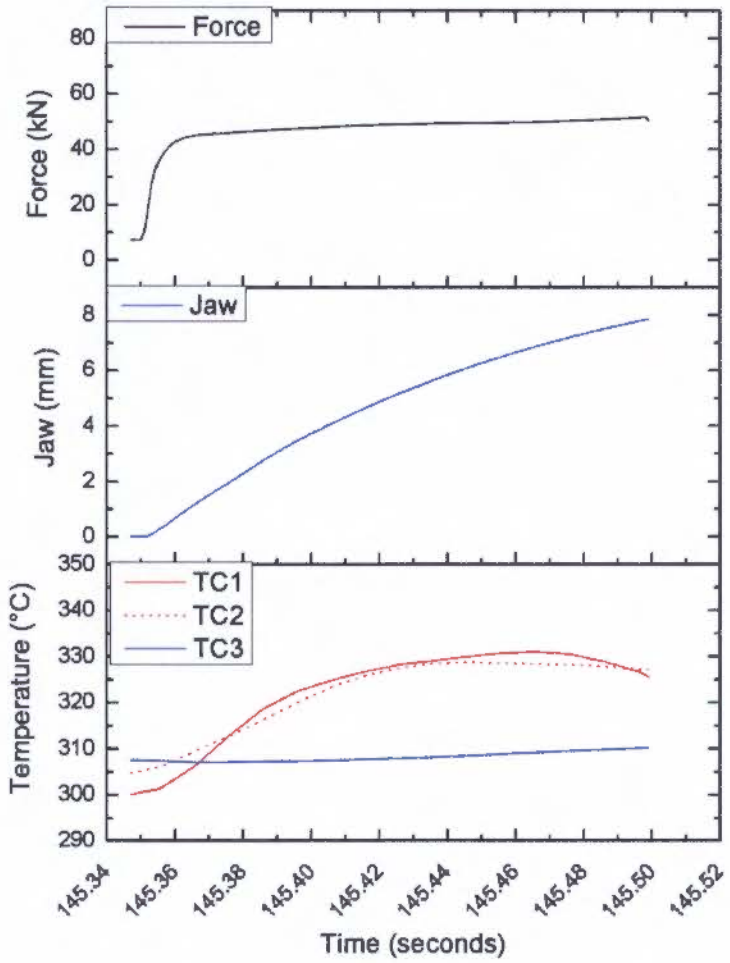

Figure 6.4: Raw data for test 1 of DSI PSC configuration under the nominal deformation conditions of 300 °C and a strain rate of 10 sec^{-1}.

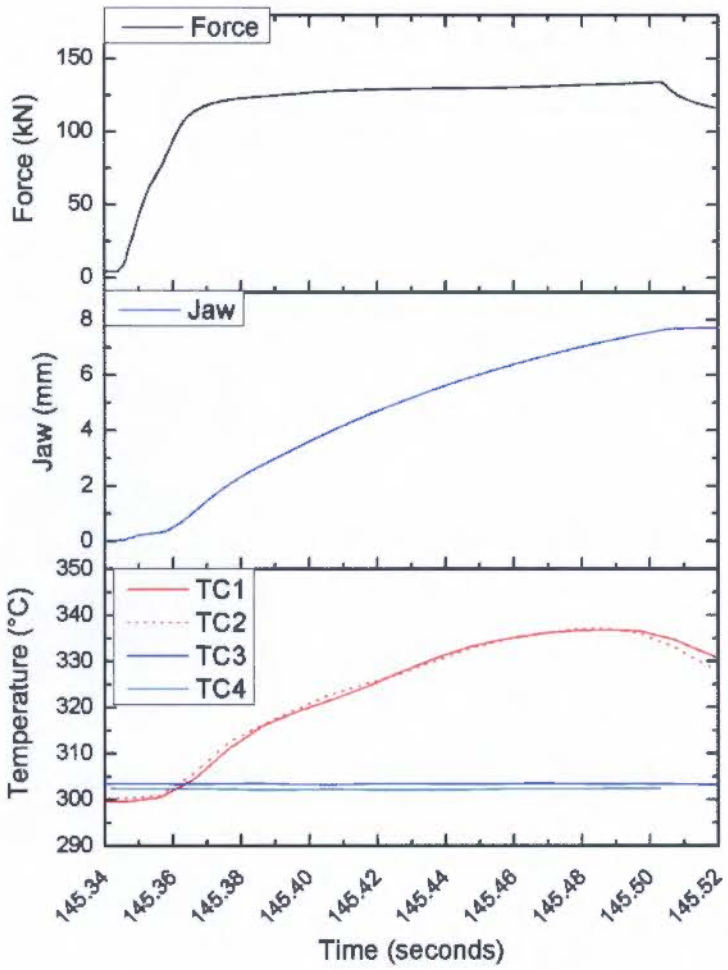

Figure 6.5: Raw data for test 1 of modified PSC configuration under the nominal deformation conditions of 300 °C and a strain rate of 10 sec^{-1}.

6.2.1 Load

The load experienced on all of PSC validation samples during the deformation of both the DSI and modified configurations followed a similar curve shape as experienced by the initial PSC tests that were lubricated with the nickel-based lubricant. This provided promising insight, demonstrating that the graphite foil provides enough lubricating properties for PSC tests as a steady state load was achieved after yielding of the aluminium alloy AA3104. This is evident as shown in Figures 6.4 and 6.5. Obviously, due to the larger surface area of the deformation zone of the modified PSC configuration, higher loads were experienced during the deformation in comparison to those of the DSI configuration. The Gleeble 3800 experienced no problems by achieving higher loads that was necessary to deform the aluminium alloy A3104 for the modified configured PSC tests.

6.2.2 Displacement

The jaw displacement of the Gleeble 3800 measures the displacement between the two faces of the PSC anvils and therefore the amount of deformation of the PSC sample can be measured. From both the DSI and modified PSC configurations, consistent displacements of the samples were measured during the deformation. The jaw displacement curves during the deformations all achieved a relatively straight curve, with perhaps a slight convex shape. This was expected, due to the 'stroke' and 'wedge' ram on the Gleeble 3800 needing to speed up and slow down during the very short time interval of the deformation ($\sim$ 0.14 sec for 10 sec^{-1}, $\sim$0.1 sec for 30 sec^{-1} and $\sim$0.02 sec for 100 sec^{-1}) and thus resulting in a slight convex shape of the jaw displacement. A similar response on the Servotest machine was also achieved in the report compiled by Evans and Ricks in their PSC tests on the aluminium alloy AA3104 [49]. This slight convex on the jaw displacement curve is not significant enough for the scope of this investigation, as a result, the jaw displacement curve during the deformation is effectively linear.

6.2.3 Temperature

The temperature measurements read from the attached thermocouples for both PSC testing configurations behaved similarly to that experienced in the initial PSC tests. The raw data of the validation PSC tests showed similar general common behaviour that was observed across the different testing conditions. It can be concluded from the results of the modified testing configuration that the two thermocouples positioned outside of the deformation zones (TC3 and TC4) depicted similar readings with negligible differences between the two over the range of testing conditions. It can also be noted that the thermocouples situated outside of the deformation zone under both testing conditions remained at a constant temperature during the deformation of the aluminium alloy AA3104. In both the DSI and modified PSC testing configurations the embedded thermocouple, TC3, in the shoulder of the sample during the deformation was $\pm$3 mm away from the deformation zone. The fact that the temperature reading of thermocouple TC3 remained constant during the deformation, shows that there was no heat transfer from the deformation zone to the material within the colder shoulders within the PSC sample greater than 3 mm for all of the nominal temperature and strain rate conditions.

The two embedded thermocouples, TC1 and TC2, within the deformation zone of the sample allow to determine the thermal gradient across the breadth of the sample, in turn, also allowing for a more informed and reliable temperature reading of the deformation zone within the sample. The minimal delay of thermal response of the embedded thermocouples, TC1 and TC2, during the deformation allows for an accurate temperature measurements of

the adiabatic temperature rise within the deformation zone under the nominal strain rates of 10 and 30 sec^{-1}. The highest nominal strain rate testing condition of 100 sec^{-1} showed a similar response to the results derived from the initial PSC tests with the reading of the adiabatic temperature rise occurring before the start of the deformation. The temperature data points for these tests also display more of an angular curve as opposed to the smoother temperature curves obtained for tests that were under the nominal strain rate conditions of 10 and 30 sec^{-1}. It is unclear why the temperature rise occurs before the start of the deformation of PSC sample but a possible explanation is that the thermocouple is reaching its limit under the nominal strain rate condition of 100 sec^{-1}. However, from the raw data, the adiabatic temperature rise can still be evaluated for the nominal strain rate of 100 sec^{-1}.

6.3 Processed Data

The raw data revealed by the validation tests for the DSI and modified PSC testing configurations were processed by using Excel and OriginLab. The same data processing steps that were utilised in the initial PSC tests were followed in order to determine the equivalent stress and strain values.

6.3.1 Temperature

DSI Configuration

Important aspects of the temperature values of the DSI testing configuration for the PSC of the aluminium alloy AA3104 are shown in Table 6.2. The values read from the thermocouples TC1, TC2 and TC3 at the beginning of the deformation are depicted in Table 6.2 as $TC1_{start}$, $TC2_{start}$ and $TC3_{start}$ respectively. These values provide the actual testing temperatures achieved at the start of the deformation, and this allows for insight into the distribution and homogeneity of the temperature within the PSC sample. The thermal gradient determined across the breadth of the PSC sample is calculated from the difference between $TC1_{start}$ and $TC2_{start}$ and it is denoted as T_{grad}. The temperature of the deformation zone was estimated by calculating the average values of TC1 and TC2. The average value of $TC1_{start}$ and $TC2_{start}$ provide the deformation testing temperature at the beginning of the deformation and it is denoted by T_{start}. Similar to what was achieved with the initial PSC tests, the average value of the temperature during the deformation was calculated from the strain range of 0.8–0.9 and it is denoted as $T_{0.8\text{-}0.9}$. Therefore, the adiabatic temperature change (Adiabatic ΔT) can be calculated from the difference between $T_{0.8\text{-}0.9}$ and T_{start}.

Table 6.2: Important calculated and measured temperature values for the DSI PSC testing configuration at the beginning of the deformation and as well as from 0.8-0.9 strain for the various thermocouples.

Nom. temp. (°C)	Nom. Strain rate (sec^{-1})		$TC1_{start}$ (°C)	$TC2_{start}$ (°C)	$TC3_{start}$ (°C)	T_{grad} (°C)	T_{start} (°C)	$T_{0.8\text{-}0.9}$ (°C)	Adiabatic ΔT
300	10	Test 1	300.1	304.7	307.6	4.6	302.4	328.3	25.9
		Test 2	304.4	311.9	308.7	7.5	308.2	331.0	22.9
300	30	Test 1	302.3	292.8	298.4	9.5	297.6	337.9	40.4
		Test 2	321.3	313.8	300.3	7.5	317.6	347.4	29.85
300	100	Test 1	306.5	295.0	300.8	11.5	300.8	345.6	44.9
		Test 2	331.6	328.3	305.6	3.3	330.0	353.7	23.8
350	10	Test 1	349.8	353.5	351.2	3.7	351.7	374.3	22.7
		Test 2	350.5	351.9	351.4	1.4	351.2	370.6	19.4
350	30	Test 1	358.7	353.4	347.8	5.3	356.1	386.0	29.9
		Test 2	362.1	357.8	355.7	4.3	360.0	387.8	27.9
350	100	Test 1	386.3	384.3	350.3	2.0	385.3	391.1	5.8
		Test 2	364.7	364.3	347.4	0.4	364.5	384.7	20.2
400	10	Test 1	401.3	402.2	402.4	0.9	401.8	418.4	16.7
		Test 2	402.5	401.9	399.2	0.6	402.2	414.6	12.4
400	30	Test 1	401.9	402.6	402.3	0.7	402.3	428.3	26.1
		Test 2	404.8	410.4	402.1	5.6	407.6	431.2	23.6
400	100	Test 1	420.8	422.0	398.1	1.2	421.4	436.8	15.4
		Test 2	421.0	424.4	399.1	3.4	422.7	433.2	10.5

Table 6.3: Holding temperature values of the DSI PSC testing configuration under the nominal strain rate condition of 100 sec^{-1}.

Nom. temp. (°C)		TC1 (°C)	TC2 (°C)	Corrected T_{start} (°C)
300	Test 2	299.2	301.2	300.2
350	Test 1	351.9	347.8	349.9
	Test 2	350.1	347.5	348.8
400	Test 1	400.4	400.3	400.4
	Test 2	399.6	397.4	398.5

It could be determined from the data presented in Table 6.2 that the average values for the thermal gradient with its standard error for all the PSC tests under the DSI testing configuration were 4.1 ±0.8 °C. This value provides very promising evidence that there was no significant thermal gradient (maximum of 1.4% of the nominal testing temperature) across the breadth of the DSI testing configuration sample. The average thermal gradient across the breadth of the sample easily falls within the temperature variation of 16 °C as shown in Table 2.3, which is recommended by the Good Practice Guide compiled by the NPL [41]. An illustrative representation of the starting deformation temperatures of the samples as well as the increase in temperature during the deformation is shown in Figure 6.6. From Figure 6.6, it can be clearly noted that the samples under the nominal strain rate condition of 100 sec^{-1} starting deformation temperatures did not achieve values close to that of the nominal testing temperatures. This is also noted from the raw temperature data

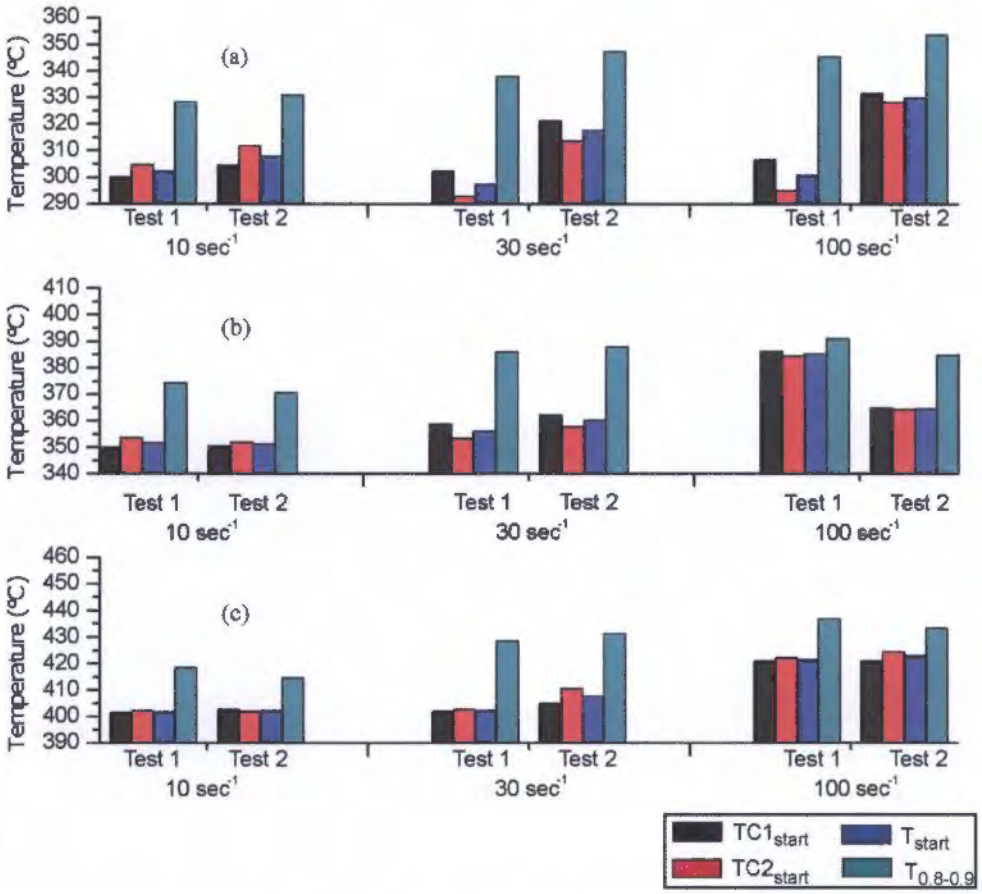

Figure 6.6: Temperature values for the DSI PSC testing configuration at the beginning of the deformation as well as the mean value of the measured temperature from strain 0.8–0.9 for the nominal testing temperatures of (a) 300 °C (b) 350 °C and (c) 400 °C under the nominal strain rate conditions of 10, 30 and 100 sec^{-1}.

as mentioned in the previous section where the recorded values of the temperature show an increase in temperature before the actual start of the deformation. This phenomenon occurred in test 2 at the nominal testing temperature of 300 °C, tests 1 and 2 at the nominal testing condition of 350 °C and as well as for tests 1 and 2 at the nominal temperature of 400 °C. Table 6.3 displays the temperature values for thermocouples TC1 and TC2 at which the PSC sample was held prior to the deformation. By averaging these two values, a corrected value for the sample's temperature prior to deformation can be estimated. The corrected temperature values as shown in Table 6.3 clearly show a very close correlation to the nominal testing deformation temperatures. This proves that the starting temperature of the sample prior to the deformation of the DSI sample did achieve the desired testing temperatures accurately and that there is a problem with the logging and recording of the initial temperature values prior to deformation at the nominal strain rate condition of 100 sec^{-1}.

Modified Configuration

Similar to the temperature results of the DSI testing configuration, Table 6.4 also provides important temperature values for the modified PSC testing configuration. The additional surface temperature value of the sample's shoulders is provided by thermocouple TC4 and the value at the beginning of the deformation denoted as $TC4_{start}$. The additional thermocouple reading from TC4 for the modified testing configuration was included due to the modified PSC sample being approximately three times larger than the DSI sample. A larger sample therefore has a higher chance of a heterogeneous temperature distribution as a result of the nature of the resistive heating of the Gleeble 3800. It was found that there is no significant temperature difference between the internal shoulder measurement of $TC3_{start}$ and the external temperature shoulder measurement of $TC4_{start}$ that would cause alarm about the modified PSC tests. The average value for the thermal gradient across the sample's breadth with its standard error for all the modified PSC testing configurations is 19.2 ±4.0 °C. This average thermal gradient value is significantly higher than that achieved in the case of the PSC tests with the DSI configuration. However, on closer inspection of the data presented in Table 6.4 and Figure 6.7 it can be seen that test 1 under the nominal testing conditions of 350 °C and 10 sec^{-1} and as well as test 1 under the nominal testing conditions of 400 °C and 10 sec^{-1} had a grossly large thermal gradient across the samples breadth of 53.3 °C and 63.9 °C, respectively. These two tests significantly skew the average value determined for the thermal gradient experienced for the modified PSC tests, and hence by not including these values in determining the average value for the thermal gradient a more acceptable value of 14.3 ±2.3 °C was achieved. However, the work by Miza and Sellars [37] as mentioned in the literature a thermal gradient of 20 °C does not significantly affect the determined flow stress values of a sample in comparison to a sample that has no thermal gradient. The series of PSC tests with the modified configuration suggest that the thermal gradient achieved was more pronounced for tests that were at the nominal temperature of 400 °C. This can lead to a greater a chance of a larger thermal gradient for the modified PSC testing configuration as the testing temperature increases. Additionally, it was found that by being able to make a very good surface contact between the sample and anvil reduces this risk considerably.

Similarly as described in the results of the DSI configuration that were subjected to the nominal strain rate condition of 100 sec^{-1}, the temperature readings started to rise before the actual start of the deformation. All the modified PSC configuration tests that were subjected to the nominal strain rate of 100 sec^{-1} displayed this phenomenon to varying degrees as is evident in Figure 6.7. Table 6.5 shows the temperature values at which the PSC sample was held prior to the deformation, therefore the corrected temperature values at the nominal strain rate of 100 sec^{-1} for the modified configuration PSC tests can be calculated

Table 6.4: Important calculated and measured temperature values of the modified PSC testing configuration at the beginning of the deformation and as well as from 0.8–0.9 strain for the various thermocouples.

Nom. temp. (°C)	Nom. Strain rate (sec^{-1})		$TC1_{start}$ (°C)	$TC2_{start}$ (°C)	$TC3_{start}$ (°C)	$TC4_{start}$ (°C)	T_{grad} (°C)	T_{start} (°C)	$T_{0.8-0.9}$ (°C)	Adiabatic ΔT
300	10	Test 1	309.2	293.9	302.2	-	15.3	301.6	323.3	21.8
		Test 2	299.6	300.3	303.4	302.4	0.7	300.0	329.7	29.7
300	30	Test 1	303.0	312.1	285.3	298.2	9.1	307.6	348.2	40.7
		Test 2	309.4	294.4	299.3	297.3	15	301.9	342.1	40.2
300	100	Test 1	324.7	309.2	293.7	291.8	15.5	317.0	346.0	29.1
		Test 2	313.4	311.3	304.1	302.9	2.1	312.4	343.6	31.3
350	10	Test 1	345.2	398.5	354.8	369.2	53.3	371.9	394.5	22.7
		Test 2	346.9	362.9	353.1	353.1	16	354.9	380.6	25.7
350	30	Test 1	353.7	361.3	357.3	356.7	7.6	357.5	396.7	39.2
		Test 2	357.7	350.5	350.2	353.4	7.2	354.9	389.1	35.0
350	100	Test 1	369.4	356.1	343.7	345.4	13.3	362.8	390.2	27.5
		Test 2	368.1	359.0	345.0	342.9	9.1	363.6	391.8	28.3
400	10	Test 1	398.8	462.7	416.0	421.3	63.9	430.8	440.4	9.6
		Test 2	399.4	407.0	403.1	402.0	7.6	403.2	424.8	21.6
400	30	Test 1	404.9	372.7	379.0	380.4	32.2	388.8	414.8	26.0
		Test 2	414.5	388.3	402.2	399.4	26.2	401.4	432.0	30.6
400	100	Test 1	440.1	470.0	447.5	447.5	29.9	455.1	477.8	22.8
		Test 2	419.1	440.6	410.9	407.7	21.5	429.9	448.9	19.1

Table 6.5: Holding temperature values of the modified PSC testing configuration under the nominal strain rate condition of 100 sec^{-1}.

Nom temp. (°C)		TC1 (°C)	TC2 (°C)	Corrected T_{start} (°C)
300	Test 1	304.3	289.4	296.85
	Test 2	300.0	297.8	298.9
350	Test 1	355.2	343.8	349.5
	Test 2	354.0	345.4	349.7
400	Test 1	400.3	438.6	420.3
	Test 2	426.1	399.7	412.9

by averaging values of thermocouples TC1 and TC2. The corrected temperature values prior to the deformation thus now correlate well with the nominal deformation temperatures for the tests that were under the nominal strain rate condition of 100 sec^{-1}.

Comparison to Evans and Ricks

Further analysis of the temperature of the PSC validation tests can be continued in order to compare results to those Evans and Ricks achieved for their findings [49]. Based on PSC tests performed on the DSI and modified configurations, Figure 6.8 compares the average temperature values with their standard error as in tests 1 and 2 for the for each specific nominal temperature and strain rate condition over the strain range of 0.8–0.9. Figure 6.8

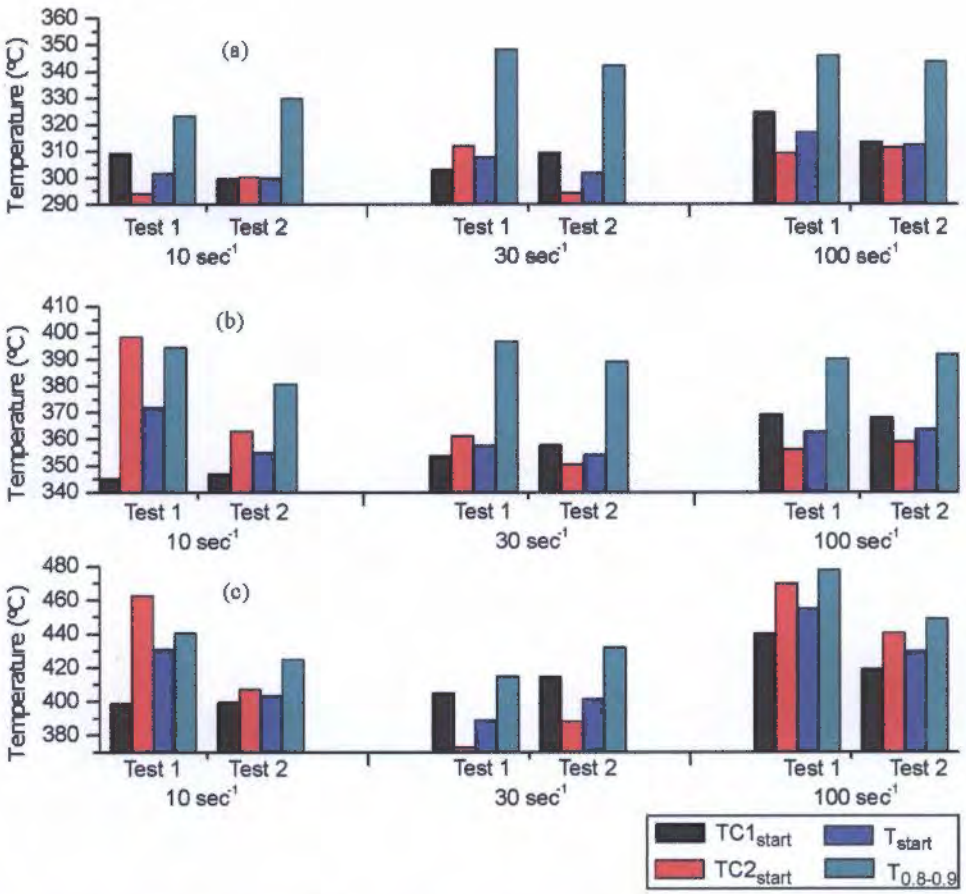

Figure 6.7: Temperature values of the modified PSC testing configuration at the beginning of the deformation as well as the mean value of the measured temperature from strain 0.8–0.9 at the nominal testing temperatures of (a) 300 °C (b) 350 °C and (c) 400 °C under the nominal strain rate conditions of 10, 30 and 100 sec^{-1}.

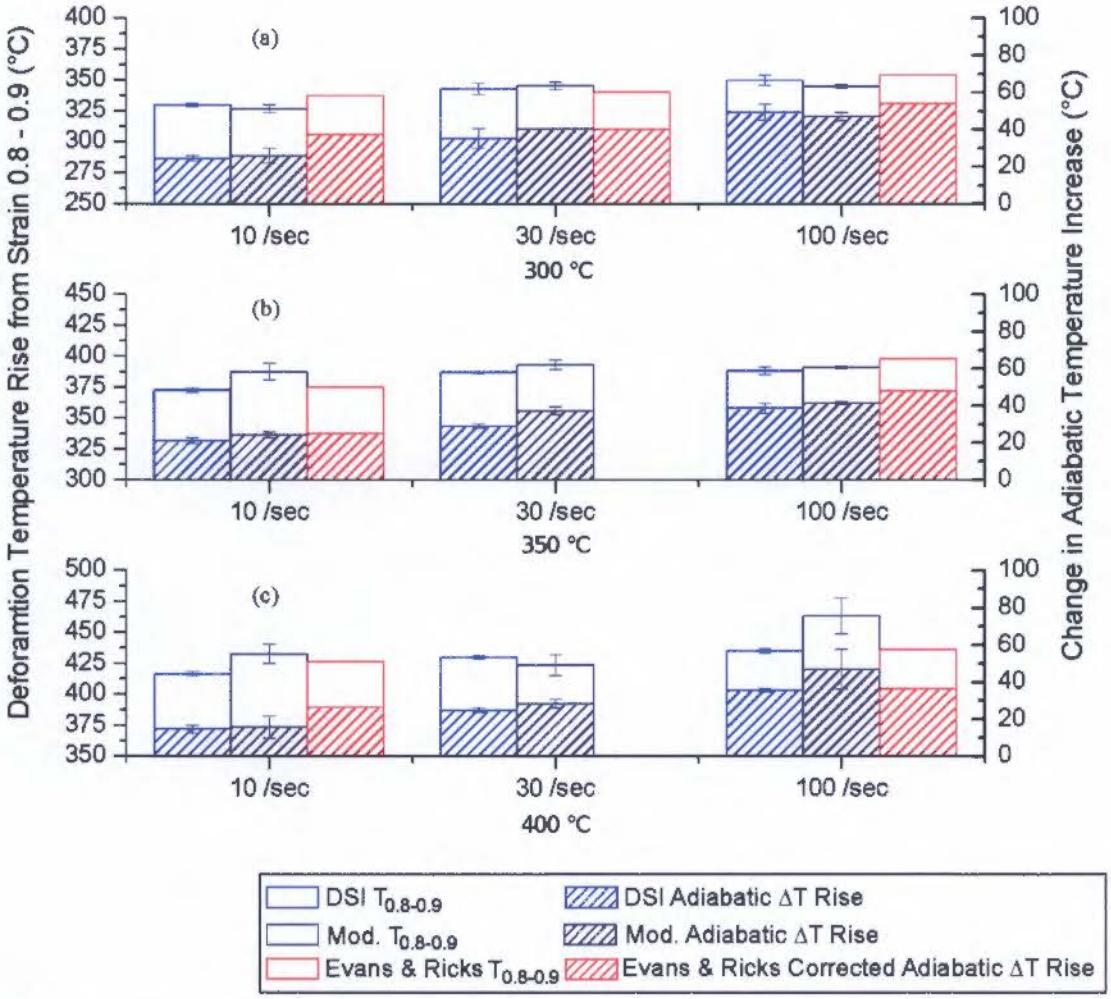

Figure 6.8: Comparison of the DSI and modified PSC testing configuration to the results of Evans and Ricks [49] of the adiabatic temperature rise at the nominal testing temperatures of (a) 300 °C, (b) 350 °C and (c) 400 °C under the nominal strain rate conditions of 10, 30 and 100 sec^{-1}.

illustrates two pieces of information: one is the absolute temperature value reached due to the adiabatic heating of the material from the deformation and the other is the change in the temperature from the initial deformation temperature to the absolute temperature value achieved during the deformation, which is the adiabatic temperature change. The results shown by Evans and Ricks are also included in Figure 6.8, with the corrected calculated values of the temperature under the 30 and 100 sec^{-1} condition. The corrected temperature values of Evans and Ricks for the nominal PSC condition of 350 °C and 30 sec^{-1} and 400 °C and 30 sec^{-1} are not included as it was not reported by Evans and Ricks [49]. As shown in Figure 6.8, the results of both the DSI and modified PSC configuration tests fared very well compared to the values achieved by Evans and Ricks over all the testing conditions. This allowed for very confident temperature readings for both the DSI and modified PSC testing configurations on the Gleeble 3800 over the full range of the testing conditions.

From the encouraging results as shown in Figure 6.8, the temperature values obtained

Table 6.6: Temperature comparison of the calculated mean values from the DSI and modified configuration to the results obtained by Evans and Ricks [49] between 0.8–0.9 strain.

		Mean values from DSI and modified configurations from 0.8-0.9 strain		Evans and Ricks mean values from 0.8 - 0.9 strain	
Nominal temperature (°C)	Nominal strain rate (sec^{-1})	Mean temperature (°C)	Change in adiabatic temperature rise (°C)	Corrected mean temperature (°C)	Corrected change in adiabatic temperature rise (°C)
300	10	328.1 ±1.7	25.1 ± 1.8	337.1	37.1
	30	343.9 ± 2.4	37.8 ± 2.6	340.0	40
	100	347.2 ± 2.2	48.1 ± 2.1	353.8	53.8
350	10	380.0 ± 5.3	22.2.6 ± 1.3	375	25.0
	30	389.9 ± 2.4	33.0 ± 2.6	N/A	N/A
	100	389.5 ± 1.6	40.0 ± 1.4	397.7	47.7
400	10	424.6 ± 5.7	15.1 ± 2.6	426.4	26.4
	30	426.6 ± 4.0	26.6 ± 1.5	N/A	N/A
	100	449.2 ± 10.1	41.2 ± 5.5	436.3	36.3

from the DSI and modified testing configurations are very similar. The two different testing configurations and ultimately different geometries therefore do not have any significant effect on the temperature readings of the PSC sample during the deformation. Along this line of thinking, the temperature results obtained in both the testing configurations can be combined in order to achieve a mean value for each specific nominal testing condition. The temperature results from the PSC testing of the aluminium alloy AA3104 on a Gleeble 3800 could therefore be summarised in Table 6.6 and evidently allow for very comparable results to those achieved by Evans and Ricks using the same material on a different PSC testing machine.

6.3.2 Strain Rate

The strain rate responses for the validation PSC tests revealed common trends for the DSI and modified PSC tests, depending on the nominal strain rate condition. The typical strain rate response for the DSI and modified PSC testing configuration is shown in Figure 6.9. Figure 6.9 shows the typical different strain rate response of test 1 of the DSI and modified testing configurations for all of the nominal strain rates at the temperature of 350 °C. The specific strain rate response in each individual PSC test is included in Appendices G and H for the DSI and modified PSC testing configurations, respectively. For the PSC tests that had noise in the derived strain rate results, smoothing of the data was achieved by using the Savitzky–Golay method as mentioned for initial PSC tests in Chapter 4. During the validation PSC tests, it was observed that there was no significant difference between the two testing configurations for the strain rate response as shown by Figure 6.9. A relatively

consistent strain rate was achieved from 0.45 strain for the PSC tests under the nominal strain rate of 10 sec^{-1}. Under both the nominal strain rate conditions of 10 and 100 sec^{-1}, a fairly flat strain rate was achieved for both testing configurations as shown in Figure 6.9. Under the nominal strain rate condition of 30 sec^{-1}, a constant strain rate was not achieved over the deformation range for both testing configurations. In the DSI testing configuration (Figure 6.9c), the strain rate steadily increases in a linear fashion up until a strain between 1.0–1.1, reaches a maximum and then steadily decreases in a linear fashion till the end of the deformation. For the modified testing configuration, the strain rate response during the deformation shows a similarly steady linear increase of the strain rate but only until the end of the deformation. This type of response under the nominal strain rate condition of 30 sec^{-1} does not achieve a constant strain rate over the full deformation range and, hence, makes it difficult to achieve the actual desired strain rate for the PSC test over the strain range 0.8–0.9. However, due to the relatively consistent strain rate response that is achieved for the nominal strain rate condition of 100 sec^{-1} this leads to the belief that a more constant strain rate can be achieved for the nominal strain rate condition of 30 sec^{-1}. The responsibility for this issue lies more with the control systems that are pre-programmed into the Gleeble 3800, rather than the actual physical capabilities of the Gleeble 3800.

The strain rate values from the validation PSC tests can have been determined for the DSI and modified PSC testing configurations as shown by Table 6.7. In order to be consistent with the testing of the PSC tests of the aluminium alloy AA3104, the mean values of the strain rate is calculated over the strain range from 0.8–0.9, and it is denoted by $\dot{\varepsilon}_{0.8-0.9}$. The average strain rate over the whole deformation range is also included in these results. The average strain rate that the PSC testing sample were subjected to the full deformation duration has been denoted as $\dot{\varepsilon}_{whole}$. For the nominal strain rate condition of 10 sec^{-1}, the $\dot{\varepsilon}_{0.8-0.9}$ and $\dot{\varepsilon}_{whole}$ have achieved similar values to the desired nominal strain rate for all of the nominal temperature conditions for both testing configurations. By reviewing the strain rate results, there is no suggestion that the different testing configurations have a significant influence on the strain rate imposed on the PSC sample during the deformation. Therefore, the average strain rate with its standard error over the whole deformation range for both of the testing configurations under the nominal strain rate condition of 10 sec^{-1} is 10.4 $\pm$0.22 sec^{-1}. Similarly for the nominal strain rate condition of 30 sec^{-1}, the average value of 33 $\pm$0.86 sec^{-1} was achieved over the full deformation and the average strain rate of 86.1 $\pm$3.22 sec^{-1} was achieved for the nominal strain rate condition of 100 sec^{-1}. From these results for the average strain rates achieved over the full deformation range, the nominal strain rate condition of 10 and 30 sec^{-1} show that the experimental strain rate values can be relatively achieved for the PSC testing of the aluminium alloy AA3104. However, under the nominal strain rate condition of 100 sec^{-1}, the average value did not satisfactorily achieve the desired strain rate conditions with the Gleeble 3800, even though a slight improvement (5.3 sec^{-1})

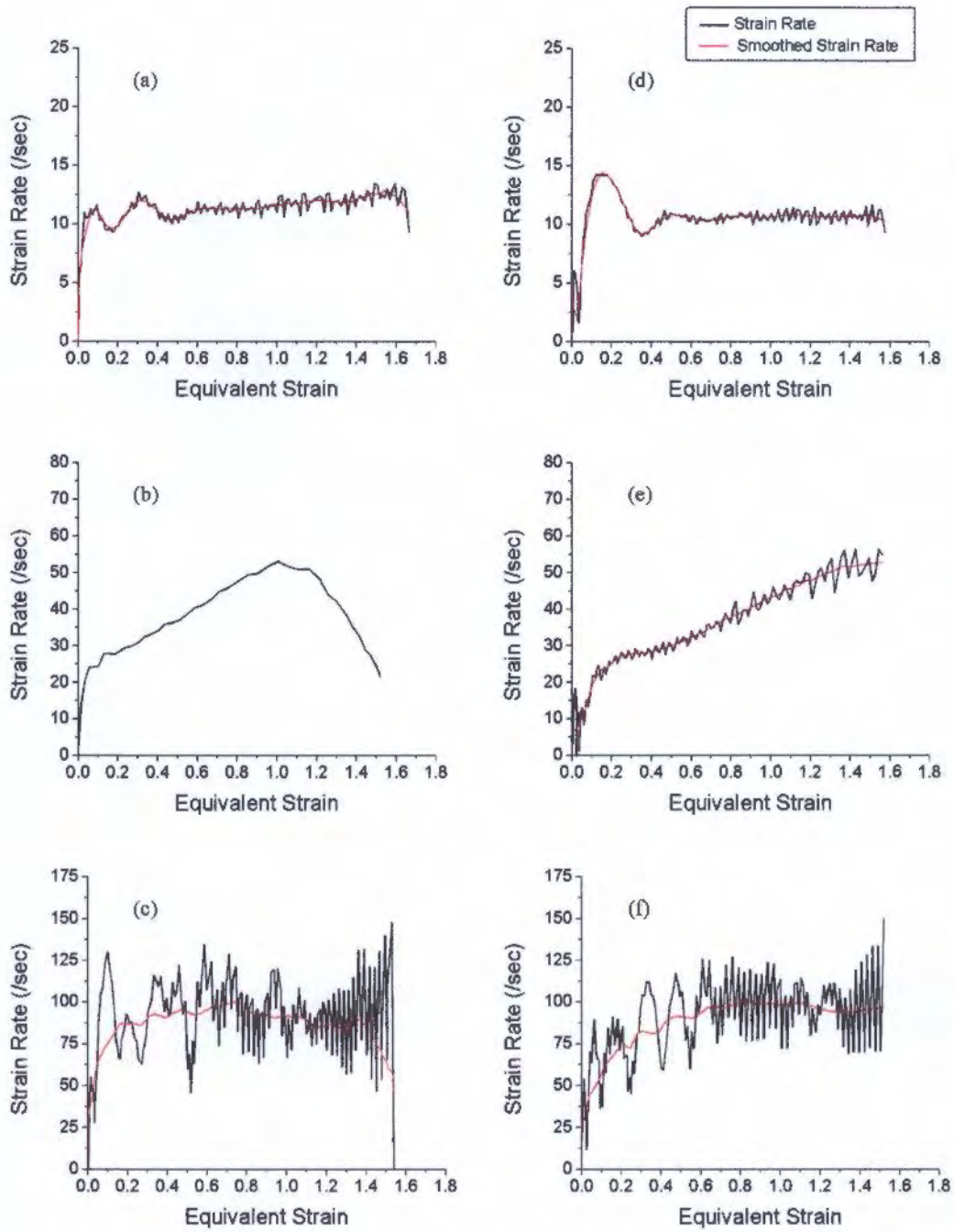

Figure 6.9: Typical strain rate responses experienced on the Gleeble 3800 for the (a-c) DSI and (d-f) modified PSC testing configurations, all these tests were performed at the nominal testing temperature of 350 °C.

Table 6.7: Strain rate results of the validation PSC tests for the DSI testing configuration and the modified testing configuration.

Nominal testing conditions			DSI configuration		Modified configuration	
			Strain rate (sec^{-1})		Strain rate (sec^{-1})	
Temp. (°C)	Strain rate (sec^{-1})		$\dot{\varepsilon}_{0.8-0.9}$	$\dot{\varepsilon}_{whole}$	$\dot{\varepsilon}_{0.8-0.9}$	$\dot{\varepsilon}_{whole}$
300	10	Test 1	11.2	10.9	10.6	9.8
		Test2	11.4	11.1	10.5	9.9
	30	Test 1	48.2	30.7	32.8	27.6
		Test2	49.9	32.6	34.3	29.0
	100	Test 1	101.6	89.6	91.9	70.6
		Test2	212.1	110.6	74.8	68.4
350	10	Test 1	11.3	11.1	10.7	10.2
		Test2	11.0	10.5	9.5	9.1
	30	Test 1	48.2	34.0	39.3	31.5
		Test2	50.30	34.2	39.6	36.1
	100	Test 1	93.3	83.6	99.7	84.8
		Test2	101.1	86.4	102.7	86.7
400	10	Test 1	11.1	10.3	10.7	10.2
		Test2	10.3	9.7	12.0	12.0
	30	Test 1	47.5	34.2	41.9	33.7
		Test2	48.0	36.3	43.5	37.5
	100	Test 1	92.1	85.0	124.3	99.5
		Test2	92.3	85.4	102.0	82.2

on the initial PSC samples was achieved. In comparison to the nominal strain rate condition of 100 sec^{-1} , the strain rates achieved by Evans and Ricks are 83.4, 97.7 and 93 sec^{-1} (the average with its standard error is 91.4± 4.21 sec^{-1}) for the nominal temperatures of 300, 350 and 400 °C respectively [49]. The strain rate results of Evans and Ricks showed that the measured strain rate was influenced by temperature during the PSC test, and that the nominal strain rate condition of only 100 sec^{-1} could be achieved as the aluminium alloy AA3104 offers less resistance at the higher temperature. This phenomenon was not observed in the case of the PSC tests on the Gleeble 3800 and, on the contrary an average strain rate over the whole deformation of 110.6 sec^{-1} was achieved for test 2 for DSI configuration at nominal temperature of 300 °C and 99.5 sec^{-1} for the test 1 of the modified configuration at the nominal condition of 400 °C at 100 sec^{-1}. This once again provides insight that the programmed controlling systems for the strain rate is what limits the Gleeble 3800 at the high strain rate and thus suggesting that the strain rate capabilities are what limits the desired strain rate. With this in mind and from these strain rate results obtained, this also shows that measured strain rate values for PSC testing on the Gleeble became more inconsistent as the nominal strain rate condition increased.

6.3.3 Flow Stress

The calculation of the equivalent flow stress values followed the same calculation process that was used for the initial PSC tests in Section 4.2.1. The value of the coefficient of friction of 0.08 based on the results of the ring compression tests in Chapter 5 was used for all the equivalent flow stress calculations in the validation PSC tests with the graphite foil lubricant. The typical flow stress curve obtained from the validation PSC tests for the DSI and modified configuration in comparison to the results by Evans and Ricks is illustrated by Figure 6.10 [49]. The results shown in Figure 6.10 are under the nominal testing temperature condition of 350 °C and a strain rate of 30 sec^{-1}. As Figure 6.10 shows, the steady state flow stress is achieved once the aluminium alloy AA3104 yields as the strain hardening of the material equals the rate of recovery. This type of behaviour is inductive of aluminium during TMP, and suggests that the material softening mechanism is dynamic recovery, mentioned in the literature review. The flow stress value of the material also has a section that steadily declines with further deformation of the material (with strain > 1.0), and this is caused by the material temperature increasing by ±38 °C due to the deformation of heating from the adiabatic temperature rise. It can be seen that there is a small but significant higher flow stress value for the modified PSC testing configuration in comparison to that of the DSI testing configuration. This type behaviour was observed for all of the validation PSC tests. The flow stress of results determined by Evans and Ricks also show the same trend of the curve, however a notable higher stress value across the strain range is achieved. This holds true for all the validation PSC tests that were investigated in this report. The equivalent flow stress curves for the DSI and modified testing configuration are included in Appendix G and H respectively.

Similar to the method used to obtain the results for the temperature and strain rate values, the flow stress from the PSC tests for the DSI and modified configurations was calculated using the mean value over the strain rang of 0.8-0.9. This allows direct comparison to the flow stress values achieved by Evans and Ricks, which are illustrated by Figure 6.11. The specific flow stress values over the strain range of 0.8–0.9 for each PSC test for the DSI and modified testing configuration are included in Appendices G and H. Evidentially as shown in Figure 6.11, the general trend for both the DSI and modified PSC testing configurations demonstrates that the flow stress of the aluminium alloy AA3104 increases with a decreasing deformation temperature and an increasing strain rate. It can also be seen in Figure 6.11 that similar flow stress values between tests 1 and 2 under each specific testing condition for the DSI and modified configurations are achieved providing strong evidence of repeatability. The only exception to this is the flow stress result from test 1 of the modified configuration under the nominal conditions of 400 °C and 100 sec^{-1} and this is due to the deformation temperature being ±20 °C higher than the nominal temperature. From the flow stress results depicted in

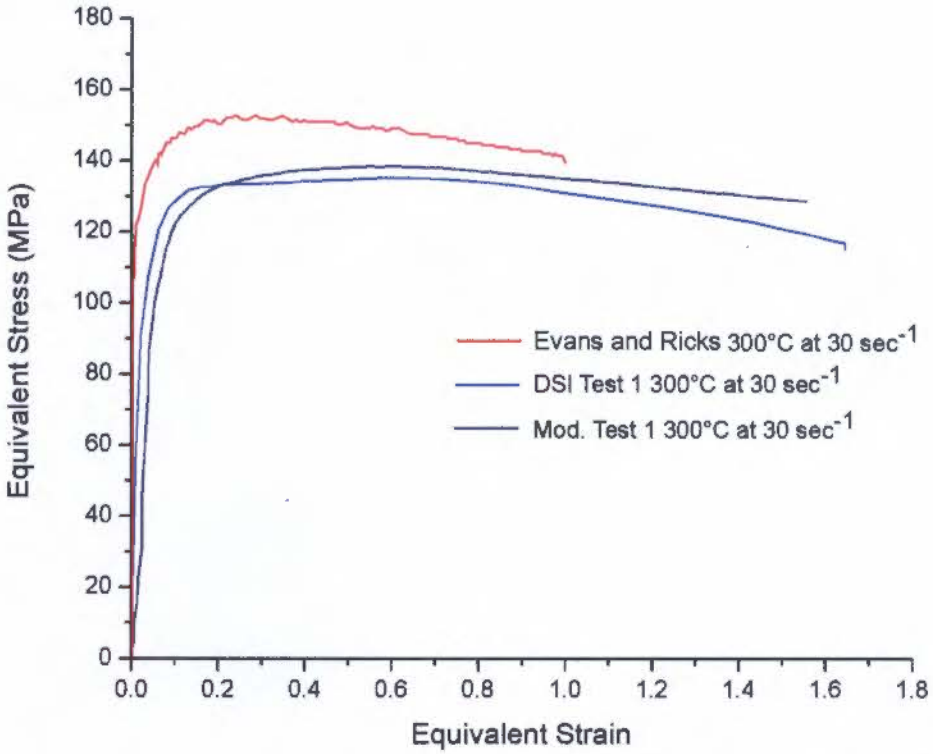

Figure 6.10: Equivalent flow stress vs. strain plot for the DSI and modified PSC testing configuration in comparison to the flow stress curve obtained by Evans and Ricks [49] under the nominal PSC testing condition of 350 °C and 30 sec^{-1}.

Figure 6.11, it can be seen that there is a fairly common and consistent difference between the flow stress values obtained by Evans and Ricks [49] in comparison to the results obtained in the PSC tests on the Gleeble 3800 for the two different testing configurations. The mean difference with its standard error between the DSI testing configurations is 14.1 ±0.8 MPa (11.6 ±0.7%) less than the flow stress results determined by Evans and Ricks. Similarly the flow stress results of the modified configuration are 10.6 ±1.2 MPa (7.7 ±0.9%) less. The difference between the DSI and the modified PSC testing configuration is on average 3.48 ±1.2 MPa (2.7 ±1.2%) lower. These results suggest that determining the flow stress for the modified PSC testing configuration is the better option for PSC testing on the Gleeble 3800.

6.3.4 Aluminium Alloy AA3104 Constitutive Equation

So far the results and analysis in this investigation for the validation PSC tests only compare the temperature, strain rate and flow stress results individually for the DSI and modified testing configurations. While comparing each portion of the TMP of the PSC testing of aluminium alloy AA3104 allows insight to how that specific area influences the behaviour of the material, a full understanding of the material's behaviour needs to combine the temperature, strain rate and flow stress in order to achieve a complete comparison. As the literature review demonstrates, the strain rate and temperature can be

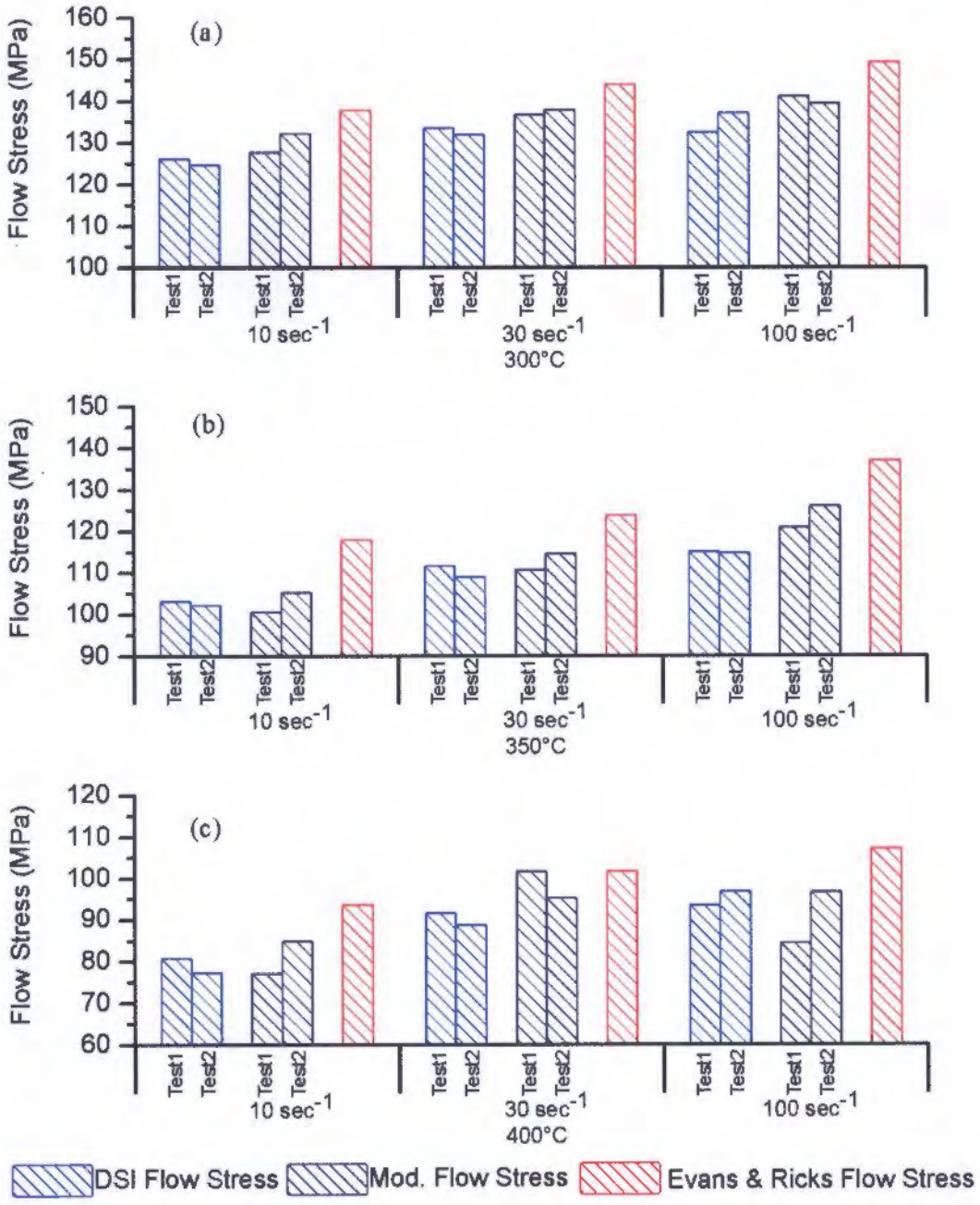

Figure 6.11: Flow stress comparisons between the DSI and modified PSC testing configurations and the results determined by Evans and Ricks [49] at the nominal testing temperatures of (a) 300 °C (b) 350 °C and (d) 400 °C nnder the nominal strain rate conditions of 10, 30 and 100 sec^{-1}.

Table 6.8: Results showing the linear fit that relates the flow stress values to lnZ for the DSI and modified PSC configurations as well as results of Evans and Ricks [49].

PSC testing scenario	Slope	Slope standard error	Y intercept (MPa)	Y intercept Standard Error
Evans and Ricks Results	10.99	-	-223.8	-
DSI configuration	10.55	0.36	-229.9	11.67
Modified configuration	10.87	0.41	-232.6	13.17

linked together to form the Zener–Holloman parameter as shown by Equation 2.1. The flow stress values determined by the PSC tests for the DSI and modified configurations are related to the Zener–Holloman parameter as shown in the literature review by Equation 2.18. Therefore by combining and rearranging Equations 2.1 and 2.18, the following equation can be formed to relate the stress value to the Zener–Holloman parameter:

$$\sigma = \frac{1}{\beta} lnZ - \frac{1}{\beta} lnA \tag{6.1}$$

This allows for sound analysis of the PSC testing data in order to compare the results of the DSI and modified PSC testing configurations to the results obtained by Evans and Ricks [49], as the strain rate and temperature values are considered for the flow stress values of the different PSC tests. The Zener–Holloman parameter has therefore been calculated for each of the PSC tests in the DSI and modified configuration by using Equation 2.1. The temperature values used in the calculation of the Zener–Holloman parameter for each PSC test of the DSI and modified configuration is the average value calculated over the strain range of 0.8–0.9 as shown in Tables 6.2 and 6.4, respectively, in Section 6.3.1. Similarly, the strain rate values used for the DSI and modified configuration are calculated from the values obtained in Table 6.7 in Section 6.3.2. The Q_{def} for the aluminium alloy AA3104 for these calculations was used as the generally accepted value of 155 JK/mol [43]. The values of lnZ for the DSI and modified configuration are included in Appendices G and H, respectively, for all of the validation PSC tests.

Figure 6.12 is therefore a plot of all the PSC test results of the DSI and modified configuration as well as the results determined by Evans and Ricks [49] for the flow stress values as a function of lnZ. A fairly good scatter of the data points was obtained for both of the testing configurations. The general trend of the data points for each testing configuration makes it possible to fit a linear regression to the data points. The results obtained from the linear fit of the data points are in included in Table 6.8. As can he seen from the results as shown in Figure 6.12 and Table 6.8 all three of the straight lines are essentially parallel. This is a very significant result, as it shows that the change of the PSC testing conditions (deformation temperature and strain rate) results is in the same the change in the flow stress for the DSI configuration and the modified configuration as the

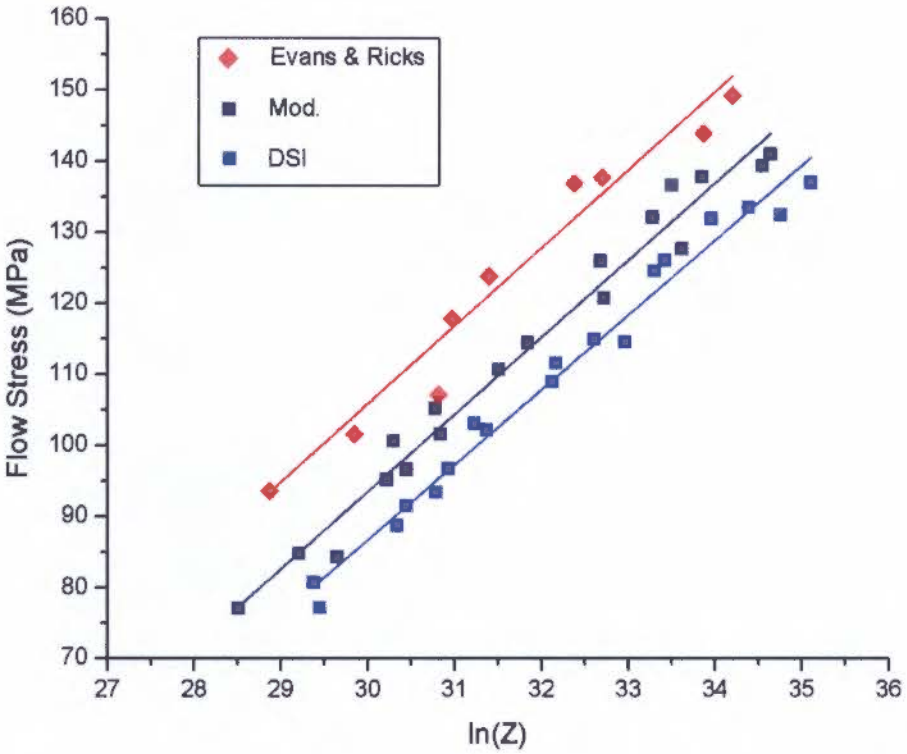

Figure 6.12: The flow stress value vs. ln(Z) parameter of each test for the DSI and modified PSC testing configuration and as well as the results determined by Evans and Ricks [49].

results from Evans and Ricks confirm.

In order for the constitutive equation to be determined the constants A and β must be determined for Equation 6.1. The inverse value of the slope from the plot in Figure 6.12 determines the β value for each testing configuration, and this, in turn allows the determination of A, as $A = \exp(-\beta \times Y_{intercept})$. The constitutive equation for the aluminium alloy can therefore be expressed as:

$$\dot{\varepsilon}\left(\frac{Q_{def}}{RT}\right) = A\exp\left(\beta\bar{\sigma}\right) \tag{6.2}$$

As shown by the results in Table 6.9, the material constant β determined across all of the PSC testing scenarios achieved very similar values. Since β is a material constant and by achieving very similar values regardless of PSC testing scenario, this provides promising results for the PSC testing on the Gleeble 3800. The only noticeable difference between the DSI and modified PSC testing configuration from the Evans and Ricks results is the material constant A. The difference between the A in the two configurations can only be explained by the different flow stress values determined from the different temperature and strain rate PSC testing conditions.

Table 6.9: Results of the different values of the material constants of the constitutive equation for aluminium alloy AA3104 determined by Evans and Ricks [49] and the DSI and modified PSC testing configuration.

PSC testing scenario	β (/MPa)	A (sec^{-1})
Evans and Ricks	0.091	7.01×10^8
DSI configuration	0.095	28.5×10^8
Modified configuration	0.092	19.6×10^8

6.4 Summary

A full and comprehensive set of PSC tests on the aluminium alloy AA3104 produced by Hulamin was carried out in order to validate the performance of the Gleeble 3800 for two different sample to anvil geometries. As mentioned in the literature review, the PSC testing geometry plays an important role in order to achieve a satisfactory and accurate PSC test. The two different PSC testing configurations utilised in this investigation are the recommended DSI configuration and the modified PSC testing configurations. The two different ratios for the geometries for these PSC testing configurations are the H_R and B_R, where the values for the two configurations are shown in Table 6.10 as well as the values used by Evans and Ricks [49]. The temperature and strain rate testing conditions for these sets of PSC tests were performed at temperatures of 300, 350 and 400 °C and at strain rates of 10, 30 and 100 sec^{-1}. Two PSC tests of a single deformation up to the strain of 1.6

Table 6.10: Different sample to anvil geometric ratios for the two different PSC testing configurations as well as Evans and Ricks ratio' [49].

	$H_R \left(\frac{b_0}{w}\right)$	$B_R \left(\frac{w}{h_0}\right)$
DSI PSC Configuration	3.0	1.0
Modified PSC Configuration	1.3	4.62
Evans and Ricks	5.0	1.5

were carried out for each testing condition for both testing configurations. Therefore a total of 36 PSC tests (18 tests per PSC testing configuration) were carried out in the validation PSC tests.

In order to validate and prove that the results obtained by the Gleeble 3800 are credible for the PSC testing of the aluminium alloy AA3104, the PSC results for this investigation are compared to the results obtained by Evans and Ricks [49] for the same aluminium alloy produced by Hulamin. Analysis of the temperature results of the DSI testing configuration resulted in an average thermal gradient of 4.1 ±0.8 °C across the PSC sample's breadth and similarly the average thermal gradient for the modified testing configuration is 19.2 ±4.0 °C. It is clear that the DSI testing configuration allows for a tighter, reliable and consistent control of the temperature distribution within PSC sample. However due to less than satisfactory heating of the PSC samples for two of the modified PSC tests, an acceptable thermal gradient is possible to achieve (14.3 ±2.3 °C) for the modified PSC testing

configuration. The severity of the thermal gradient set-up across the sample's breadth on the effect it has on the microstructural evolution is of concern and further investigation should be conducted on this possible effect. Care with the testing preparation should be taken into consideration when making use of the modified testing configuration to achieve a very good surface contact between the anvil and sample. On the whole, measurements of the adiabatic temperature increase for both of the DSI and modified testing configuration was achieved and the results fared very well by achieving similar results values to that Evans and Ricks determined. This compelling evidence proves that reliable and accurate temperature recordings of the aluminium alloy AA3104 over the full range of temperature and strain rate conditions were achieved while performing PSC tests on the Gleeble 3800.

Analysis of the strain rate response during the deformation process of the DSI and modified PSC testing configuration did not show any significant differences between each testing configuration, and similar trends for each testing condition were observed. PSC tests that were deformed at the nominal strain rate of 10 sec^{-1} achieved a good strain rate response with an average strain rate over the full deformation of 10.4 ± 0.22 sec^{-1}. In the PSC tests that were deformed at the nominal strain rate of 30 sec^{-1} the average strain rate over the full deformation achieved satisfactory results with an average strain rate of 33 ± 0.86 sec^{-1}. However this figure is not truly representative of the strain rate during the deformation as a rising increase of the value of the strain rate was generally followed from the start of the deformation till the end. The 100 sec^{-1} strain rate tests did not achieve an acceptable nominal strain rate value with the average strain rate of 86.1 ± 3.22 sec^{-1} for both of the testing configurations. However, in comparison to the results obtained by Evans and Ricks the average strain rate of 91.4$\pm$ 4.21 sec^{-1} [49] was achieved, and therefore only a small difference exists on average between the results on the Gleeble 3800 and the results obtained by Evans and Ricks for the nominal strain rate tests of 100 sec^{-1}.

As expected, the flow stress of the aluminium alloy AA3104 increases with a decreasing deformation temperature and an increasing strain rate. In both PSC testing configurations on the Gleeble 3800 repeatable flow stress values were determined, however, tighter tolerances of the flow stress values were achieved with the DSI configuration. This is a direct result of the more consistent and tighter temperature control of the DSI configuration. Under all the testing conditions, the flow stress values determined by Evans and Ricks proved to be consistently higher than the results determined by the DSI and modified PSC testing configuration. The modified PSC testing configuration achieved a small but significant higher flow stress value in comparison to the DSI testing configuration. The DSI testing configuration was on average 11.6 $\pm 0.7\%$ less than the results obtained by Evans and Ricks, where the modified testing configuration obtained an average of 7.7 $\pm 0.9\%$ lower. The flow stress difference of 3.48 ± 1.2 MPa (2.7 $\pm 1.2\%$) between the DSI and modified PSC testing configuration can he largely based on the

different geometric ratios employed (H_R and B_R) for each testing configuration.

The Zener–Holloman parameter was utilised to directly compare the effect of the temperature and strain rate on the flow stress of the aluminium alloy AA3104, in order to combine the temperature and strain value for each specific testing condition. A linear relationship between the Zener–Holloman parameter and the flow stress values for both testing configurations were obtained by fitting a linear best fit curve to the data sets of the DSI and modified data sets. The constitutive equation for the aluminium alloy in the form of $\dot{\varepsilon}\left(\frac{Q_{def}}{RT}\right) = A\exp\left(\beta\bar{\sigma}\right)$ was determined by using the best fitted lines. Based on the results of the DSI testing configuration, the constitutive equation for the aluminium alloy AA3104 is:

$$\dot{\varepsilon}\left(\frac{Q_{def}}{RT}\right) = 28.5 \times 10^8 \exp\left(0.095\sigma\right) \tag{6.3}$$

Similarly, based on the results of the modified PSC testing configuration the constitutive equation for the aluminium alloy AA3104 is:

$$\dot{\varepsilon}\left(\frac{Q_{def}}{RT}\right) = 19.6 \times 10^8 \exp\left(0.092\sigma\right) \tag{6.4}$$

The only significant difference between the constitutive equations determined is the value of the material constant. The A constant relies on the flow stress results of each testing condition of the different PSC configurations. The difference in the values of the A constant determined from the results of the DSI and the modified testing configurations can be explained by the different geometric values employed for the H_R and B_R, and as a result the more geometrically favoured (modified PSC testing configuration) configuration yielded closer flow stress values to those Evans and Ricks achieved in their PSC tests. However, the difference between the constitutive equations obtained by Evans and Ricks and the PSC tests on the Gleeble 3800 cannot be based solely on the different sample to anvil geometric ratios. Therefore, there is a systematic difference between the PSC test results achieved by this investigation and the PSC test results achieved by Evans and Ricks. The one logical reason for this systematic difference can be the different frictional conditions achieved at the sample and anvil interface in the two investigations.

Chapter 7

Results and Discussion of Rolling Simulation Tests

Multi-pass PSC tests were carried out on the aluminium alloy AA3104 for the modified PSC testing configuration in order to simulate the industrial hot rolling conditions that occur on the hot finishing mill at Hulamin. The results of these tests will be discussed and analysed in this chapter. The results for each PSC test that simulated the different rolling routes and conditions are included in Appendix J.

7.1 Temperature Values:

The temperature measurements for the hot rolling simulation tests were analysed for the first, second and third pass simulations. The temperature measurements of the PSC sample prior to the deformation was recorded in order to determine the temperature in the specific simulated rolling pass, as well as the temperature of the sample during the deformation. The temperature of the PSC sample is estimated as the average value between thermocouples TC1 and TC2, while the thermal gradient across the sample breadth is determined by the difference between these two values. The measured temperature of the deformation was determined from the average strain value from 0.4–0.5.

7.1.1 PSC Simulation of the First Industrial Pass

The temperature of the first simulated pass of the industrially hot rolling of the LE of the aluminium alloy AA3104 was 358 °C. The temperature values for the first pass of the rolling simulation are shown in Table 7.1. From these measured temperature values for the PSC

test that only simulated the first pass of the rolling condition, a fairly noticeable thermal gradient was present for test 2 (25.9 °C). In the PSC test that simulated all three rolling conditions, a very noticeable thermal gradient existed for both tests (47.3 and 31.4 °C). As a result, the starting temperature of the sample in both of these PSC testing simulations was not ideal for the simulation of the first industrial rolling condition, with the exception of test 1 of the PSC test that only simulated the first industrial condition. The noticeable thermal gradient would have an effect on the flow stress values as well as the microstructure. The average value with its standard error of the thermal gradient for both of the PSC test routes that encountered the first rolling condition was 30.0 ±6.7 °C.

Table 7.1: Temperature measurement of the simulated first pass of the industrial hot finishing rolling mill on the Gleeble 3800 by PSC tests that (a) only simulated the first rolling condition as well as (b) PSC tests that simulated all three of the industrial hot rolling conditions.

Hot PSC test route		$TC1_{start}$ (°C)	$TC2_{start}$ (°C)	T_{grad} (°C)	T_{start} (°C)	Temp. difference to nom. (°C)	$T_{0.4\text{-}0.5}$ (°C)	Adiabatic ΔT (°C)
(a) 1st. rolling condition	Test 1	365.3	349.8	15.5	357.6	0.4	380.6	23.1
	Test 2	357.9	332.1	25.9	345.0	13.0	366.6	21.6
(b) 1st., 2nd, 3rd rolling conditions	Test 1	357.5	310.2	47.3	333.9	24.1	359.7	25.8
	Test 2	359.8	328.4	31.4	344.1	13.9	372.5	28.4

7.1.2 PSC Simulation of the Second Industrial Pass

The temperature measurements of the second simulated rolling pass are shown in Table 7.2, where the values derived from the PSC test that simulated the second and third industrial rolling pass conditions as well as the PSC test that simulated all three of the industrial rolling conditions are shown. The temperature of the second simulated pass of the industrial hot rolling of the LE of the aluminium alloy AA3104 was 349 °C. The data as shown in Table 7.2 indicates that acceptable temperature values were achieved for both simulated PSC testing routes. There is no significant thermal gradient across the breath of the sample and, as a result, the starting temperature of the sample was within an acceptable range for the nominal rolling temperature. The average value with its standard error of the thermal gradient for both PSC tests that underwent the second rolling condition was 7.8 ±1.8 °C.

Table 7.2: Temperature measurement of the simulated second pass of the industrial hot finishing rolling mill on the Gleeble 3800 by PSC tests that (a) simulated the second and third rolling condition as well as (b) PSC tests that simulated all three of the industrial hot rolling conditions.

Hot PSC test route		$TC1_{start}$ (°C)	$TC2_{start}$ (°C)	T_{grad} (°C)	Temp. difference to nom. (°C)	T_{start} (°C)	$T_{0.4\text{-}0.5}$ (°C)	Adiabatic ΔT (°C)
(a) 2nd., 3rd rolling conditions	Test 1	349.0	338.6	10.4	5.2	343.8	374.7	30.9
	Test 2	349.0	339.8	9.2	4.6	344.4	367.8	23.4
(b) 1st., 2nd, 3rd rolling conditions	Test 1	349.0	351.3	2.3	2.3	351.3	367.6	16.3
	Test 2	349.4	358.7	9.3	9.7	358.7	377.2	18.5

7.1.3 PSC Simulation of the Third Industrial Pass

Table 7.3 demonstrates the temperature values for the simulated third pass of the hot finishing rolling conditions at Hulamin. The PSC test that simulated the second and third industrial rolling condition as well as the PSC test that simulated all three of the industrial rolling conditions are described in Table 7.3. From these values of the two PSC testing routes of the simulated third industrial hot rolling pass, acceptable temperature values were obtained within range of the nominal 262 °C. The average value of the thermal gradient with its standard error for both simulated PSC testing routes of the third rolling condition was 10.8 ±5.6 °C.

Table 7.3: Temperature measurement of the simulated third pass of the industrial hot finishing rolling mill on the Gleeble 3800 by PSC tests that (a) simulated the second and third rolling condition as well as (b) PSC tests that simulated all three of the industrial hot rolling conditions.

Hot PSC test route		$TC1_{start}$ (°C)	$TC2_{start}$ (°C)	T_{grad} (°C)	Temp. difference to nom. (°C)	T_{start} (°C)	$T_{0.4\text{-}0.5}$ (°C)	Adiabatic $\triangle T$ (°C)
(a) $2^{nd.}$, 3^{rd} rolling conditions	Test 1	273.0	268.3	4.7	8.6	270.6	295.2	24.6
	Test 2	259.0	255.6	3.43	4.7	257.3	273.0	15.7
(b) $1^{st.}$, 2^{nd}, 3^{rd} rolling conditions	Test 1	262.5	289.9	27.3	14.2	276.2	287.9	11.7
	Test 2	272.0	279.9	7.86	13.9	275.9	284.6	8.7

7.2 Equivalent Stress and Strain

The PSC test data for each deformation step of the simulated rolling passes was used to determine the equivalent stress and strain values for their respective deformation routes and conditions. The same procedural steps as explained in Section 4.2.1 were followed for each deformation pass which simulated the different rolling passes experienced in the hot finishing mill at Hulamin. The plot of the equivalent stress and strain values for all of the PSC tests which simulated the rolling scheduled passes of the hot finishing mill at Hulamin are shown in Figure 7.1. It can be seen that there is a noticeable range in the flow stress values for the first simulated pass but the other simulated passes achieved relatively good agreement. The flow stress, strain and strain rate for each simulated rolling pass are explained in this section. The flow stress values depicted for each simulated rolling pass was determined from the mean values over the strain range from 0.5–0.4, as the transient effects that influence the PSC test have been minimised, and evidently the steady state flow stress condition was met for each deformation.

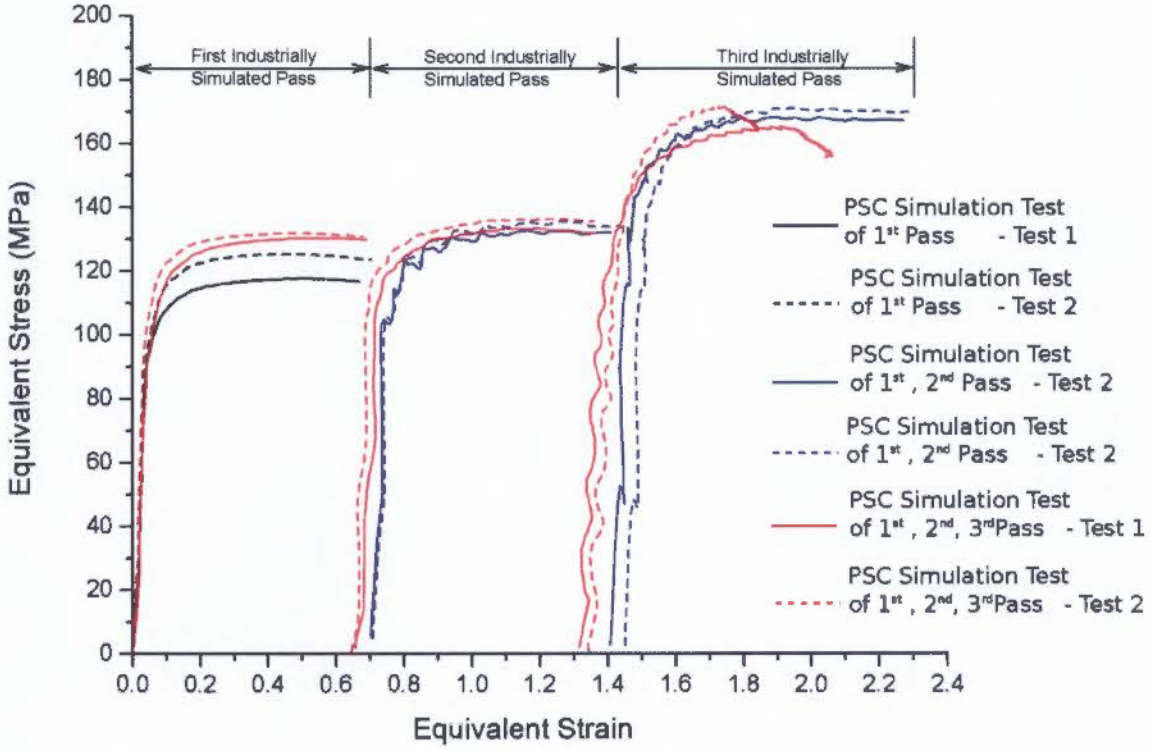

Figure 7.1: Flow stress curves of the LE of the aluminium alloy AA3104 for the PSC tests that simulate the respective different passes experienced on the hot finishing rolling mill at Hulamin.

7.2.1 PSC Simulation of the First Industrial Pass

Table 7.4 illustrates the amount of strain, average strain rate and the flow stress values of the first simulated rolling pass. In the two different PSC rolling simulated routes of the first industrial rolling condition, the strain rates achieved across board achieved acceptable values (19.6, 19.9, 19.9 and 19.5 sec^{-1}) within the nominal strain rate of 21 sec^{-1}. The nominal total strain value for the first rolling pass was 0.7 and the values of the total strain achieved for each test were also acceptable, with the exception of test 1 (strain of 0.66) for the PSC testing condition that simulated just the first pass. However, the amount of strain for this test was not widely inaccurate (0.04) and thus did not affect the mechanical testing procedure significantly. The results of the flow stress values show that there is a range of 14.4 MPa from the lowest to highest value across both simulated PSC testing routes. The reason for this can be explained by the different starting temperatures of the individual PSC tests. The average value with its standard error for the flow stress for all of the PSC tests that simulated the first rolling pass is 126.1 $\pm$3.2 MPa.

Table 7.4: Strain rate, strain and flow stress values of the simulated first pass of the industrial hot finishing rolling mill on the Gleeble 3800 by PSC tests that (a) simulated only the first rolling condition as well as (b) PSC tests that simulated all three of the industrial hot rolling conditions.

Hot PSC test route		$\dot{\varepsilon}_{whole}$ (sec^{-1})	Strain	Flow stress (MPa)
(a) $1^{st.}$ rolling condition	Test 1	19.6	0.66	117.4
	Test 2	19.9	0.7	125.3
(b) $1^{st.}$, 2^{nd}, 3^{rd} rolling conditions	Test 1	19.9	0.69	130.0
	Test 2	19.5	0.68	131.8

7.2.2 PSC Simulation of the Second Industrial Pass

The strain, strain rate and flow stresses are portrayed in Table 7.5 for the simulated PSC tests the encountered the second industrial rolling pass. The PSC tests that simulated the second and third rolling route achieved marginally higher values of the strain rate (52.1 and 54.0 sec^{-1}) in comparison to the strain rates for the PSC tests that simulated all three of the rolling routes (47.4 and 45.6 sec^{-1}). However, neither of these two PSC rolling simulation routes was able to achieve acceptable values close to those of the nominal strain rate of 77 sec^{-1} for the second hot industrial rolling pass. However, the strain rate values achieved were relatively consistent. This further confirms that the strain rate controlling software is limiting the desired strain rate values. The total amount of strain in all the tests achieved an accuracy of 0.01 to the nominal strain value, thus providing an encouraging result, as well fairly consistent values for the flow stress. This stems from the tighter tolerances achieved by the temperatures values. The results of the flow stress values indicate there is no noticeable significant difference in terms of the mechanical performance between the transfer bar material from the PSC test that simulated all three of the industrial rolling conditions and the industrial rolled strip (after the first industrial pass), which was used for the PSC test that simulated the second and third rolling route. The average value with its standard error for the flow stress for all of the simulated PSC tests that encountered the second rolling pass is 133.9 $\pm$0.8 MPa.

Table 7.5: Strain rate, strain and flow stress values of the second pass of the industrial hot finishing rolling mill on the Gleeble 3800 by PSC tests that (a) simulated the first and second rolling condition as well as (b) PSC tests that simulated all three of the industrial hot rolling conditions.

Hot PSC test route		$\dot{\varepsilon}_{whole}$ (sec^{-1})	Strain	Flow stress (MPa)
(a) $2^{nd.}$, 3^{rd} rolling conditions	Test 1	52.1	0.71	132.1
	Test 2	54.0	0.73	134.6
(b) $1^{st.}$, 2^{nd}, 3^{rd} rolling conditions	Test 1	47.4	0.71	133.0
	Test 2	45.6	0.71	135.9

7.2.3 PSC Simulation of the Third Industrial Pass

The values of the strain, strain rate and flow stress are shown in Table 7.6 for the third industrially simulated pass. Disappointing values of the strain rate for all the simulated PSC tests of the third industrial rolling pass did not achieve the values of the nominal strain rate condition of 125 sec^{-1}. The PSC that simulated the second and third rolling route was only able to achieve strain rate (54.8 and 52.1 sec^{-1}) values which are similar to what was achieved for the prior simulated second rolling passes (52.1 and 54.0 sec^{-1}). This suggests that a strain rate of the order of 50 sec^{-1} is the limit for the multi-pass simulated PSC rolling tests, this limit either being reached mechanically or electronically. Very poor values of the simulated third rolling pass of the strain rate (15 and 9.3 sec^{-1}) and strain (0.73 and 0.5) were achieved for the PSC test that simulated all three rolling passes. The explanation for the poor performance experienced during this simulated PSC testing route could be the limited amount of material remaining on the transfer bar to be deformed in the last simulated rolling pass. The PSC sample had already undergone two previous deformations (totalling to 1.42 strain) with the result that too little material remained to be accurately deformed. However, for the PSC test that simulated the second and third rolling schedule achieved acceptable values of strain (0.87 and 0.89). The flow stress values achieved for the third rolling pass are fairly consistent despite the disappointing strain and strain rate issues, however these flow stress values cannot be representative of the third rolling pass based on the poor strain rates achieved . The average value with its standard error for the flow stress for all the simulated PSC tests that encountered the third rolling pass is 167.2 $\pm$1.5 MPa.

Table 7.6: Strain rate, strain and flow stress values of the simulated third pass of the industrial hot finishing rolling mill on the Gleeble 3800 by PSC tests that (a) simulated the first and second rolling condition as well as (b) PSC tests that simulated all three of the industrial hot rolling conditions.

Hot PSC test route		$\dot{\varepsilon}_{whole}$ (sec^{-1})	Strain	Flow stress (MPa)
(a) $2^{nd.}$, 3^{rd} rolling conditions	Test 1	54.8	0.87	167.5
	Test 2	52.1	0.89	170.5
(b) $1^{st.}$, 2^{nd}, 3^{rd} rolling conditions	Test 1	15	0.73	163.4
	Test 2	9.3	0.5	167.5

7.3 Flow Stress Prediction

The flow stress values obtained in the various PSC tests that simulated the different industrial pass conditions can be compared to the predicted flow stress values of the aluminium alloy AA3104 by utilising the constitutive Equation 6.4. The constitutive equation determined for the aluminium alloy AA3104 for the modified PSC testing configuration in Chapter 6 was used to predict the steady state flow stress values for each of the simulated PSC passes

of the rolling simulation.

7.3.1 PSC Simulation of the First Industrial Pass

The predicted flow stress value for the first simulated industrial rolling pass of the aluminium alloy AA3104 was 121.8 MPa. The flow stress values for each PSC test that simulated the first rolling pass is compared to the predicted value of the flow stress as shown in Table 7.7. As the results of the first industrially simulated pass in the PSC tests show, it is evident that only the first rolling condition achieved a closer value to the predicted flow stress (4.4 and 3.5 MPa difference). This is directly due to these PSC tests having a lesser thermal gradient than the PSC tests that simulated all three of the industrial rolling routes. This highlights the importance of achieving a low thermal gradient for hot PSC testing. The mean difference with its standard error for all the PSC tests that simulated the first rolling condition is 3.5 ±2.6% (4.30 ±3.21 MPa) higher than the predicted flow stress (121.8 MPa) value. Despite the thermal gradient across the breadth of the sample, the mean flow stress determined (126.1 ±3.2 MPa) by these tests is therefore a respectable value for the first industrially simulated pass.

Table 7.7: Flow stress comparison of the predicted value of the first pass for the industrial hot finishing rolling mill simulated on the Gleeble 3800 by PSC tests that (a) simulated only the first rolling condition as well as (b) PSC tests that simulated all three of the industrial hot rolling conditions.

Flow stress prediction (MPa)		121.8		
Hot PSC test route		Flow stress (MPa)	Difference to predicted flow stress (MPa)	Difference to predicted flow stress (%)
(a) 1st. rolling condition	Test 1	117.4	4.4	3.6
	Test 2	125.3	3.5	2.9
(b) 1st., 2nd, 3rd rolling conditions	Test 1	130.0	8.2	6.7
	Test 2	131.8	10.0	8.1

7.3.2 PSC Simulation of the Second Industrial Pass

The predicted flow stress value for the second rolling pass of the aluminium alloy AA3104 was 140.6 MPa. Table 7.8 displays the difference between the predicted flow stress value and the simulated PSC tests that underwent the second industrial rolling pass. The mean difference with its standard error for all of the simulated PSC tests is 4.8 ±0.6% (6.70 ±0.84 MPa) lower than the predicted flow stress value (140.6 MPa). The mean flow stress of 133.9 ±0.84 MPa in comparison to the predicted value of the second simulated rolling pass is acceptable despite these tests not acceptably achieving the desired strain rate, hence the lower mean flow stress value.

Table 7.8: Flow stress comparison of the predicted value of the second pass for the industrial hot finishing rolling mill simulated on the Gleeble 3800 by PSC tests that (a) simulated the first and second rolling condition as well as (b) PSC tests that simulated all three of the industrial hot rolling conditions.

Flow stress prediction (MPa)		140.6		
Hot PSC test route		Flow stress (MPa)	Difference to predicted flow stress (MPa)	Difference to predicted flow stress (%)
(a) $2^{nd.}$, 3^{rd} rolling conditions	Test 1	132.1	8.5	6.0
	Test 2	134.6	6.0	4.3
(b) $1^{st.}$, 2^{nd}, 3^{rd} rolling conditions	Test 1	133.0	7.6	5.4
	Test 2	135.9	4.7	3.3

7.3.3 PSC Simulation of the Third Industrial Pass

The predicted flow stress value for the third rolling pass of the aluminium alloy AA3104 was 198.9 MPa. Similarly, for the third rolling pass simulations the difference of flow stress values to the predicted flow stress is depicted in Table 7.9. Based on the poor performance of the strain rates achieved in the PSC simulated third rolling pass, the difference of the experimental simulated flow stress values in comparison to the predicted flow stress values is therefore considerably large. The mean value with its standard error for the difference between the experimental simulation flow stress values and the predicted value is 15.9 $\pm$0.7% (31.6 $\pm$1.46 MPa) lower. It can be clearly noted that the PSC tests that simulate the third rolling pass do not represent the third rolling pass on the Hulamin hot rolling mill – this is due to the poor performance of the required strain rate.

Table 7.9: Flow stress comparison of the predicted value of the third pass for the industrial hot finishing rolling mill simulated on the Gleeble 3800 by PSC tests that (a) simulated the first and second rolling condition as well as (b) PSC tests that simulated all three of the industrial hot rolling conditions.

Flow stress prediction (MPa)		198.9		
Hot PSC test route		Flow stress (MPa)	Difference to predicted flow stress (MPa)	Difference to predicted flow stress (%)
(a) $2^{nd.}$, 3^{rd} rolling conditions	Test 1	167.5	31.4	15.8
	Test 2	170.5	28.4	14.3
(b) $1^{st.}$, 2^{nd}, 3^{rd} rolling conditions	Test 1	163.4	35.5	17.8
	Test 2	167.5	31.4	15.8

7.4 Summary

PSC tests were carried out on the Gleeble 3800 in order to simulate the hot finishing rolling conditions for the LE of the aluminium alloy AA3104 experienced at Hulamin. Three different PSC rolling simulations procedures were carried out. The three PSC rolling simulation schedules that were performed were to simulate 1) just the first rolling pass, 2)

just the second and third passes and 3) all three of the rolling passes that experienced the hot finishing mill at Hulamin. The nominal testing conditions to simulate the first rolling pass was 358 °C at a strain rate of 21 sec^{-1} to a strain of 0.7, where the conditions for the second rolling pass were 349 °C at a strain rate of 77 sec^{-1} to a strain of 0.72 and the third simulated rolling condition was 262 °C at a strain rate of 125 sec^{-1} to a strain of 0.88. The interpass time between the first and second passes was estimated as 188 seconds and the interpass time between the second and third passes was 35 seconds. The PSC simulated rolling tests were used to calculate and analyse the temperature, strain, strain rate and flow stress values in order to determine if multi-pass hot rolling conditions could be met for each industrial rolling condition.

Acceptable temperature values were achieved for the PSC simulated tests in the second and third rolling conditions. However, thermal gradients in the PSC rolling tests (average 30.0 ±6.7 °C) across the breath of the samples caused a concern about the reliability of the modified PSC testing configuration as shown by the results of the first rolling pass simulation. It is interesting to note that, once the PSC sample had been deformed by a previous simulated rolling pass, the thermal gradient across the breadth of the samples (average of 7.8 ±1.8 °C for second pass and 10.8 ±5.6 °C for the third pass) diminished significantly despite of an initial large thermal gradient established during the previously simulated rolling deformation. This can, therefore, be used for future hot PSC tests to ensure tight control of the thermal gradient – a small deformation (as long as it does not significantly influence the test) prior to heating would reduce this issue. The strain value for each simulated pass condition was met with satisfactory results, except for three consecutive deformations. This was due to the height of the sample being significantly reduced by the previous two simulated rolling passes, and thus not enough material remained to be deformed to the correct amount of strain accurately. These PSC rolling simulation tests proved that a multi-pass PSC test with up to three simulated passes totalling to strain of 2.3 cannot be achieved on the Gleeble 3800. The strain rate values achieved for each rolling simulation was only acceptably achieved for the first rolling condition. The second simulated rolling condition did not achieve the required (49.8 ±1.96 sec^{-1}) strain rate of 77 sec^{-1}. The third rolling simulation failed dismally by not achieving the nominal strain rate condition of 125 sec^{-1}. These results suggest that the upper limit of the multi-pass simulation tests of the aluminium alloys is of the order of 50 sec^{-1}.

The experimental mean flow stress values for the first, second and third simulated hot finishing rolling conditions are 126.1 ±3.2, 133.9 ±0.8 and 167.2 ±1.5 MPa, respectively. The predicted flow stress values for the first, second and third rolling conditions were calculated from the constitutive equation of the aluminium alloy determined for the modified PSC configuration. The experimental flow stress values are 3.5 ±2.6% higher, 4.8 ±0.6% and 15.9 ±0.7% lower than the predicted flow stress values for the first, second and third simulated

rolling conditions, respectively. The experimental flow stress values for the first and second rolling passes provided pleasing results with respect to the predicted values based on the constitutive equation. Despite the unfavourable thermal gradients in the first simulated rolling test and the lower than expected strain rates in the second rolling simulation test, the PSC simulation hot finishing rolling tests of the aluminium alloy AA3104 were successful for the first two rolling passes. Further optimisation of the PSC rolling simulation tests are therefore needed in order to successfully achieve the full rolling schedule and multi-pass PSC tests greater than two passes.

Chapter 8

Results and Discussion of the Polarized Light Optical Microscopy

The results derived from the PLOM of the aluminium alloy AA3104 are shown and discussed in this chapter. Micrographs of the industrially rolled AA3104, validation PSC tests and the rolling PSC simulation tests were created.

8.1 Hulamin Industrially Rolled Samples

An array of micrographs of the different industrially rolled strips of the aluminium alloy AA3104 at Hulamin were taken for each of the subsequent industrial hot finishing rolling passes in the RD and ND plane. An array of micrographs has then been digitally stitched together with the software Microsoft Image Composite Editor. These stitched micrographs are shown in Figure 8.1, showing the transfer bar (Figure 8.1a), the strip after the first pass (Figure 8.1b) and the sheet after the third pass (Figure 8.1c). The stitched micrographs allow for an overall view of the microstructure of the aluminium alloy AA3104 during the rolling passes performed on the Hulamin hot finishing mill.

The grain structure at the surfaces ($\pm$2.5 mm thick) of the transfer bar has undergone recrystallisation and grain growth with few grains achieving an equiaxed structure and the majority of the recrystallised grains aligning in the RD. The material at the centre of the transfer bar is highly deformed with very long and elongated microstructure in the RD depicting a fibrous-type structure. There is also a somewhat 'transitional' area ($\pm$ 2.5 mm thick) between the fibrous grain structure and the recrystallised surface grains. This area did not reveal the grain structure as well as the remainder of the transfer bar and this area could be due to a substantial amount of recovery. However, this cannot be confirmed by

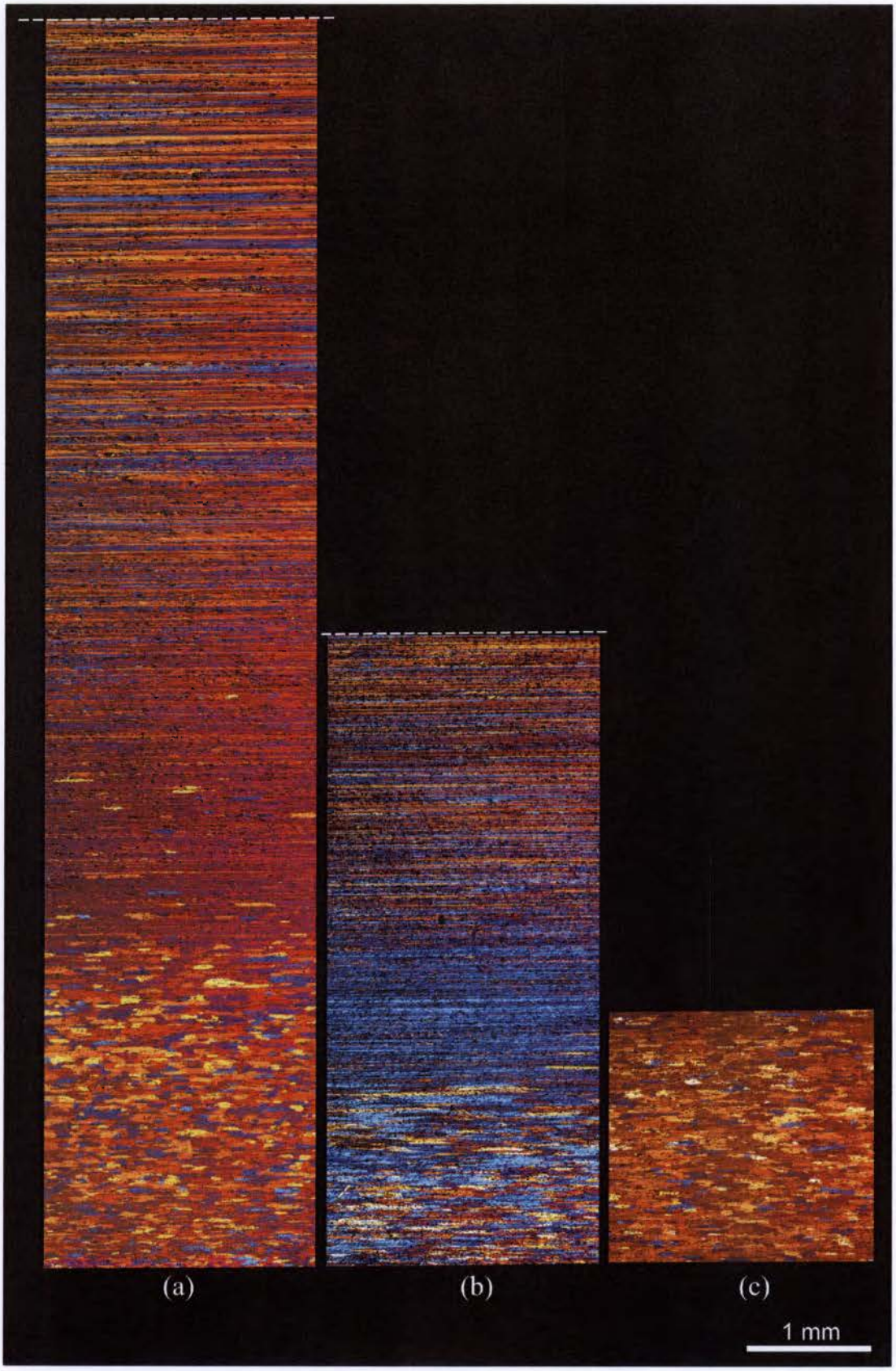

Figure 8.1: Aluminium alloy AA3104 stitched micrographs of (a) half the thickness of the transfer bar, (b) half the thickness of the first pass of the industrially rolled plate and (c) the full thickness of the third pass of the industrially rolled sheet which has undergone laboratory recrystallisation.

PLOM and an EBSD analysis would therefore be necessary to determine the structure of the 'transitional' area. Since the PSC samples used in the validation PSC test were machined from the centre region of the transfer bar, the microstructure of the validation PSC sample consists of the fibrous microstructure. The microstructure of the aluminium alloy AA3104 after the first pass on the hot finishing rolling mill at Hulamin is similar to that of the transfer bar with the fibrous microstructure at the centre of the plate, however, with a more deformed and elongated structure. The recrystallised grains on the surface of the transfer bar can now be seen as deformed and elongated in the RD (up to a depth of ± 1.4 mm) as a result after the first hot rolling pass. The PSC samples that simulated the second and third pass conditions will have the same initial microstructure as shown by Figure 8.1b. The third rolling pass on the hot finishing mill, which underwent a post-annealing heat treatment at 365 °C for three hours carried out by Hulamin [55], revealed a microstructure showing recrystallised grains throughout the whole thickness of the hot rolled sheet.

8.2 Validation PSC Samples

Similarly, an array of micrographs were stitched together in order to display the overall microstructure of the deformed validation PSC samples. The micrographs of the deformed area of the PSC samples in the ND and RD plane are shown in Figures 8.2 and 8.3 for the DSI and modified PSC testing configurations, respectively. Higher resolution micrographs of the validation PSC test samples are included in Appendix K. The micrographs of the DSI testing configuration subjected to the nominal strain rate of 10 sec^{-1} (Figures 8.2a and c) display symmetrically deformed samples and thus a symmetrical flow pattern around the centre line of the sample. The PSC sample that was subjected to the nominal testing conditions of 300 °C and 100 sec^{-1} (Figure 8.2b) reveals a slight asymmetrical deformation that had taken place and, as such, this is evident from the slightly asymmetrical flow pattern of the microstructure, and indicates that more of a heterogeneous strain distribution within the sample exists. Similarly, in the modified PSC test sample under the same nominal testing conditions (Figure 8.3b) the asymmetrical deformation flow pattern also exists, albeit, it is more prominent. It is clear that far more strain within the activated slip-lines occurred in the case of the modified PSC sample. Figure 8.3 which illustrates the PSC condition of 300 °C at 10 sec^{-1} also displays a slight asymmetrical flow pattern within the deformed area of the modified PSC sample. It can be seen, to a lesser degree of Figure 8.3b, that a fairly consistent and heterogeneous band along the middle line of the PSC samples exists in both DSI and modified PSC testing configuration.

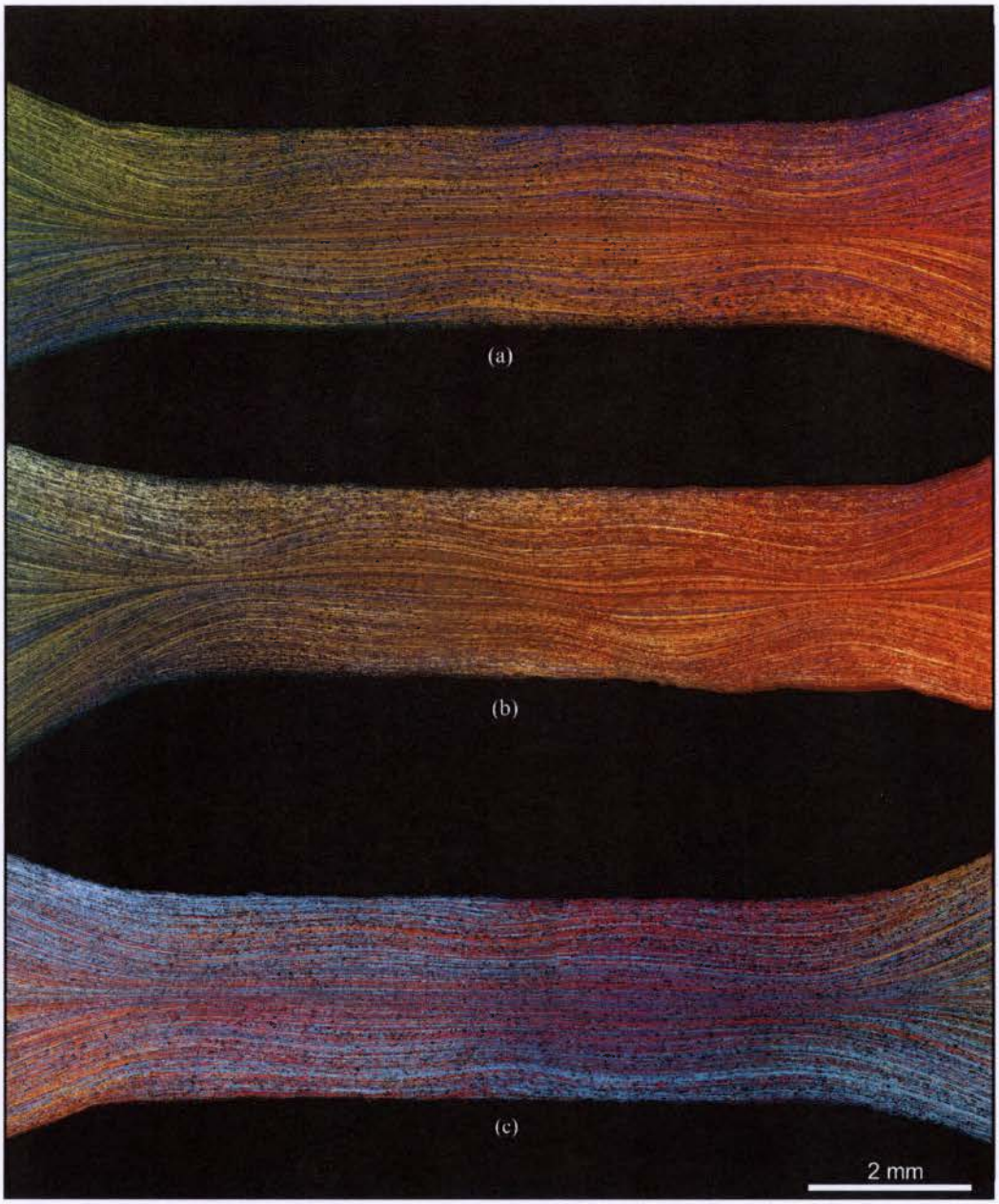

Figure 8.2: Stitched micrographs of the water-quenched DSI configured samples that have been deformed to a total strain of 1.6 under the nominal testing conditions of (a) 300 °C at 10 sec^{-1} (b) 300 °C at 100 sec^{-1} and (d) 400 °C at 10 sec^{-1}.

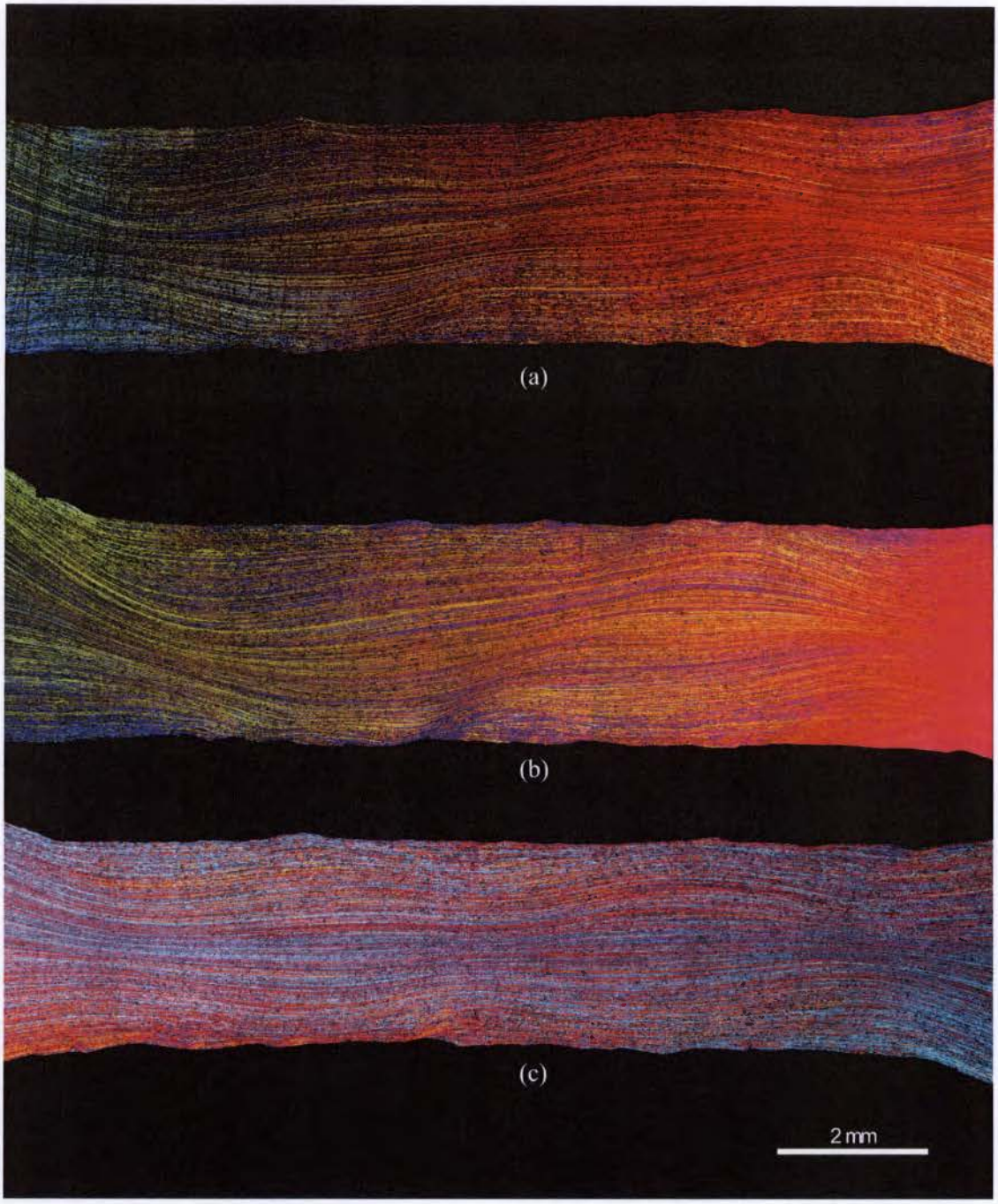

Figure 8.3: Stitched micrographs of the water-quenched modified configured PSC samples that have been deformed to a total strain of 1.6 under the nominal testing conditions of (a) 300 °C at 10 sec^{-1} (b) 300 °C at 100 sec^{-1} and (d) 400 °C at 10 sec^{-1}.

The flow pattern of the microstructure as shown in Figure 8.3c for the modified PSC testing configuration in comparison to the sample of the DSI in Figure 8.2c reveals that there is a slightly more heterogeneous flow pattern in nature than can be seen in the DSI sample. Sharper flow lines of the DSI sample are more evident at the start of the deformation area. However, the centre and middle regions of the deformation area of the DSI and modified samples are fairly similar. The DSI PSC testing configuration produces a more predictable flow stress pattern based on the consistent symmetrical deformations of

this configuration. This type of feature is, therefore, more desirable in terms of the ability to reproduce consistent microstructure. However as stated in the literature review, the research conducted by Duckham and Knusten [39] found that the comparison of the texture of the symmetric and asymmetric deformed and recrystallised samples demonstrated no significant influence on the texture evolution when only the midsection of the sample was investigated. This similar observation suggests that this could be the case for this investigation as well and that the asymmetrical PSC samples produced by the modified PSC testing configuration still allow for credible investigation. However, in order to validate this claim a quantitative comparison of the texture evolution between the two different PSC testing configurations would necessarily have to be performed. Microstructural analysis, such as EBSD, can perform this study; however this is beyond of the scope of this investigation.

The micrographs as shown in Figures 8.2 and 8.3 suggest that no recrystallisation took place during the deformation. This was expected as aluminium alloys prominently undergo dynamic recovery during TMP illustrated by the characteristic steady state recovery flow stress curves produced in below in this Chapter 6. These optical microstructural observations provide no evidence that the PSC testing conditions influence the flow structure of the material. The only influencing aspect on hot PSC testing is the geometric testing configuration and whether the sample has been deformed symmetrically or not.

8.3 Rolling Simulation Samples

The array of micrographs taken of the rolling simulated PSC samples in the ND and RD plane were stitched in order to produce an overall microstructural evaluation. The micrograph of the PSC rolling simulation test that mimicked the hot finishing rolling condition during the first pass is shown in Figure 8.4, and the simulated hot rolling condition in the second and third passes is shown in Figure 8.5. The PSC test that simulated all three passes on the hot finishing rolling mill is shown in Figure 8.6. From all of the different PSC tests that simulated the different aspects of the hot finishing rolling conditions, a relatively symmetrical flow pattern is noticeable. A relatively symmetrical flow pattern is noticeable on examination of all the different PSC tests that simulated the different aspects of the hot finishing rolling conditions. A noticeable aspect of the sample of the PSC test that simulated the second and third pass conditions on the hot finishing mill is that large surface grains as shown in Figure 8.1b are clearly seen at the surface of the PSC sample, shown in Figure 8.5. These more noticeable grains highlight the 'dead zone' that exists during PSC tests: this is the area between the slip-line 'crosses' formed during deformation. There is very little deformation of the material within the 'dead zone',

and this is clearly shown by the preservation of the larger surface grains after two multi-pass PSC simulated rolling tests. This phenomenon demonstrates that the midsection of the deformation zone of PSC tests should be the investigated area due to the homogeneity of local strain occurring outside of this section. In all three PSC tests that simulated the various tested rolling passes, the micrographs reveal no evidence of recrystallisation within the deformed area. However on further observation of the PSC test that simulated all three rolling conditions, recrystallisation on the surface of the sample was evident in the case of material outside the deformation area. The section is found in the 'transitionary' area on the sloped section, as illustrated by Figure 8.7, which is between the undeformed section of the sample's shoulders and the deformed PSC area. The recrystallised grains are up to a depth of 400 μm from the surface as is evident in Figure 8.7. This suggests that the recrystallisation process took place during the time between the second and third simulated interpass times. It is promising that recrystallisation occurred at the surface of the sample as this behaviour is similar to the behaviour as shown by the surface recrystallisation of the transfer bar. The internal energy imposed on the sample from the subsequent rolling processes coupled with the interpass times at high temperatures allow for recrystallisation to occur in the aluminium alloy AA3104. Higher resolution images of rolling simulated PSC test samples are included in Appendix K.

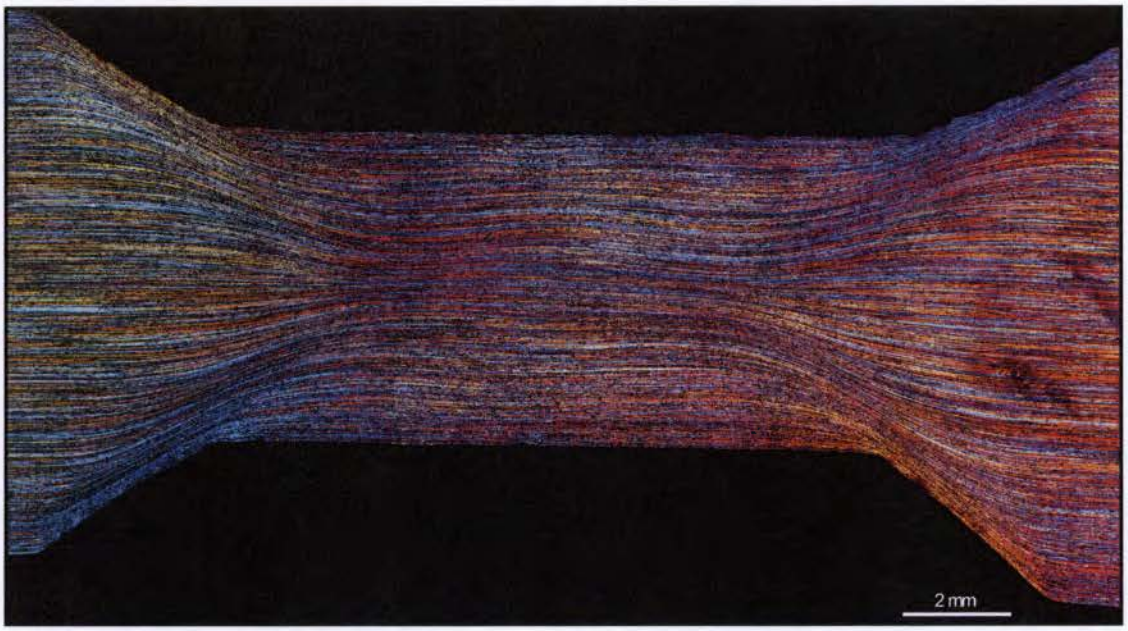

Figure 8.4: Micrograph of the transfer bar that has been subjected to the first pass of the simulated PSC rolling test.

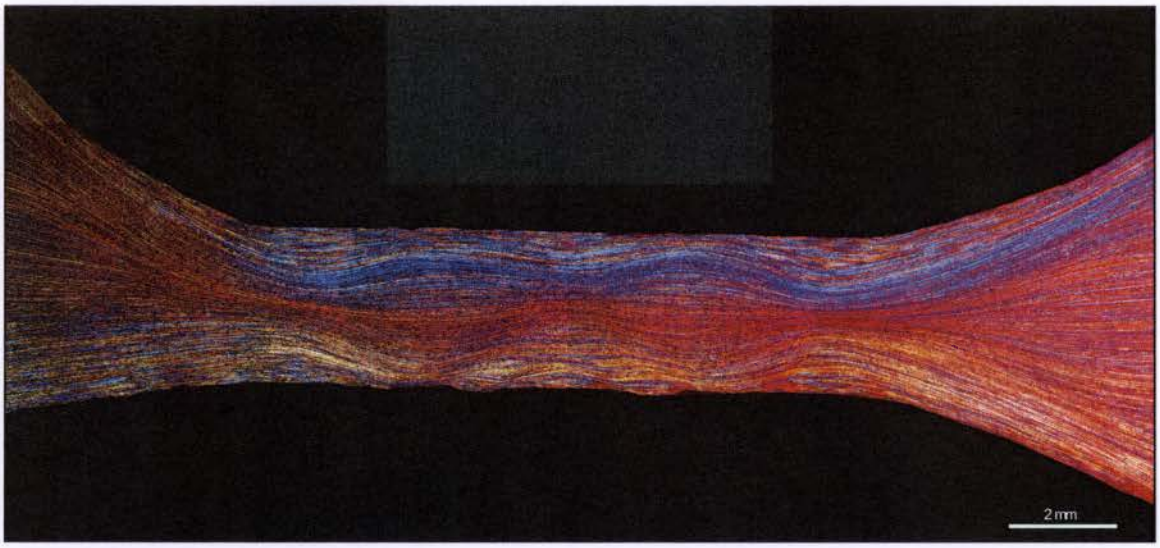

Figure 8.5: Micrograph of the first pass industrially rolled strip that was subjected to the second and third passes of the simulated PSC rolling test.

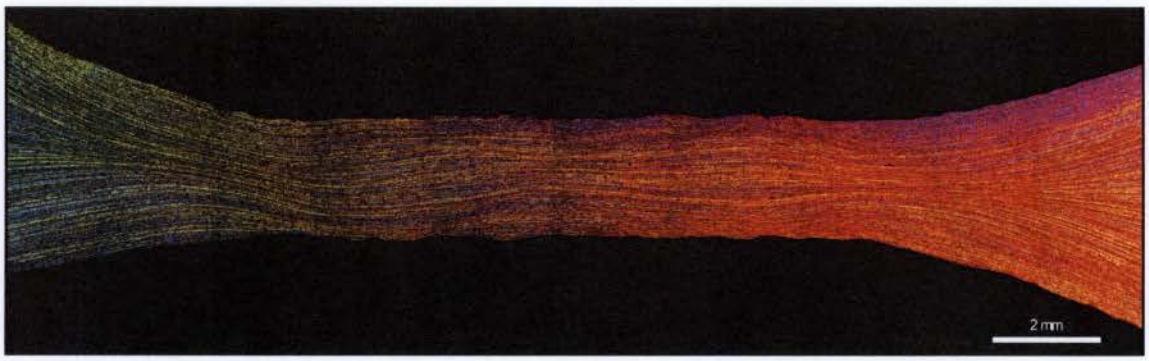

Figure 8.6: Micrograph of the transfer bar that was subjected to all three of the simulated PSC simulated rolling tests.

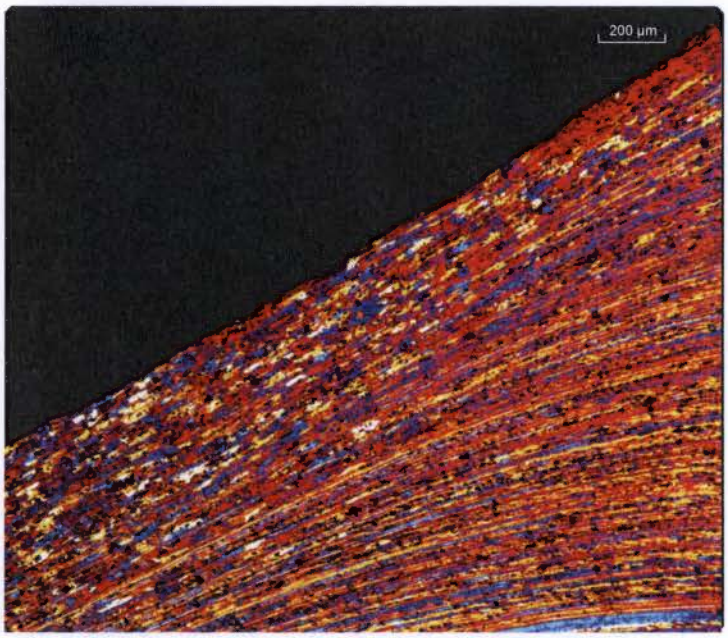

Figure 8.7: Recrystallised structure occurring at the surface of the PSC sample that has undergone all three passes of the PSC simulated rolling tests.

8.4 Summary

PLOM was performed on the aluminium alloy AA3104 in the RD and ND orientation of the industrially rolled material as well as on PSC samples. The industrially rolled samples of the aluminium alloy AA3104 investigated were the transfer bar, the strip after the first hot finishing rolling pass and the sheet (post rolling laboratory heat treatment) after the full hot finishing rolling schedule. The PSC samples investigated were from the validation PSC tests and the PSC rolling simulation tests. After the validation PSC tests, samples of the testing conditions at 300 °C at 10 sec^{-1}, 300 °C at 100 sec^{-1} and 400 °C at 10 sec^{-1} for both the DSI and modified PSC testing configurations were investigated. The PLOM of this investigation were used to stitch a series of micrographs in order to reveal the overall microstructure and the microstructural flow. The PLOM of the PSC tests that simulated the rolling conditions were investigated in the case of the samples that represented the rolling conditions during the second and third rolling passes only, and all three rolling conditions on the hot finishing rolling mill at Hulamin.

The results of the industrially rolled samples of the transfer bar and the first industrially rolled sheet show that the majority of the microstructure is fibrous in nature with high levels of elongation along the RD as well as recrystallised grains at samples surfaces. Furthermore the validation PSC tests indicated that there is no immediate significant difference in the microstructural flow lines of the material within the middle and centre sections of the deformed area of the PSC sample. However, there is slightly more

heterogeneity of the strain distribution in the DSI sample at the starting section of the deformed area. In the samples that were deformed asymmetrically, the asymmetrical flow lines were more prominent in the modified PSC samples as the modified PSC samples have a higher tendency to deform more asymmetrically. Where PSC samples are highly deformed asymmetrically, the majority of the strain occurs within one of activated slip-lines – the midsection of the sample does not display the same amount of asymmetry as experienced in the material outside the middle section of the sample. It appears that there is little noticeable significant difference between the microstructure of the sample of the DSI and modified PSC samples within the midsection of the deformed samples. However, it is necessary to carry out further analysis in order to quantify the differences that may exist between the two different testing configurations. Concern about the noticeable thermal gradient and lower temperature control in the modified PSC samples leads to the belief that this will also influence the microstructure and thus a different microstructure in comparison to the DSI sample will exist for the same condition. This, however, will also need to be investigated further. Fairly symmetrical microstructural flow lines were achieved under the different simulated rolling conditions in the PSC rolling simulation tests. Isolated recrystallisation on the surface of the PSC sample outside the deformation zone occurred during the PSC test that was subjected to the full hot finishing rolling PSC simulation test. The recrystallisation occurred during the interpass time between the second and third simulated rolling pass. Further microstructural techniques need to be performed to quantify the microstructure of the PSC samples, especially the texture and form of the various PSC tests and simulations.

Chapter 9

Conclusions

Based from the literature and experimental work of this investigation, a number of conclusions can be made. This investigation can be split and viewed as two broad sections, 1) the hot PSC tests of the aluminium alloy AA3104 carried out on the Gleeble 3800 thermomechanical testing machine and 2) tbe PLOM observations of the hot PSC tested samples.

9.1 Hot PSC Tests

9.1.1 Single Deformation PSC Tests

Single deformation hot PSC tests on the aluminium alloy AA3104 was carried out for three different temperature (300, 350 and 400 °C) and three different strain rate (10, 30 and 100 sec^{-1}) conditions. In addition two different anvil and sample testing geometries were investigated at the aforementioned temperature and strain rate conditions. The standard geometric testing configuration recommended by DSI has a $B_R = 3$ and $H_R = 1$, where the modified testing configuration achieved more favourable testing geometric ratios, with the $B_R = 4.62$ and $H_R = 1.3$. From these series of tests, it can be concluded that:

- The temperature control of the PSC sample for both of the DSI and modified PSC testing configuration proved to achieved acceptable values for all three of the temperature testing conditions. The DSI testing configuration, however proved to provide better temperature control in comparison to the modified configuration, as demonstrated by the thermal gradient achieved across the samples breadth. The average thermal gradient with its standard error achieved for the DSI and modified testing configuration is 4.1 ±0.8°C and 19.2 ±4.0°C respectively.

- The temperature measurement of the adiabatic temperature rise due to the deformation of heating was successfully determined for both of the testing configurations for all of the temperature and strain rate conditions testing in this investigation. The DSI and modified testing geometries did not effect the adiabatic temperature rise and similar values were achieved across all of the testing conditions.

- Acceptable, successful and repeatable strain rate values for both testing configurations were achieved by PSC testing on the aluminium alloy AA3104 on the Gleeble 3800 for the nominal strain rate conditions of 10 and 30 sec^{-1}. It was found that there is no significant influence difference between the DSI and modified PSC testing configurations on the strain rate response.

- An average strain rate of 86.1 $\pm$3.22 sec^{-1} was achieved by the Gleeble 3800 for the 100 sec^{-1} nominal condition, this value is therefore the upper limit strain rate condition that can be achieved for single hot PSC tests of the aluminium alloy AA3104.

- Repeatable flow stress values were obtained for both testing configurations over the the temperature and strain rate testing conditions. The DSI testing configuration achieved slightly better consistent and repeatable flow stress values to the modified testing configuration due to the better temperature control for this configuration. However, the lower temperature control for the modified PSC tests did not significantly effect the flow stress result, and it is acceptable.

- The modified PSC testing configuration achieved a consistently higher flow stress value to the DSI configuration of the aluminium alloy AA3104 for each temperature and strain rate testing condition. A small but significantly higher value of 3.48 $\pm$1.2 MPa (2.7 $\pm$1.2%) on average was achieved by the modified PSC testing configuration resulting closer values to to work of Evans and Ricks [49]. This small but significant difference of flow stress values between the DSI and modified PSC testing configuration are of a result from the different B_R and H_R employed for each testing configuration.

- While the modified PSC testing configuration achieved more representative flow stress value for the aluminium alloy AA3104, the use of this testing configuration is not as practical as the DSI testing configuration. The temperamental behaviour of the temperature gradient set up across the samples breadth for the modified PSC testing configuration does not provide confidence during the testing procedure, causing possible needed retests. This testing configuration is therefore not recommended based on the unreliable thermal gradient control.

- Constitutive equations of the aluminium alloy AA3104 have been successfully determined for each testing configuration in the form of $\dot{\varepsilon}\left(\frac{Q_{def}}{RT}\right) = A\exp(\beta\sigma)$. The

material constant β value determined from both of the testing configurations revealed no significant difference between the DSI and modified PSC testing configuration, however based from the small but significant difference of the flow stress values between the two testing configurations, a significant difference (37.0%) between the A value is established.

- The constitutive equation determined of the aluminium alloy AA3104 determined from the DSI testing configuration is $\dot{\varepsilon}\left(\frac{Q_{def}}{RT}\right) = 28.5 \times 10^8 \exp(0.095\sigma)$, and the constitutive equation determined by the modified PSC testing configuration is $\dot{\varepsilon}\left(\frac{Q_{def}}{RT}\right) = 19.6 \times 10^8 \exp(0.092\sigma)$.

- The Gleeble 3800 is a very capable thermomechanical testing machine for the use of hot PSC tests of aluminium alloys. Consistent, reliable and credible results are able to be extracted with the correct use of the Gleeble 3800 within its boundaries as a PSC testing machine.

9.1.2 Multi-Pass PSC Test

Multi-pass PSC tests were performed in order to simulate different hot rolling scheduled passes of the LE of the aluminium alloy AA3104 experienced on hot finishing rolling mill at Hulamin. Three stages of multi-pass PSC tests were carried out, where they simulated: just the first rolling pass, the first and second rolling pass and all three of the rolling passes experienced on the hot finishing rolling mill at Hulamin. The hot rolling PSC simulation tests simulated the temperature, strain, strain rate and interpass times which are found on the hot finishing mill at Hulamin. From these series of tests, the following can be concluded:

- The multi-pass PSC tests revealed that the modified PSC testing configuration is an inconstant configuration in terms of temperature reliability and control. While acceptable thermal gradients were achieved for the multi-pass tests that simulated the second (average 7.8 ±1.8°C) and third (average 10.8 ±5.6 °C) rolling pass, inconsistent and unacceptable values of the thermal gradient was achieved for the first simulated pass (average 30.0 ±6.7 °C). However, the thermal gradient across the samples breadth diminishes significantly with prior deformation of the sample and thus allowing for far greater and acceptable temperature control

- Up to two multi-pass PSC tests can successfully deform the aluminium alloy AA3104 to the desired amount of strain, either it being to simulate the first and second pass (strain total of 1.42) or the second and third (pass strain total of 1.6). Due the limited amount of remaining material after two multi PSC tests, three multi-pass PSC tests cannot be used to successfully simulate the full rolling deformation schedule (strain

total of 2.3) as experienced on the Hulamin hot finishing rolling of the aluminium alloy AA3104.

- The upper limit of the strain rate for multi-pass PSC tests of the aluminium alloy is 50 sec^{-1}, and as a result the strain rate conditions for the second and third hot rolling finishing pass could not be met. It is not recommend to exceed the strain rate of 50 sec^{-1} for multi-pass hot PSC tests of aluminium.
- The derived constitutive equation of the aluminium alloy AA3104 for the modified PSC testing configuration provides pleasing flow stress predictions when acceptable testing conditions are met.

9.2 Polarized Light Optical Microscopy

PLOM was carried out in the RD and ND orientation of the industrially rolled aluminium alloy AA3104 and laboratory deformed PSC samples in order to obtain the overall microstructural representation and the microstructural flow of the investigated sample. From the obtained results, the following can be concluded:

- The modified PSC testing configuration yields a higher chance by producing asymmetrical PSC testing samples, this results in more of a heterogeneous strain distribution of the deformed sample. However, by only taking the middle centre region into consideration this effect does not drastically influence the microstructural flow of the material.
- The microstructural flow of the deformed material are all similar in nature about the centre line and middle section of deformed PSC sample for both of the DSI and modified PSC samples of the single PSC validation tests across all testing temperature and strain rate conditions.
- The rolling simulation PSC tests displayed no evidence of recrystallization within the deformed area of the PSC samples, however evidence of localised recrystallised grains outside of the deformation area between the shoulder of the sample suggests that recrystallisation of AA3104 occurs during the interpass time during the hot finishing rolling mill.

Chapter 10

Future Work and Recommendations

From the results and conclusions of this investigation, further future work and recommendations for hot PSC testing on the Gleeble 3800 can be carried out in order to expand further testing capabilities. In addition, future microstructural scope is available based from the initial findings of this investigation. It is, therefore, recommended that future work can be carried out:

- Additional testing geometries should be investigated in order to achieved the best balance of testing reliability and favourable geometric PSC testing ratios. From this investigation, achieving a favourable H_R is more advantageous than a B_R if microstructural analysis is performed at half of the samples breadth. Hence, an investigation with B_R value of 4 and a H_R value 1.5 should be considered.
- A further in depth microstructural study on this investigation's PSC samples produced from the DSI and modified configuration should be further investigated. It would be interesting determine a quantitative difference between the two testing configurations
- A variety of different lubricants should be investigated for hot PSC testing and the affect each different lubricant has.
- Automated software program that processes the relevant PSC data post deformation and this should be implemented into the existing Gleeble 3800 set up.
- An investigation into improving the high strain rate capabilities (>50 sec^{-1}) for PSC tests. This investigation should be investigated on the Gleeble 3800 for different materials and geometries.
- An investigation in order to successfully achieve a three multi-pass hot finishing PSC rolling simulation that achieves all of necessary rolling conditions that are experienced at Hulamin for the aluminium alloy AA3104. A microstructural study

can then be investigated to study the effect of the different rolling conditions (interpass time, temperature, strain rate and strain) have on the formed textures. The microstructural study can also continue to determine what textures are formed on the rolling mill in comparison to the simulated PSC rolling tests.

- It is recommended that the DSI testing configuration should be used as the standard PSC testing configuration, until a more suitable and reliable configuration is developed.

List of References

[1] Sayers Publishing Group Ltd., "Frequently Asked Questions," 2014. [Online]. Available: http://www.canmaker.com/news/latestnews/faqs

[2] Rexam, "Overview: global beverage can market," 2014. [Online]. Available: http://www.rexam.com/index.asp?pageid=246

[3] Nampak Limited, "Intergrated Annual Report 2013," Nampak Limited, South Africa, Tech. Rep., 2013. [Online]. Available: http://www.nampak.com/DynamicData/AnnualReport/Current/NampakIAR2013.pdf

[4] N. Odendaal, "SA follows global trend in move to all-aluminium cans," *Engineering News*, Nov. 2012.

[5] Collect a Can, "March 2013 - Collect-a-Can is turning 20!" 2013. [Online]. Available: http://www.collectacan.co.za/index.php/press-office-25

[6] D. Faku, "Hulamin invests in recycling," *Cape Times*, p. 24, 2014.

[7] S. de Ryhove, "Conversion to aluminium beverage cans to facilitate job creation," *Creamer Media*, Oct. 2013.

[8] Hulamin Limited, "Intergrated annual report 2013," Hulamin Limited, Tech. Rep., 2013. [Online]. Available: http://hulamin.co.za/iar2013/overview_feature_aluminium.html

[9] K. R. Van Horn, *Aluminum Vol.I. Properties, Physical Metallurgy and Phase Diagrams*. Materials Park, Ohio: American Society for Metals, 1967.

[10] O. Ryen, O. Nijs, E. Sjölander, B. Holmedal, H. Ekström, and E. Nes, "Strengthening Mechanisms in Solid Solution Aluminum Alloys," *Materials Transactions A*, vol. 37, no. June, pp. 1999–2006, 2006.

[11] "Alumatter." [Online]. Available: http://aluminium.matter.org.uk/

[12] The Aluminum Association, "International Alloy Designations and Chemical Composition Limits for Wrought Aluminum and Wrought Aluminum Alloys," Arlington, 2009.

[13] F. King, *Aluminium and Its Alloys*. Chichester: Ellis Horwood Limited, 1987.

[14] E. Howard, Boyer, and L. Timothy, *Metals Handbook*. Materials Park, Ohio: American Society for Metals, 1985.

[15] Hulamin Limited, "Hulamin - All Trials Rev 1," Tech. Rep., 2012.

[16] F. Humphreys and M. Hatherly, *Recrystallization and Related Annealing Phenomena*. Oxford, OX, UK: Pergamon, 2004.

[17] W. F. Hosford, *Physical Metallurgy*, 2nd ed. London: CRC Press - Taylor & Francis, 2010.

[18] J. E. Hatch, *Aluminum: Properties and Physical Metallurgy*. Materials Park, Ohio: American Society for Metals, 1984.

[19] J. M. Buchanan, "Determination of Thermo-Mechanical Variables During Plane Strain Compression Testing," MSc Thesis, University of Cape Town, 2002.

[20] I. Polmear, *Light Alloys From Taditional Alloys to Nanocrystals*, 4th ed. Oxford: Elsevier/Butterworth-Heinemann, 2006.

[21] C. Zener and H. J. H, "Effect of Strain Rate Upon Plastic Flow of Steel," *Journal of Applied Physics*, vol. 15, p. 22, 1944.

[22] G. E. Dieter, H. A. Kuhn, and S. L. Semiatin, *Handbook of Workability and Process Design*. Materials Park, Ohio: American Society for Metals, 2003.

[23] M. Mostafaei and M. Kazeminezhad, "A Novel Approach to Find the Kinetics of Dynamic Recovery Based on Hot Flow Curves," *Materials Science and Engineering: A*, vol. 544, pp. 88–91, May 2012.

[24] Q. Guo-zheng, "Characterization for Dynamic Recrystallization Kinetics Based on Stress-Strain Curves," in *Recent Developments in the Study of Recrystallization*, 1st ed., P. Wilson, Ed. InTech, 2013, pp. 61 – 64.

[25] J. J. Jonas, C. M. Sellars, and W. J. M. Tegart, "Strength and Structure Under Hot-Working Conditions," *International Materials Reviews*, vol. 14, no. 1, pp. 1–24, 1969.

[26] O. Daaland and E. Nes, "Origin of Cube Texture During Hot Rolling of Commercial Al-Mn-Mg Alloys," *Acta Materialia*, vol. 44, no. 4, pp. 1389–1411, 1996.

[27] E. Orowan, "The Calculation of Roll Pressure in Hot and Cold Flat Rolling," *Proceedings of the Institution of Mechanical Engineers*, vol. 150, pp. 140–167, 1943.

[28] N. J. Silk and M. R. van der Winden, "Interpretation of Hot Plane Strain Compression Testing of Aluminum Specimens," *Materials Science and Technology*, vol. 15, pp. 295–300, 1999.

[29] H. Ford, "Researches into the Deformation of Metals by Rold Rolling," *Proceedings of the Institution of Mechanical Engineers*, vol. 159, pp. 115–143, 1948.

[30] S. M. Rehlaendar, "Plane Strain Compression of Aluminum Alloy 6061," MSc Thesis, The University of British Columbia, 1994.

[31] R. Hill, E. H. Lee, and S. J. Tupper, "A Method of Numerical Analysis of Plastic Flow in Plane Strain and its Application to the Compression of a Ductile Material Between Rough Plates," *The American Society of Mechanical Engineers Transactions, Journal of Applied Mechanics*, vol. 18, pp. 44–52, 1951.

[32] A. P. Green, "A Theoretical Investigation of the Compression of a Ductile Material Between Smooth Flat Dies," *Philosophical Magazine*, vol. 42, no. 331, pp. 900–918, 1951.

[33] J. H. Beynon and C. M. Sellars, "Strain Distribution Patterns During Plane Strain Compression," *Journal of Testing and Evaluation*, vol. 13, pp. 28–38, 1985.

[34] R. Colas and C. M. Sellars, "Strain Distribution and Temperature Increase During Plane Strain Compression Testing," *Journal of Testing and Evaluation*, vol. 15, pp. 342–349, 1987.

[35] M. S. Mirza and C. M. Sellars, "Modelling the Hot Plane Strain Compression Test Part 1 - Effect of Specimen Geometry, Strain Rate and Friction on Deformation," *Materials Science and Technology*, vol. 17, pp. 1133–1141, 2001.

[36] ——, "Modelling the Hot Plane Strain Compresion Test Part 2 - Effect of friction and Specimen Geometry on Spread," *Materials Science and Technology*, vol. 17, pp. 1142–1148, 2001.

[37] ——, "Modelling Hot Plane Strain Compression Tests Part 3 - Effect of Asymmetric Conditions," *Materials Science and Technology*, vol. 23, pp. 567–576, 2001.

[38] A. J. Lacey, "Interaction of Testing Machine Characteristics and Specimen Geometry in Plane Strain Compression Testing," MPhil Thesis, University of Sheffield, 2003.

[39] A. Duckham and R. Knutsen, "Asymmetric Flow During Plane Strain Compression Testing of Aluminum Alloys," *Materials Science and Engineering: A*, vol. 256, pp. 220–226, Nov. 1998.

[40] A. Duckham, "The Formation of Copper Type Shear Bands in Al-1Mg and their Influence on Recrystallization Behaviour," Ph.D. dissertation, University of Cape Town, 1998.

[41] M. S. Loveday, G. J. Mahon, B. Roebuck, A. J. Lacey, E. J. Palmiere, C. M. Sellars, and M. R. van der Winden, "Measurement of the Flow Stress in Hot Plane Strain Compression Tests," *Materials at High Temperature*, vol. 23, pp. 85–118, 2006.

[42] C. M. Sellars, J. P. Sah, J. H. Beynon, and S. R. Foster, "Report on the Research Work Supported by SRC Grant B/RG/1481," University of Sheffield, Tech. Rep., 1976.

[43] H. Shi, A. J. McLaren, C. M. Sellars, R. Shahani, and R. Bolingbroke, "Hot Plane Strain Compression Testing of Aluminum Alloys," *Journal of Testing and Evaluation*, vol. 25, pp. 61–73, 1997.

[44] N. J. Silk, "Derivation of Friction Equations for Plane Strain Compression testing," University of Sheffield, Tech. Rep., 1997.

[45] R. J. Hand, S. R. Foster, and C. M. Sellars, "Temperature Chamges During Hot Plane Strain Compression Testing," *Materials Science and Technology*, vol. 16, pp. 442–450, 2000.

[46] S. B. Davenport, N. J. Silk, C. N. Sparks, and C. M. Sellars, "Development of Constitutive Equations for Modelling of Hot Rolling," *Materials Science and Technology*, vol. 16, pp. 539–546, 2000.

[47] W. J. M. Tegart and C. M. Sellars, "No Title," *Mém. Sci. Rev. Métall.*, vol. 63, pp. 731–746, 1966.

[48] B. Kowalski, A. J. Lacey, and C. M. Sellars, "Correction of Plane Strain Compression Dara for the Effects of Inhomogeneous Deformation," *Material Science and Technology*, vol. 19, pp. 1564–1570, 2003.

[49] P. Evans and R. Ricks, "TSC REPORT: TR11-121 Plane Strain Compression Testing of Hulamin AA3104," Technology Strategy Consultants, Warwickshire, United Kingdom, Tech. Rep. November, 2011.

[50] H. Sofuoglu, H. Gedikli, and J. Rasty, "Determination of Friction Coefficient by Employing the Ring Compression Test," *Journal of Engineering Materials and Technology*, vol. 123, no. 3, p. 338, 2001.

[51] M. Kunogi, "A New Method of Cold Extrusion," *Journal of the Scientific Research Institute*, vol. 50, pp. 215–246, 1956.

[52] A. T. Male and M. G. Cockcroft, "A Method for the Determination of the Coefficient of Friction of Metals under Condition of Bulk Plastic Deformation," *Journal of the Institute of Metals*, vol. 93, 1965.

[53] L. Li, D. Peng, J. Liu, and Z. Liu, "An Experiment Etudy of the Lubrication Behavior of Graphite in Hot Compression Tests of Ti-6Al-4V Alloy," *Journal of Materials Processing Technology*, vol. 112, pp. 1–5, May 2001.

[54] B. Avitzur, "Forging of Hollow Disks," *Israel Journal of Technology*, vol. 9, pp. 295–304., 1964.

[55] F. Vlok, "Private Communications," 2014.

[56] G. E. Dieter, *Mechanical Metallurgy*. New York: McGraw-Hill Book Company, 1961.

[57] Dynamic Systems Incorporated, "Gleeble 3800 System," 2014. [Online]. Available: http://gleeble.com/index.php/products/gleeble-3800.html

[58] ——, "Hydrawedge," 2014. [Online]. Available: http://gleeble.com/index.php/products/mcu.html

[59] L. Li, D. Peng, J. Liu, Z. Liu, and Y. Jiang, "An Experimental Study of the Lubrication Behavior of A5 Glass Lubricant by means of the Ring Compression Test," *Journal of Materials Processing Technology*, vol. 102, pp. 138–142, May 2000.

[60] L. Cheng, H. Chang, B. Tang, H. Kou, and J. Li, "Characteristics of Metadynamic Recrystallization of a High Nb Containing TiAl alloy," *Materials Letters*, vol. 92, pp. 430–432, Feb. 2013.

[61] B. Roebuck, M. Brooks, and M. Gee, "Load Cell Ringing in High Rate Compression Tests," 2002.

Appendices

Appendix A: Technical Drawings

- Evans and Ricks PSC sample technical drawing [49]
- Recommended DSI sample technical drawing
- Ring compression tests technical drawings
- Modified PSC configuration technical drawings
- Standard DSI anvil technical drawing machined from K460 Böhler steel

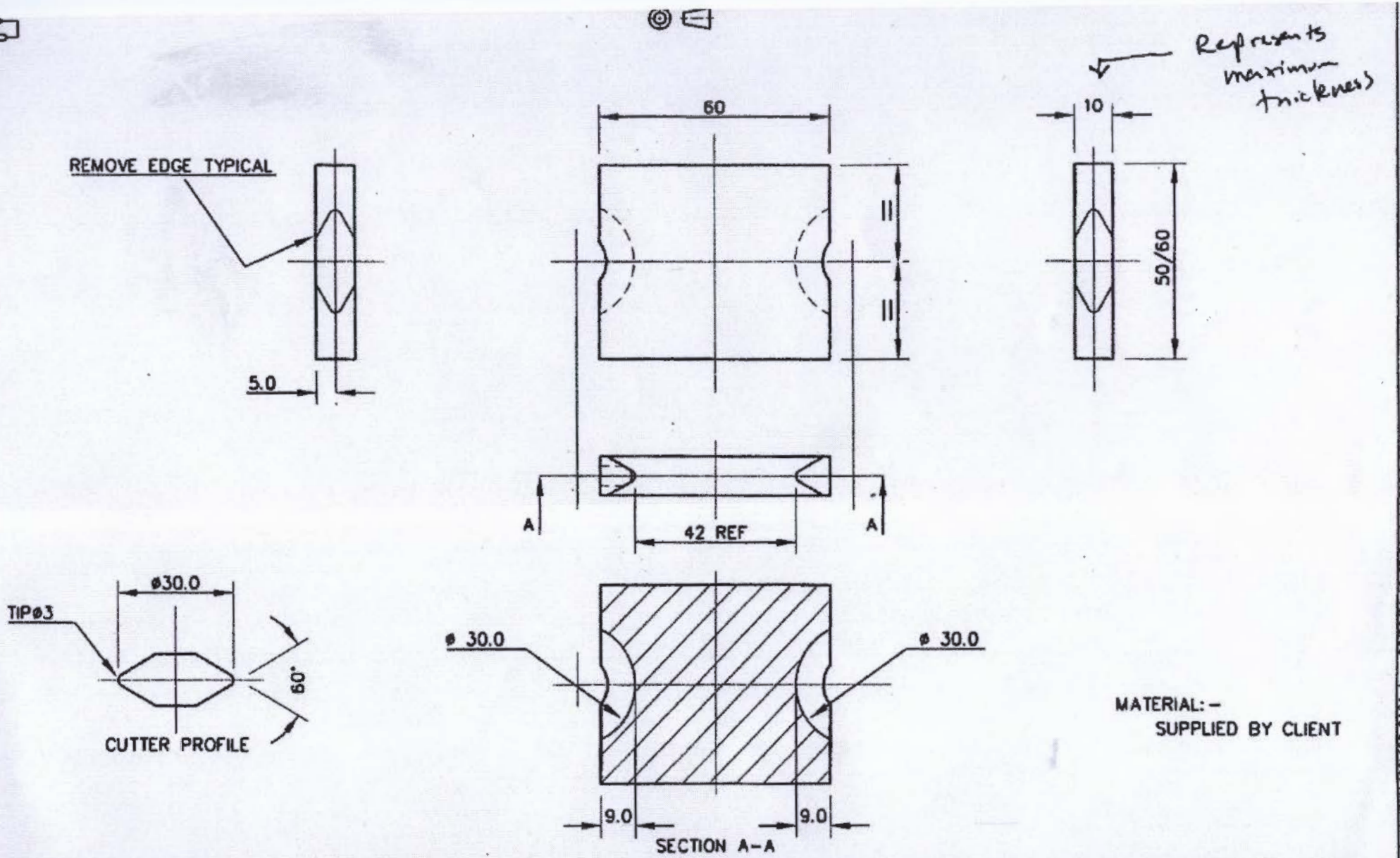

MATERIAL:-
SUPPLIED BY CLIENT

GEOMETRIC CHARACTERISTIC SYMBOLS

maximum material condition	perpendicularity
runout	parallelism
flatness of a surface	concentricity
straightness of a line	symmetry
profile of a surface	angularity
profile of a line	roundness
true position	basic dimension
cylindricity	datum

FEATURE CONTROL SYMBOL

total tolerance diameter | datum reference

geometric characteristic symbol

tolerance in mms. or inches

Form positional tolerances & related datum are regardless of feature size unless specified.

ISSUE	DATE		JOB No	DRAWN
1	17-4-01	ORIGINAL ISSUE	61141	T.RINTS

All Dimensions in millimetres & refer to finished sizes
Tolerances:-
No decimal places ±0.4
One decimal place ±0.1
Angular ±0.5°
Squareness 0.1 per 100mm
hole depths to drill point
Surface texture 3.2um
Remove all burrs & break sharp edges rad 0.1/0.5 unless otherwise stated

SERVOTEST© 2000

TITLE: PLAIN STRAIN SPECIMEN

MATERIAL SEE ABOVE		FINISH
DATE 17-4-01	SCALE 1:1	DRW.No. D603-2181
DRN T.RINTS	CHKD.	

M:\603\603-2181.dwg, 25/09/01 12:39:31, 1:1.37276

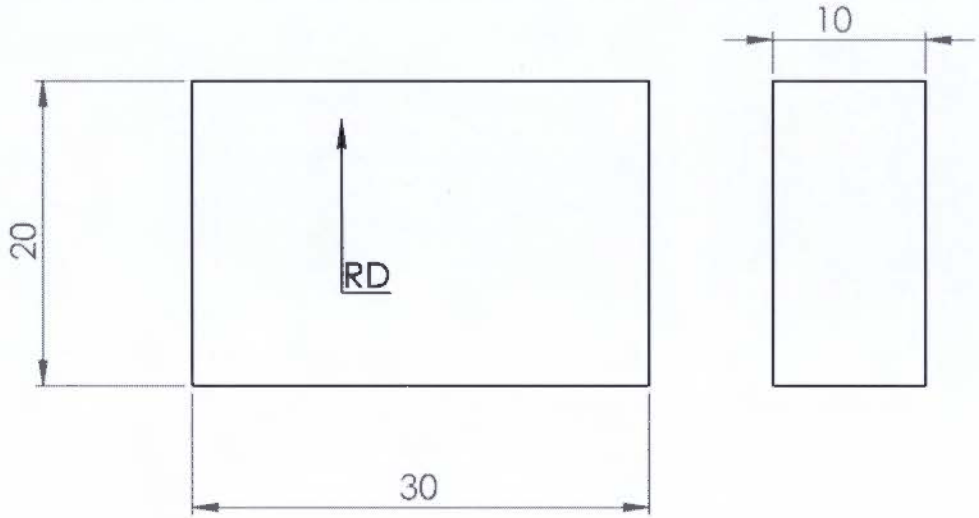

Note: Orientation
RD -Rolling Direction

UNLESS OTHERWISE SPECIFIED: DIMENSIONS ARE IN MILLIMETERS SURFACE FINISH: TOLERANCES: LINEAR: ANGULAR:		FINISH:			DEBUR AND BREAK SHARP EDGES	DO NOT SCALE DRAWING	REVISION
	NAME	SIGNATURE	DATE			TITLE: Plane Strain Compression Samples	
DRAWN	Chase Hyde		25/06/2012				
CHK'D							
APPV'D							
MFG							
Q.A				MATERIAL: Aluminium Plate - Provided		DWG NO 30(b)x20(l)x10(h)	A4
				WEIGHT:		SCALE:2:1	SHEET 1 OF 1

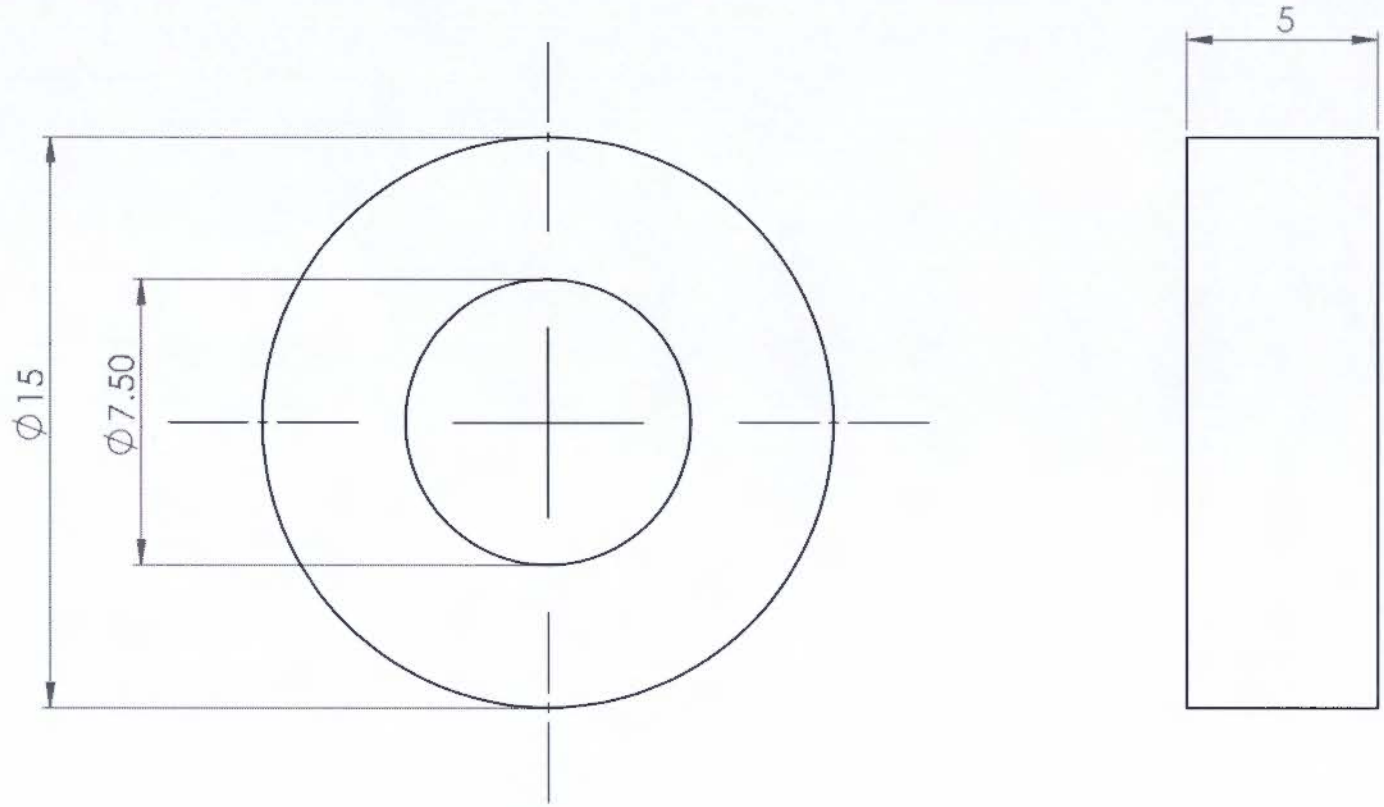

UNLESS OTHERWISE SPECIFIED: DIMENSIONS ARE IN MILLIMETERS SURFACE FINISH: TOLERANCES: LINEAR: ANGULAR:	FINISH:		DEBUR AND BREAK SHARP EDGES	DO NOT SCALE DRAWING	REVISION	
	NAME	SIGNATURE	DATE	TITLE:		
DRAWN	CK HYDE		31/05/13	Ring Compression Sample		
CHK'D						
APPV'D						
MFG						
Q.A						
MATERIAL: Aluminium AA3014 -Provided				DWG NO. Sample Drawing		A4
WEIGHT:				SCALE:5:1	SHEET 1 OF 1	

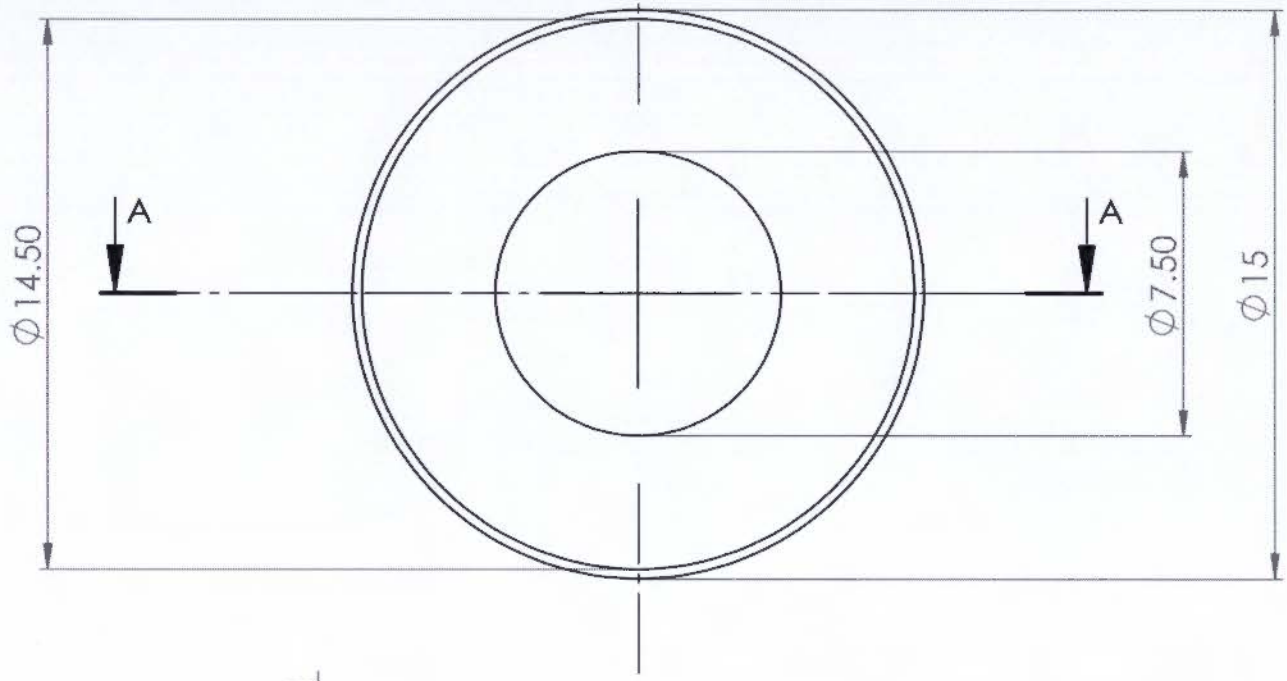

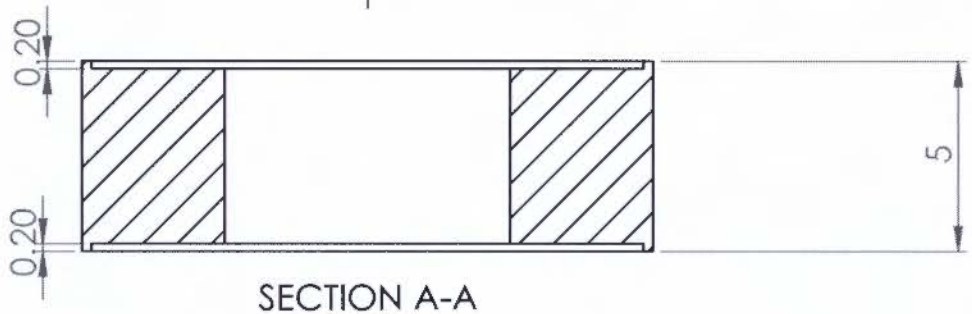

SECTION A-A

UNLESS OTHERWISE SPECIFIED: DIMENSIONS ARE IN MILLIMETERS SURFACE FINISH: TOLERANCES: LINEAR: ANGULAR:		FINISH:			DEBUR AND BREAK SHARP EDGES	DO NOT SCALE DRAWING	REVISION
	NAME	SIGNATURE	DATE			TITLE: Ring Compression Recess - Test Sample	
DRAWN	CK HYDE		19/03				
CHK'D							
APPV'D							
MFG							
Q.A				MATERIAL: Aluminium AA3104 (provided)		DWG NO. Sample	A4
				WEIGHT:		SCALE:5:1	SHEET 1 OF 1

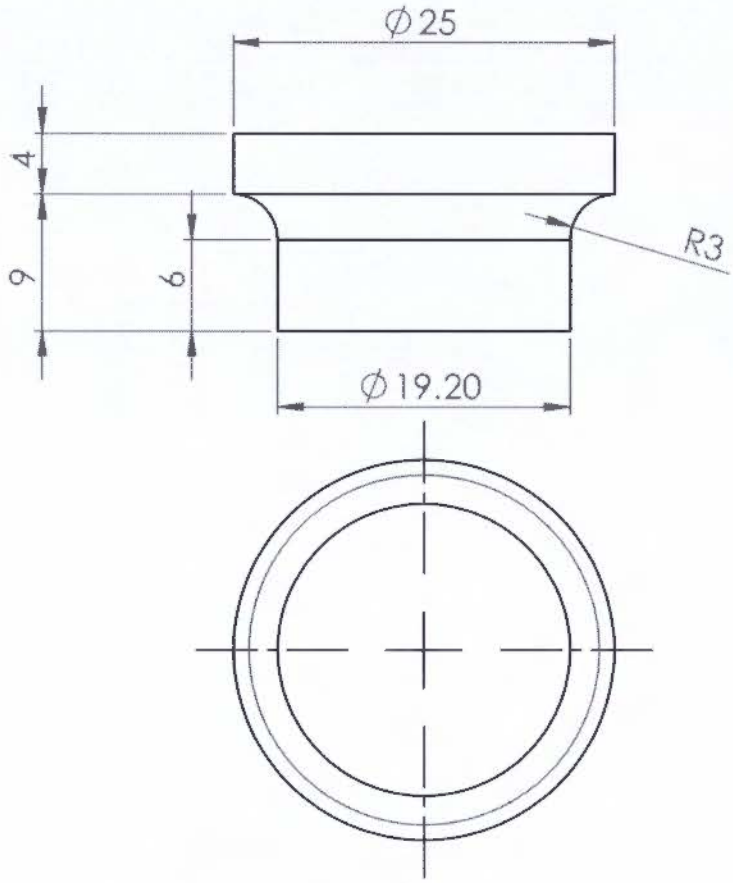

Quantity: x2

UNLESS OTHERWISE SPECIFIED: DIMENSIONS ARE IN MILLIMETERS SURFACE FINISH: TOLERANCES: LINEAR: ANGULAR:	FINISH:	DEBUR AND BREAK SHARP EDGES	DO NOT SCALE DRAWING / REVISION

	NAME	SIGNATURE	DATE
DRAWN	CK Hyde		19/04/2013
CHK'D			
APPV'D			
MFG			
Q.A			

TITLE:

Ring Compression Anvil End Cap

MATERIAL: K460 Steel

DWG NO. Ring_Comp_End Cap

A4

WEIGHT:

SCALE:2:1

SHEET 1 OF 1

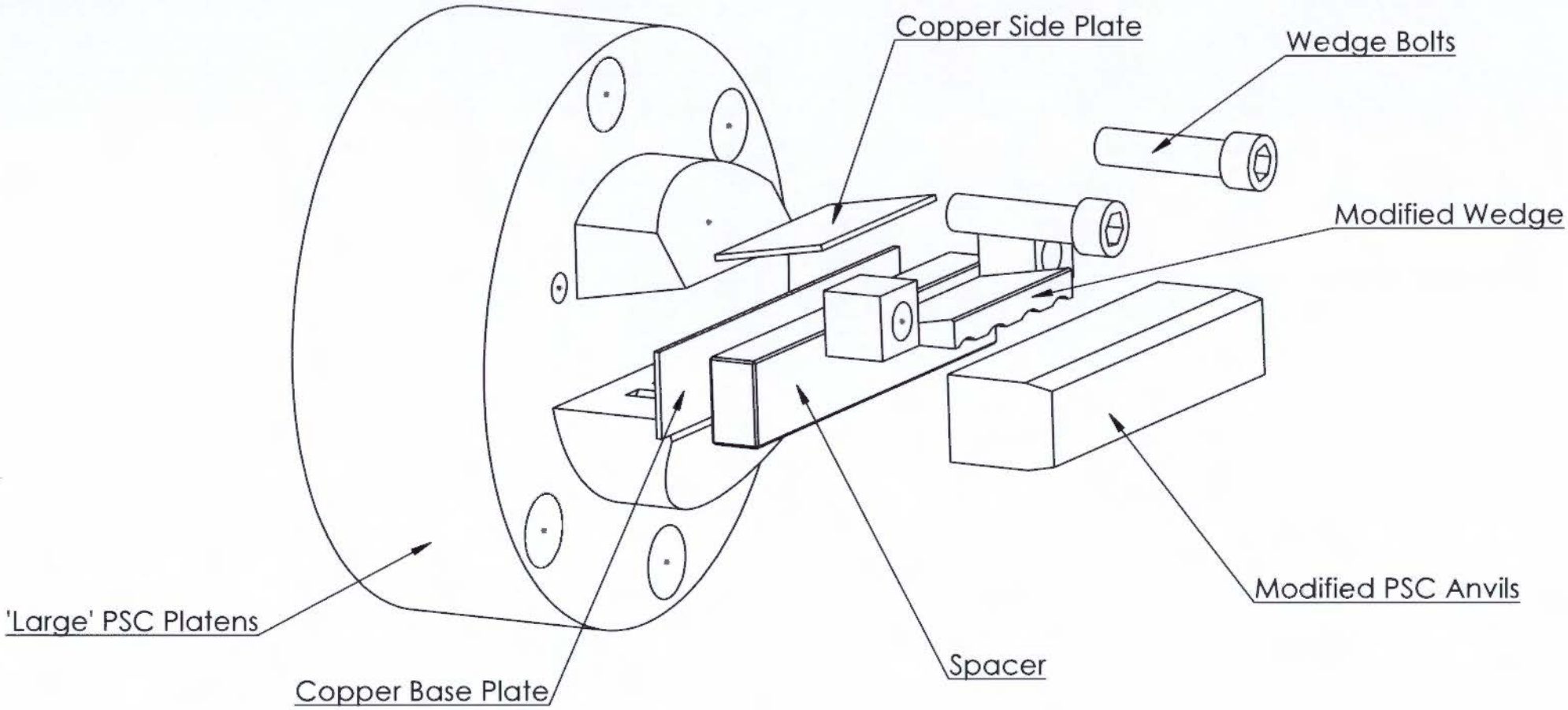

UNLESS OTHERWISE SPECIFIED: DIMENSIONS ARE IN MILLIMETERS SURFACE FINISH: TOLERANCES: LINEAR: ANGULAR:	FINISH:	DEBUR AND BREAK SHARP EDGES	DO NOT SCALE DRAWING / REVISION

	NAME	SIGNATURE	DATE
DRAWN	C K Hyde		
CHK'D			
APPV'D			
MFG			
Q.A			

MATERIAL:

WEIGHT:

TITLE:

Modified PSC Configuration - One Half

DWG NO.

PSC Set Up - One half

SCALE:1:1

SHEET 1 OF 1

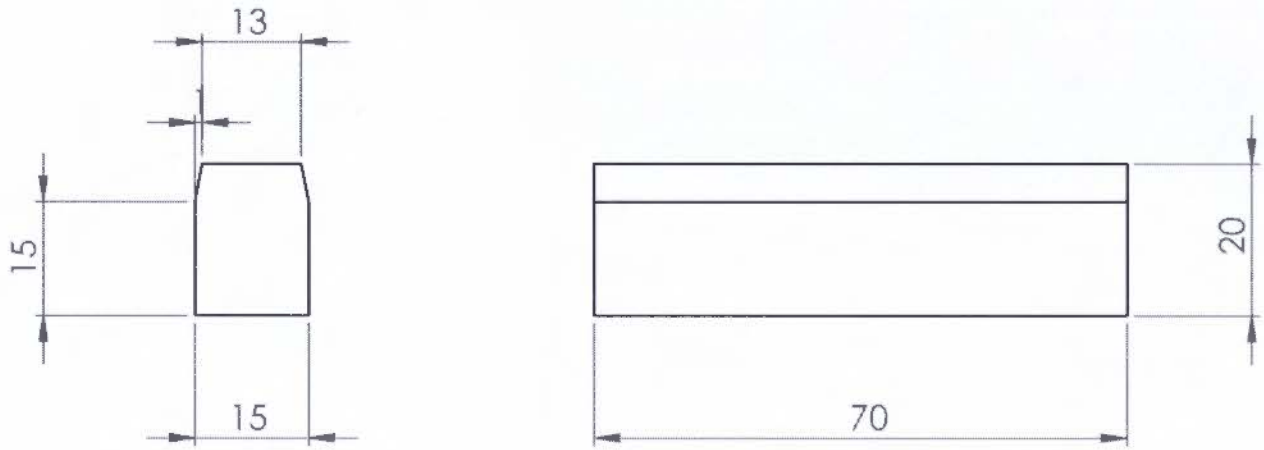

Quantity: 2 sets (Total 4)

Heat treatment to be performed

UNLESS OTHERWISE SPECIFIED: DIMENSIONS ARE IN MILLIMETERS SURFACE FINISH: TOLERANCES: LINEAR: ANGULAR:	FINISH:		DEBUR AND BREAK SHARP EDGES	DO NOT SCALE DRAWING	REVISION
	NAME	SIGNATURE	DATE	TITLE:	
DRAWN	C K HYDE		3/10/12	Modified PSC Anvils	
CHK'D					
APPV'D					
MFG					
Q.A					
				DWG NO. Anvil_Modified	A4
			MATERIAL: Böhler K460 steel.		
			WEIGHT:	SCALE:1:1	SHEET 1 OF 1

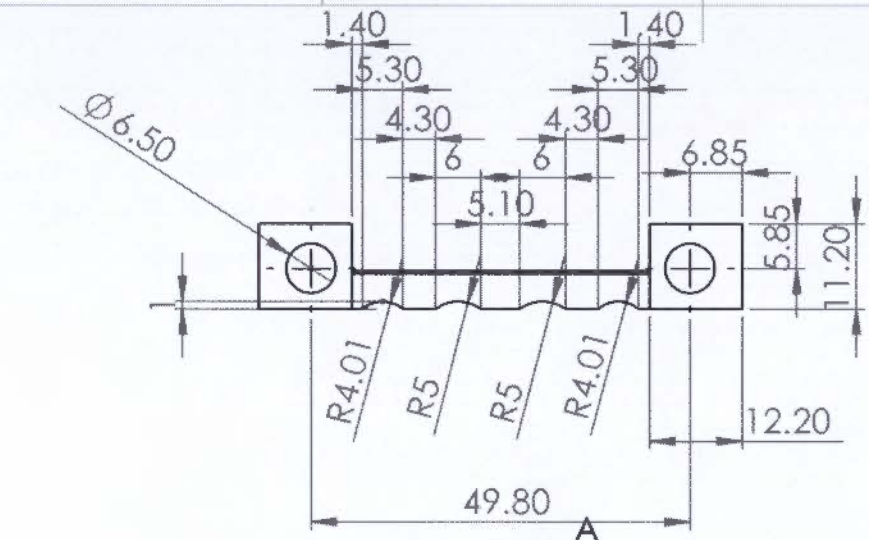

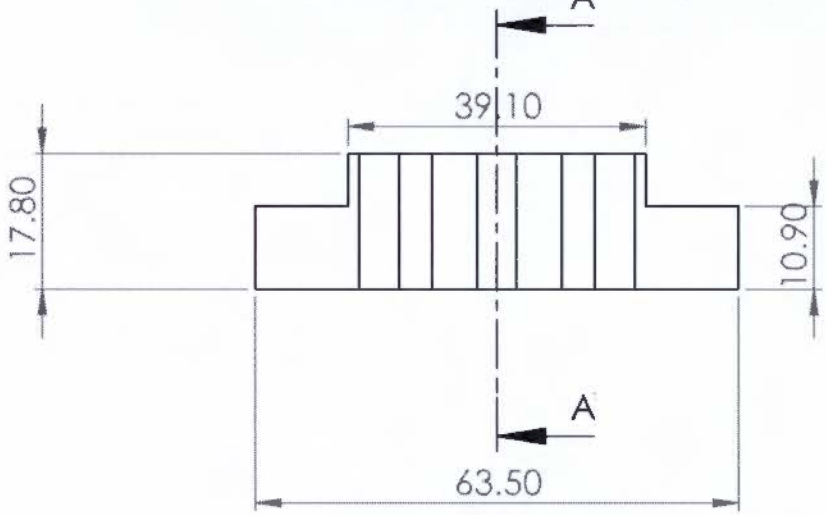

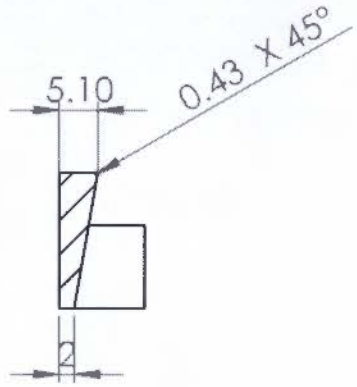

SECTION A-A

Quantity: x 2

UNLESS OTHERWISE SPECIFIED: DIMENSIONS ARE IN MILLIMETERS SURFACE FINISH: TOLERANCES: LINEAR: ANGULAR:	FINISH:		DEBUR AND BREAK SHARP EDGES	DO NOT SCALE DRAWING	REVISION
	NAME	SIGNATURE	DATE	TITLE:	
DRAWN	C K HYDE		1/10/12	PSC Wedge Component	
CHK'D					
APP'V'D					
MFG					
Q.A					
				DWG NO. Wedge_Mod_2.0	A4
			MATERIAL: Böhler K460 steel.		
			WEIGHT:	SCALE:1:1	SHEET 1 OF 1

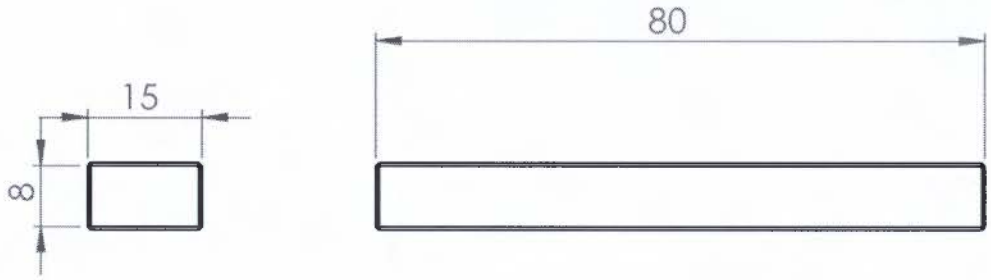

Quantity: x2
All edges: 45 degree chamfer

UNLESS OTHERWISE SPECIFIED: DIMENSIONS ARE IN MILLIMETERS SURFACE FINISH: TOLERANCES: LINEAR: ANGULAR:	FINISH:		DEBUR AND BREAK SHARP EDGES	DO NOT SCALE DRAWING	REVISION	
	NAME	SIGNATURE	DATE	TITLE:		
DRAWN	C K HYDE		3/10/12	Modified PSC Spacer		
CHKD						
APPV'D						
MFG						
Q.A				MATERIAL:	DWG NO.	A4
				Böhler K460 steel.	Spacer_Modified	
				WEIGHT:	SCALE:1:1	SHEET 1 OF 1

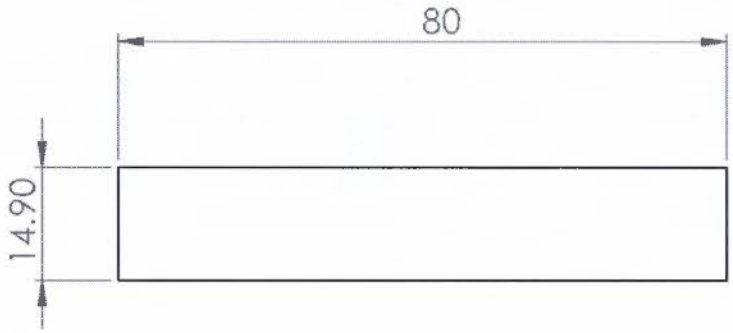

Amount: x 2

UNLESS OTHERWISE SPECIFIED: DIMENSIONS ARE IN MILLIMETERS SURFACE FINISH: TOLERANCES: LINEAR: ANGULAR:		FINISH:			DEBUR AND BREAK SHARP EDGES	DO NOT SCALE DRAWING	REVISION
	NAME	SIGNATURE	DATE			TITLE: Copper Conducting Base Plate	
DRAWN	C.K Hyde		27/11/12				
CHK'D							
APPV'D							
MFG							
Q.A				MATERIAL: Copper plate (provided)		DWG NO. Copper_Base_Plate_Modifi	A1
				WEIGHT:		SCALE:1:1	SHEET 1 OF 1

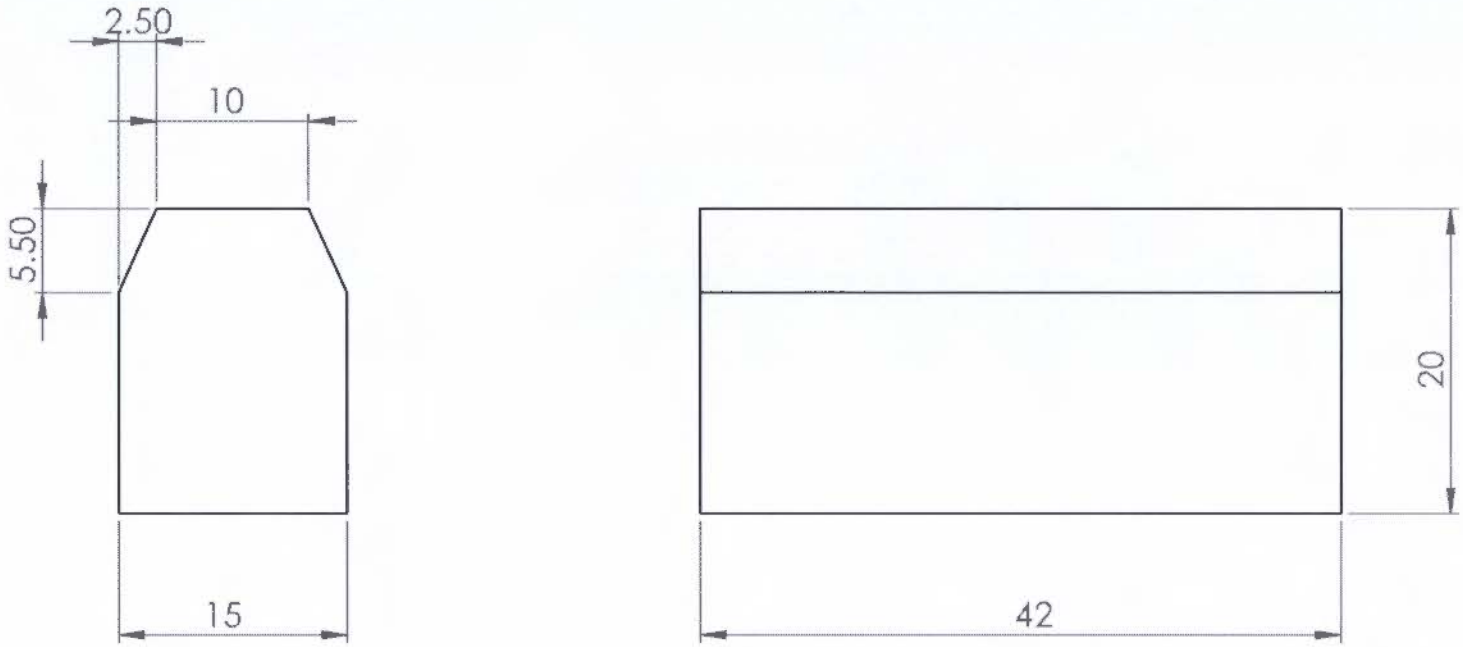

Quantity: x2

UNLESS OTHERWISE SPECIFIED: DIMENSIONS ARE IN MILLIMETERS SURFACE FINISH: TOLERANCES: LINEAR: ANGULAR:	FINISH:		DEBUR AND BREAK SHARP EDGES	DO NOT SCALE DRAWING	REVISION	
	NAME	SIGNATURE	DATE	TITLE:		
DRAWN	Chase Hyde		25/05/2012	Plane Strain Anvil		
CHK'D						
APPV'D						
MFG						
Q.A						
MATERIAL: BÖHLER K460 Steel				DWG NO. Anvil_b10mm_l42mm		A4
WEIGHT:				SCALE:1:1 2:1	SHEET 1 OF 1	

Technical Drawings of the PSC Validation Test Samples

- DSI PSC configuration sample technical drawing with drilled thermocouple holes
- Modified PSC configuration sample technical drawing with drilled thermocouple holes
- Rolling PSC simulation technical drawing

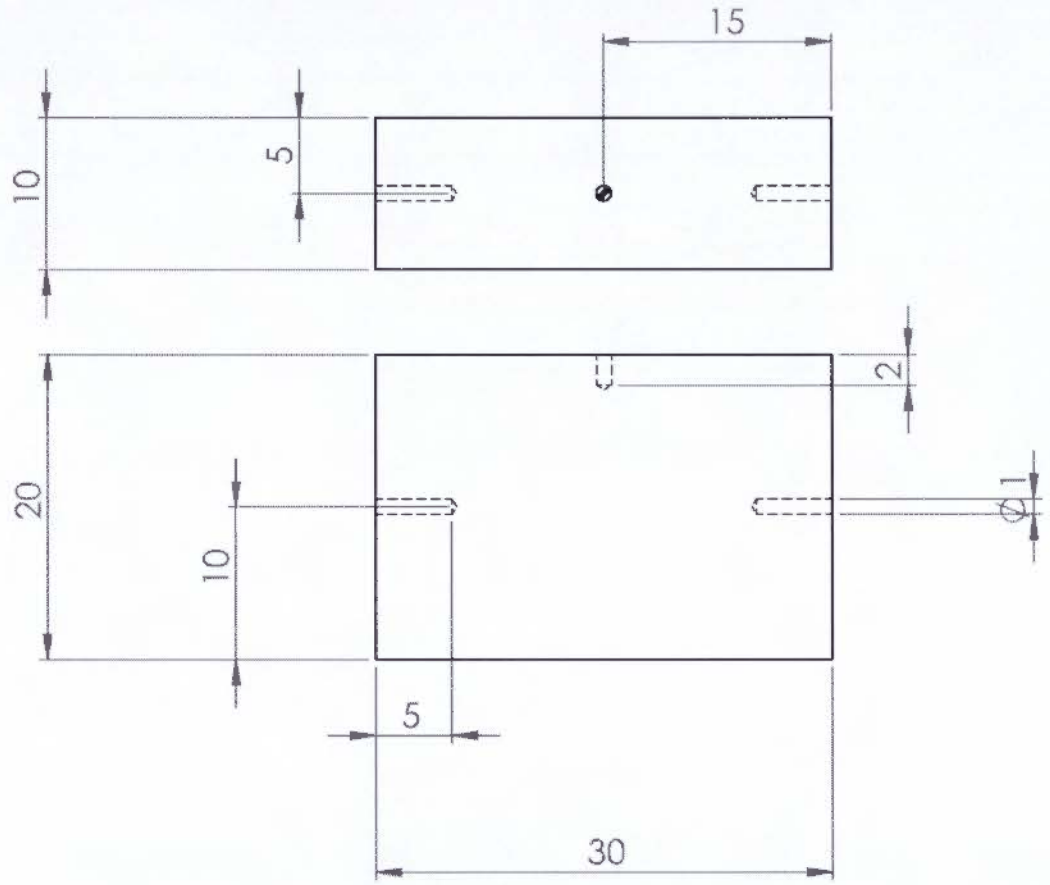

Note: Orientation
RD -Rolling Direction

UNLESS OTHERWISE SPECIFIED: DIMENSIONS ARE IN MILLIMETERS SURFACE FINISH: TOLERANCES: LINEAR: ANGULAR:	FINISH:	DEBUR AND BREAK SHARP EDGES	DO NOT SCALE DRAWING / REVISION

	NAME	SIGNATURE	DATE
DRAWN	Chase Hyde		25/05/2012
CHK'D			
APPV'D			
MFG			
Q.A			

TITLE: Standard DSI PSC Samples

MATERIAL: Aluminium Plate - Provided

DWG NO: 30(b)x20(l)x10(h)

A4

WEIGHT:

SCALE:2:1

SHEET 1 OF 1

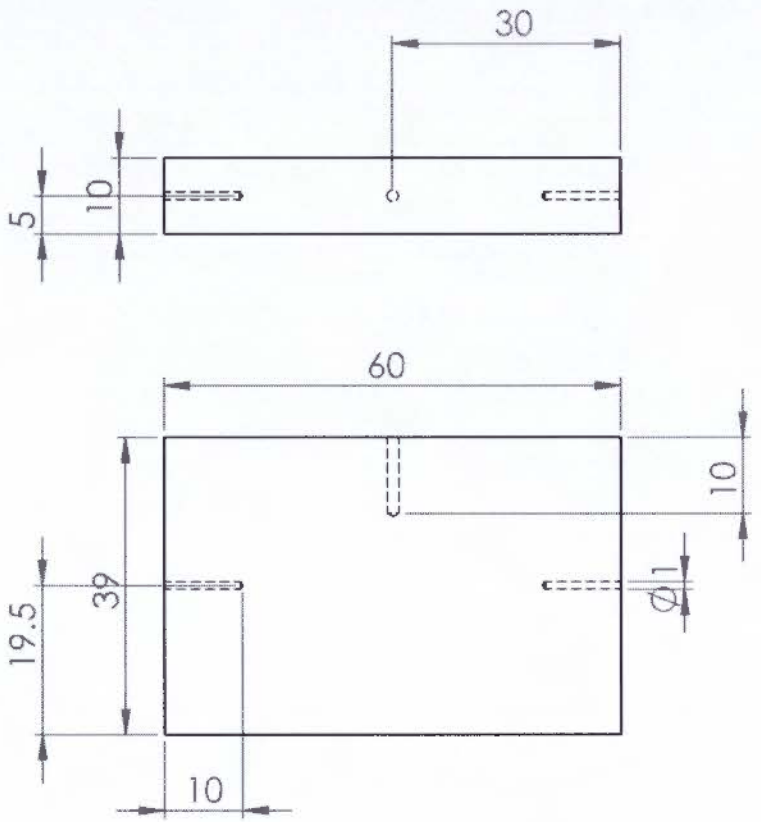

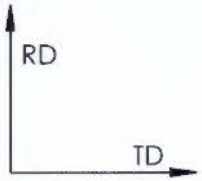

Note: Orientation

UNLESS OTHERWISE SPECIFIED: DIMENSIONS ARE IN MILLIMETERS SURFACE FINISH: TOLERANCES: LINEAR: ANGULAR:	FINISH:		DEBUR AND BREAK SHARP EDGES	DO NOT SCALE DRAWING	REVISION	
	NAME	SIGNATURE	DATE	TITLE: PSC Samples		
DRAWN	C.K Hyde		25/10/12			
CHK'D						
APP'D						
MFG						
Q.A						
MATERIAL: Aluminium Plate (Provided)				DWG NO: 39(l)x60(b)x10(h)		A4
WEIGHT:				SCALE:1:1	SHEET 1 OF 1	

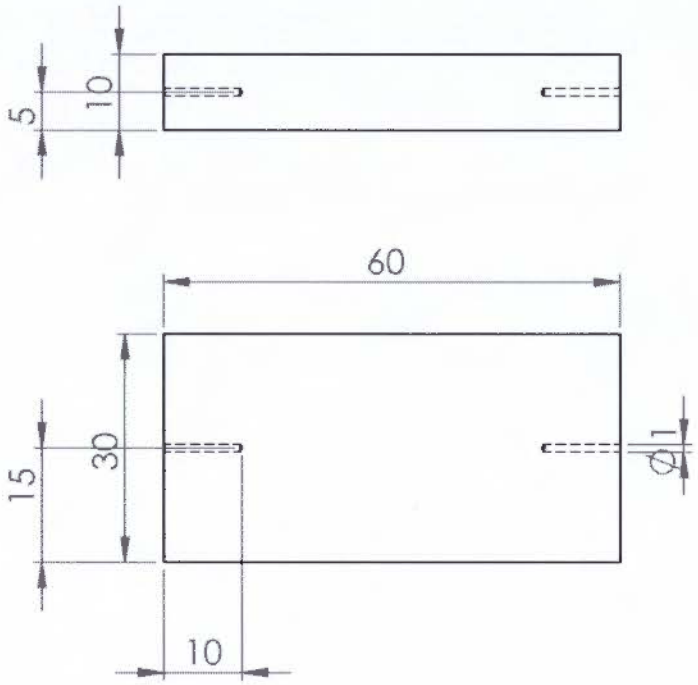

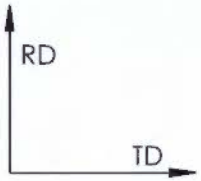

Note: Orientation

UNLESS OTHERWISE SPECIFIED: DIMENSIONS ARE IN MILLIMETERS SURFACE FINISH: TOLERANCES: LINEAR: ANGULAR:	FINISH:		DEBUR AND BREAK SHARP EDGES	DO NOT SCALE DRAWING	REVISION	
	NAME	SIGNATURE	DATE	TITLE:		
DRAWN	C.K Hyde		25/10/12	PSC Simulation Samples		
CHK'D						
APPV'D						
MFG						
Q.A						
				MATERIAL: Aluminium AA3104	DWG NO. 30(l)x60(b)x10(h)	A4
				WEIGHT:	SCALE:1:1	SHEET 1 OF 1

Appendix B: Testing Procedure Flow Charts

Testing Flow Chart:

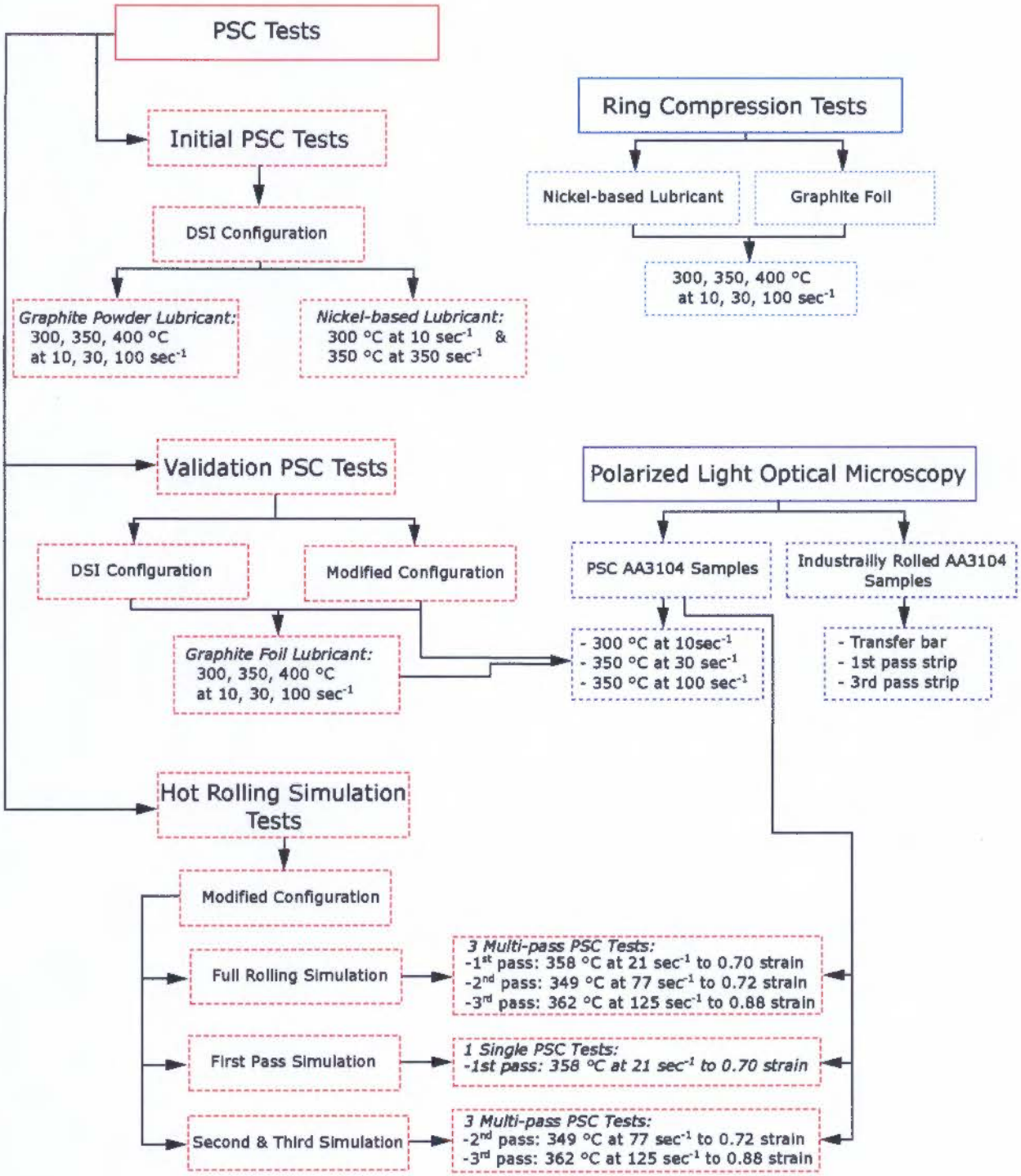

Gleeble 3800 Testing Procedure:

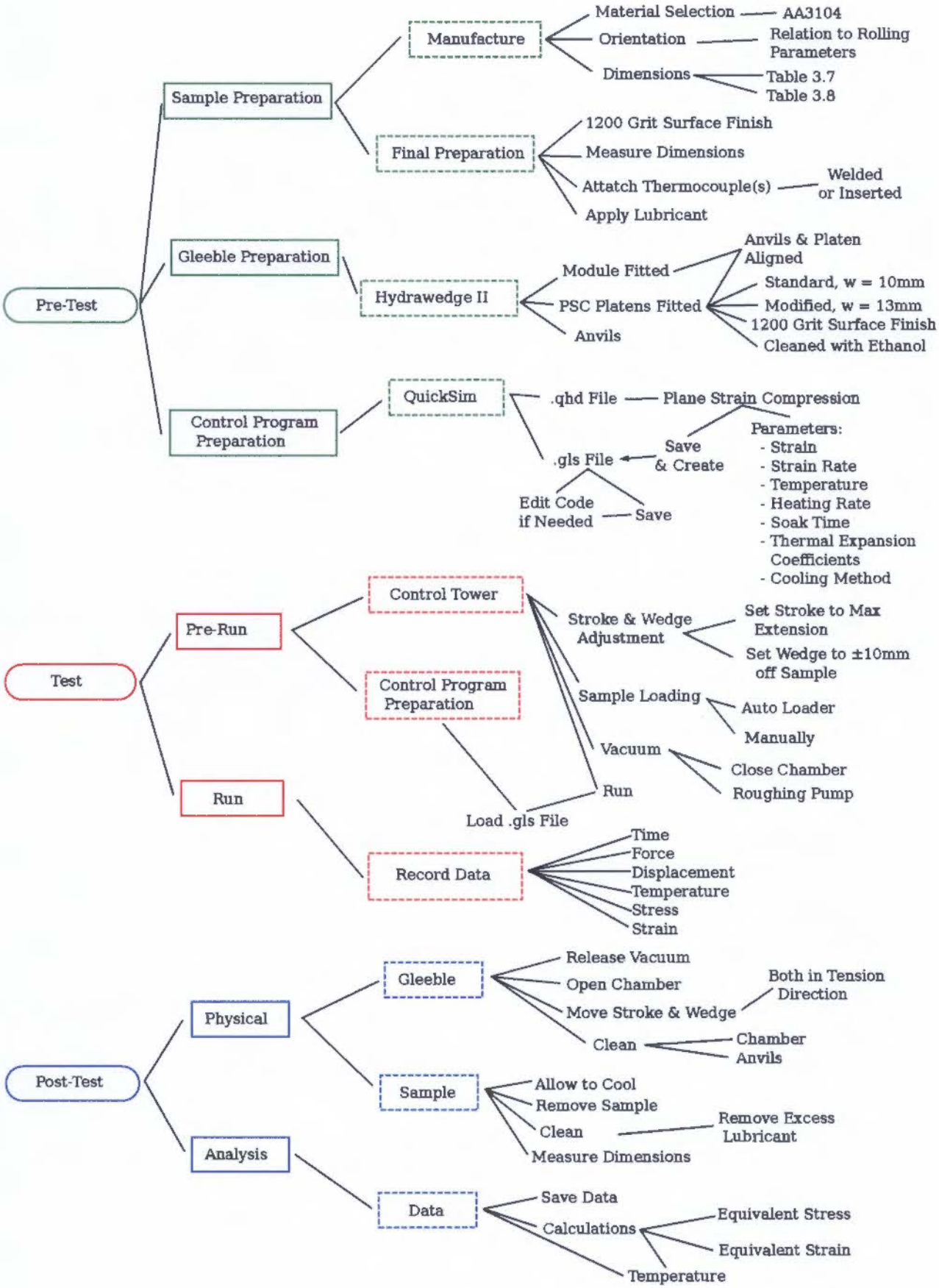

Appendix C: PSC Testing Form

Date:	
Sample Name:	
Material:	

Sample Dimensions:		
Breadth, mm		
Initial	b_1	
	b_2	
	b_3	
Average:	$\mathbf{b_0}$	
Standard Deviation:	S_{b0}	
Final	$\mathbf{b_f}$	
Height, mm		
Initial	h_1	
	h_2	
	h_3	
	h_4	
	h_5	
Average:	$\mathbf{h_0}$	
Standard Deviation:	S_{h0}	
Final	h_6	
	h_7	
	h_8	
	h_9	
	h_{10}	
Average:	$\mathbf{h_f}$	
Standard Deviation:	S_{hf}	

Important Variables:

strain: (ε)		
strain rate: (ε')		/sec
Δh:		mm
h_f		mm
Test Temp:		°C
Heating Rate:		°C/sec
Holding @ Test Temp:		sec
Time to Deformation:	min	sec
Cooling Method:		
Lubricant:		
Air Ram Pressure:		kN
Variac Setting:		

w =	mm	
/ =	mm	
B_R (b_0/w) =		[>5]
H_R (w/h_0) =		[>1.5]
$/_R$ (//w) =		[>3]

Thermocouple Positions

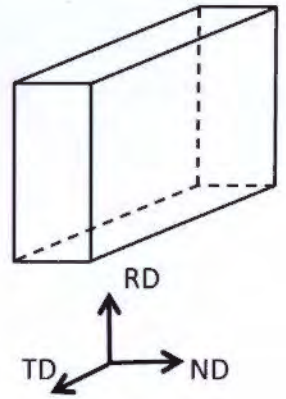

Comments:

Appendix D: Initial PSC Tests

Temperature: 300°C | Strain rate: 10 sec^{-1} | Strain 0.9 | Graphite Powder Lubrication

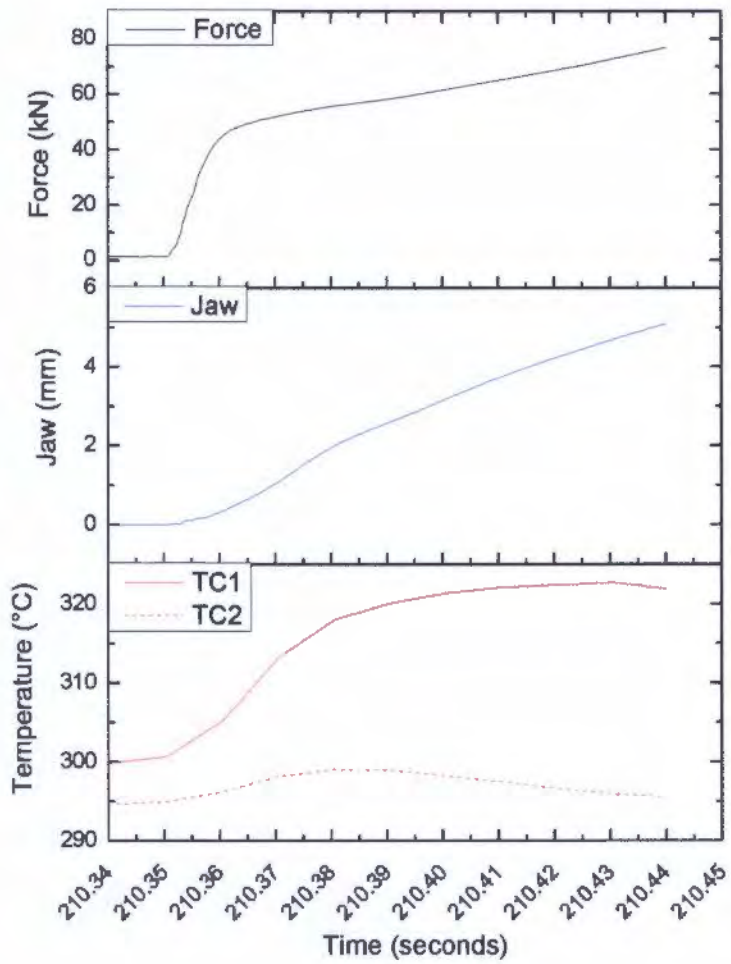

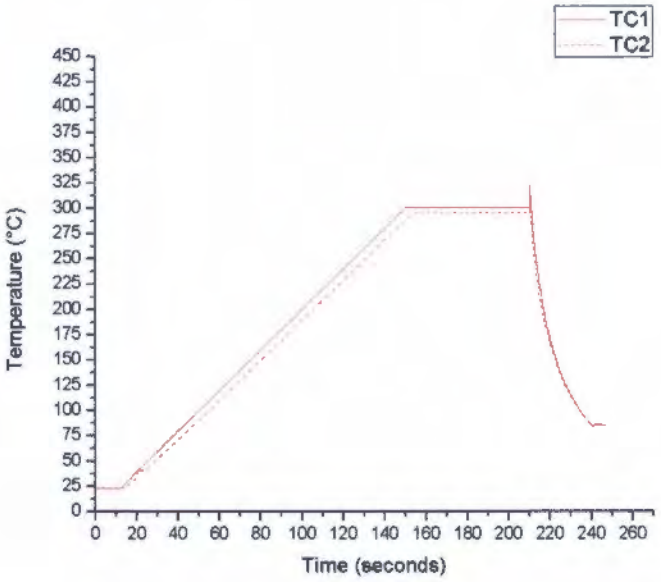

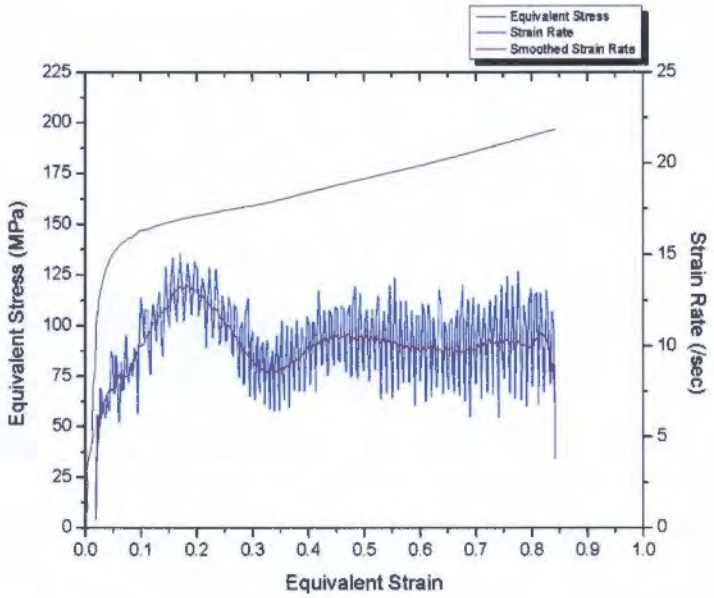

Summary:

	Value from 0.8 - 0.9 strain			Overall value	
Starting Temperature (°C)	Temperature (°C)	Flow stress (MPa)	Strain rate (sec^{-1})	Strain rate (sec^{-1})	△Temperature (°C)
300.6	322.1	195.2	9.73	9.79	21.5

Temperature: 300°C | Strain rate: 30 sec^{-1} | Strain 0.9 | Graphite Powder Lubrication

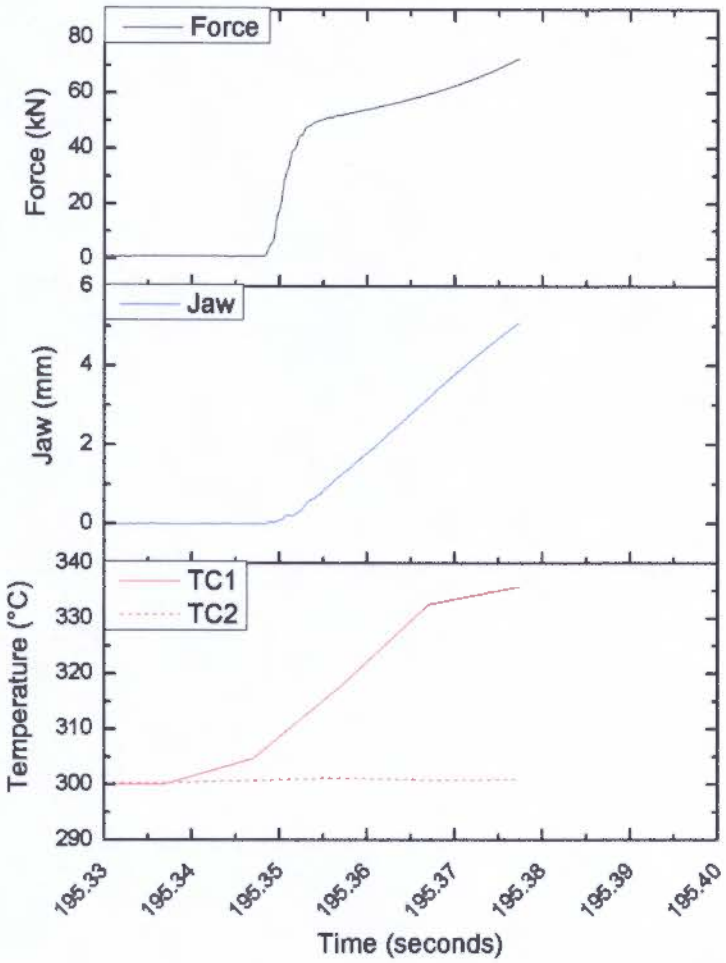

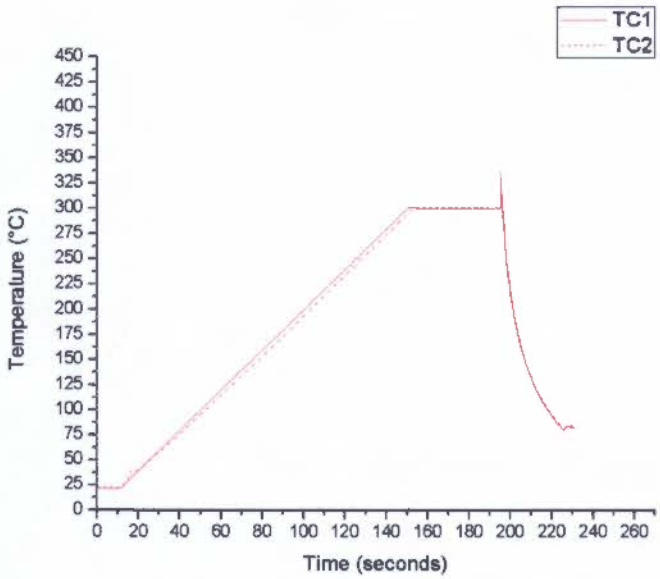

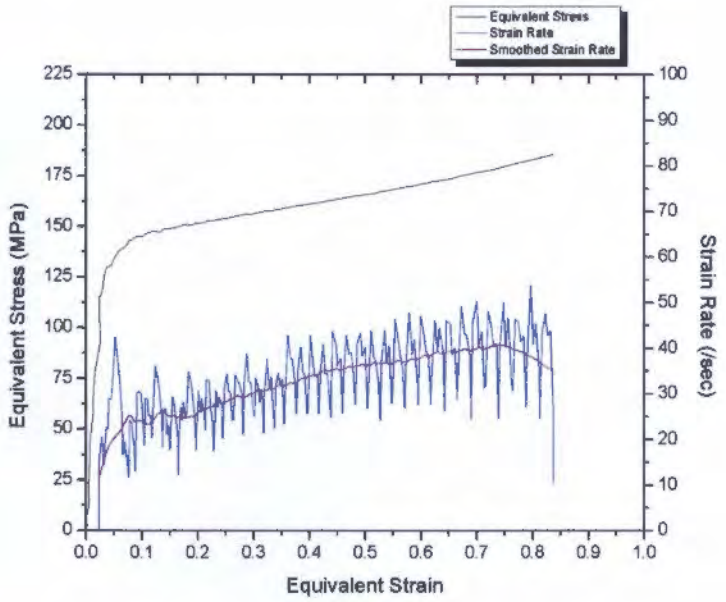

Summary:

	Value from 0.8 - 0.9 strain			Overall value	
Starting Temperature (°C)	Temperature (°C)	Flow stress (MPa)	Strain rate (sec^{-1})	Strain rate (sec^{-1})	△Temperature (°C)
304.0	335.5	184.6	36.4	31.0	31.5

Temperature: 300°C | Strain rate: 100 sec^{-1} | Strain 0.9 | Graphite Powder Lubrication

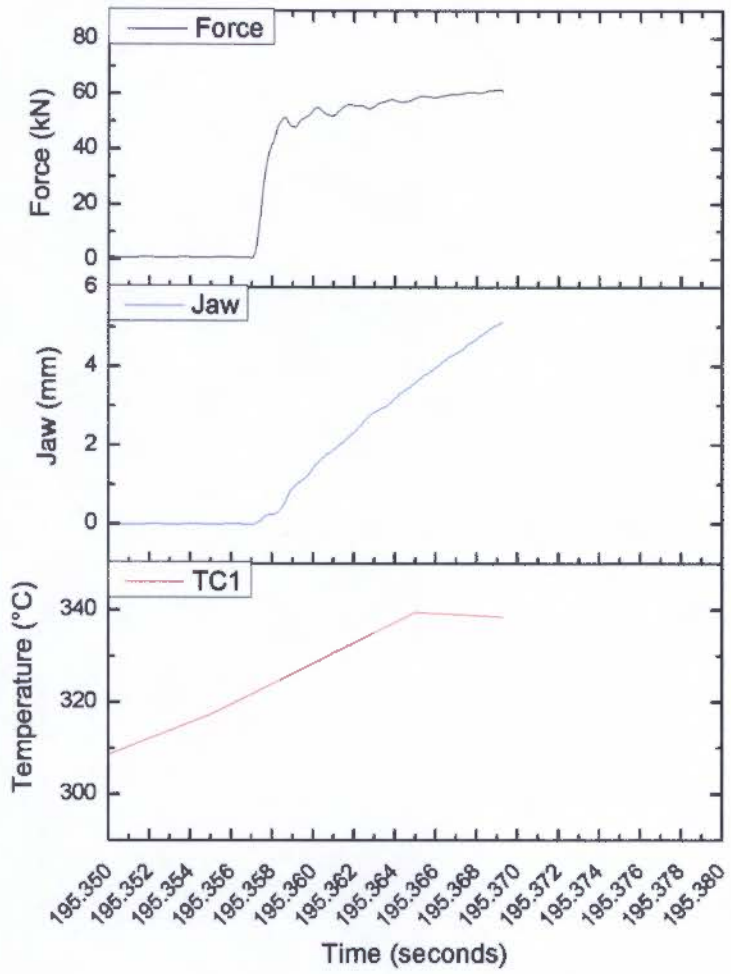

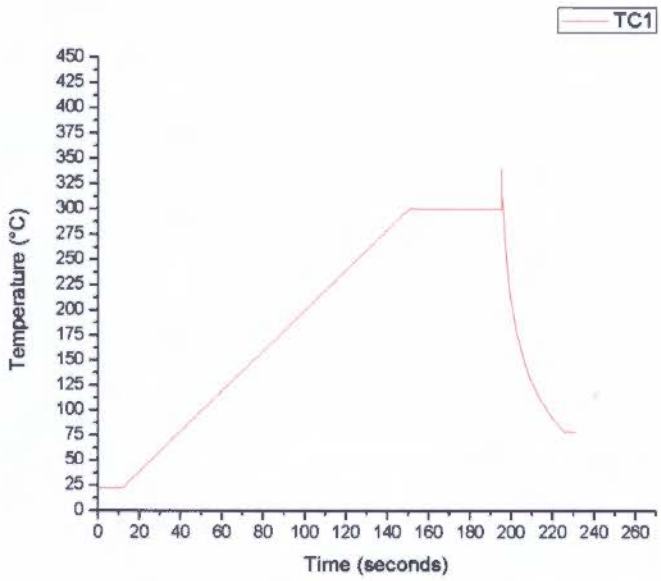

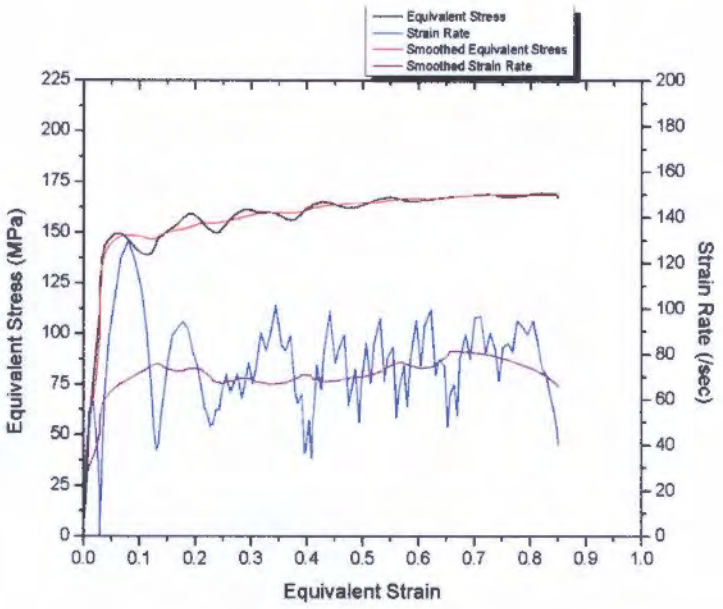

Summary:

	Value from 0.8 - 0.9 strain			Overall value	
Starting Temperature (°C)	Temperature (°C)	Flow stress (MPa)	Strain rate (sec^{-1})	Strain rate (sec^{-1})	△Temperature (°C)
300.0	338.6	169.0	76.1	68.5	38.6

Temperature: 350°C | Strain rate: 10 sec^{-1} | Strain 0.9 | Graphite Powder Lubrication

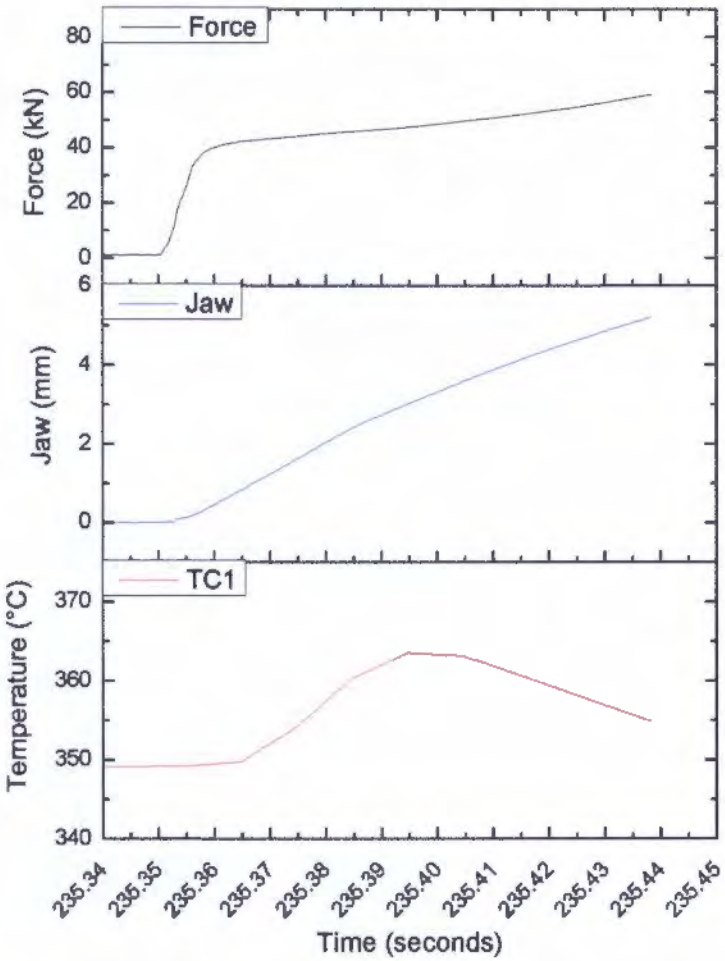

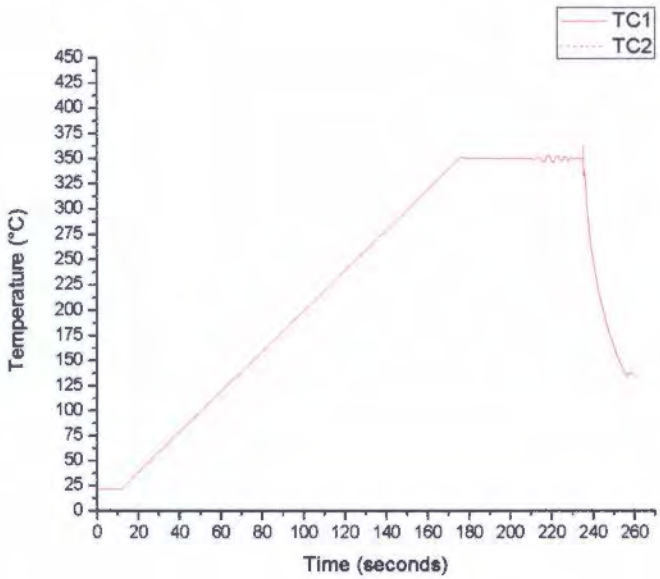

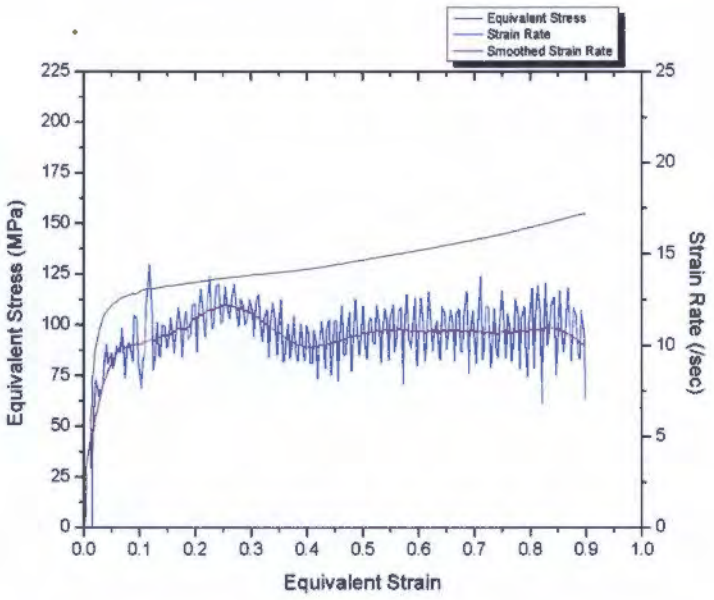

Summary:

	Value from 0.8 - 0.9 strain			Overall value	
Starting Temperature (°C)	Temperature (°C)	Flow stress (MPa)	Strain rate (sec^{-1})	Strain rate (sec^{-1})	△Temperature (°C)
349.3	355.9	151.7	10.7	10.4	6.6

Temperature: 350°C | Strain rate: 30 sec^{-1} | Strain 0.9 | Graphite Powder Lubrication

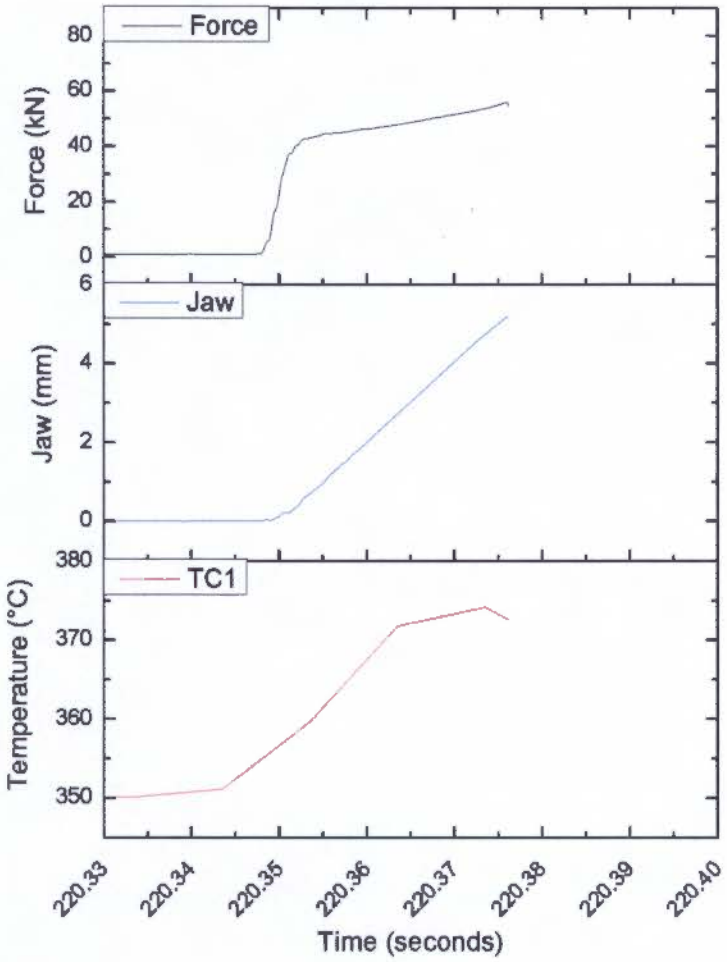

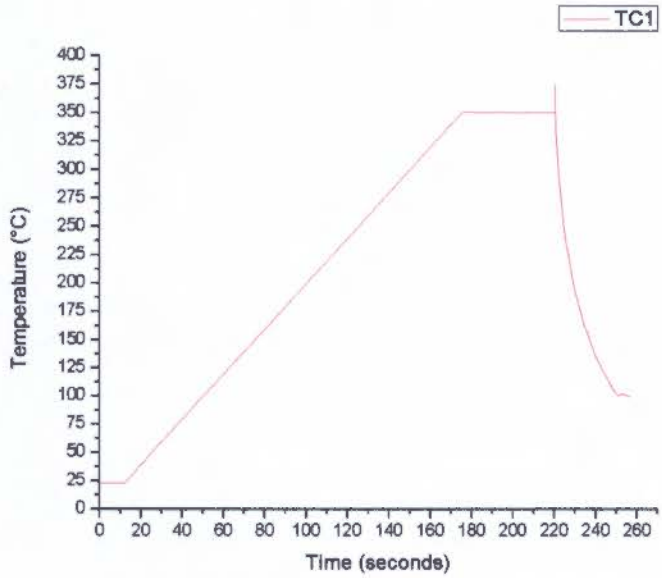

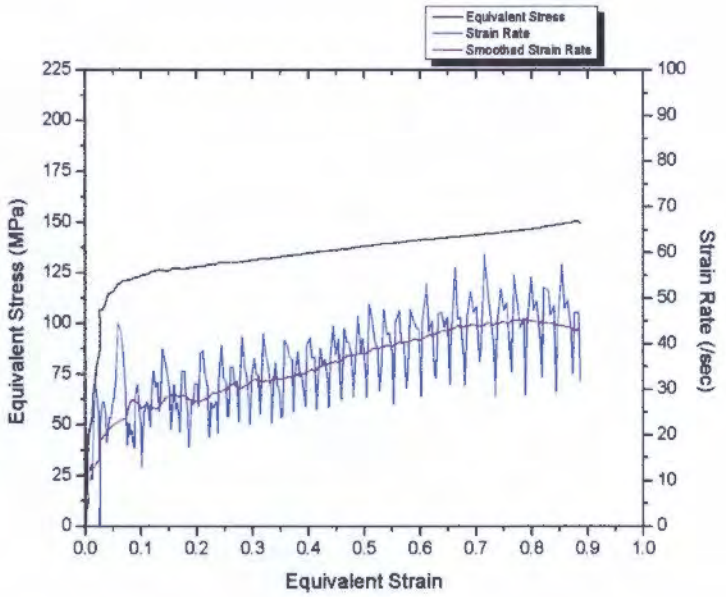

Summary:

	Value from 0.8 - 0.9 strain			Overall value	
Starting Temperature (°C)	Temperature (°C)	Flow stress (MPa)	Strain rate (sec^{-1})	Strain rate (sec^{-1})	△Temperature (°C)
351.0	373.2	148.6	44.1	33.1	22.2

Temperature: 350°C | Strain rate: 100 sec^{-1} | Strain 0.9 | Graphite Powder Lubrication

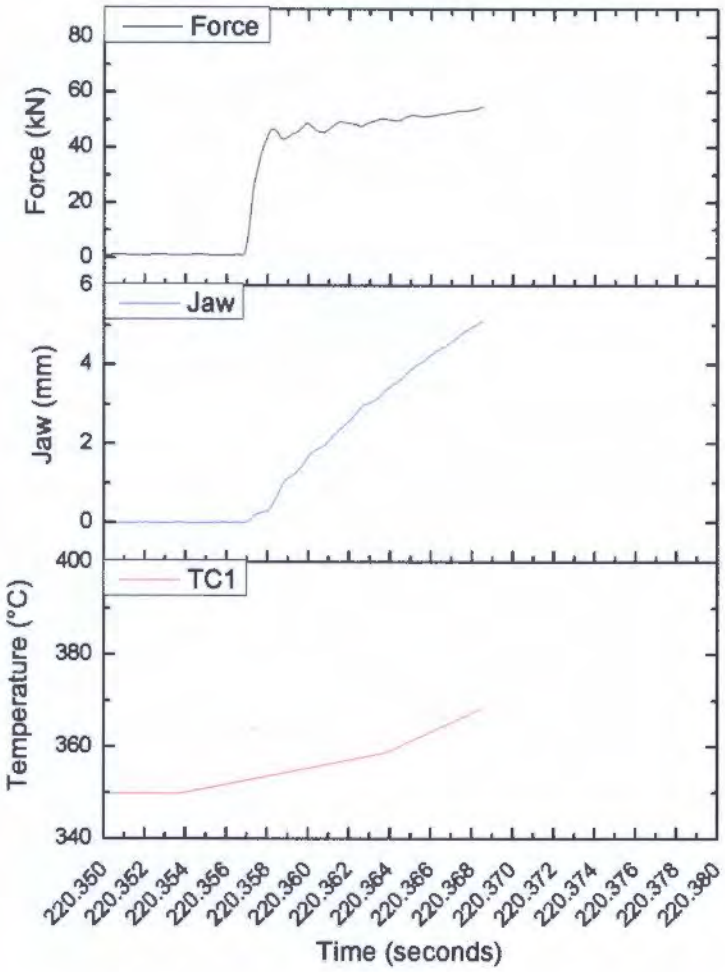

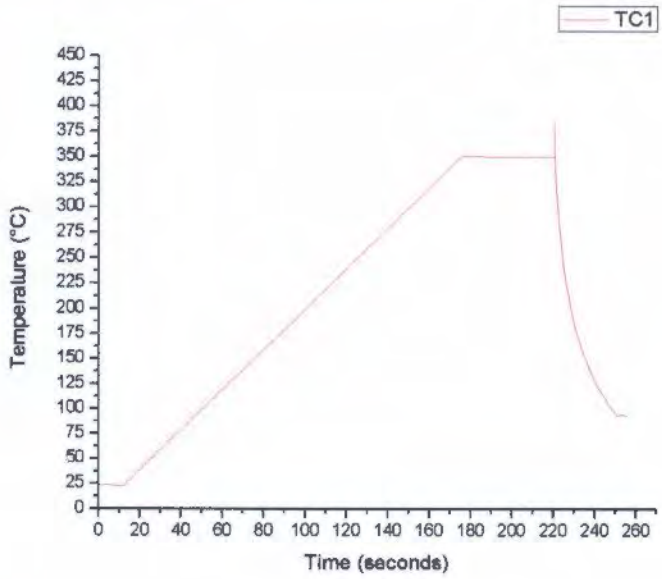

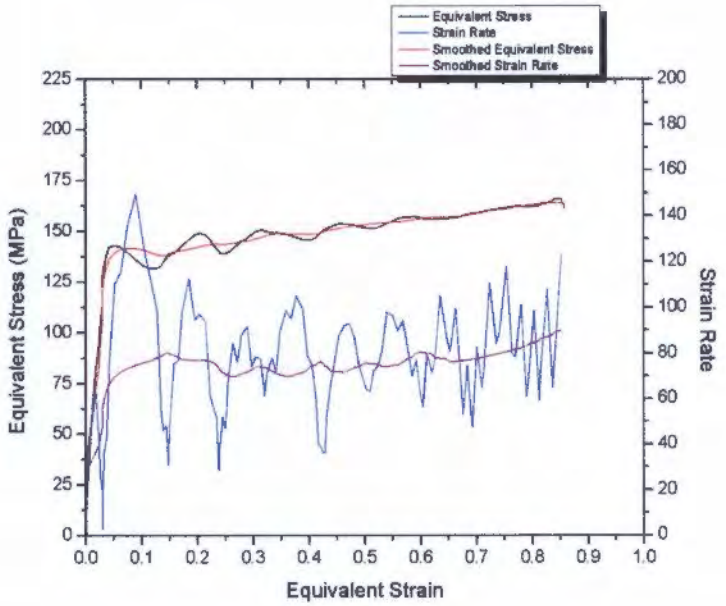

Summary:

	Value from 0.8 - 0.9 strain			Overall value	
Starting Temperature (°C)	Temperature (°C)	Flow stress (MPa)	Strain rate (sec^{-1})	Strain rate (sec^{-1})	△Temperature (°C)
349.9	367.6	163.2	86.7	71.1	17.7

Temperature: 400°C | Strain rate: 10 sec^{-1} | Strain 0.9 | Graphite Powder Lubrication

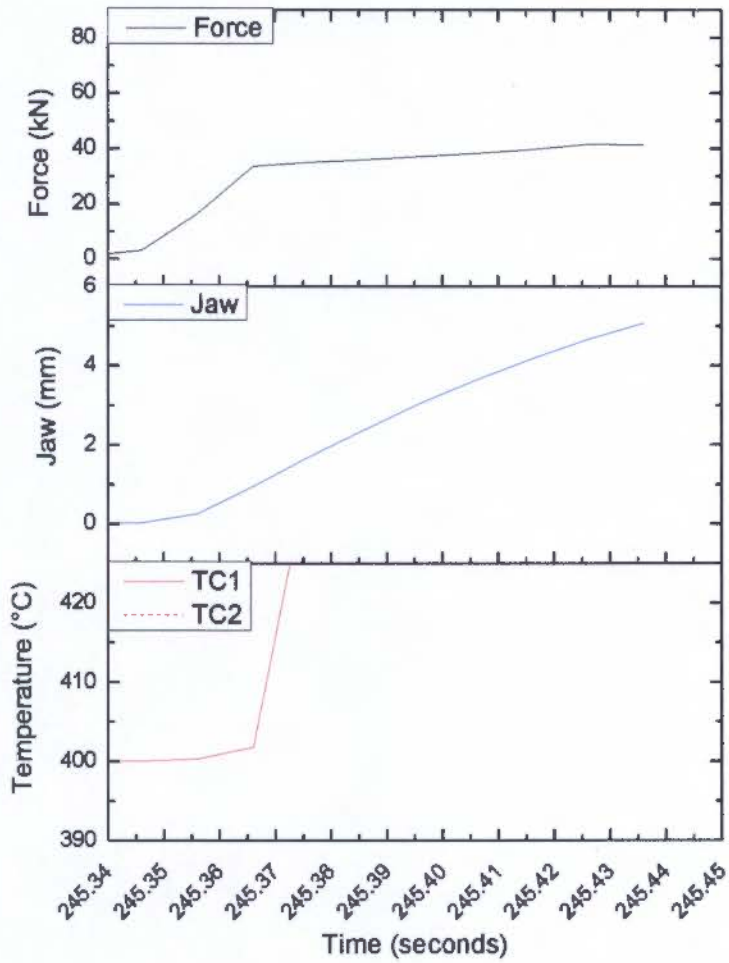

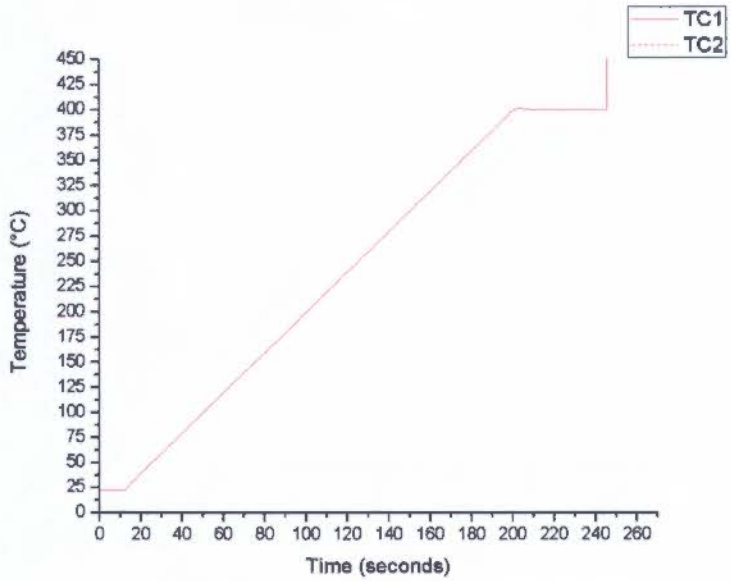

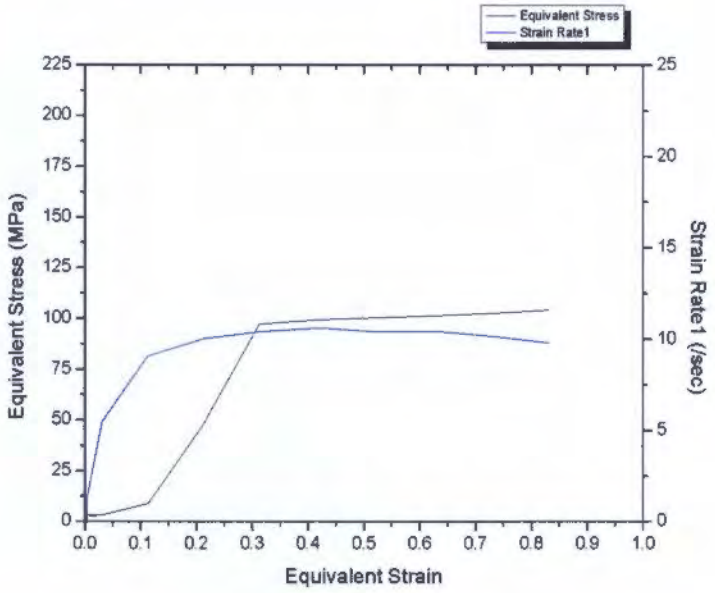

Summary:

	Value from 0.8 - 0.9 strain			Overall value	
Starting Temperature (°C)	Temperature (°C)	Flow stress (MPa)	Strain rate (sec^{-1})	Strain rate (sec^{-1})	△Temperature (°C)
-	-	104.5*	10.2*	-	-

Temperature: 400°C | Strain rate: 30 sec^{-1} | Strain 0.9 | Graphite Powder Lubrication

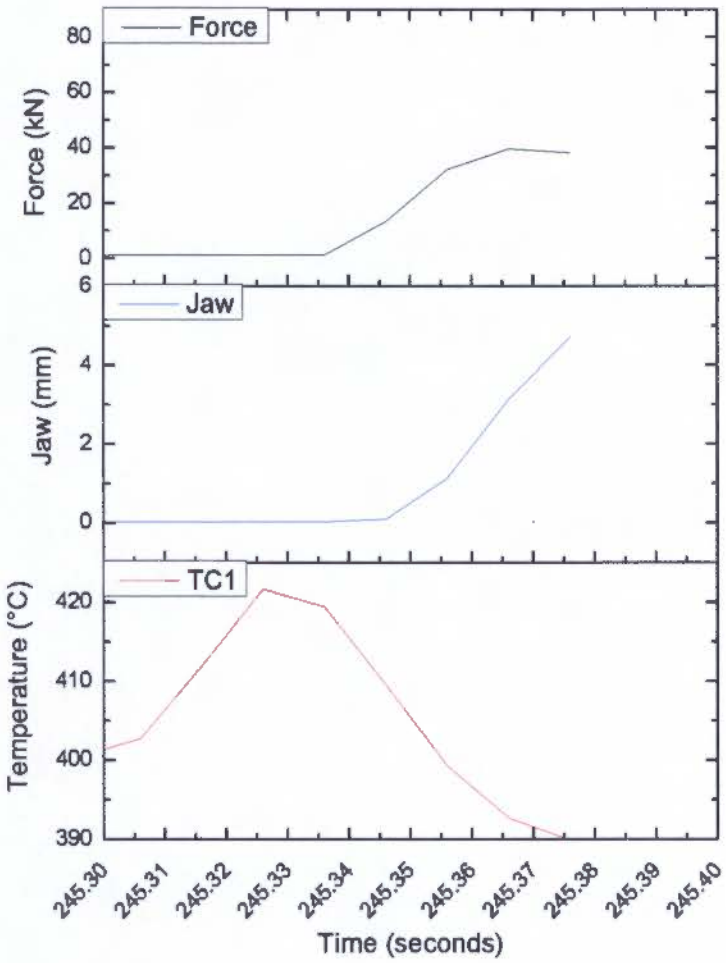

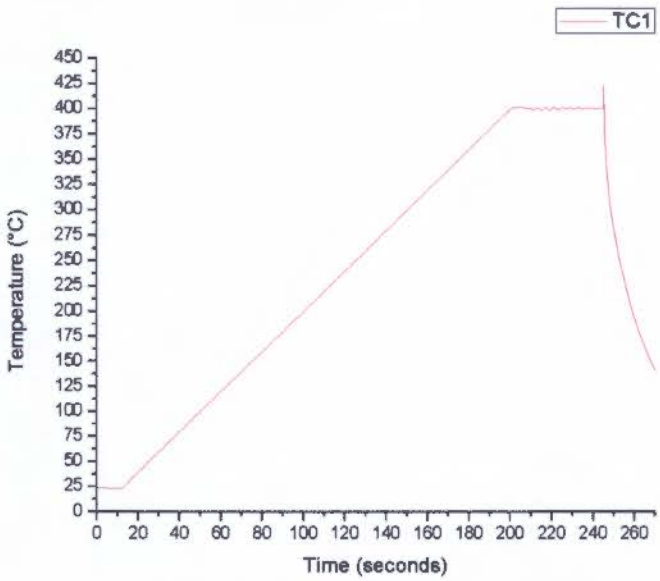

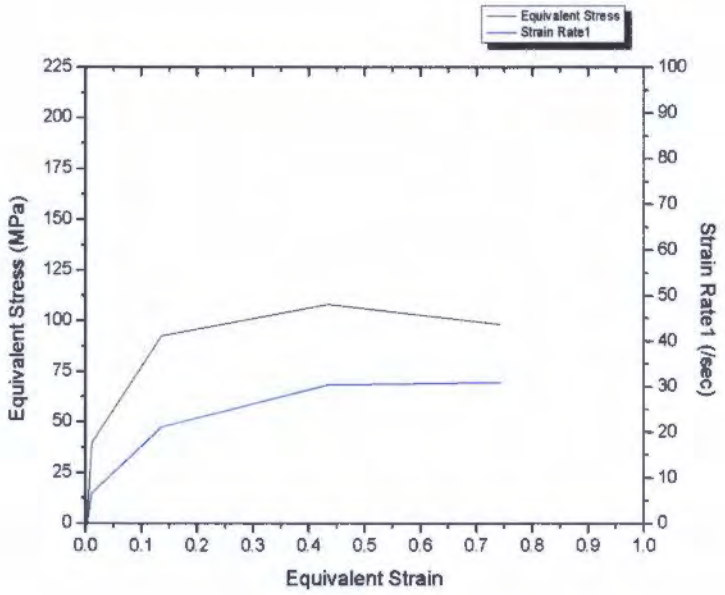

Summary:

	Value from 0.8 - 0.9 strain			Overall value	
Starting Temperature (°C)	Temperature (°C)	Flow stress (MPa)	Strain rate (sec^{-1})	Strain rate (sec^{-1})	△Temperature (°C)
400.1	391.2*	103.1*	30.7*	-	-8.9*

Temperature: 400°C | Strain rate: 100 sec^{-1} | Strain 0.9 | Graphite Powder Lubrication

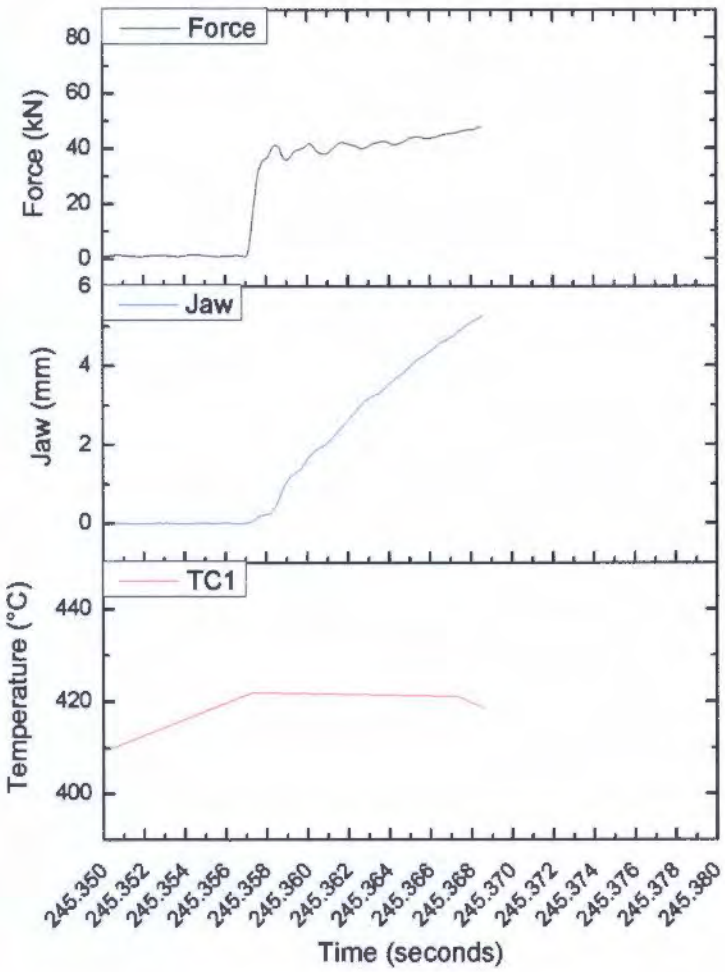

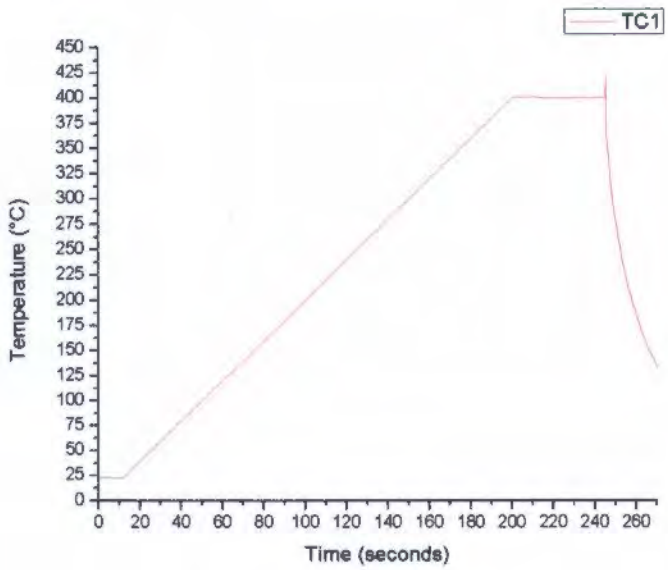

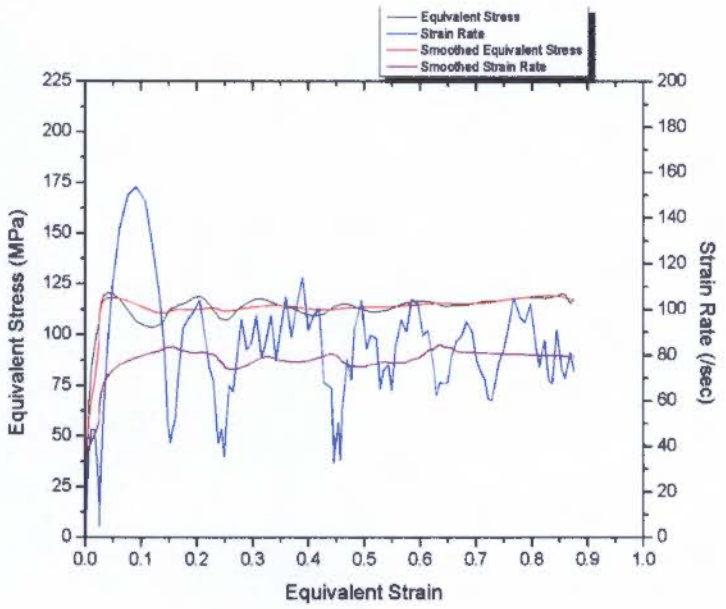

Summary:

	Value from 0.8 - 0.9 strain			Overall value	
Starting Temperature (°C)	Temperature (°C)	Flow stress (MPa)	Strain rate (sec^{-1})	Strain rate (sec^{-1})	△Temperature (°C)
400.0	419.4	118.5	79.7	71.2	19.4

Nickel-based Lubricated PSC Tests:

Temperature: 300°C | Strain rate: 10 sec^{-1} | Strain 1.6 | Nicke Based Lubricant

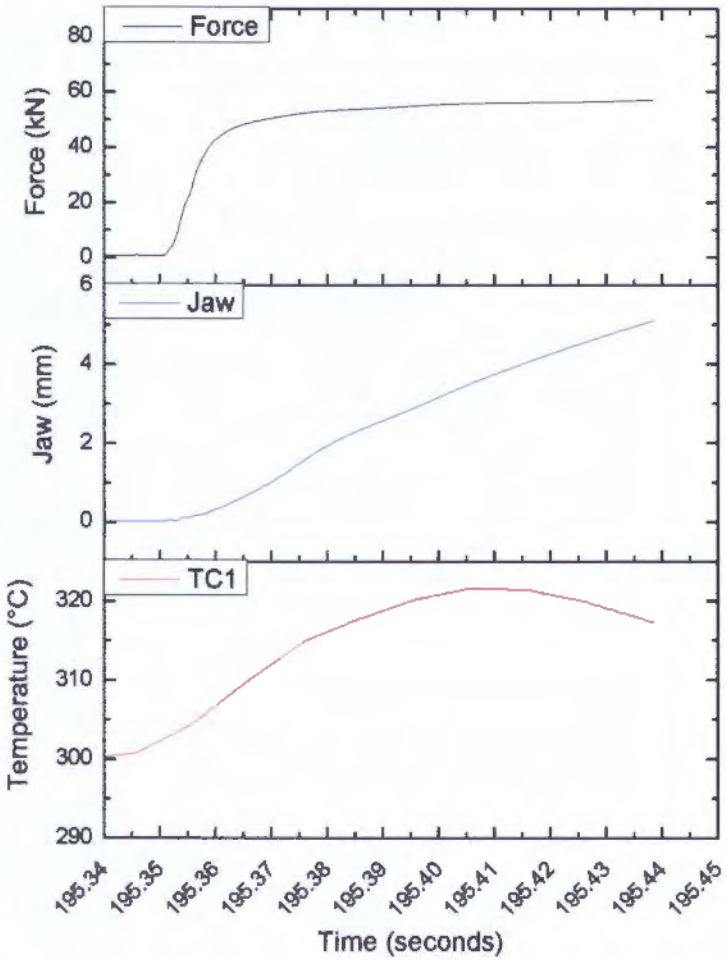

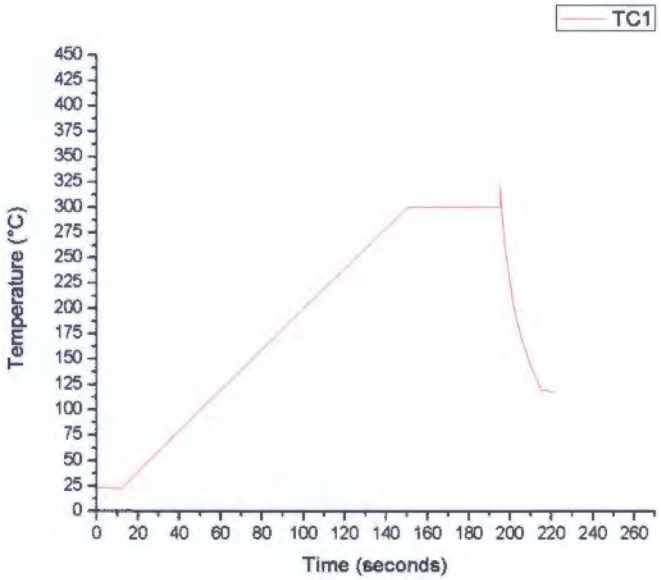

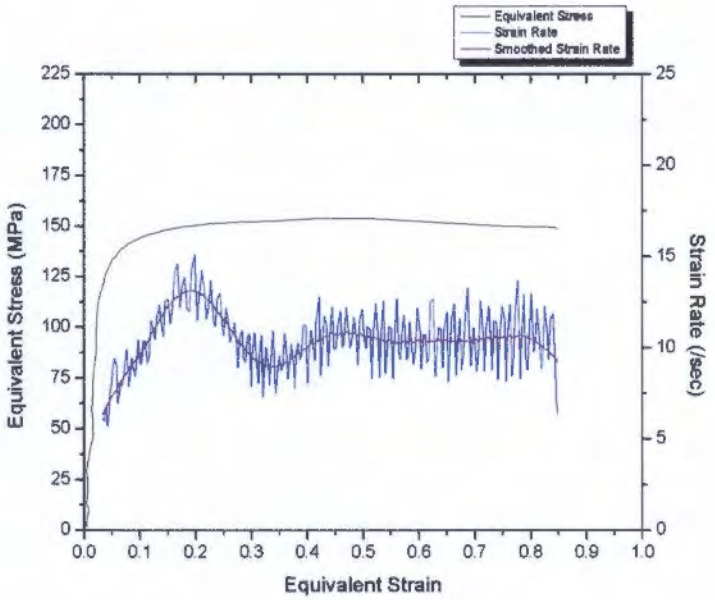

Summary:

	Value from 0.8 - 0.9 strain			Overall value	
Starting Temperature (°C)	Temperature (°C)	Flow stress (MPa)	Strain rate (sec^{-1})	Strain rate (sec^{-1})	△Temperature (°C)
300.08	317.8	149.6	9.95	10.2	17.72

Temperature: 350°C | Strain rate: 30 sec^{-1} | Strain 1.6 | Nicke Based Lubricant

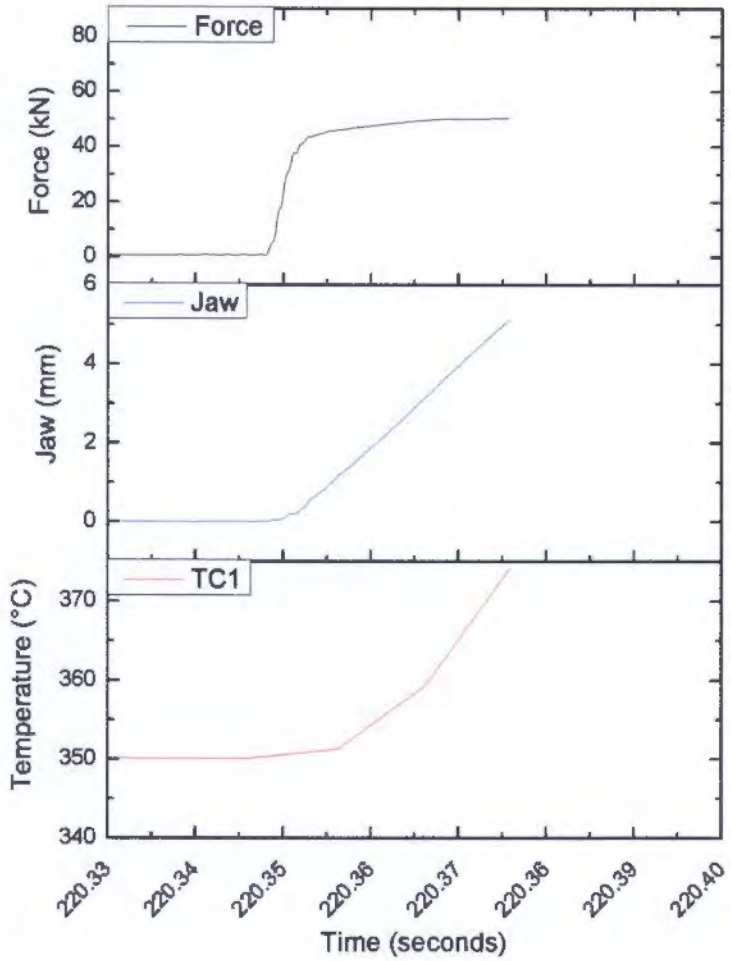

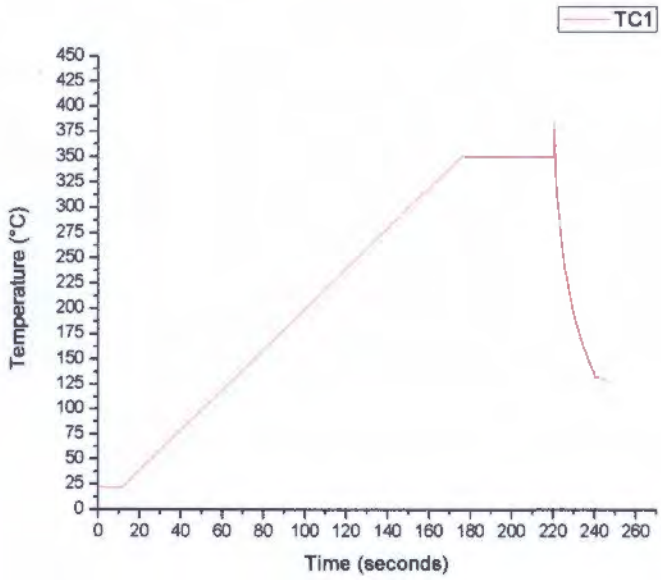

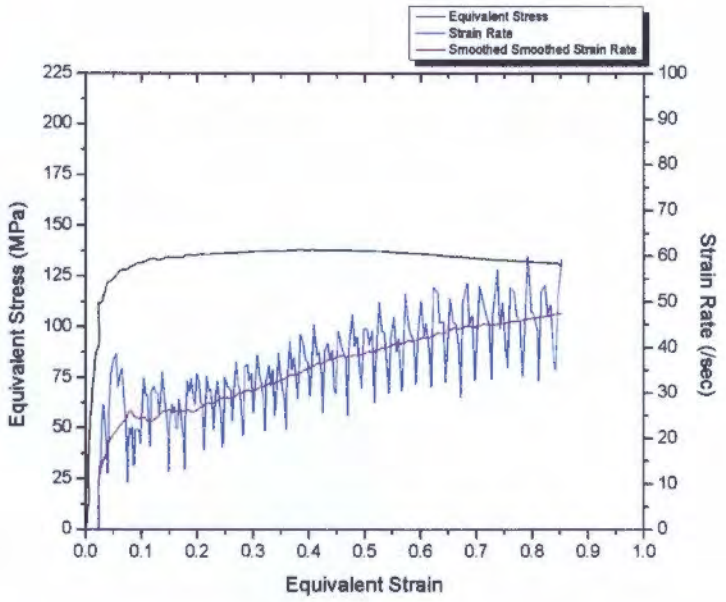

Summary:

	Value from 0.8 - 0.9 strain			Overall value	
Starting Temperature (°C)	Temperature (°C)	Flow stress (MPa)	Strain rate (sec^{-1})	Strain rate (sec^{-1})	△Temperature (°C)
350.07	373.3	131.6	46.9	33.5	23.23

Appendix E: Evans and Ricks PSC Results [49]

Nominal temperature (°C)	Mean temperature (°C)	Nominal strain rate (sec^{-1})	Mean strain rate (sec^{-1})	Mean flow stress (MPa)
300	337.1	10	10.1	137.8
300	324.4	30	30.7	144.0
300	316.1	100	83.4	149.3
350	375.0	10	10.2	117.9
350	375.7	30	30.7	123.8
350	365.2	100	97.7	136.9
400	426.4	10	9.9	93.6
400	417.6	30	30.8	101.6
400	412.7	100	93.0	107.1

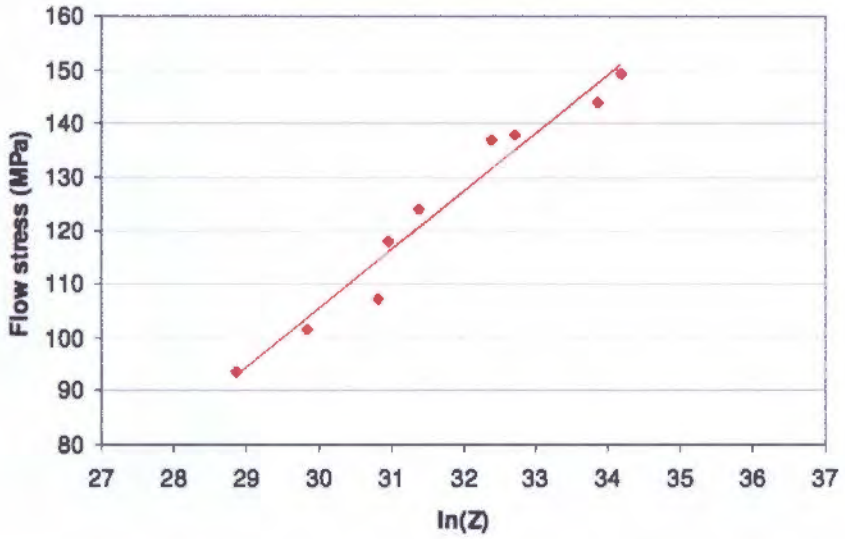

$$\dot{\varepsilon}\left(\frac{Q_{def}}{RT}\right) = A\exp\left(\beta\bar{\sigma}\right)$$

Constant	Unit	Value
Q_{def}	J/mol	155000
A	/sec	7.01×10^{8}
β	/MPa	0.091

Appendix F: Ring Compression Results

Sample No.	Strain Rate (/sec)	Temp. (°C)	Lubricant	Initial Height h0 (mm)	Deformed Height h1 (m)	Height Reduction (%)	Initial Internal Diameter d0 (mm)	Deformed Internal Diameter d1(mm)	Internal Diameter Reduction (%)
2	10	300	Nickel Base	5.14	3.14	38.98	7.49	8.60	-14.82
3	10	300	Nickel Base	5.25	2.99	42.98	7.46	8.17	-9.52
4	30	300	Nickel Base	5.10	2.22	56.47	7.39	8.73	-18.13
5	30	300	Nickel Base	5.05	3.18	37.03	7.46	8.47	-13.54
6	100	300	Nickel Base	5.01	2.91	41.98	7.44	8.47	-13.84
7	100	300	Nickel Base	5.14	2.37	53.96	7.47	8.68	-16.20
8	10	400	Nickel Base	5.10	2.63	48.37	7.47	8.25	-10.44
9	10	400	Nickel Base	5.08	3.35	33.99	7.46	8.22	-10.19
10	30	400	Nickel Base	5.12	3.39	33.85	7.44	8.22	-10.48
11	100	400	Nickel Base	4.95	2.29	53.67	7.47	7.86	-5.22
12	10	350	Nickel Base	4.94	2.42	51.01	7.46	8.46	-13.40
13	30	350	Nickel Base	5.10	2.92	42.75	7.46	8.63	-15.68
14	100	350	Nickel Base	5.02	2.72	45.82	7.46	9.14	-22.52
15	10	300	Graphite Foil	5.04	3.22	36.11	7.40	7.08	4.32
16	10	350	Graphite Foil	5.04	3.08	38.89	7.46	6.88	7.77
17	30	300	Graphite Foil	5.00	2.86	42.80	7.46	6.71	10.05
18	10	400	Graphite Foil	5.02	2.85	43.29	7.44	6.79	8.74
19	30	350	Graphite Foil	5.06	2.79	44.80	7.44	6.61	11.16
20	30	400	Graphite Foil	5.02	2.57	48.87	7.46	6.14	17.69
21	100	300	Graphite Foil	5.08	2.83	44.36	7.50	6.46	13.87
22	100	350	Graphite Foil	5.02	2.94	41.43	7.46	6.61	11.39
23	100	400	Graphite Foil	5.06	2.95	41.77	7.34	6.67	9.13
24	10	300	Graphite Foil	5.00	2.55	49.07	7.42	6.47	12.80
25	10	350	Graphite Foil	5.08	2.36	53.54	7.46	5.77	22.65
26	10	400	Graphite Foil	5.01	2.02	59.68	7.50	4.45	40.67
28	30	300	Graphite Foil	4.98	2.73	45.11	7.42	6.11	17.65
29	30	350	Graphite Foil	5.00	2.49	50.13	7.46	5.75	22.92
30	30	400	Graphite Foil	5.04	2.30	54.37	7.46	5.26	29.49
32	100	300	Graphite Foil	5.06	2.28	54.94	7.46	6.36	14.75
33	100	350	Graphite Foil	5.06	2.30	54.55	7.46	5.95	20.24

Appendix G: DSI Validation PSC Tests

Temperature: 300°C | Strain rate: 10 sec^{-1} | Strain 1.6 | Graphite Foil Lubrication

Test 1: Water Quenched

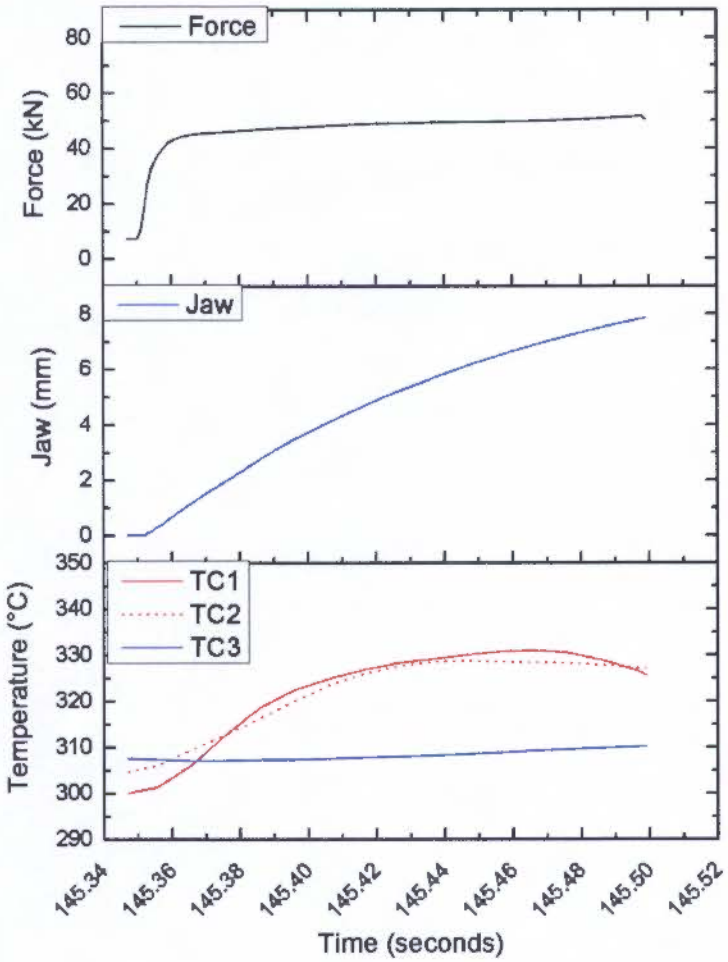

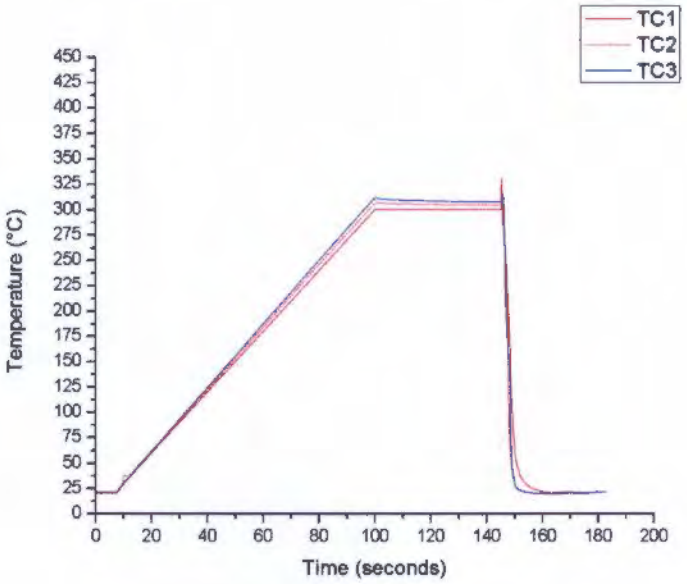

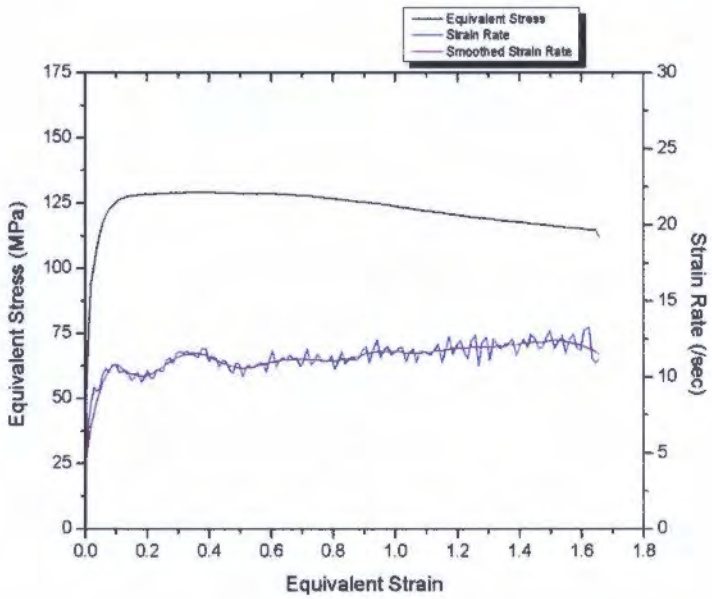

Summary:

	Value	Unit		Value	Unit
$TC1_{start}$	300.1	°C	$TC3_{start}$	307.6	°C
$TC2_{start}$	304.7	°C	$TC4_{start}$	N/A	°C
T_{grad}	4.6	°C	T_{start}	302.4	°C
$T_{0.8\text{-}0.9}$	328.3	°C	ΔT	25.9	°C
$\dot{\varepsilon}_{whole}$	10.9	sec^{-1}	$\dot{\varepsilon}_{0.8-0.9}$	11.2	sec^{-1}
Flow Stress	126.1	MPa	$ln(Z)$	33.42	

Test 2: Water Quenched

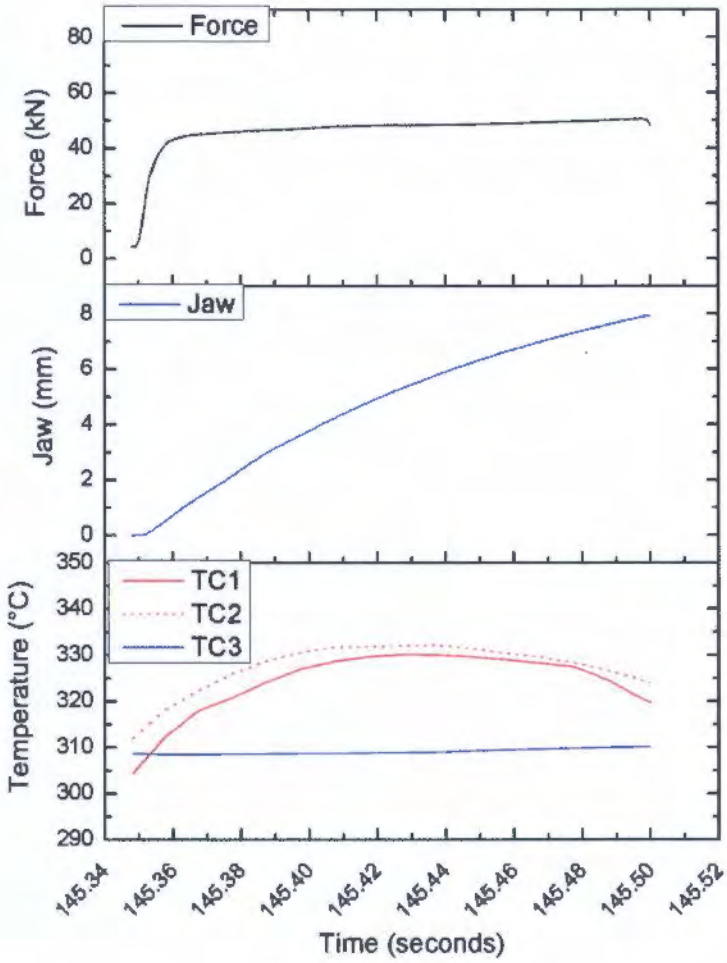

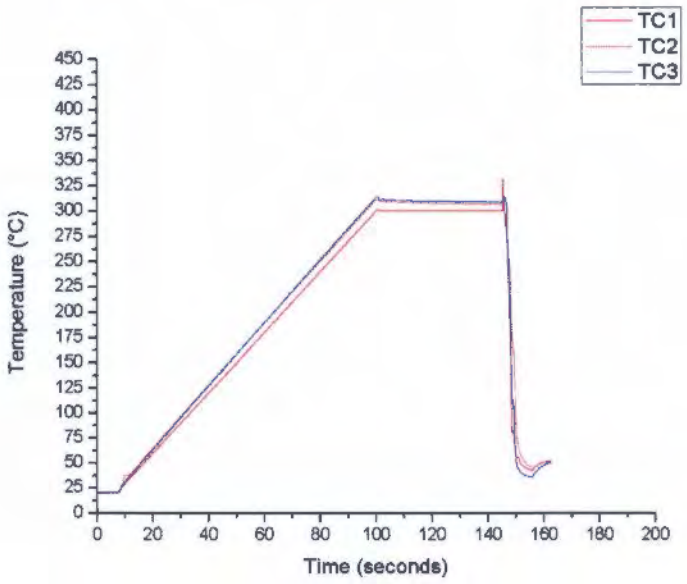

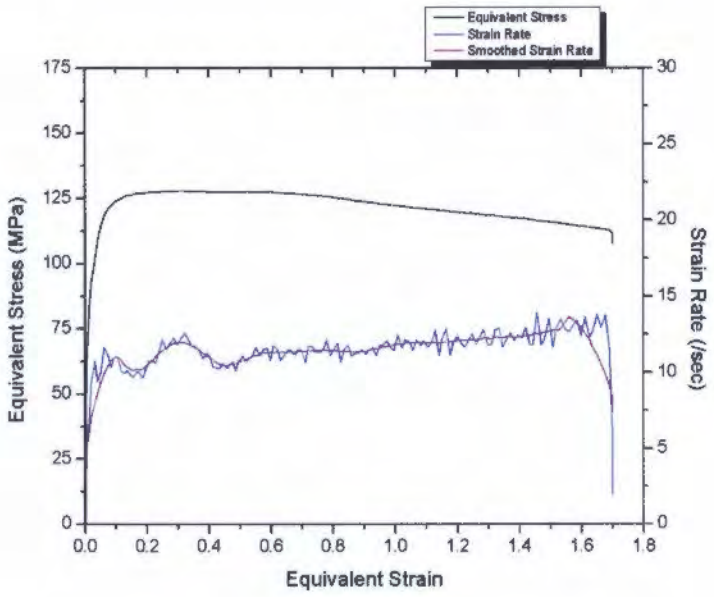

Summary:

	Value	Unit		Value	Unit
$TC1_{start}$	304.4	°C	$TC3_{start}$	308.7	°C
$TC2_{start}$	311.9	°C	$TC4_{start}$	N/A	°C
T_{grad}	7.5	°C	T_{start}	308.2	°C
$T_{0.8\text{-}0.9}$	331.0	°C	ΔT	22.9	°C
$\dot{\varepsilon}_{whole}$	11.1	sec^{-1}	$\dot{\varepsilon}_{0.8-0.9}$	11.4	sec^{-1}
Flow Stress	124.6	MPa	$ln(Z)$	33.3	

Temperature: 300°C | Strain rate: 30 sec^{-1} | Strain 1.6 | Graphite Foil Lubrication

Test 1: Water Quenched

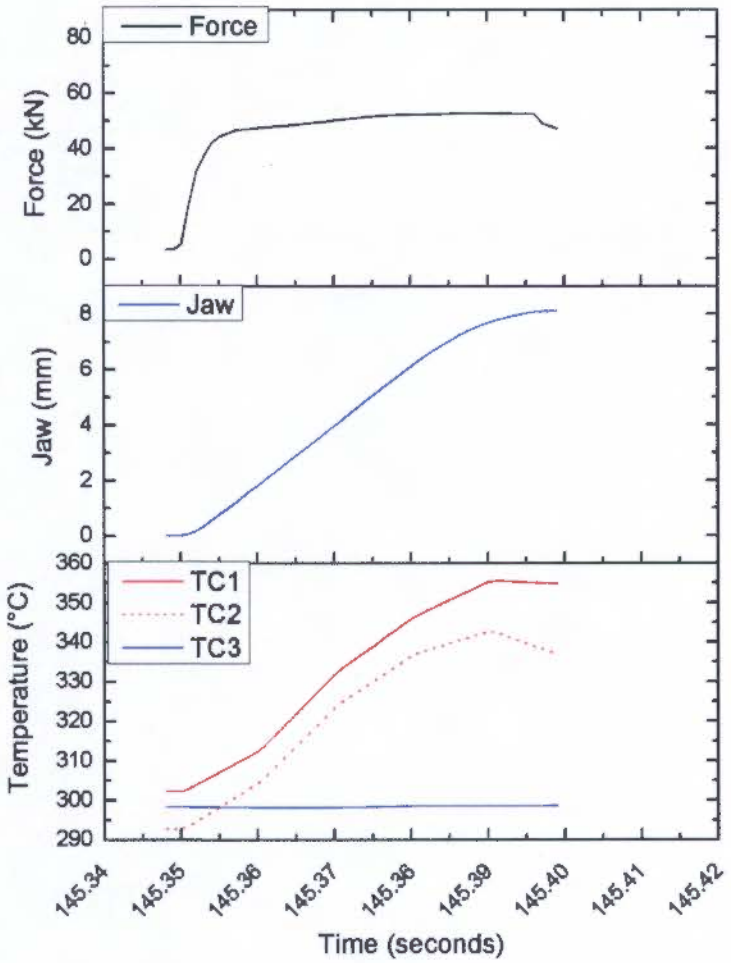

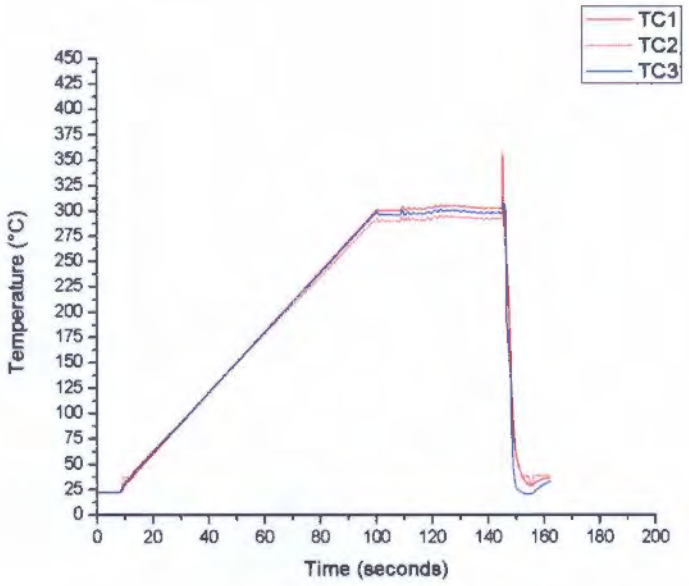

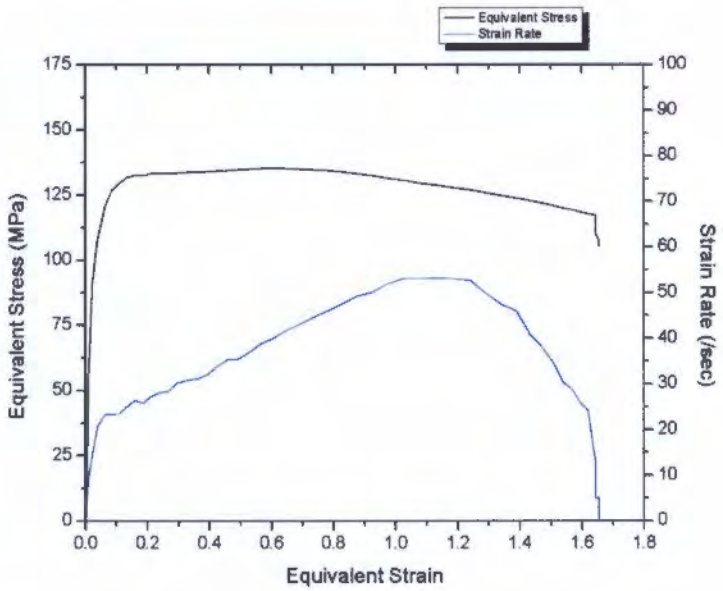

Summary:

	Value	Unit		Value	Unit
$TC1_{start}$	302.3	°C	$TC3_{start}$	298.4	°C
$TC2_{start}$	292.8	°C	$TC4_{start}$	N/A	°C
T_{grad}	9.5	°C	T_{start}	297.6	°C
$T_{0.8\text{-}0.9}$	337.9	°C	ΔT	40.4	°C
$\dot{\varepsilon}_{whole}$	30.7	sec^{-1}	$\dot{\varepsilon}_{0.8-0.9}$	48.2	sec^{-1}
Flow Stress	133.6	MPa	$ln(Z)$	34.39	

Test 2: Water Quenched

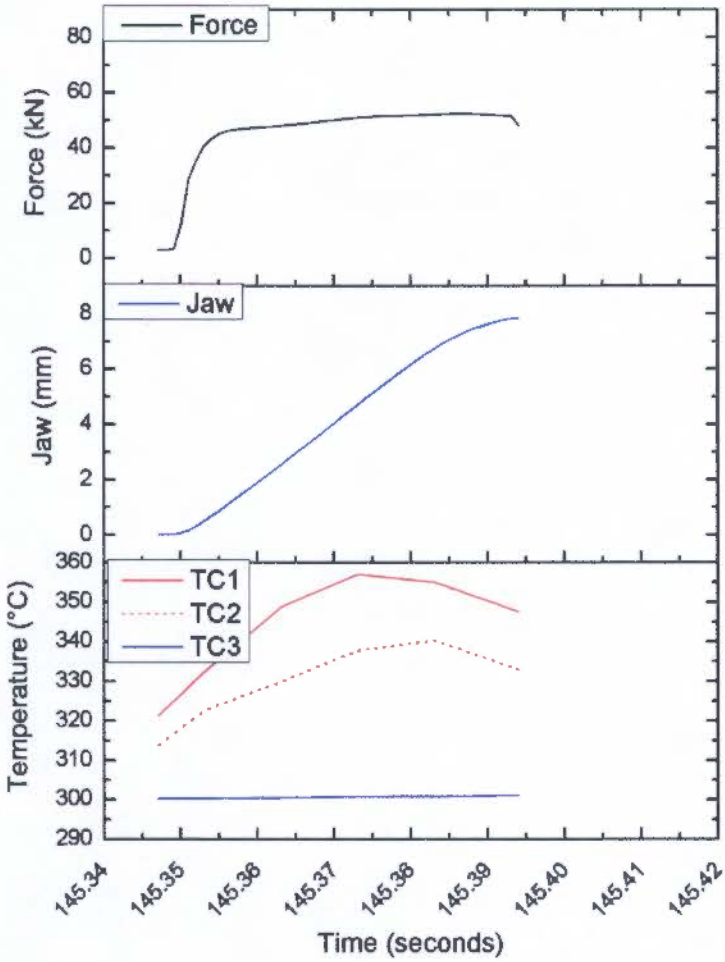

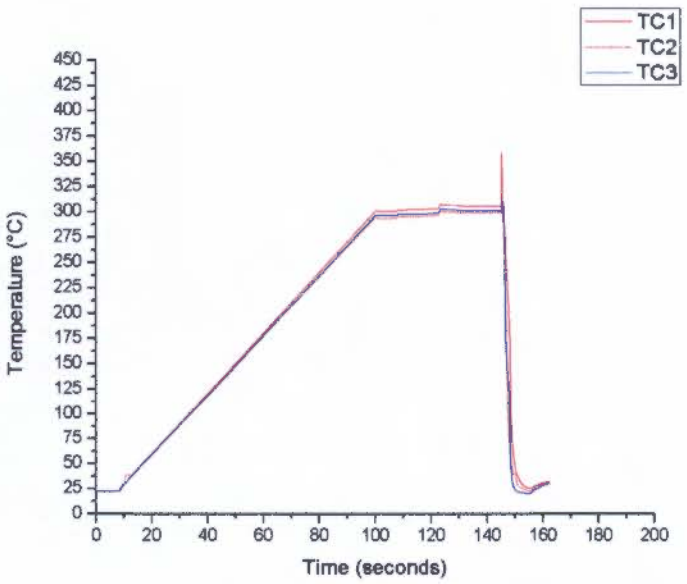

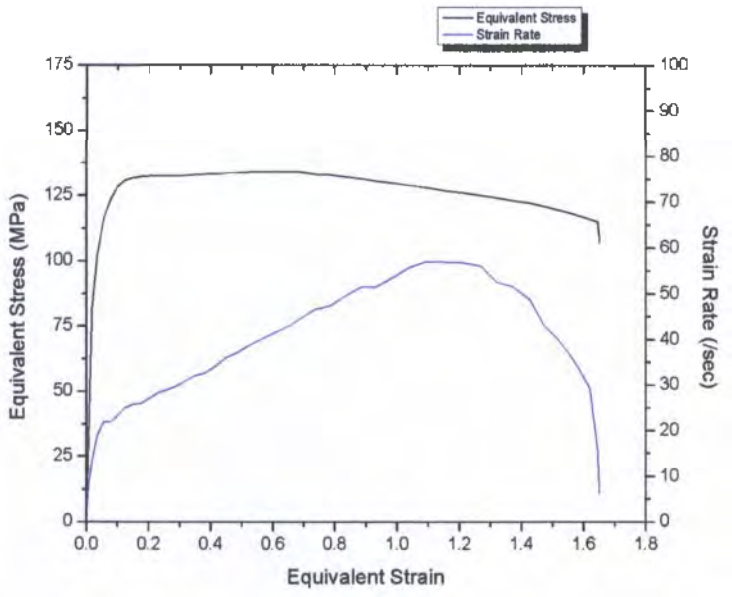

Summary:

	Value	Unit		Value	Unit
$TC1_{start}$	321.3	°C	$TC3_{start}$	300.3	°C
$TC2_{start}$	313.8	°C	$TC4_{start}$	N/A	°C
T_{grad}	7.5	°C	T_{start}	317.6	°C
$T_{0.8\text{-}0.9}$	347.4	°C	$\triangle T$	29.85	°C
$\dot{\varepsilon}_{whole}$	32.6	sec^{-1}	$\dot{\varepsilon}_{0.8-0.9}$	49.9	sec^{-1}
Flow Stress	132	MPa	$ln(Z)$	33.96	

Temperature: 300°C | Strain rate: 100 sec^{-1} | Strain 1.6 | Graphite Foil Lubrication

Test 1: Water Quenched

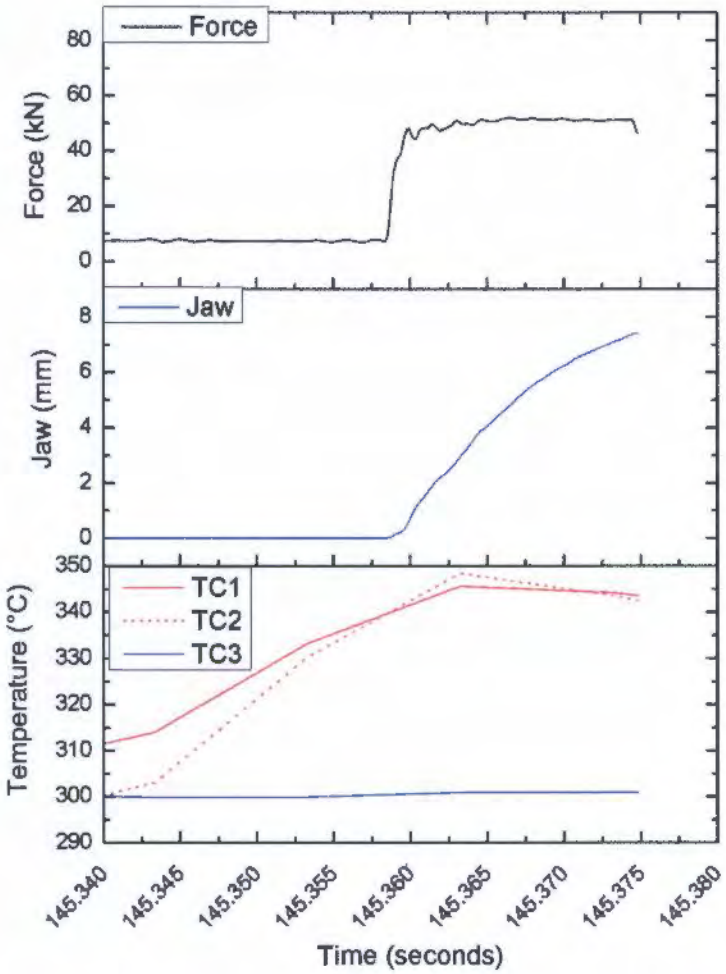

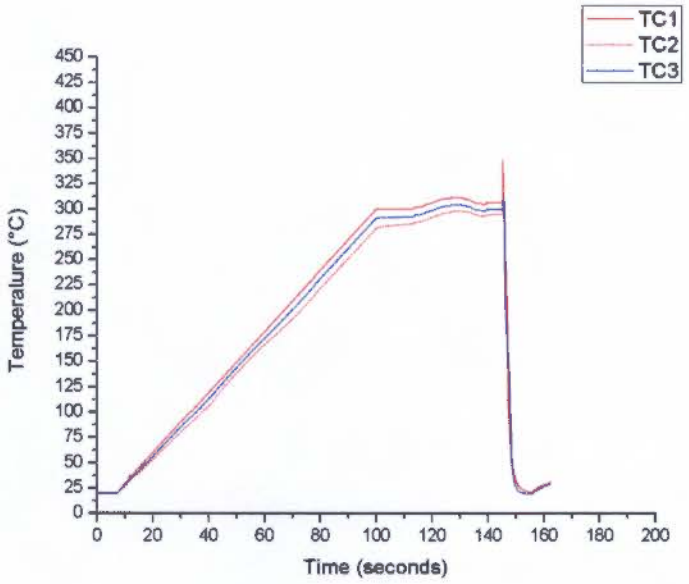

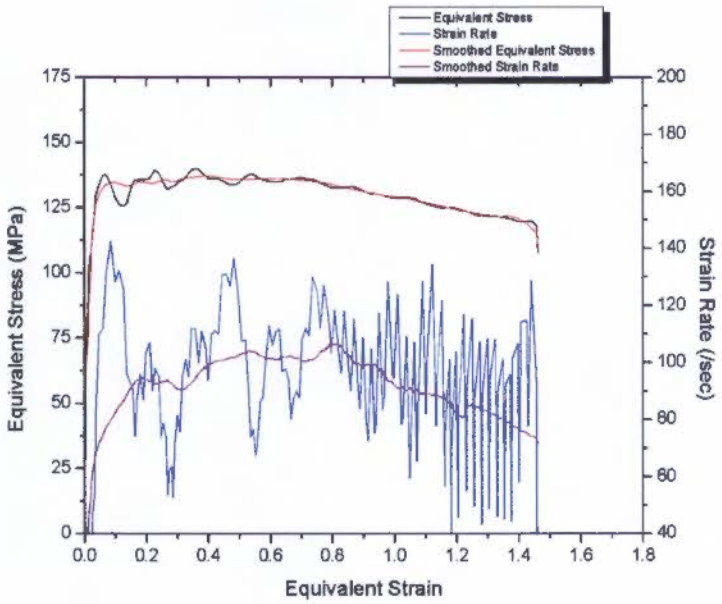

Summary:

	Value	Unit		Value	Unit
$TC1_{start}$	306.5	°C	$TC3_{start}$	300.8	°C
$TC2_{start}$	295.0	°C	$TC4_{start}$	N/A	°C
T_{grad}	11.5	°C	T_{start}	300.8	°C
$T_{0.8\text{-}0.9}$	345.6	°C	ΔT	44.9	°C
$\dot{\varepsilon}_{whole}$	89.6	sec^{-1}	$\dot{\varepsilon}_{0.8-0.9}$	101.6	sec^{-1}
Flow Stress	132.5	MPa	$ln(Z)$	34.76	

Test 2: Water Quenched

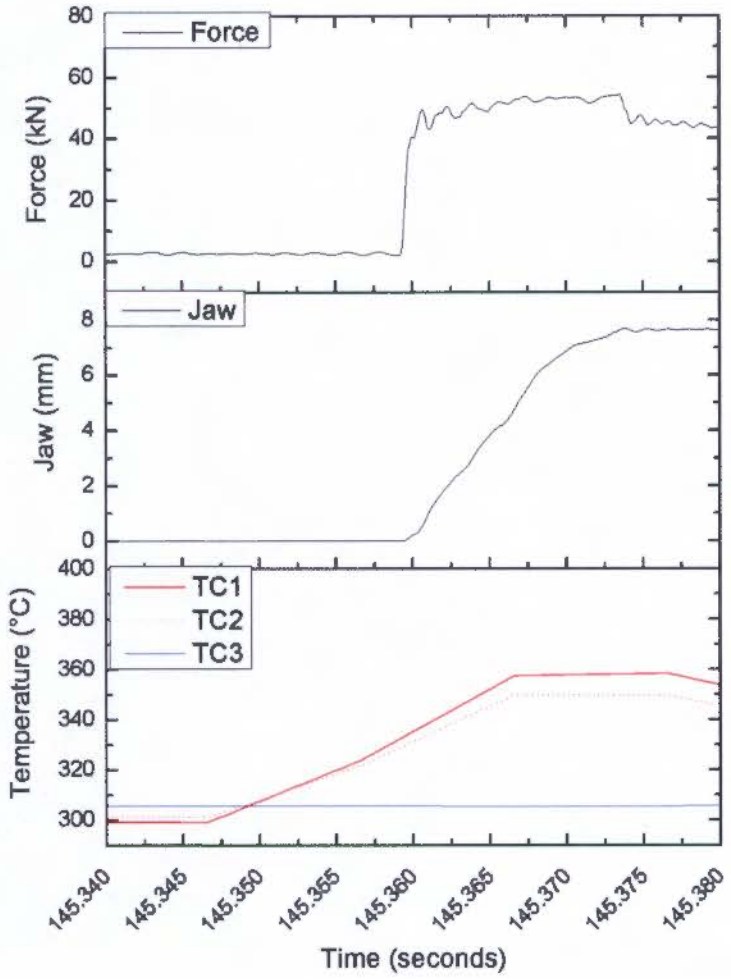

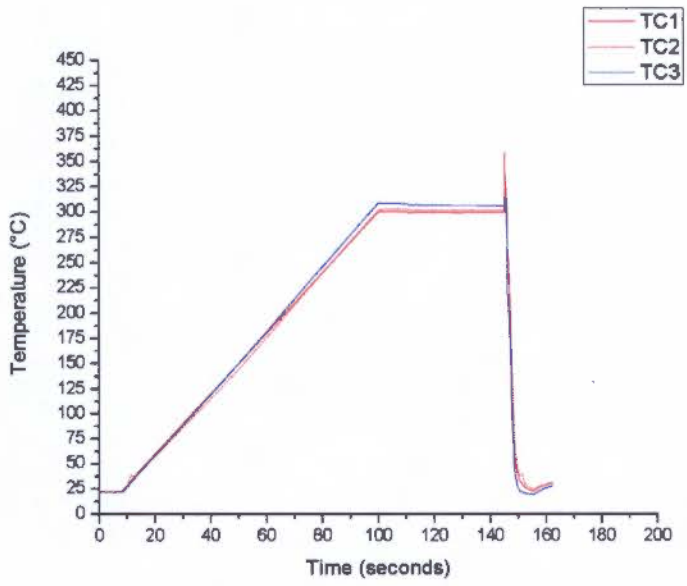

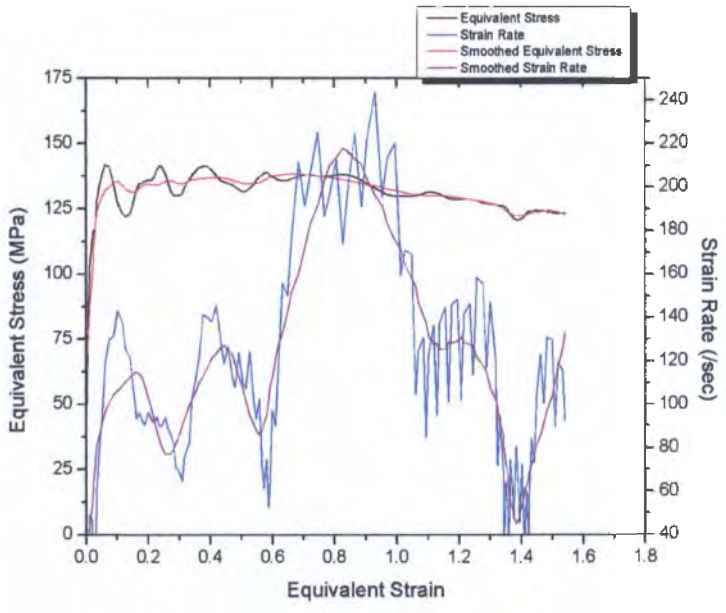

Summary:

	Value	Unit		Value	Unit
$TC1_{start}$	331.6	°C	$TC3_{start}$	305.6	°C
$TC2_{start}$	328.3	°C	$TC4_{start}$	N/A	°C
T_{grad}	3.3	°C	T_{start}	330.0	°C
$T_{0.8\text{-}0.9}$	353.7	°C	$\triangle T$	23.8	°C
$\dot{\varepsilon}_{whole}$	110.6	sec^{-1}	$\dot{\varepsilon}_{0.8-0.9}$	212.1	sec^{-1}
Flow Stress	137.1	MPa	$ln(Z)$	35.11	

Temperature: 350°C | Strain rate: 10 sec^{-1} | Strain 1.6 | Graphite Foil Lubrication

Test 1: Water Quenched

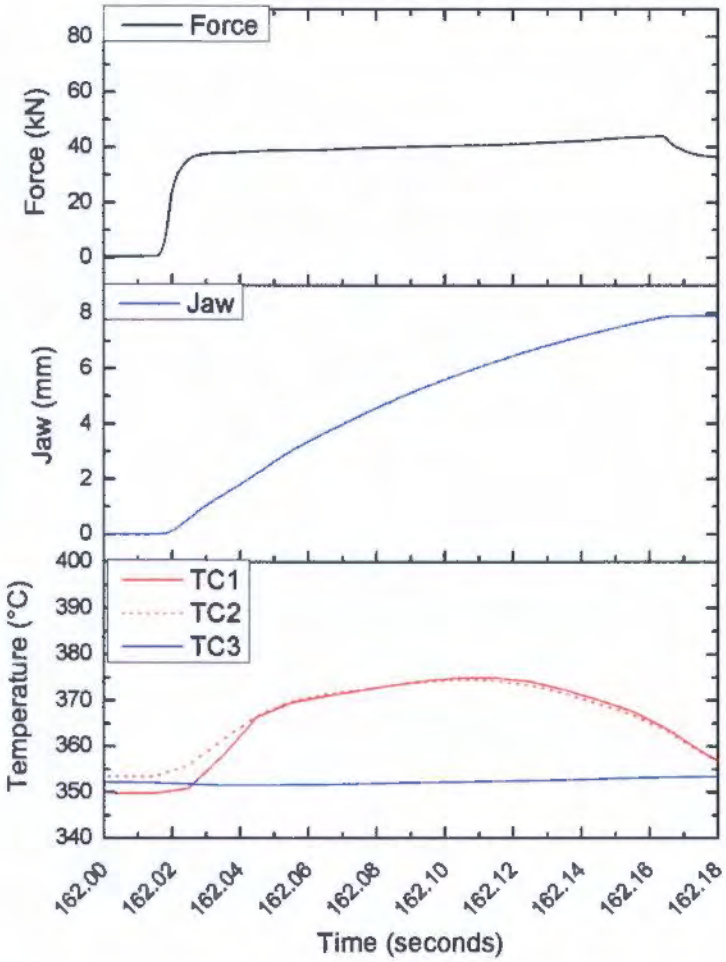

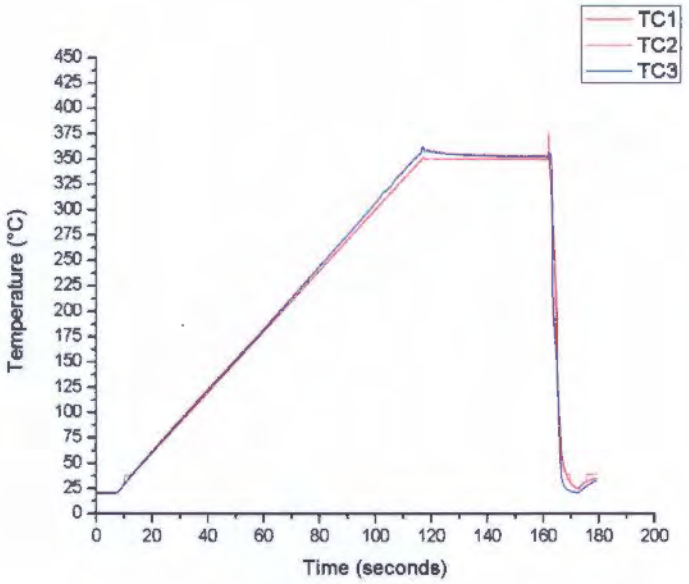

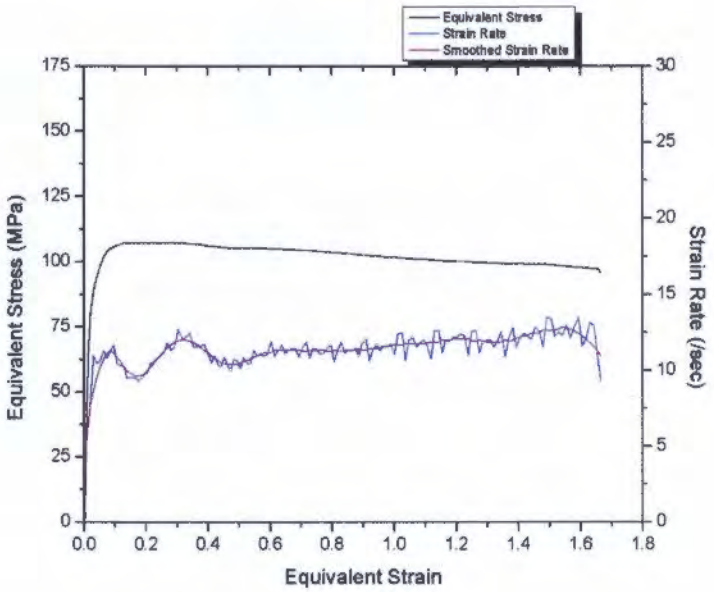

Summary:

	Value	Unit		Value	Unit
$TC1_{start}$	349.8	°C	$TC3_{start}$	351.2	°C
$TC2_{start}$	353.5	°C	$TC4_{start}$	N/A	°C
T_{grad}	3.7	°C	T_{start}	351.7	°C
$T_{0.8\text{-}0.9}$	374.3	°C	$\triangle T$	22.7	°C
$\dot{\varepsilon}_{whole}$	11.1	sec^{-1}	$\dot{\varepsilon}_{0.8-0.9}$	11.3	sec^{-1}
Flow Stress	103.1	MPa	$ln(Z)$	31.23	

Test 2: Water Quenched

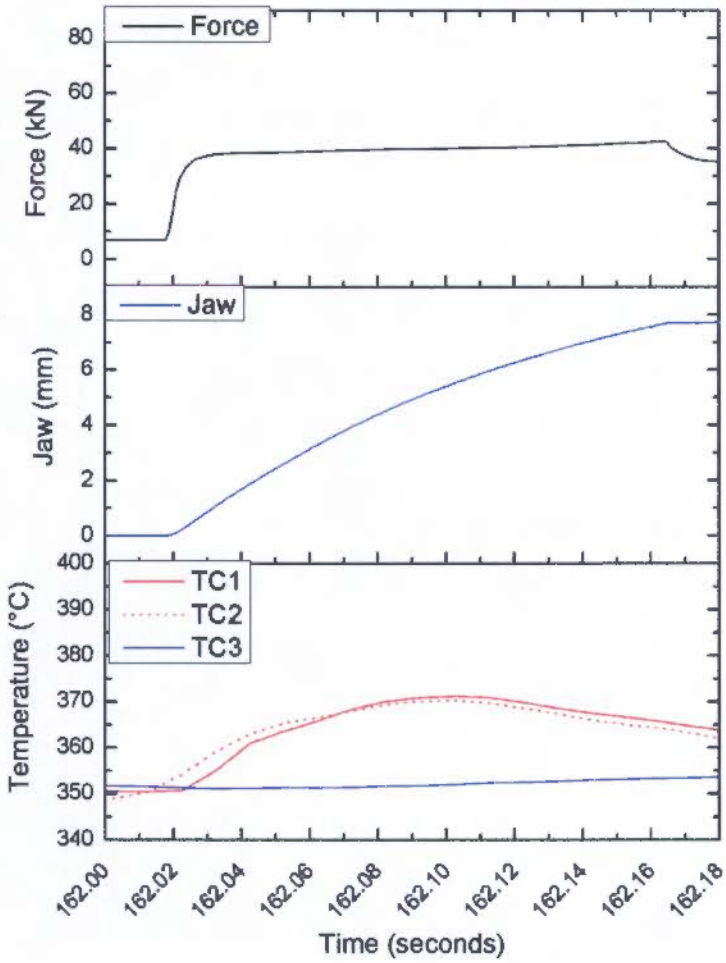

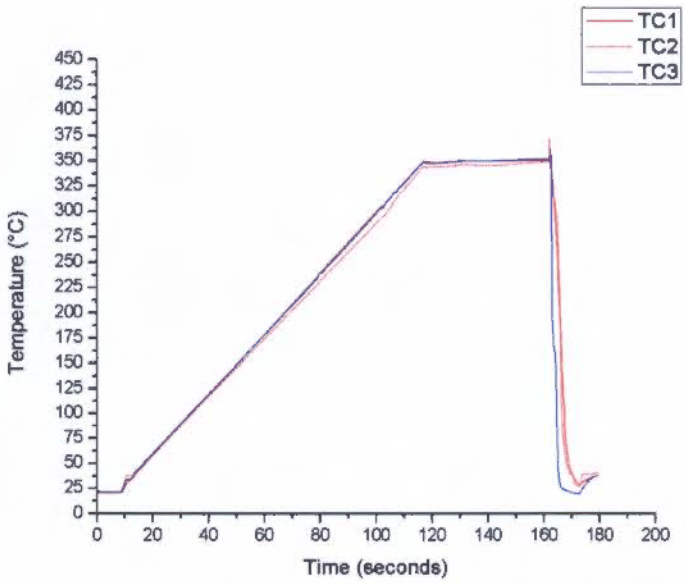

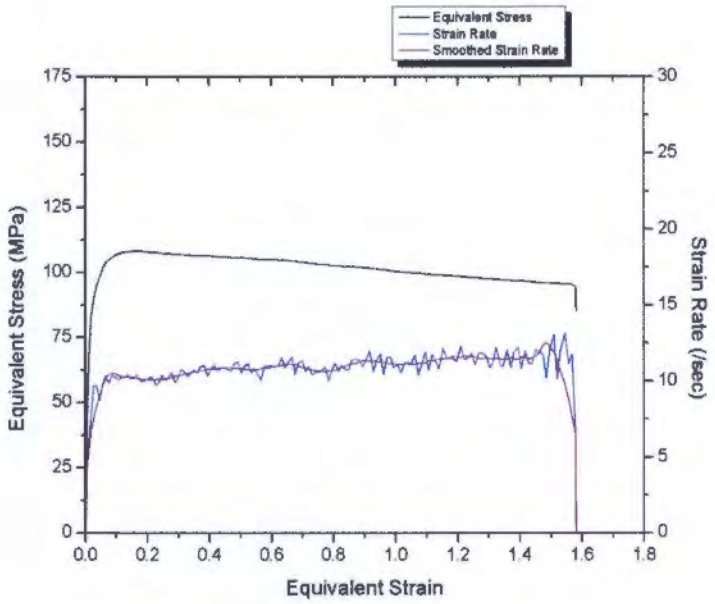

Summary:

	Value	Unit		Value	Unit
$TC1_{start}$	350.5	°C	$TC3_{start}$	351.4	°C
$TC2_{start}$	351.9	°C	$TC4_{start}$	N/A	°C
T_{grad}	1.4	°C	T_{start}	351.2	°C
$T_{0.8\text{-}0.9}$	370.6	°C	ΔT	19.4	°C
$\dot{\varepsilon}_{whole}$	10.5	sec^{-1}	$\dot{\varepsilon}_{0.8-0.9}$	11.0	sec^{-1}
Flow Stress	102.2	MPa	$ln(Z)$	31.37	

Temperature: 350°C | Strain rate: 30 sec^{-1} | Strain 1.6 | Graphite Foil Lubrication

Test 1: Water Quenched

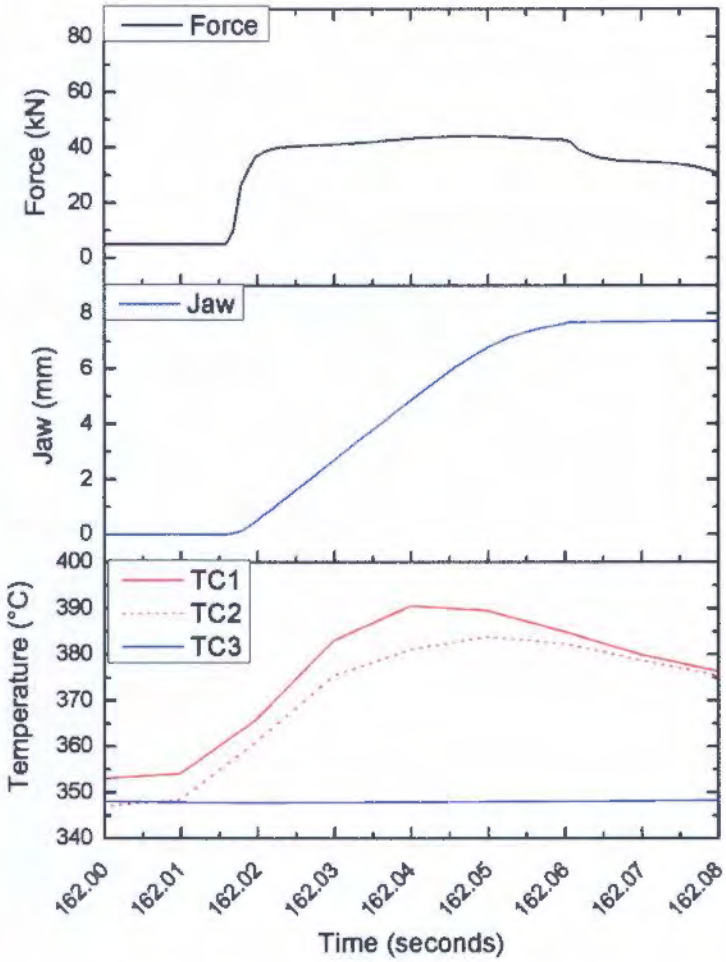

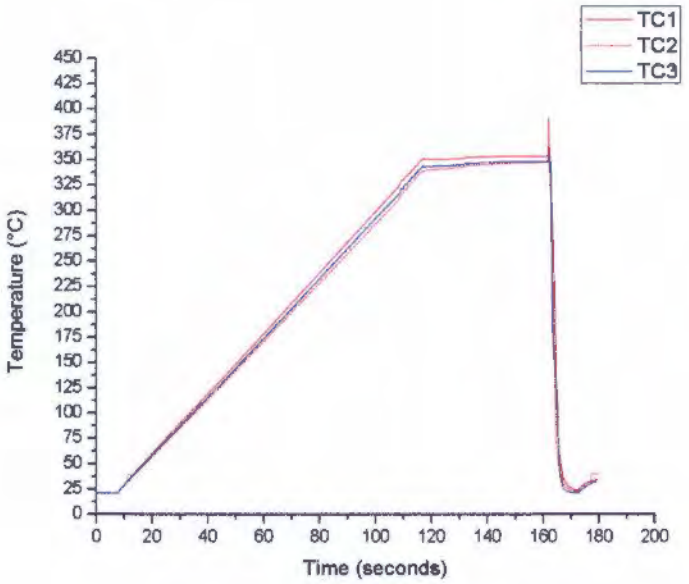

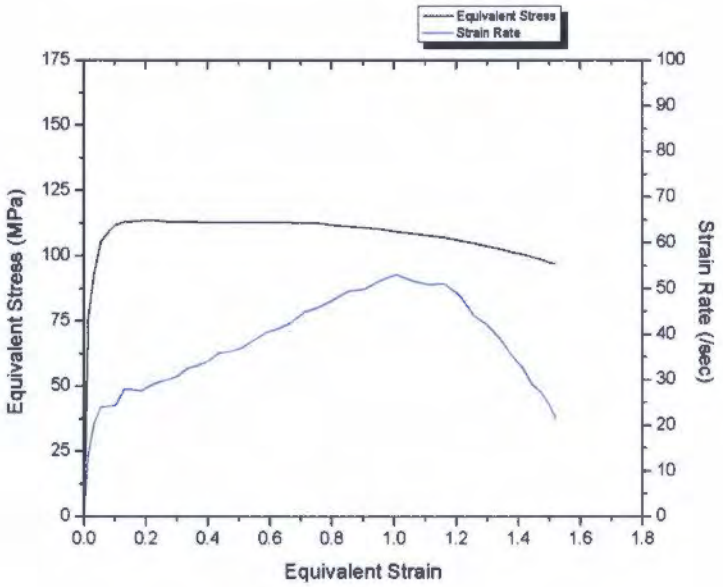

Summary:

	Value	Unit		Value	Unit
$TC1_{start}$	358.7	°C	$TC3_{start}$	347.8	°C
$TC2_{start}$	353.4	°C	$TC4_{start}$	N/A	°C
T_{grad}	5.3	°C	T_{start}	356.1	°C
$T_{0.8\text{-}0.9}$	386.0	°C	ΔT	29.9	°C
$\dot{\varepsilon}_{whole}$	34.0	sec^{-1}	$\dot{\varepsilon}_{0.8-0.9}$	48.2	sec^{-1}
Flow Stress	111.6	MPa	$ln(Z)$	32.17	

Test 2: Water Quenched

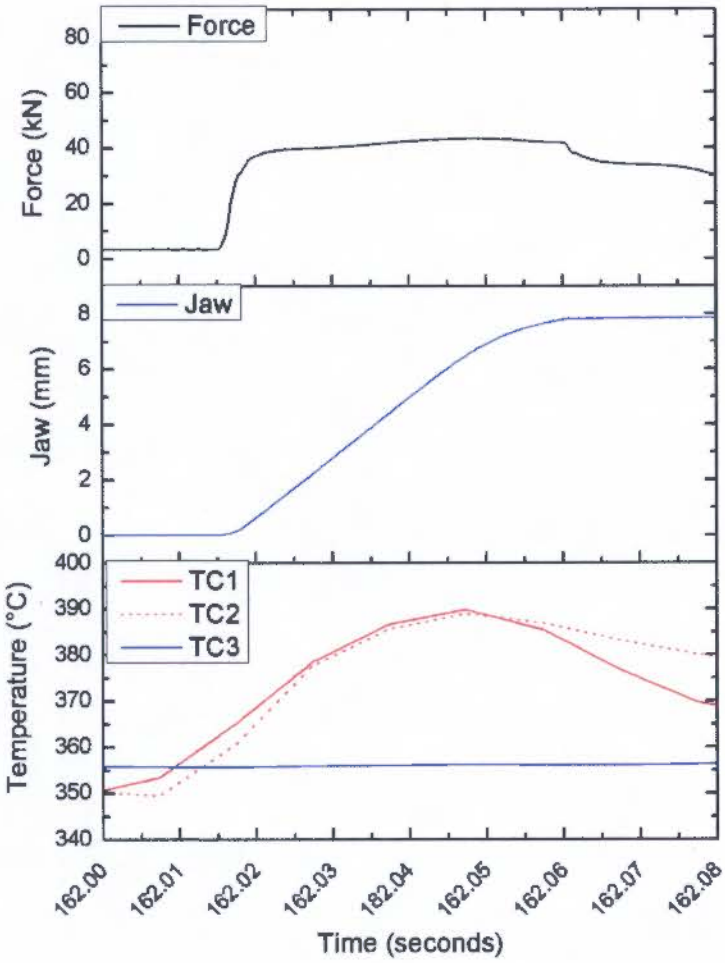

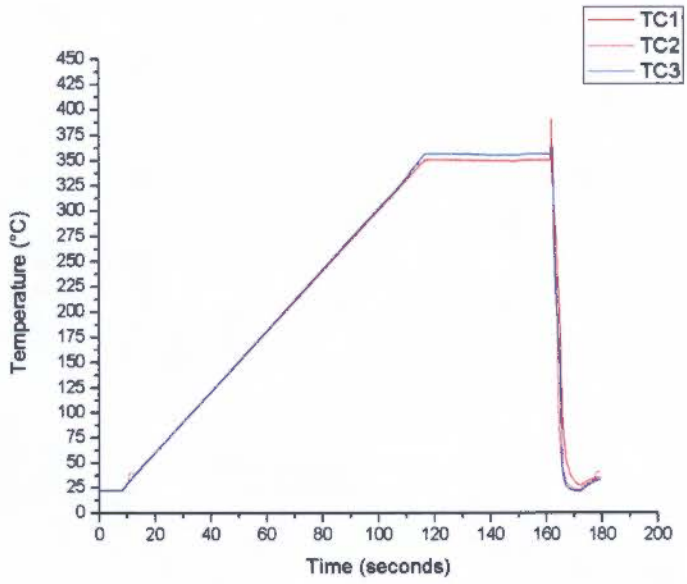

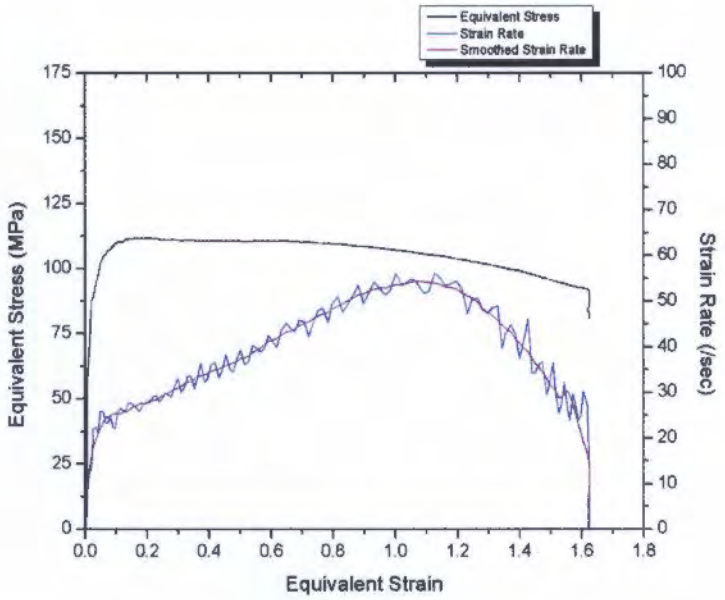

Summary:

	Value	Unit		Value	Unit
$TC1_{start}$	362.1	°C	$TC3_{start}$	355.7	°C
$TC2_{start}$	357.8	°C	$TC4_{start}$	N/A	°C
T_{grad}	4.3	°C	T_{start}	360.0	°C
$T_{0.8\text{-}0.9}$	387.8	°C	ΔT	27.9	°C
$\dot{\varepsilon}_{whole}$	34.2	sec^{-1}	$\dot{\varepsilon}_{0.8-0.9}$	50.30	sec^{-1}
Flow Stress	109	MPa	$ln(Z)$	32.13	

Temperature: 350°C | Strain rate: 100 sec^{-1} | Strain 1.6 | Graphite Foil Lubrication

Test 1: Water Quenched

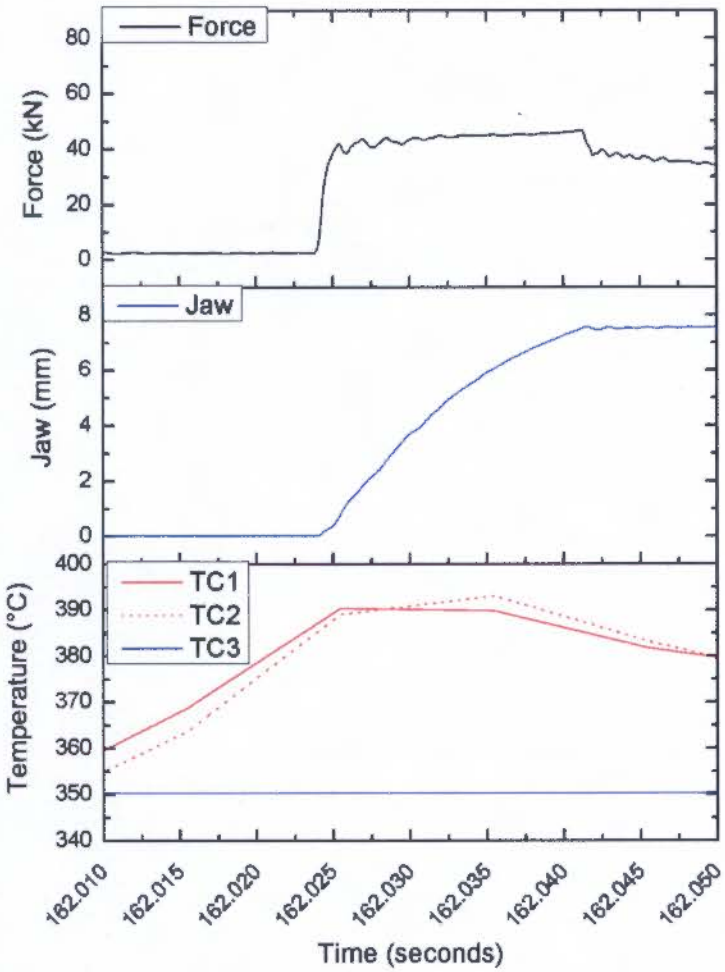

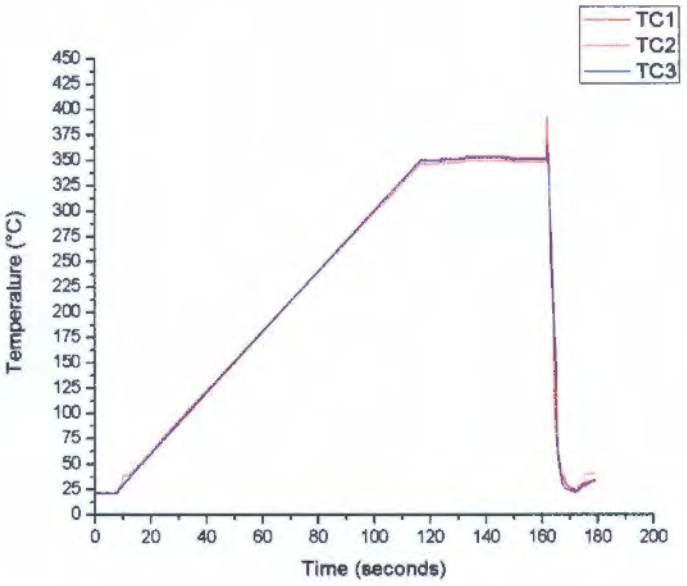

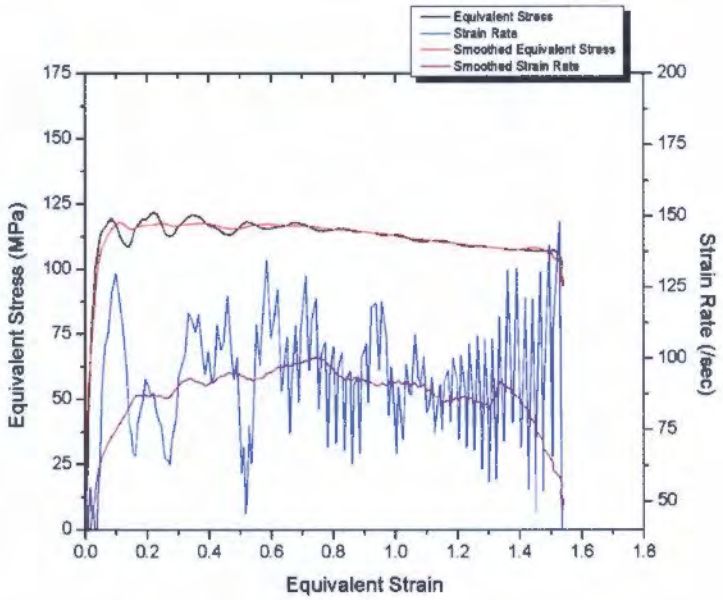

Summary:

	Value	Unit		Value	Unit
$TC1_{start}$	386.3	°C	$TC3_{start}$	350.3	°C
$TC2_{start}$	384.3	°C	$TC4_{start}$	N/A	°C
T_{grad}	2.0	°C	T_{start}	385.3	°C
$T_{0.8\text{-}0.9}$	391.1	°C	ΔT	5.8	°C
$\dot{\varepsilon}_{whole}$	83.6	sec^{-1}	$\dot{\varepsilon}_{0.8-0.9}$	93.3	sec^{-1}
Flow Stress	115	MPa	$ln(Z)$	32.61	

Test 2: Water Quenched

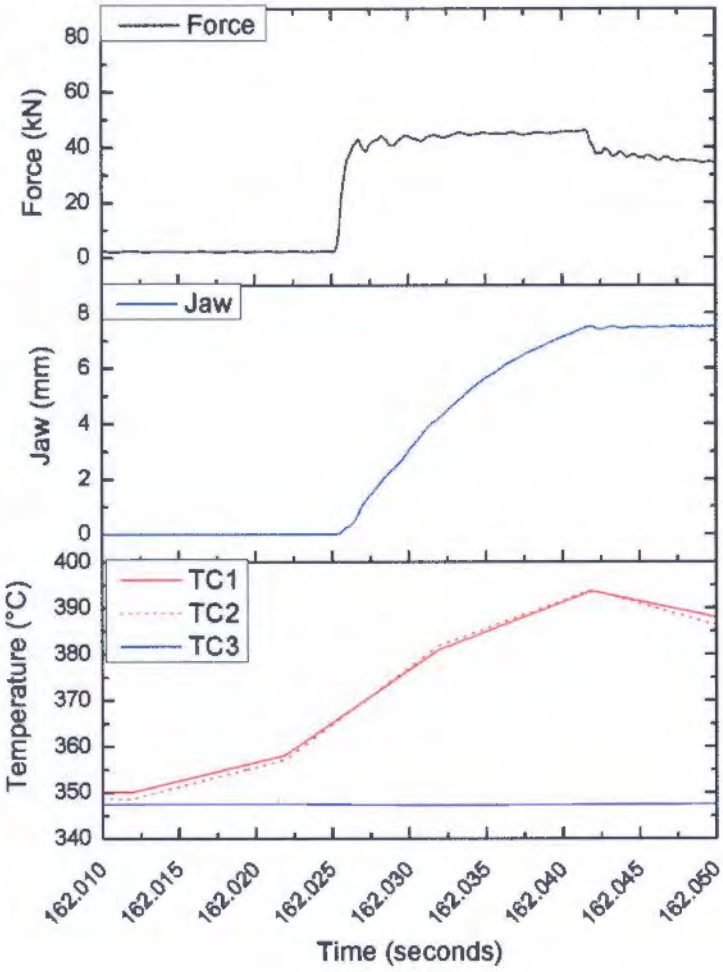

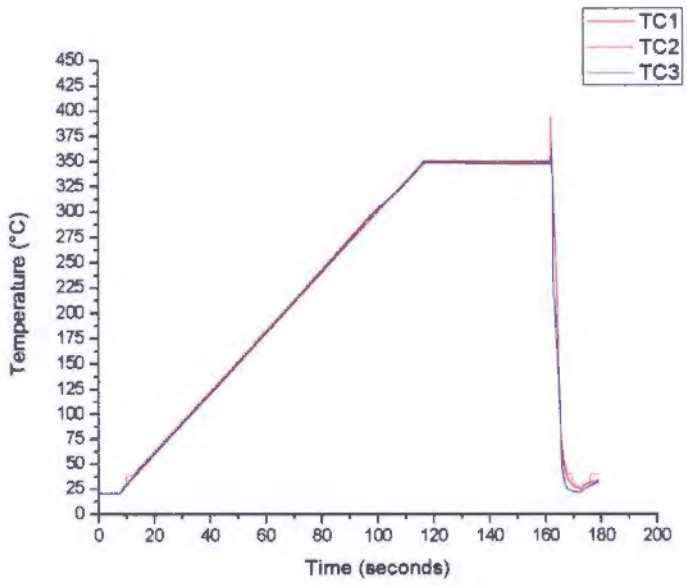

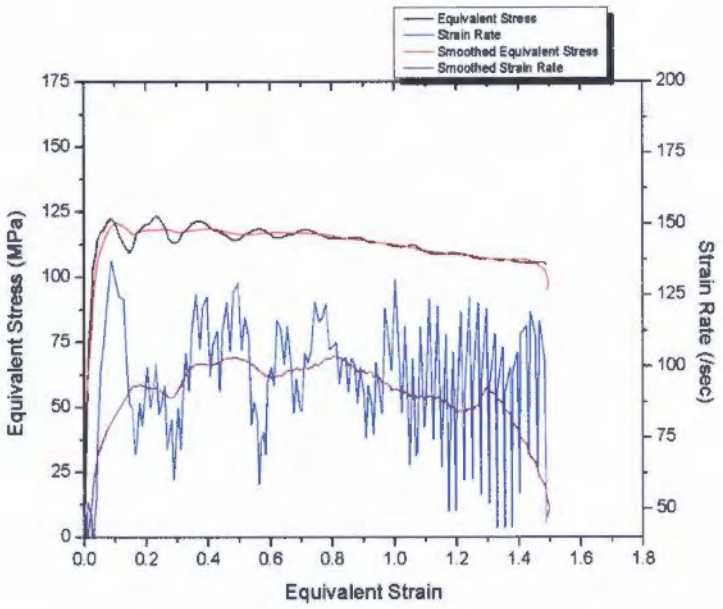

Summary:

	Value	Unit		Value	Unit
$TC1_{start}$	364.7	°C	$TC3_{start}$	347.4	°C
$TC2_{start}$	364.3	°C	$TC4_{start}$	N/A	°C
T_{grad}	0.4	°C	T_{start}	364.5	°C
$T_{0.8\text{-}0.9}$	384.7	°C	ΔT	20.2	°C
$\dot{\varepsilon}_{whole}$	86.4	sec^{-1}	$\dot{\varepsilon}_{0.8-0.9}$	101.1	sec^{-1}
Flow Stress	114.6	MPa	$ln(Z)$	32.96	

Temperature: 400°C | Strain rate: 10 sec^{-1} | Strain 1.6 | Graphite Foil Lubrication

Test 1: Water Quenched

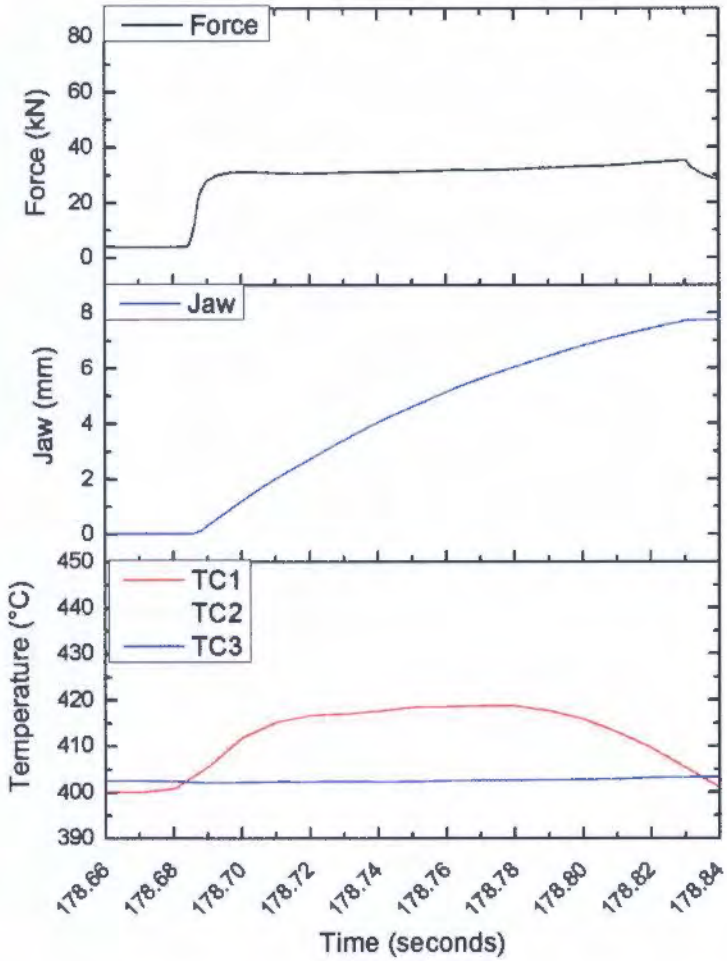

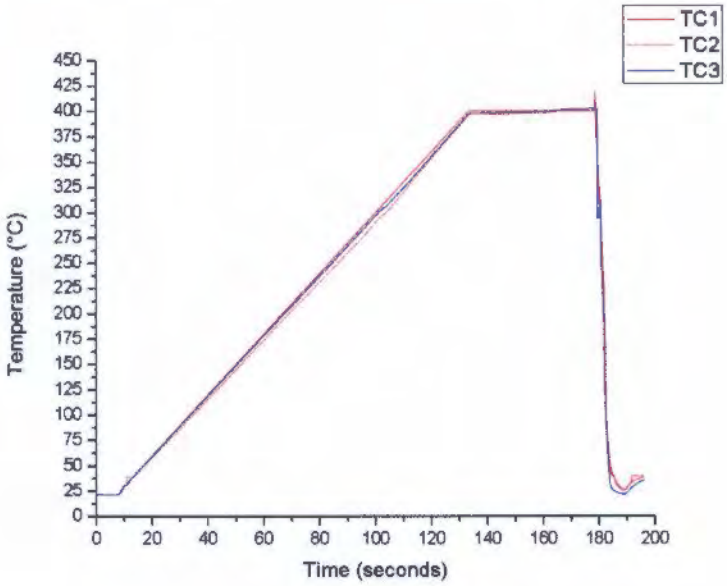

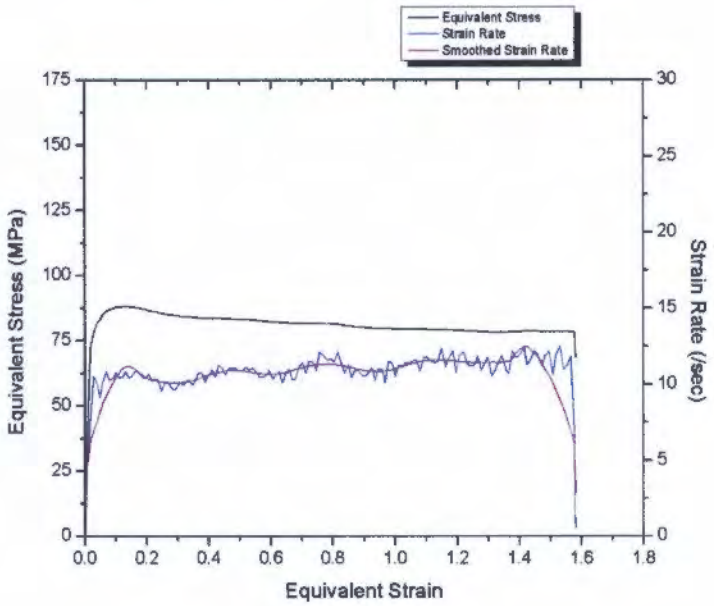

Summary:

	Value	Unit		Value	Unit
$TC1_{start}$	401.3	°C	$TC3_{start}$	402.4	°C
$TC2_{start}$	402.2	°C	$TC4_{start}$	N/A	°C
T_{grad}	0.9	°C	T_{start}	401.8	°C
$T_{0.8\text{-}0.9}$	418.4	°C	$\triangle T$	16.7	°C
$\dot{\varepsilon}_{whole}$	10.3	sec^{-1}	$\dot{\varepsilon}_{0.8-0.9}$	11.1	sec^{-1}
Flow Stress	80.76	MPa	$ln(Z)$	29.38	

Test 2: Water Quenched

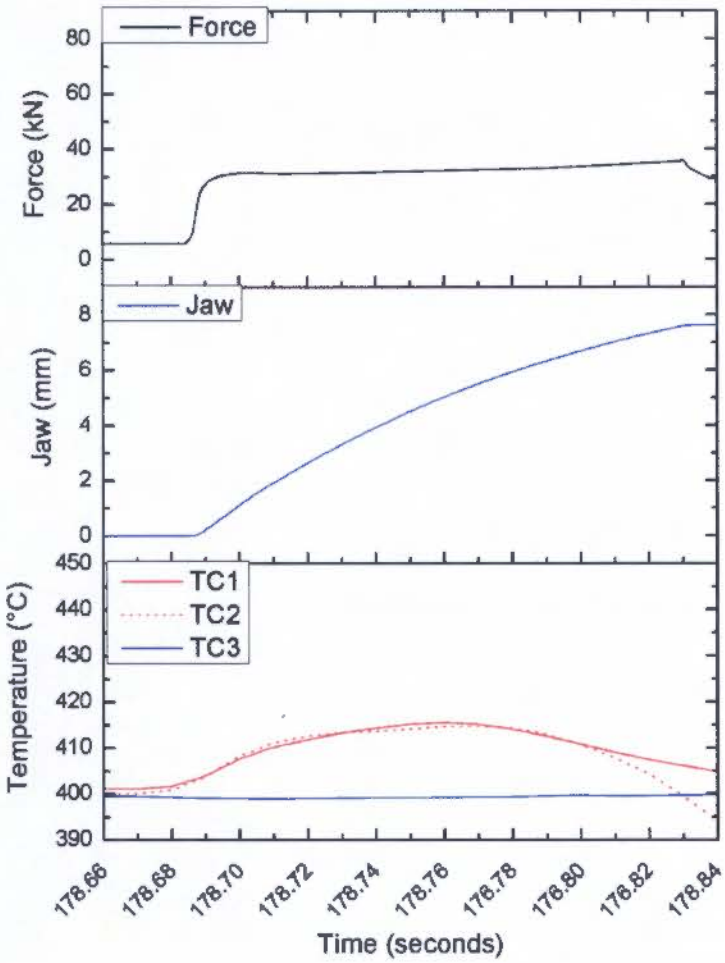

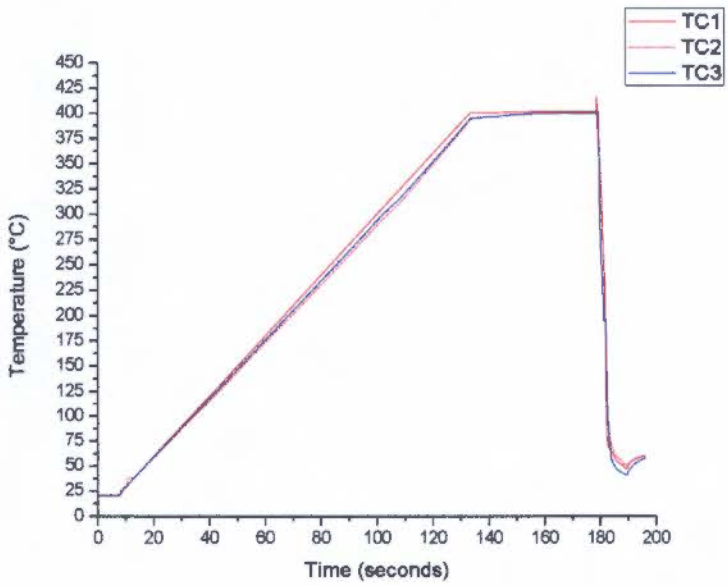

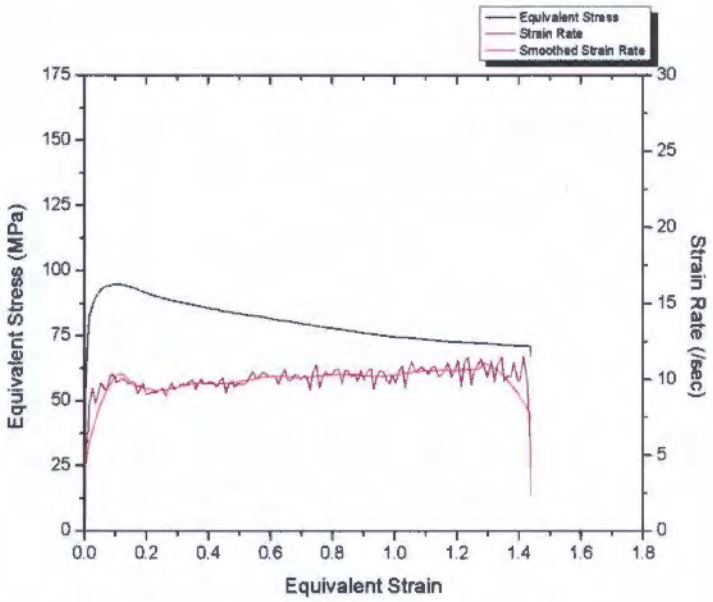

Summary:

	Value	Unit		Value	Unit
$TC1_{start}$	402.5	°C	$TC3_{start}$	399.2	°C
$TC2_{start}$	401.9	°C	$TC4_{start}$	N/A	°C
T_{grad}	0.6	°C	T_{start}	402.2	°C
$T_{0.8\text{-}0.9}$	414.6	°C	$\triangle T$	12.4	°C
$\dot{\varepsilon}_{whole}$	9.7	sec^{-1}	$\dot{\varepsilon}_{0.8-0.9}$	10.3	sec^{-1}
Flow Stress	77.19	MPa	$ln(Z)$	29.45	

Temperature: 400°C | Strain rate: 30 sec^{-1} | Strain 1.6 | Graphite Foil Lubrication

Test 1: Water Quenched

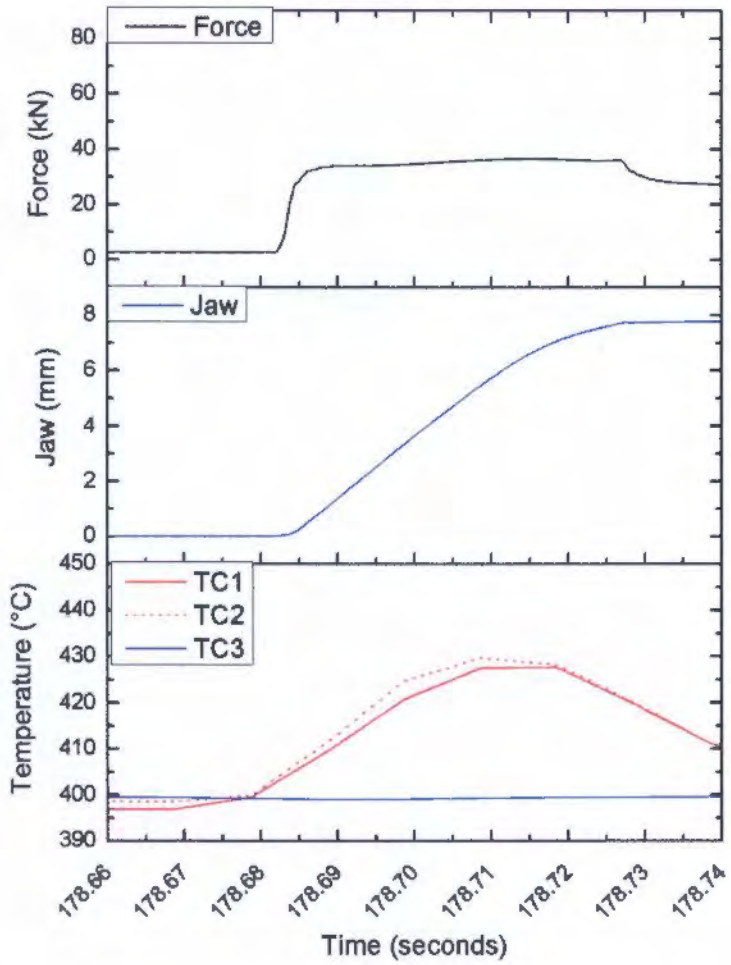

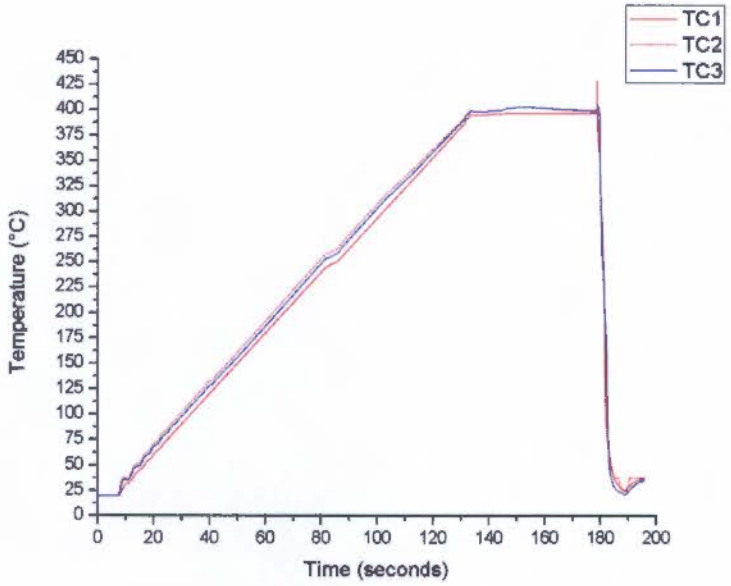

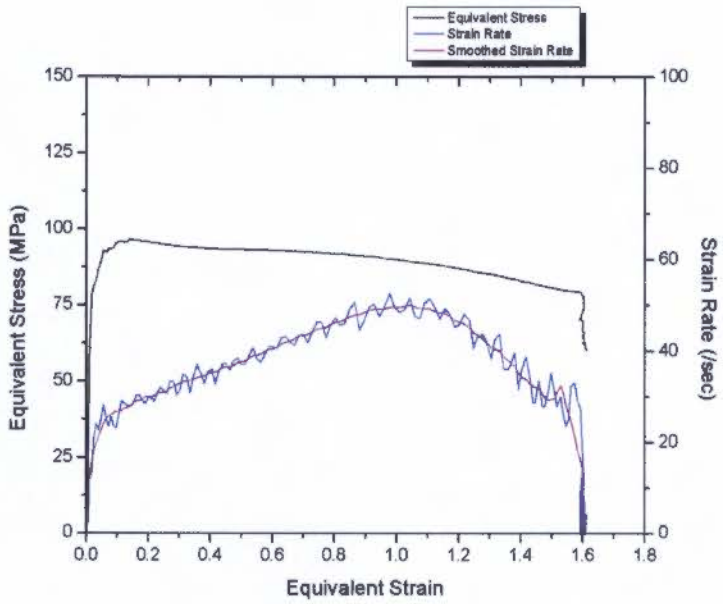

Summary:

	Value	Unit		Value	Unit
$TC1_{start}$	401.9	°C	$TC3_{start}$	402.3	°C
$TC2_{start}$	402.6	°C	$TC4_{start}$	N/A	°C
T_{grad}	0.7	°C	T_{start}	402.3	°C
$T_{0.8\text{-}0.9}$	428.3	°C	$\triangle T$	26.1	°C
$\dot{\varepsilon}_{whole}$	34.2	sec^{-1}	$\dot{\varepsilon}_{0.8-0.9}$	47.5	sec^{-1}
Flow Stress	91.54	MPa	$ln(Z)$	30.45	

Test 2: Water Quenched

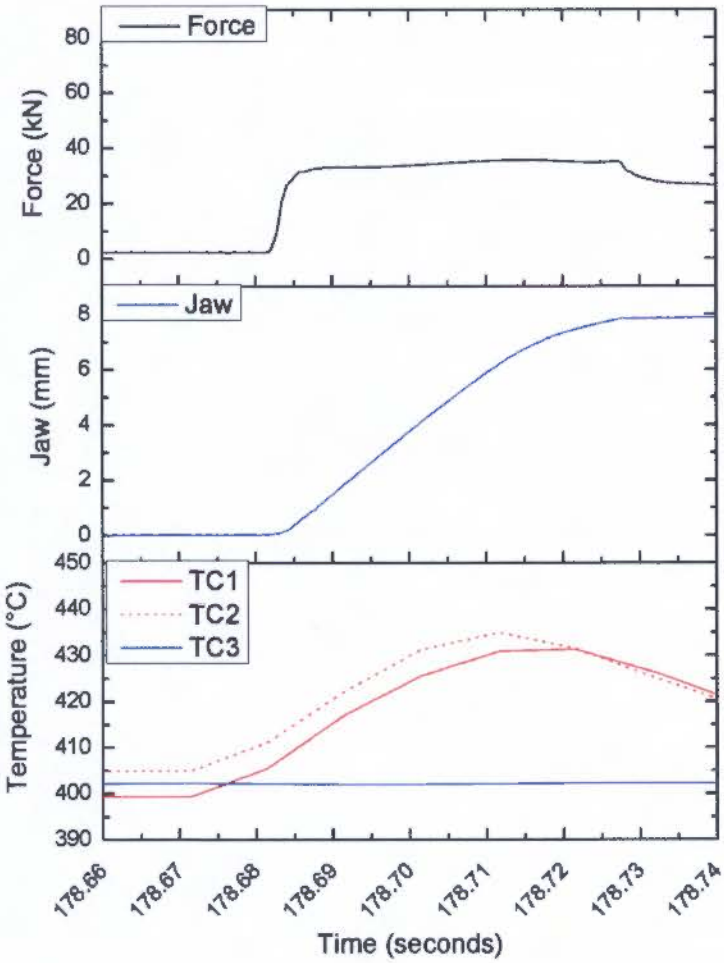

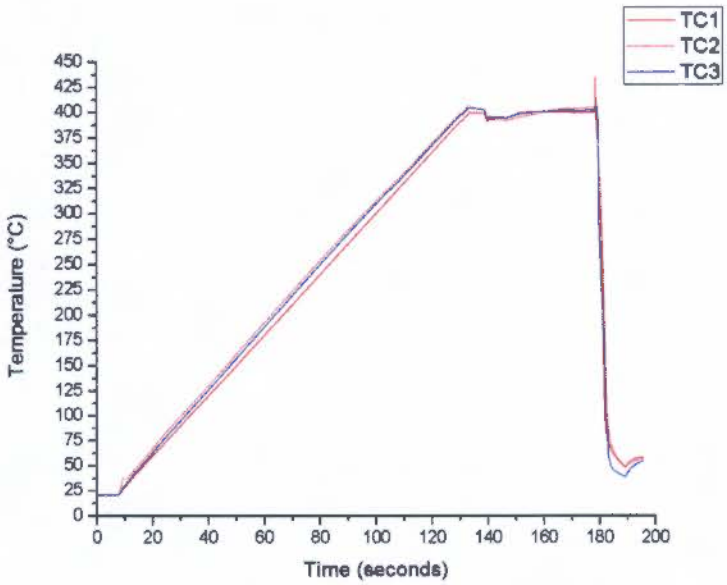

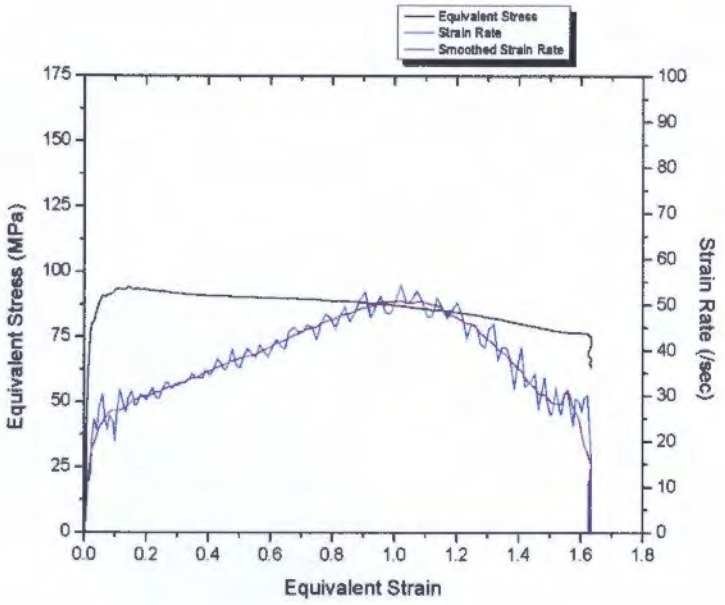

Summary:

	Value	Unit		Value	Unit
$TC1_{start}$	404.8	°C	$TC3_{start}$	402.1	°C
$TC2_{start}$	410.4	°C	$TC4_{start}$	N/A	°C
T_{grad}	5.6	°C	T_{start}	407.6	°C
$T_{0.8\text{-}0.9}$	431.2	°C	ΔT	23.6	°C
$\dot{\varepsilon}_{whole}$	36.3	sec^{-1}	$\dot{\varepsilon}_{0.8-0.9}$	48.0	sec^{-1}
Flow Stress	88.74	MPa	$ln(Z)$	30.34	

Temperature: 400°C | Strain rate: 100 sec^{-1} | Strain 1.6 | Graphite Foil Lubrication

Test 1: Water Quenched

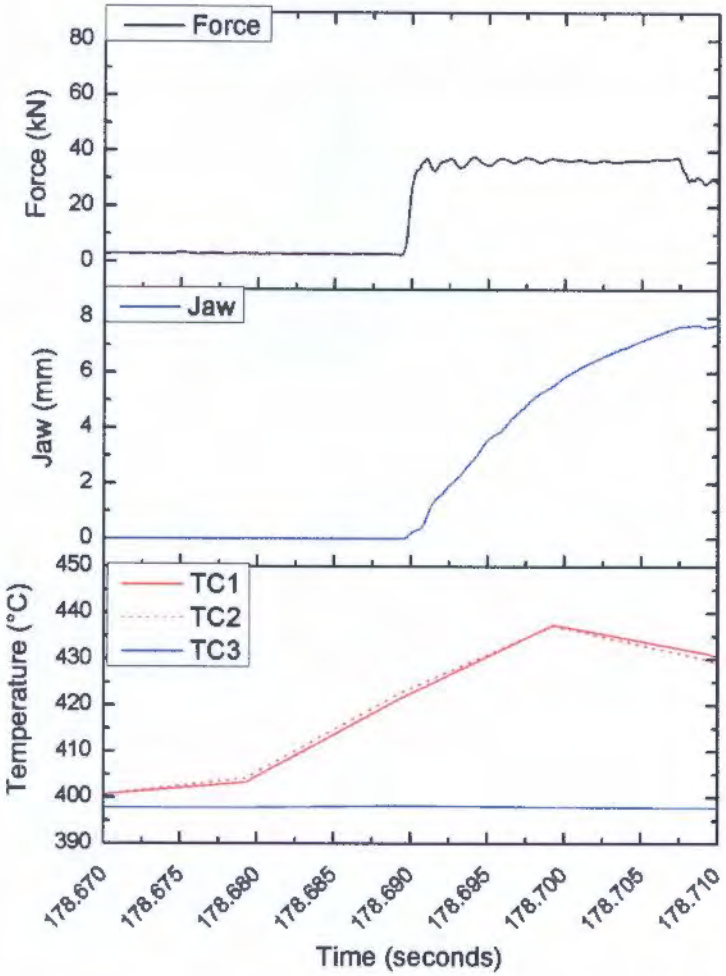

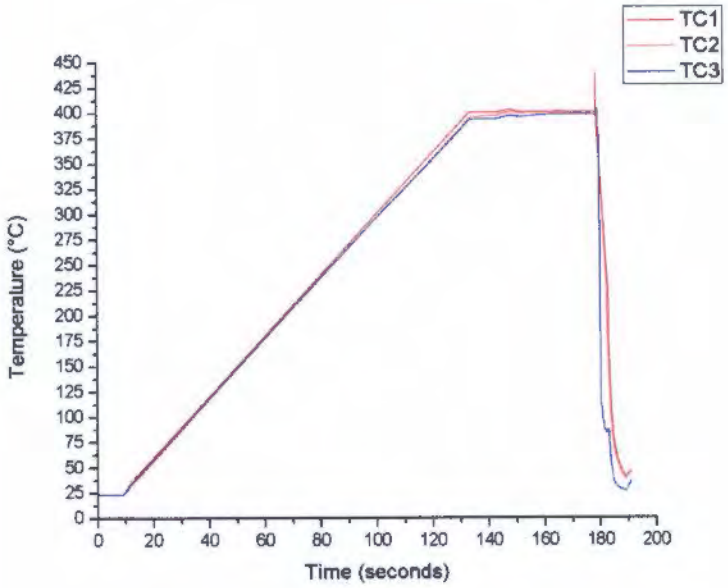

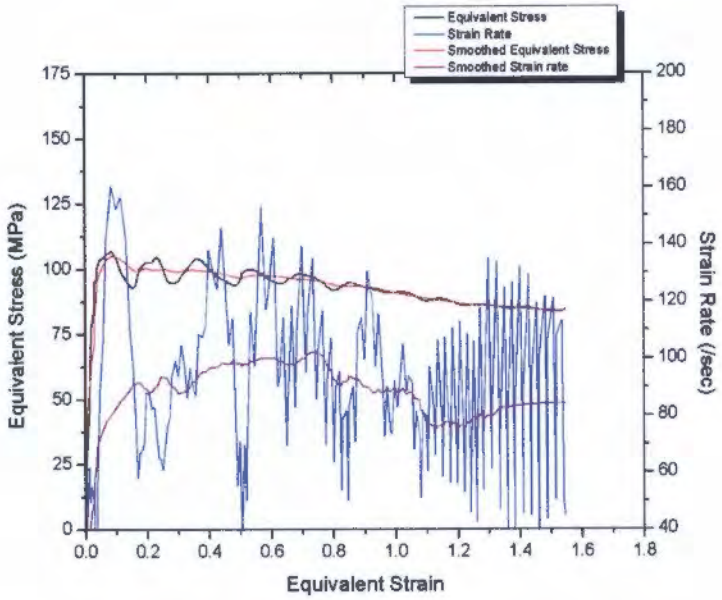

Summary:

	Value	Unit		Value	Unit
$TC1_{start}$	420.8	°C	$TC3_{start}$	398.1	°C
$TC2_{start}$	422.0	°C	$TC4_{start}$	N/A	°C
T_{grad}	1.2	°C	T_{start}	421.4	°C
$T_{0.8\text{-}0.9}$	436.8	°C	ΔT	15.4	°C
$\dot{\varepsilon}_{whole}$	85.0	sec^{-1}	$\dot{\varepsilon}_{0.8-0.9}$	92.1	sec^{-1}
Flow Stress	93.45	MPa	$ln(Z)$	30.79	

Test 2: Water Quenched

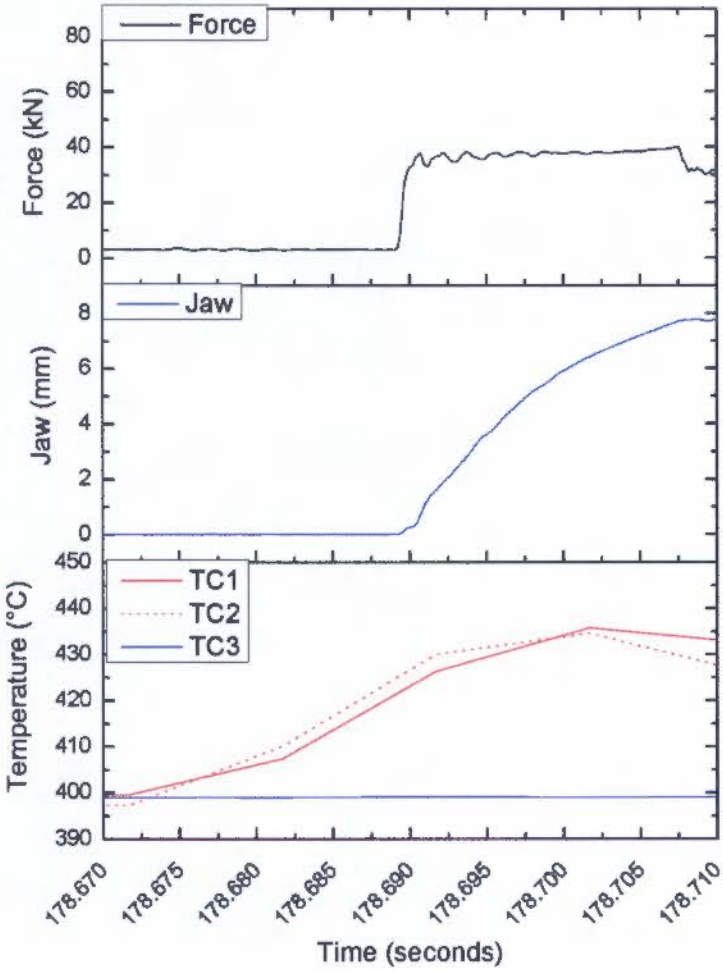

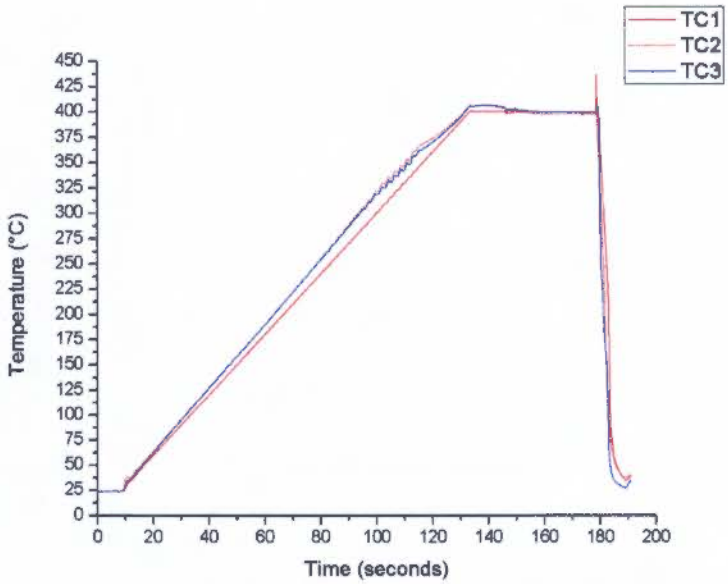

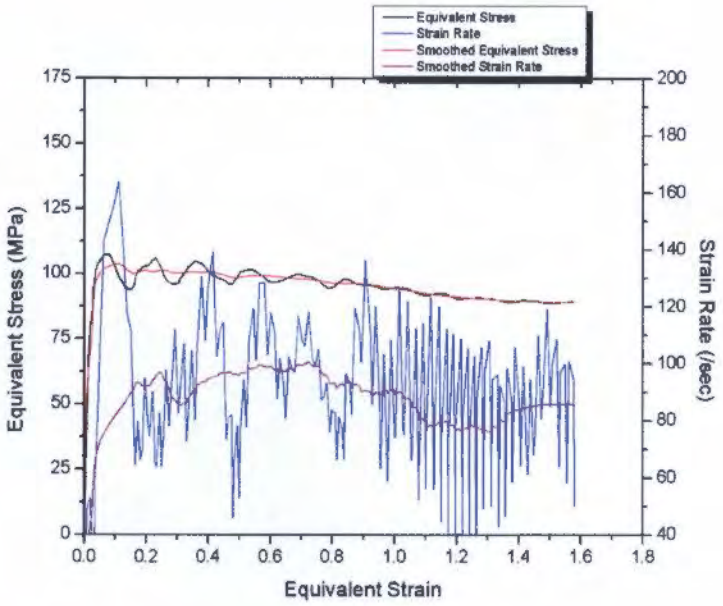

Summary:

	Value	Unit		Value	Unit
$TC1_{start}$	421.0	°C	$TC3_{start}$	399.1	°C
$TC2_{start}$	424.4	°C	$TC4_{start}$	N/A	°C
T_{grad}	3.4	°C	T_{start}	422.7	°C
$T_{0.8\text{-}0.9}$	433.2	°C	$\triangle T$	10.5	°C
$\dot{\varepsilon}_{whole}$	92.3	sec^{-1}	$\dot{\varepsilon}_{0.8-0.9}$	85.4	sec^{-1}
Flow Stress	96.72	MPa	$ln(Z)$	30.93	

Appendix H: Modified PSC Validation Tests

Temperature: 300°C | Strain rate: 10 sec^{-1} | Strain 1.6 | Graphite Foil Lubrication

Test 1: Water Quenched

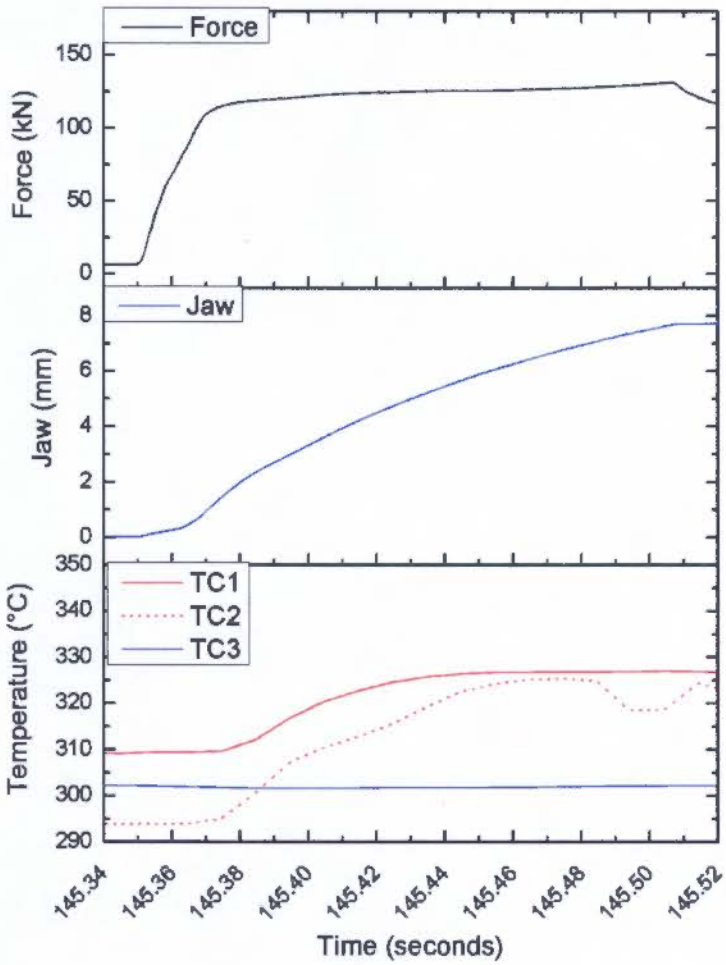

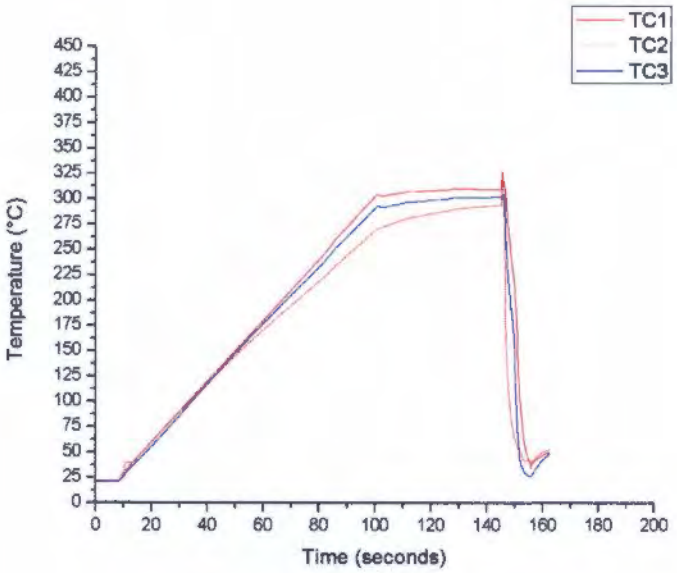

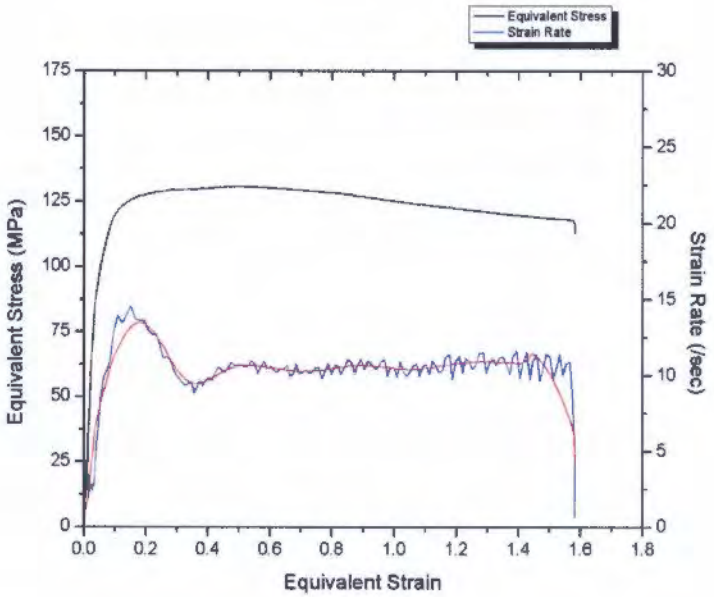

Summary:

	Value	Unit		Value	Unit
$TC1_{start}$	309.2	°C	$TC3_{start}$	302.2	°C
$TC2_{start}$	293.9	°C	$TC4_{start}$	-	°C
T_{grad}	15.3	°C	T_{start}	301.6	°C
$T_{0.8\text{-}0.9}$	323.3	°C	$\triangle T$	21.8	°C
$\dot{\varepsilon}_{whole}$	9.8	sec^{-1}	$\dot{\varepsilon}_{0.8-0.9}$	10.6	sec^{-1}
Flow Stress	127.7	MPa	$ln(Z)$	33.62	

Test 2: Air Quenched

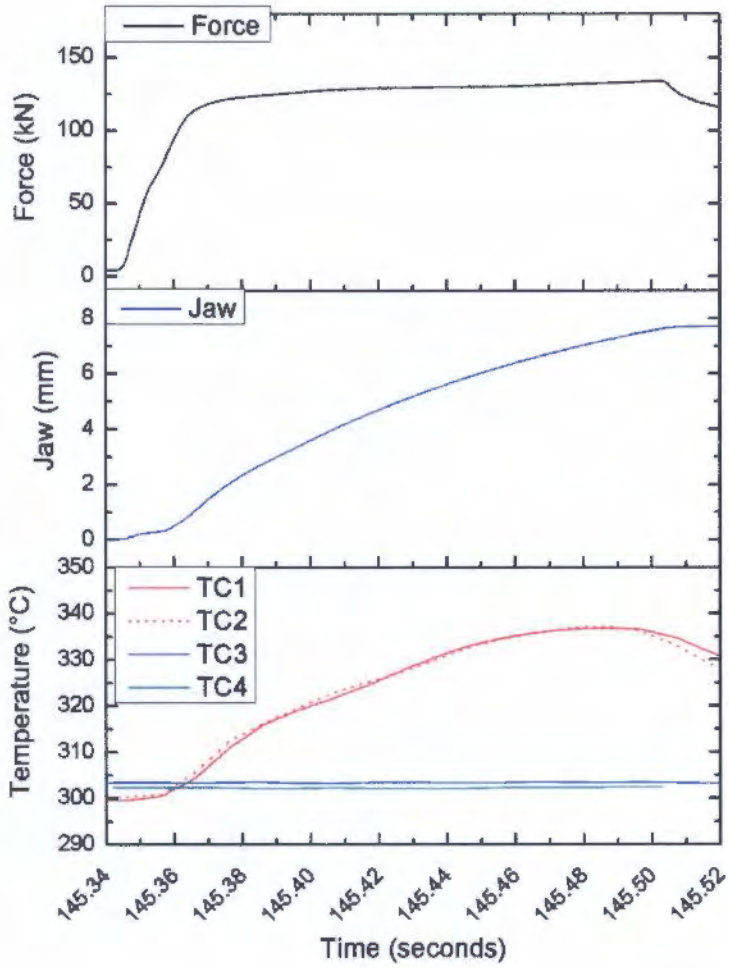

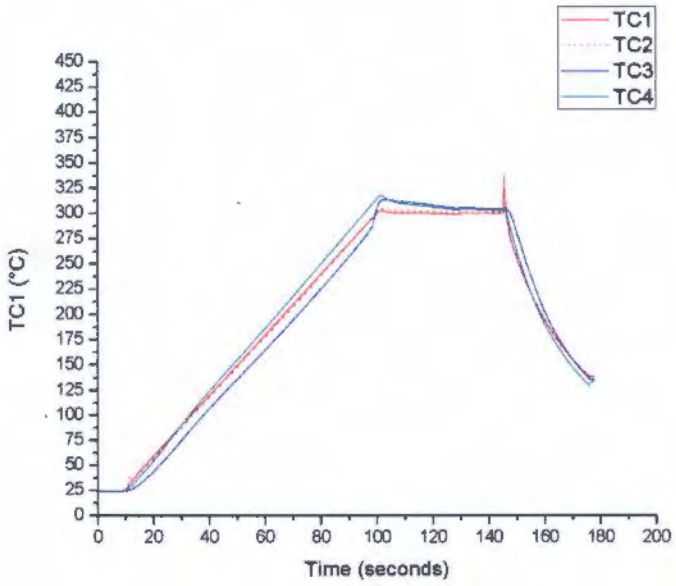

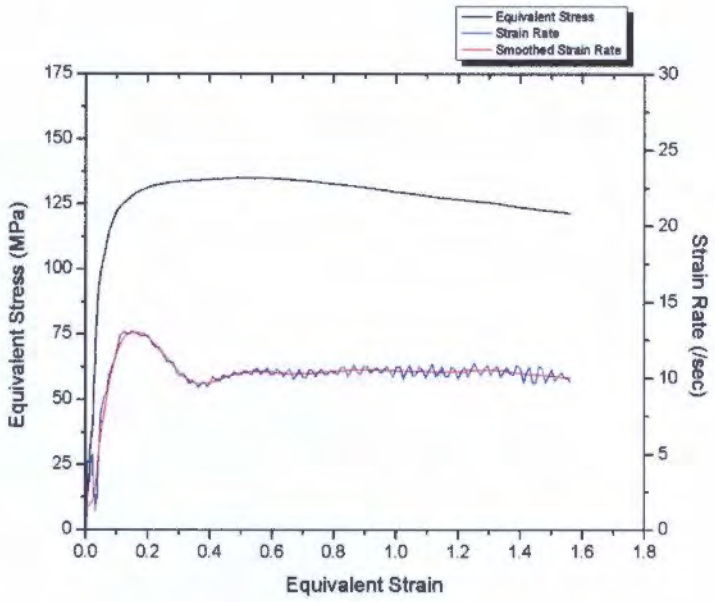

Summary:

	Value	Unit		Value	Unit
$TC1_{start}$	299.6	°C	$TC3_{start}$	303.4	°C
$TC2_{start}$	300.3	°C	$TC4_{start}$	302.4	°C
T_{grad}	0.7	°C	T_{start}	300.0	°C
$T_{0.8\text{-}0.9}$	329.7	°C	ΔT	29.7	°C
$\dot{\varepsilon}_{whole}$	9.9	sec^{-1}	$\dot{\varepsilon}_{0.8-0.9}$	10.5	sec^{-1}
Flow Stress	132.2	MPa	$ln(Z)$	33.28	

Temperature: 300°C | Strain rate: 30 sec^{-1} | Strain 1.6 | Graphite Foil Lubrication

Test 1: Water Quenched

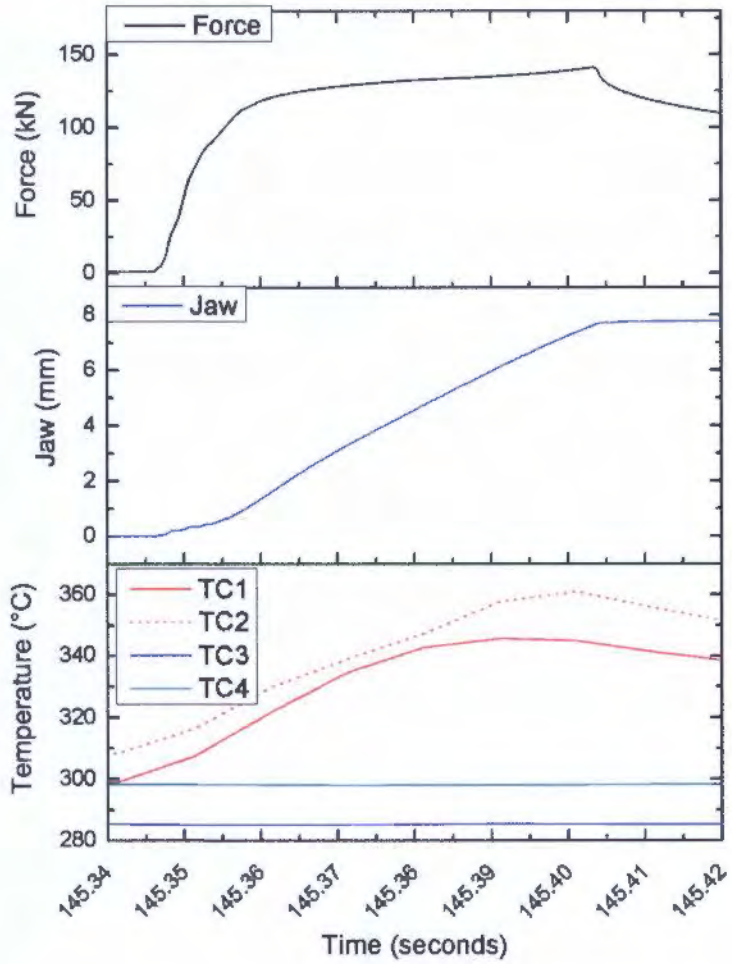

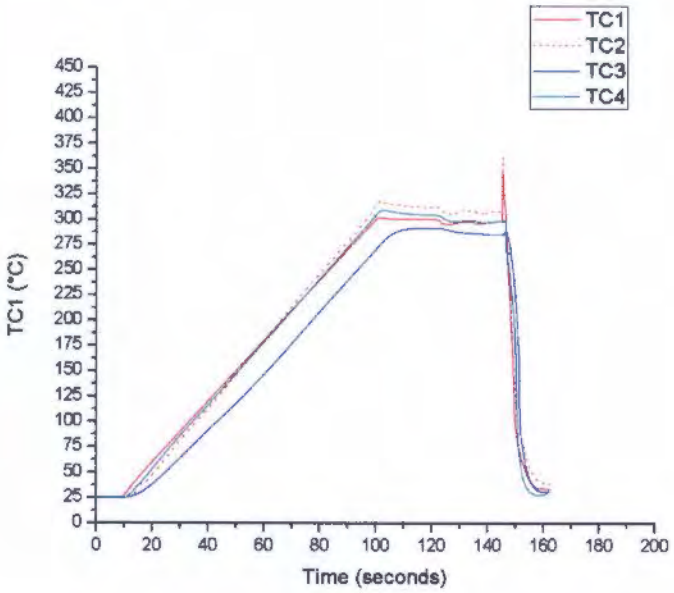

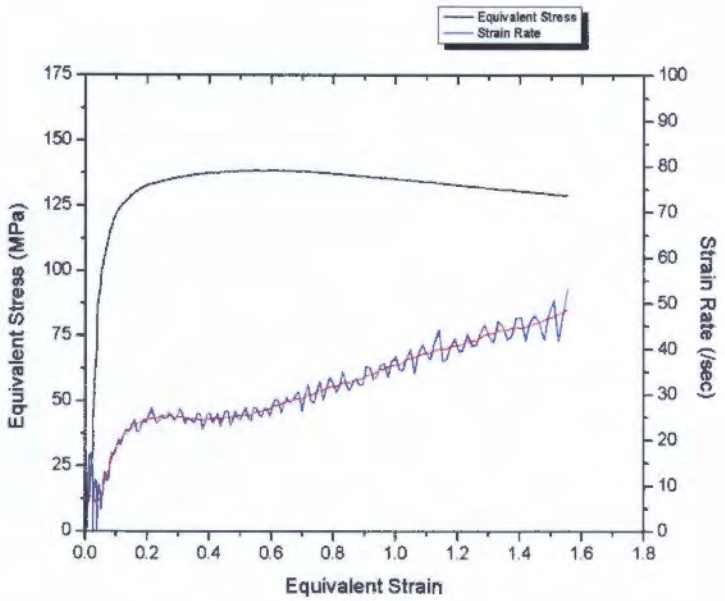

Summary:

	Value	Unit		Value	Unit
$TC1_{start}$	303.0	°C	$TC3_{start}$	285.3	°C
$TC2_{start}$	312.1	°C	$TC4_{start}$	298.2	°C
T_{grad}	9.1	°C	T_{start}	307.6	°C
$T_{0.8\text{-}0.9}$	348.2	°C	$\triangle T$	40.7	°C
$\dot{\varepsilon}_{whole}$	27.6	sec^{-1}	$\dot{\varepsilon}_{0.8-0.9}$	32.8	sec^{-1}
Flow Stress	136.7	MPa	$ln(Z)$	33.5	

Test 2: Air Quenched

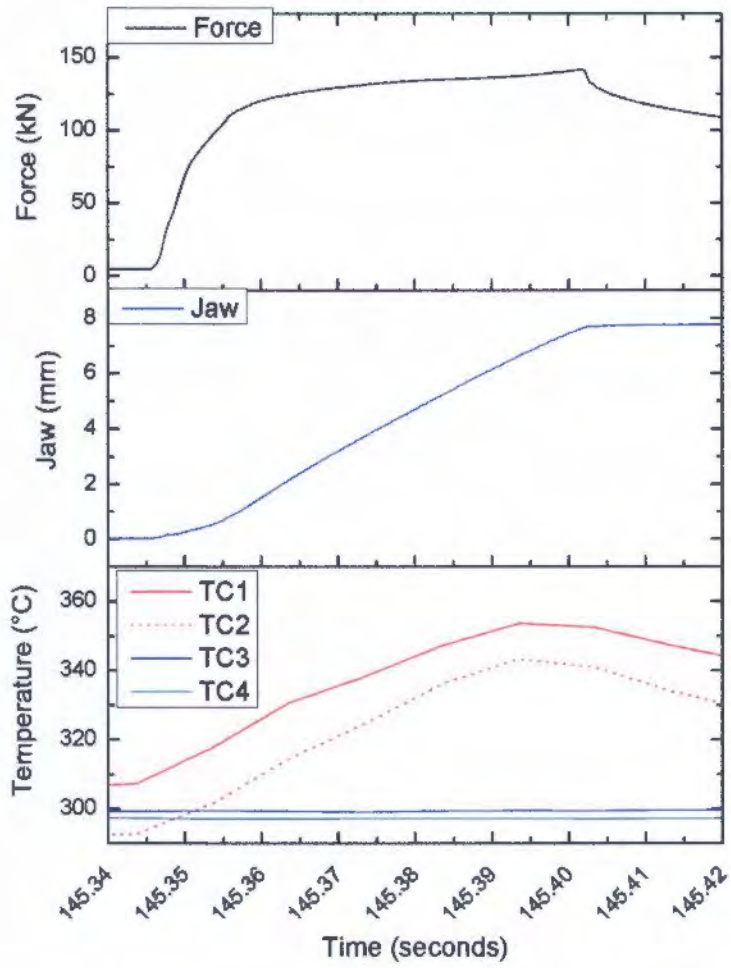

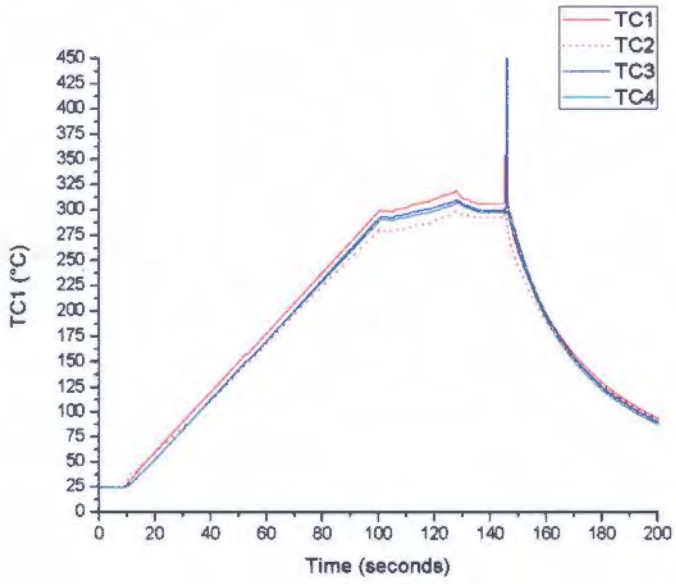

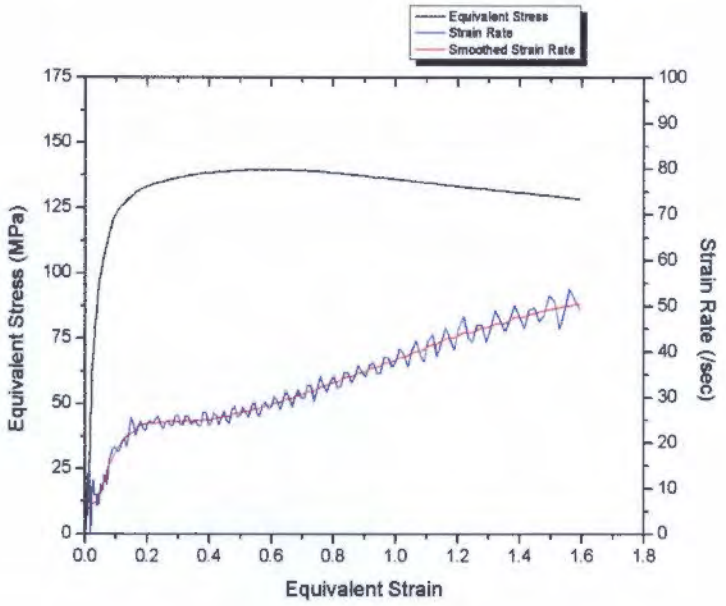

Summary:

	Value	Unit		Value	Unit
$TC1_{start}$	309.4	°C	$TC3_{start}$	299.3	°C
$TC2_{start}$	294.4	°C	$TC4_{start}$	297.3	°C
T_{grad}	15.0	°C	T_{start}	301.9	°C
$T_{0.8\text{-}0.9}$	342.1	°C	$\triangle T$	40.2	°C
$\dot{\varepsilon}_{whole}$	29.0	sec^{-1}	$\dot{\varepsilon}_{0.8-0.9}$	34.3	sec^{-1}
Flow Stress	137.9	MPa	$ln(Z)$	33.85	

Temperature: 300°C | Strain rate: 100 sec^{-1} | Strain 1.6 | Graphite Foil Lubrication

Test 1: Water Quenched

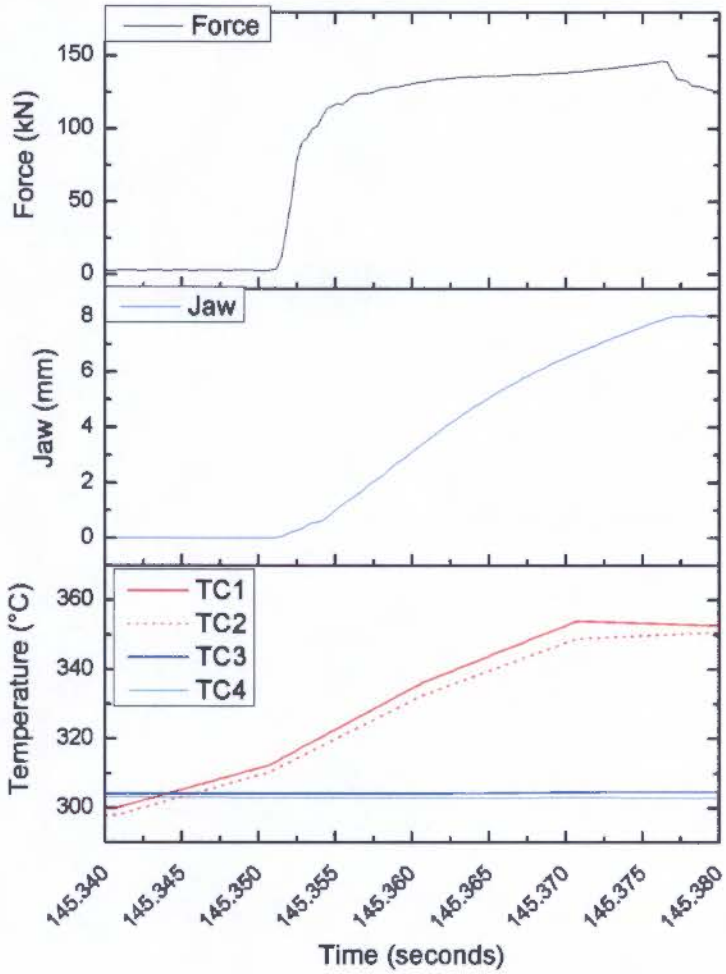

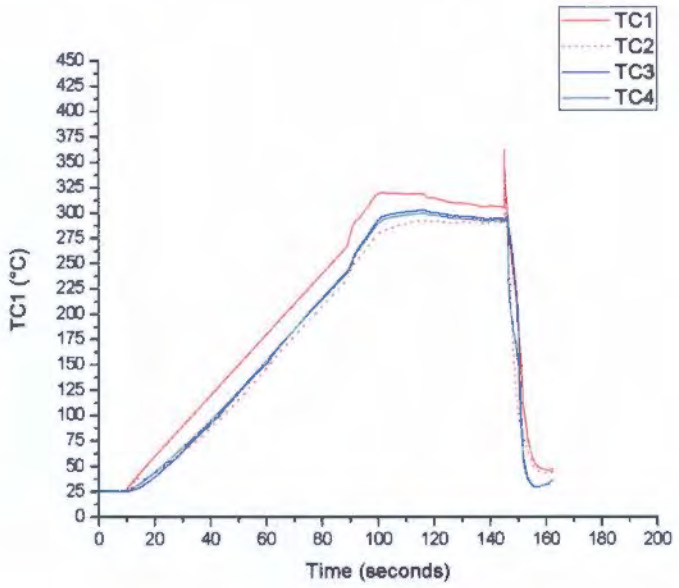

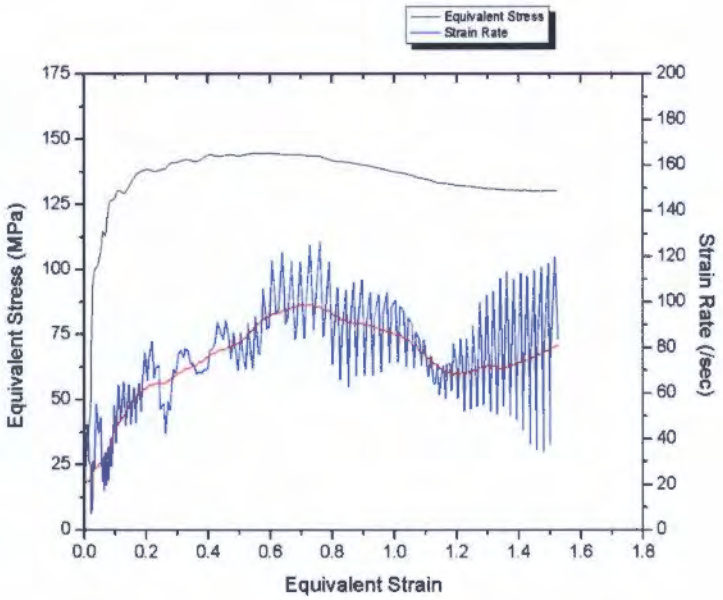

Summary:

	Value	Unit		Value	Unit
$TC1_{start}$	324.7	°C	$TC3_{start}$	293.7	°C
$TC2_{start}$	309.2	°C	$TC4_{start}$	291.8	°C
T_{grad}	15.5	°C	T_{start}	317.0	°C
$T_{0.8\text{-}0.9}$	346.0	°C	ΔT	29.1	°C
$\dot{\varepsilon}_{whole}$	70.6	sec^{-1}	$\dot{\varepsilon}_{0.8-0.9}$	91.9	sec^{-1}
Flow Stress	141.1	MPa	$ln(Z)$	34.64	

Test 2: Air Quenched

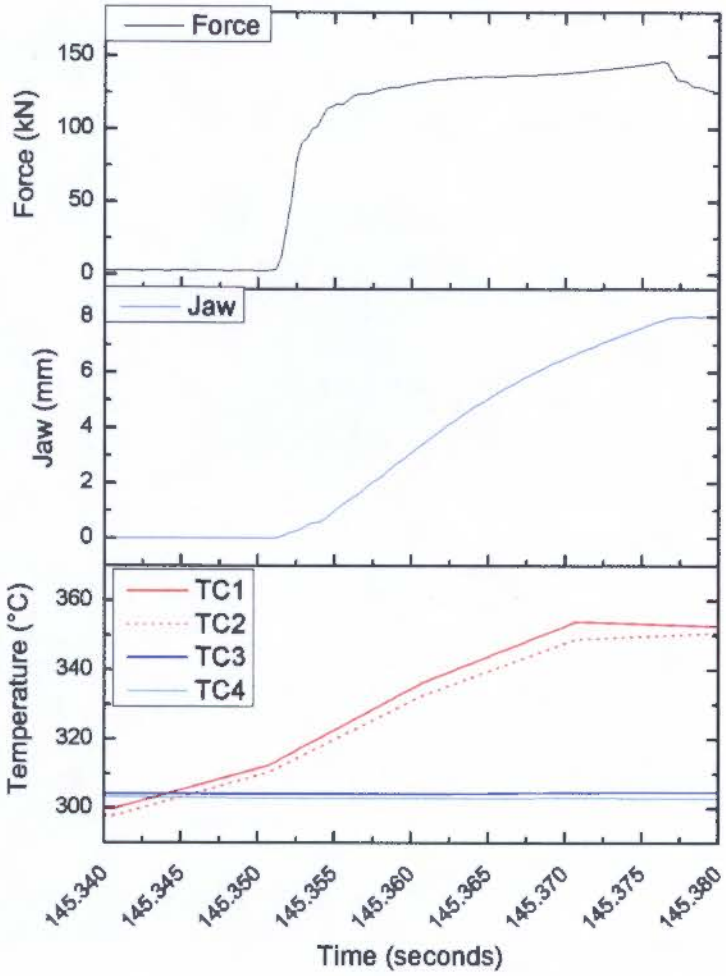

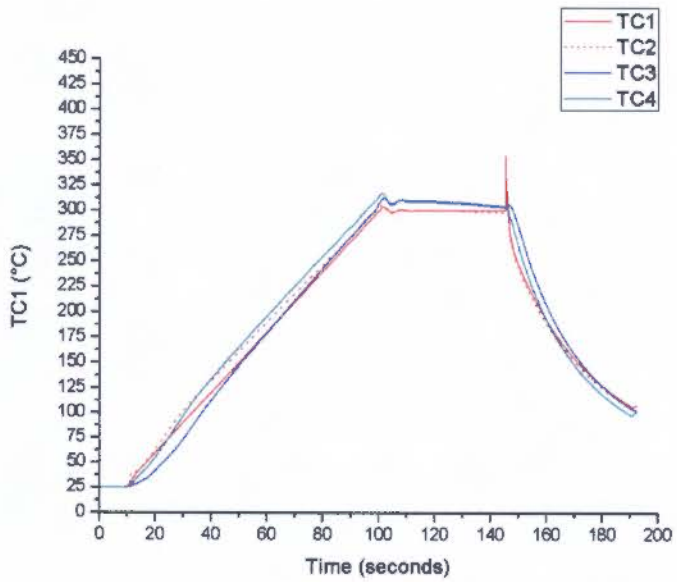

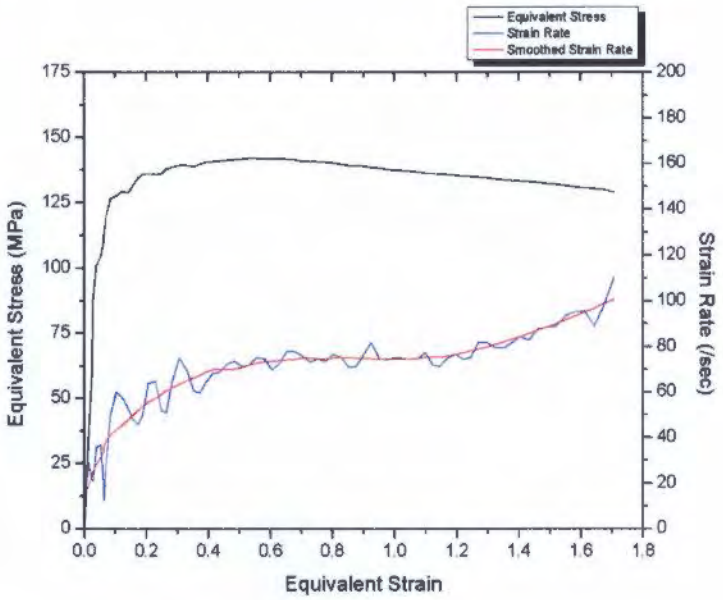

Summary:

	Value	Unit		Value	Unit
$TC1_{start}$	313.4	°C	$TC3_{start}$	304.1	°C
$TC2_{start}$	311.3	°C	$TC4_{start}$	302.9	°C
T_{grad}	2.1	°C	T_{start}	312.4	°C
$T_{0.8\text{-}0.9}$	343.6	°C	ΔT	31.3	°C
$\dot{\varepsilon}_{whole}$	68.4	sec^{-1}	$\dot{\varepsilon}_{0.8-0.9}$	74.8	sec^{-1}
Flow Stress	139.4	MPa	$ln(Z)$	34.55	

Temperature: 350°C | Strain rate: 10 sec^{-1} | Strain 1.6 | Graphite Foil Lubrication

Test 1: Water Quenched

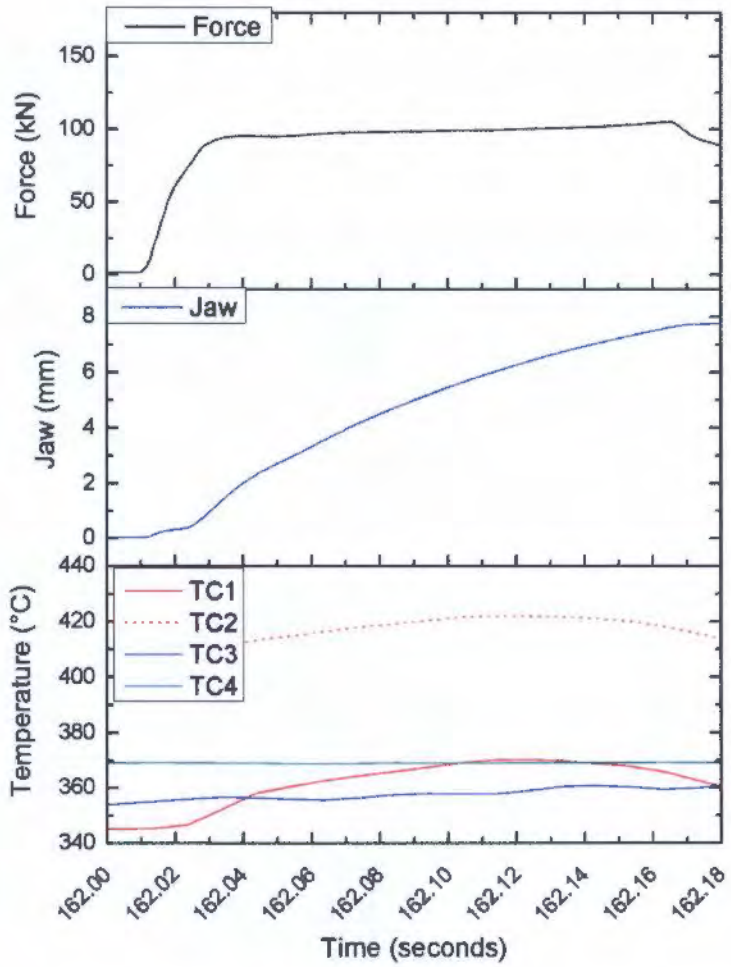

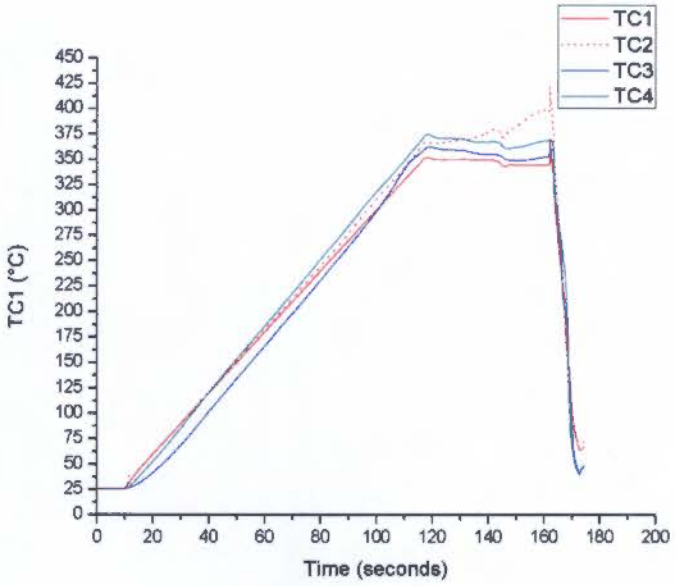

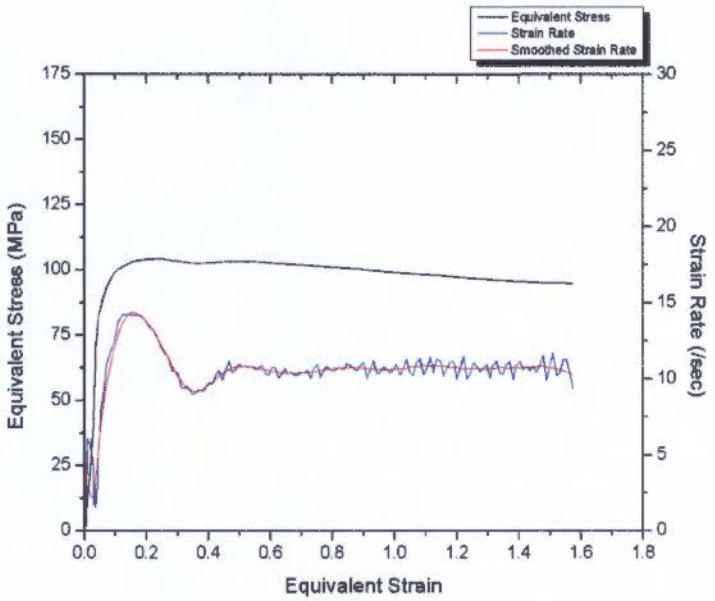

Summary:

	Value	Unit		Value	Unit
$TC1_{start}$	345.2	°C	$TC3_{start}$	354.8	°C
$TC2_{start}$	398.5	°C	$TC4_{start}$	369.2	°C
T_{grad}	53.3	°C	T_{start}	371.9	°C
$T_{0.8\text{-}0.9}$	394.5	°C	$\triangle T$	22.7	°C
$\dot{\varepsilon}_{whole}$	10.2	sec^{-1}	$\dot{\varepsilon}_{0.8-0.9}$	10.7	sec^{-1}
Flow Stress	100.6	MPa	$ln(Z)$	30.3	

Test 2: Air Quenched

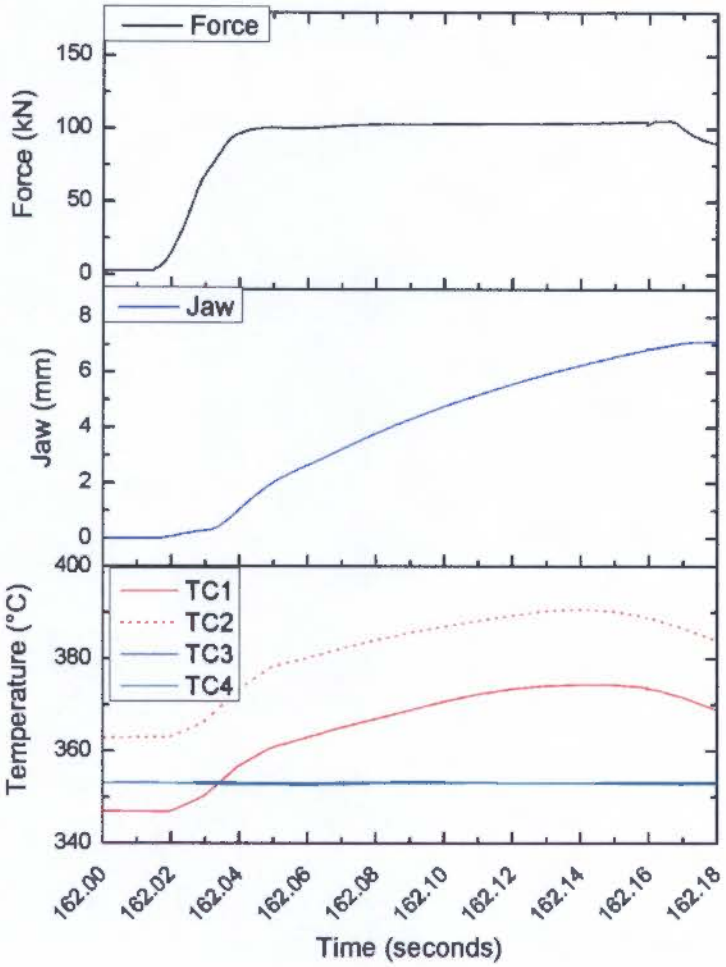

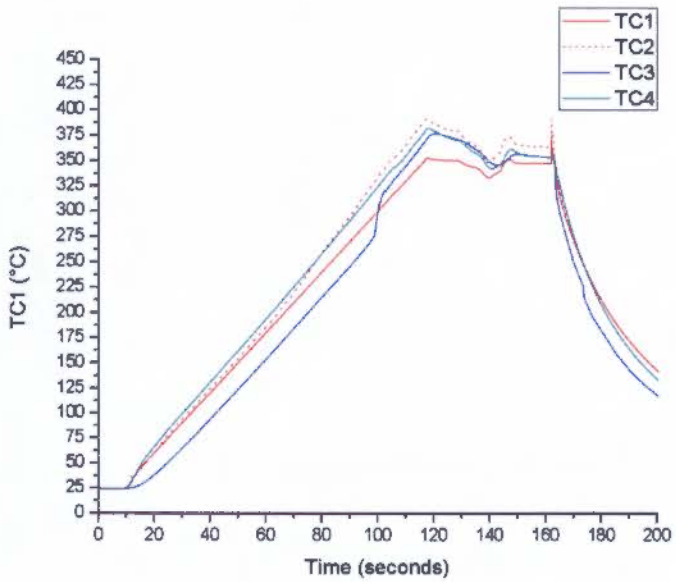

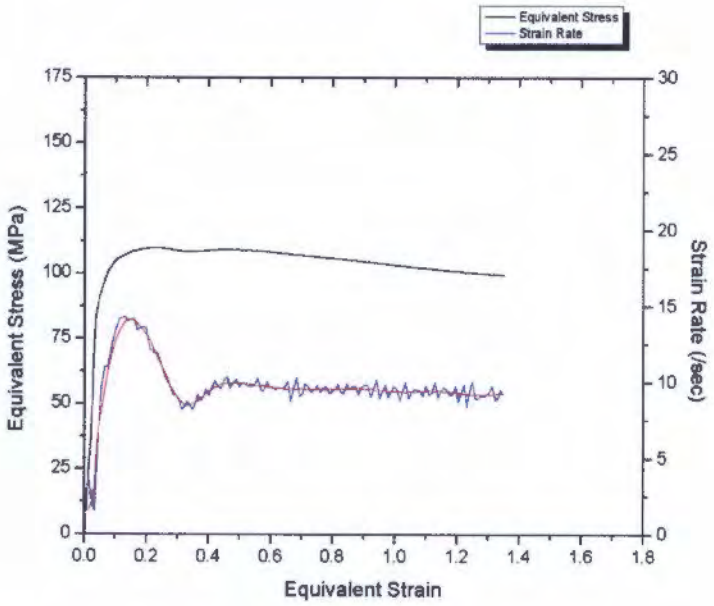

Summary:

	Value	Unit		Value	Unit
$TC1_{start}$	346.9	°C	$TC3_{start}$	353.1	°C
$TC2_{start}$	362.9	°C	$TC4_{start}$	353.1	°C
T_{grad}	16.0	°C	T_{start}	354.9	°C
$T_{0.8\text{-}0.9}$	380.6	°C	$\triangle T$	25.7	°C
$\dot{\varepsilon}_{whole}$	9.1	sec^{-1}	$\dot{\varepsilon}_{0.8-0.9}$	9.5	sec^{-1}
Flow Stress	105.2	MPa	$ln(Z)$	30.78	

Temperature: 350°C | Strain rate: 30 sec^{-1} | Strain 1.6 | Graphite Foil Lubrication

Test 1: Water Quenched

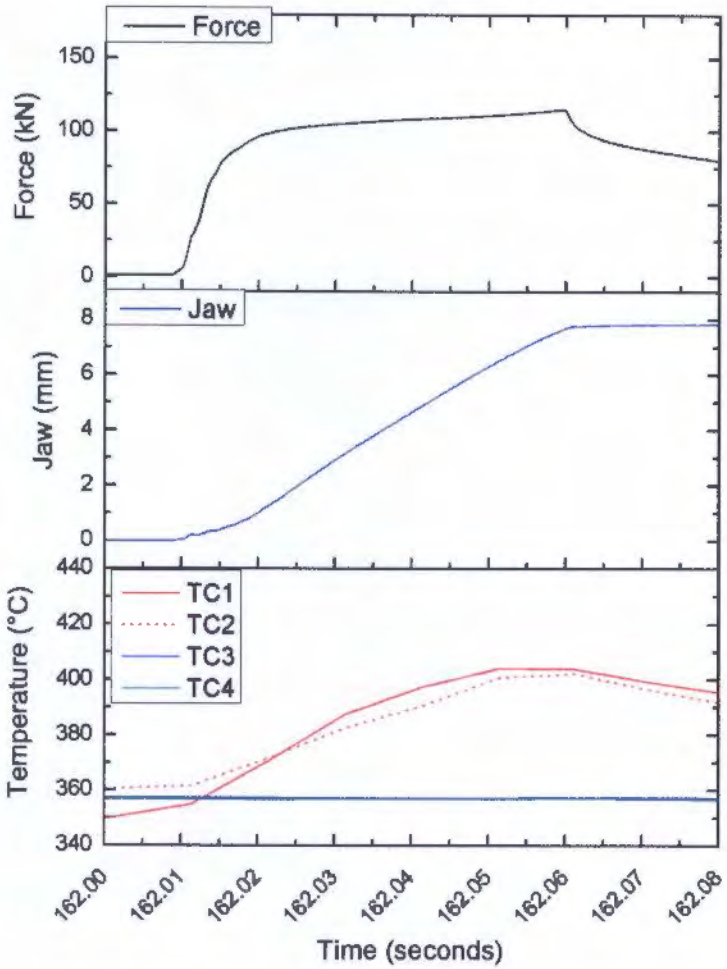

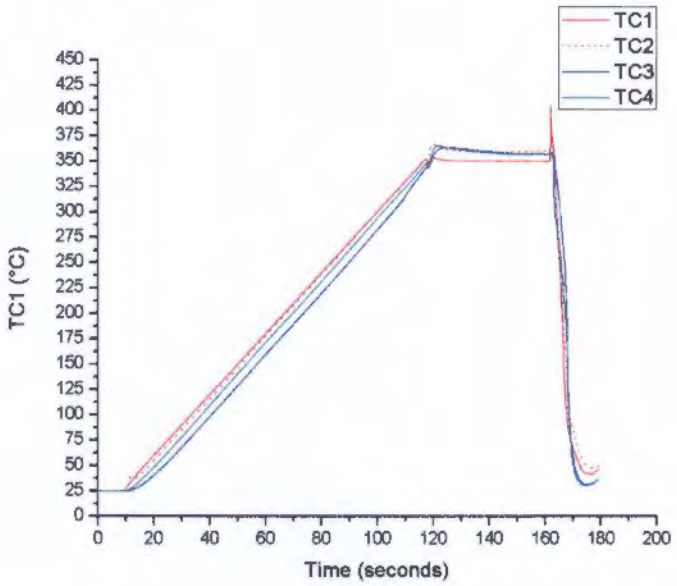

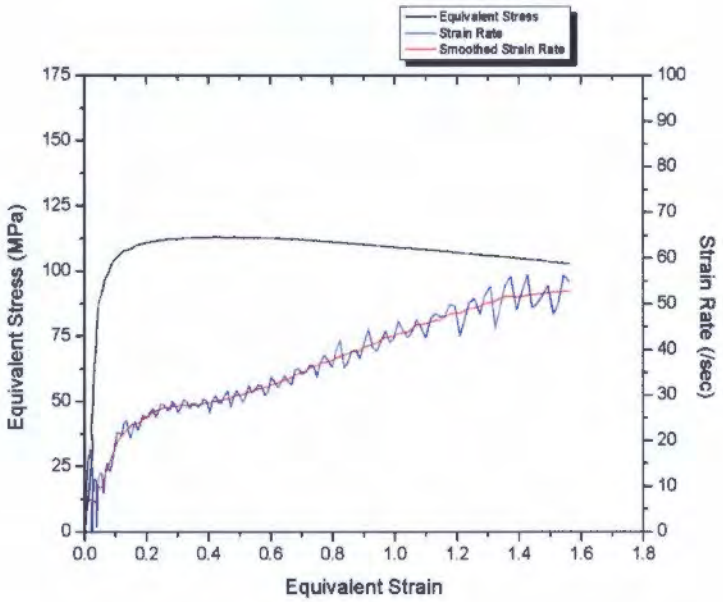

Summary:

	Value	Unit		Value	Unit
$TC1_{start}$	353.7	°C	$TC3_{start}$	357.3	°C
$TC2_{start}$	361.3	°C	$TC4_{start}$	356.7	°C
T_{grad}	7.6	°C	T_{start}	357.5	°C
$T_{0.8\text{-}0.9}$	396.7	°C	$\triangle T$	39.2	°C
$\dot{\varepsilon}_{whole}$	31.5	sec^{-1}	$\dot{\varepsilon}_{0.8-0.9}$	39.3	sec^{-1}
Flow Stress	110.7	MPa	$ln(Z)$	31.51	

Test 2: Air Quenched

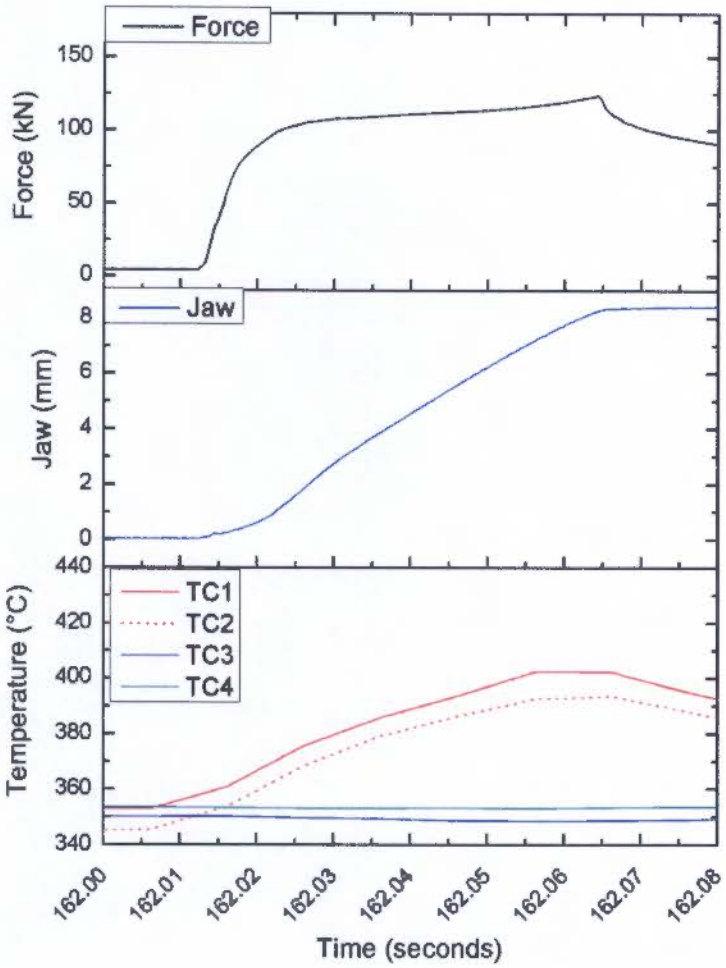

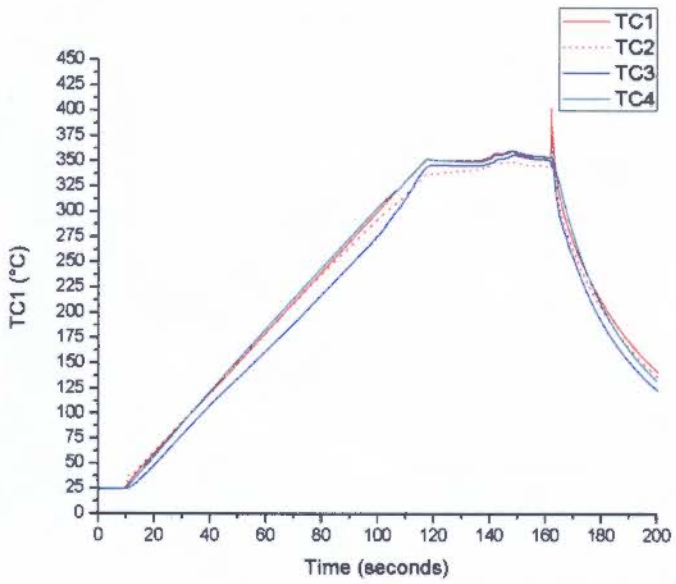

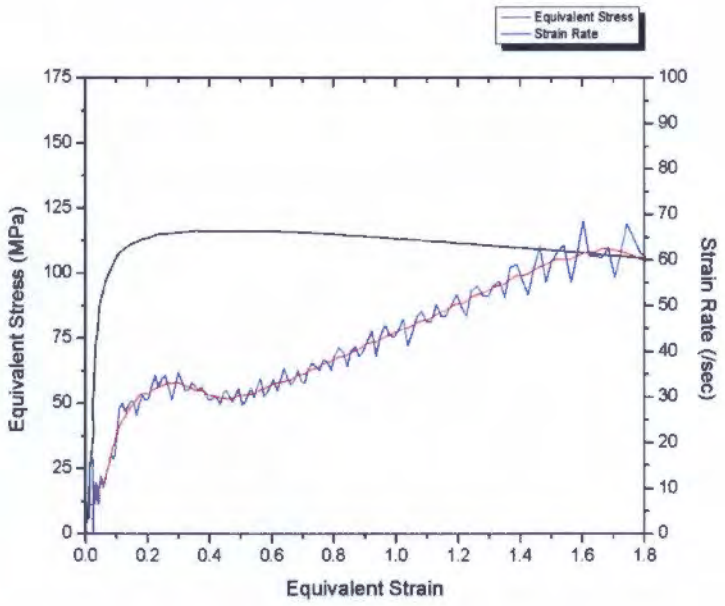

Summary:

	Value	Unit		Value	Unit
$TC1_{start}$	357.7	°C	$TC3_{start}$	350.2	°C
$TC2_{start}$	350.5	°C	$TC4_{start}$	353.4	°C
T_{grad}	7.2	°C	T_{start}	354.9	°C
$T_{0.8\text{-}0.9}$	389.1	°C	$\triangle T$	35.0	°C
$\dot{\varepsilon}_{whole}$	36.1	sec^{-1}	$\dot{\varepsilon}_{0.8-0.9}$	39.6	sec^{-1}
Flow Stress	114.5	MPa	$ln(Z)$	31.84	

Temperature: 350°C | Strain rate: 100 sec^{-1} | Strain 1.6 | Graphite Foil Lubrication

Test 1: Water Quenched

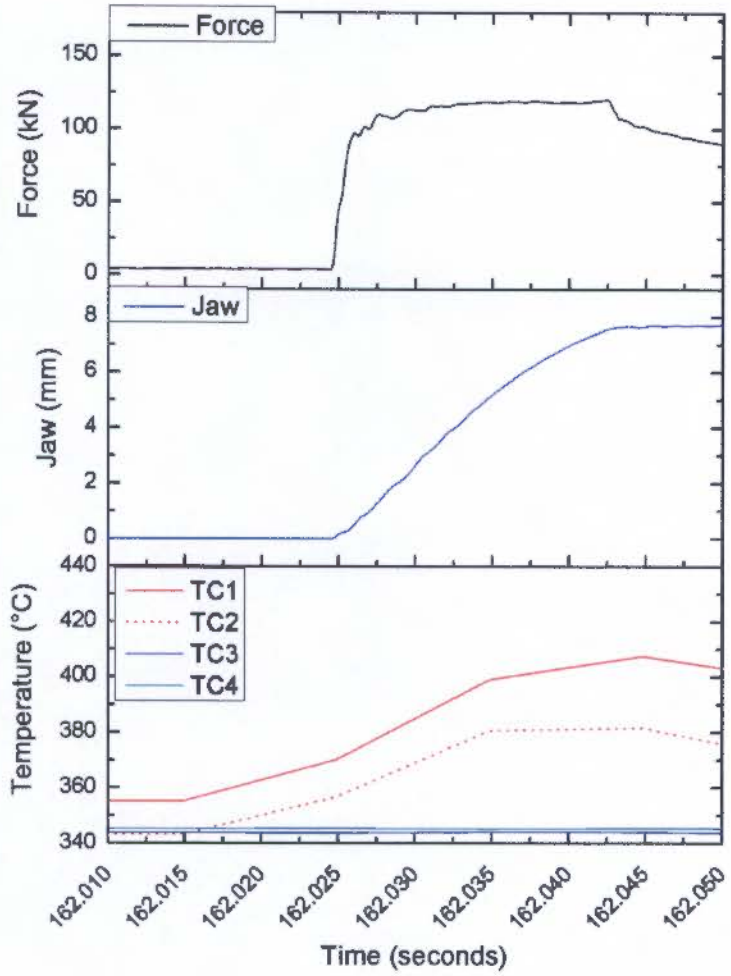

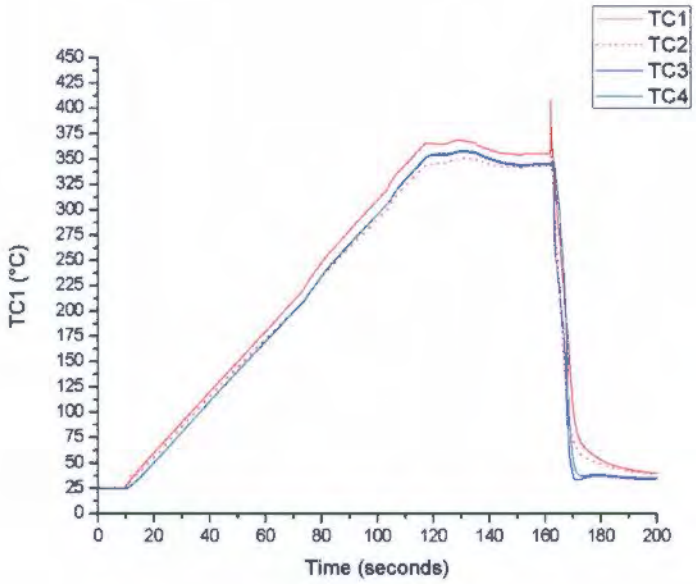

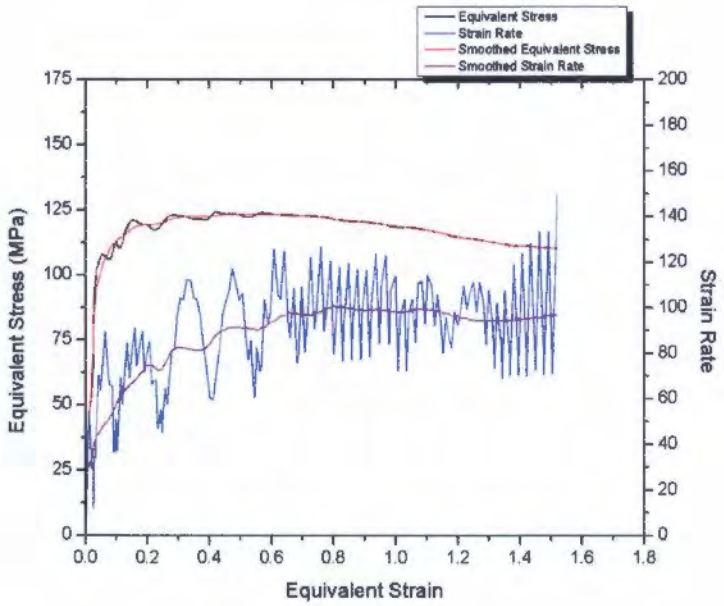

Summary:

	Value	Unit		Value	Unit
$TC1_{start}$	369.4	°C	$TC3_{start}$	343.7	°C
$TC2_{start}$	356.1	°C	$TC4_{start}$	345.4	°C
T_{grad}	13.3	°C	T_{start}	362.8	°C
$T_{0.8\text{-}0.9}$	390.2	°C	ΔT	27.5	°C
$\dot{\varepsilon}_{whole}$	84.8	sec^{-1}	$\dot{\varepsilon}_{0.8-0.9}$	99.7	sec^{-1}
Flow Stress	120.8	MPa	$ln(Z)$	32.72	

Test 2: Air Quenched

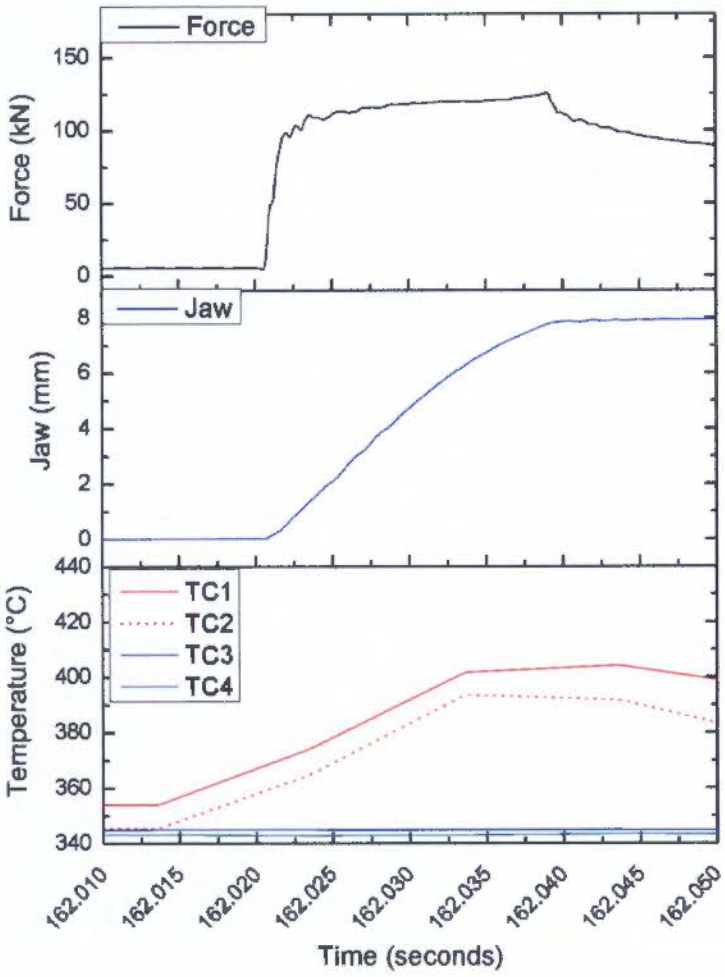

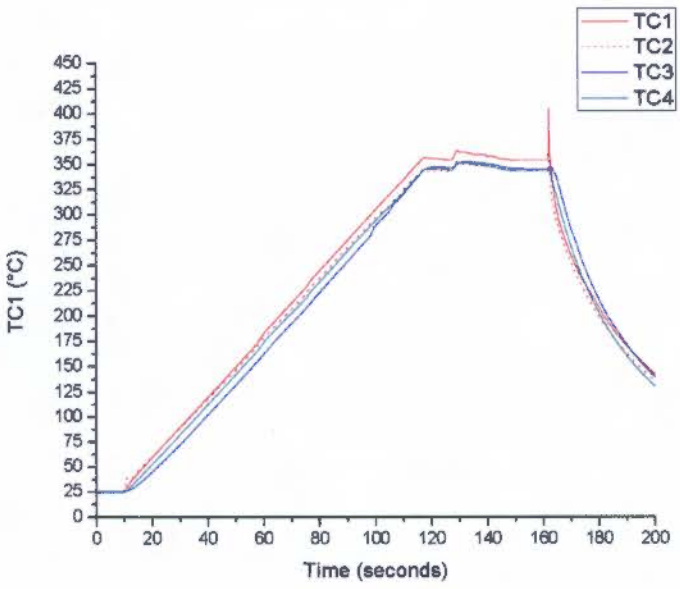

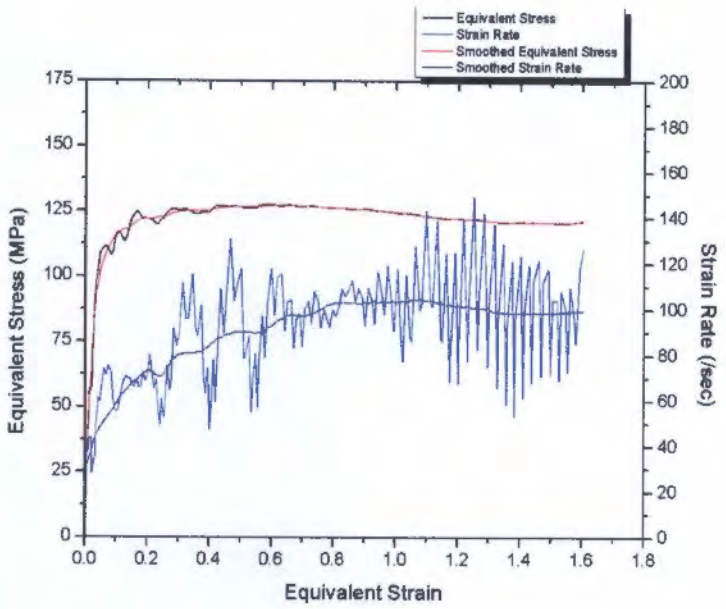

Summary:

	Value	Unit		Value	Unit
$TC1_{start}$	368.1	°C	$TC3_{start}$	345.0	°C
$TC2_{start}$	359.0	°C	$TC4_{start}$	342.9	°C
T_{grad}	9.1	°C	T_{start}	363.6	°C
$T_{0.8\text{-}0.9}$	391.8	°C	$\triangle T$	28.3	°C
$\dot{\varepsilon}_{whole}$	86.7	sec^{-1}	$\dot{\varepsilon}_{0.8-0.9}$	102.7	sec^{-1}
Flow Stress	126.0	MPa	$ln(Z)$	32.68	

Temperature: 400°C | Strain rate: 10 sec^{-1} | Strain 1.6 | Graphite Foil Lubrication

Test 1: Water Quenched

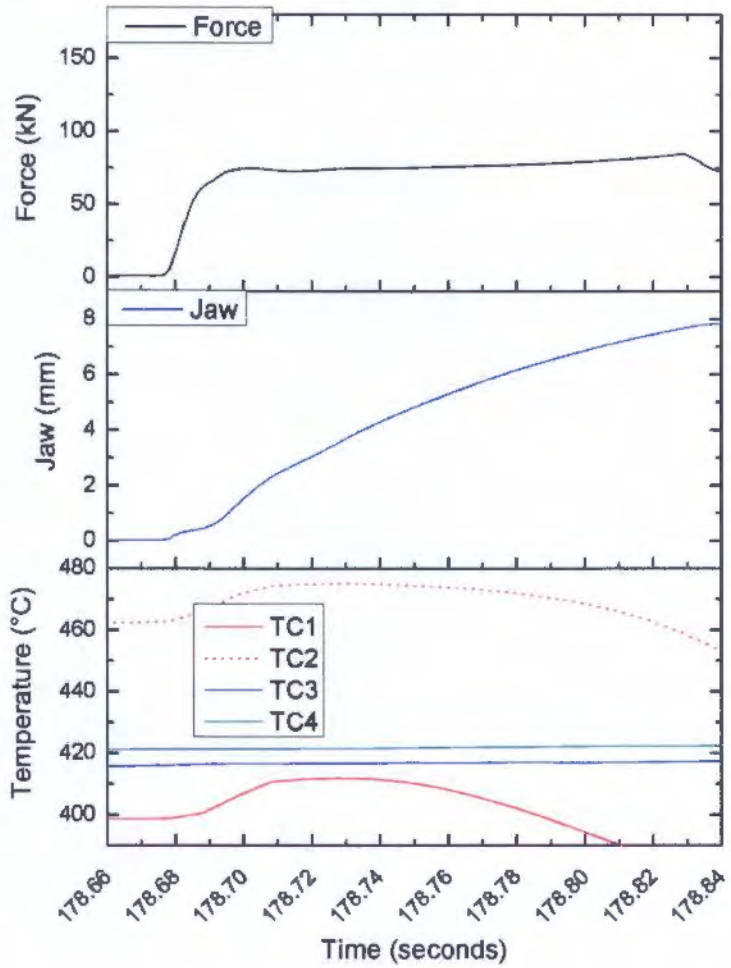

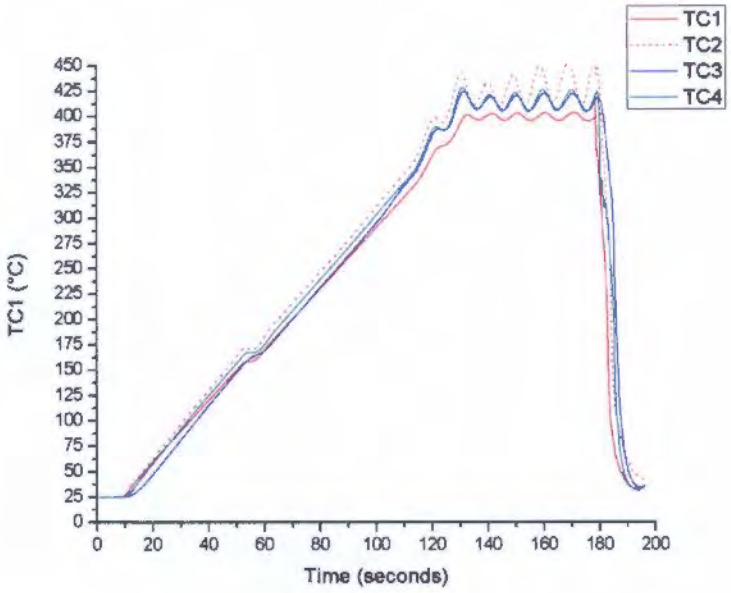

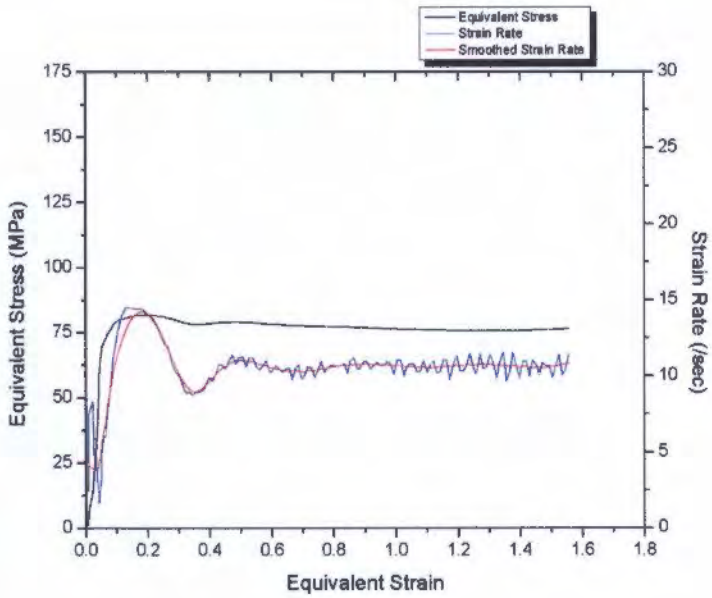

Summary:

	Value	Unit		Value	Unit
$TC1_{start}$	398.8	°C	$TC3_{start}$	416.0	°C
$TC2_{start}$	462.7	°C	$TC4_{start}$	421.3	°C
T_{grad}	63.9	°C	T_{start}	430.8	°C
$T_{0.8\text{-}0.9}$	440.4	°C	ΔT	9.6	°C
$\dot{\varepsilon}_{whole}$	10.2	sec^{-1}	$\dot{\varepsilon}_{0.8-0.9}$	10.7	sec^{-1}
Flow Stress	77.07	MPa	$ln(Z)$	28.51	

Test 2: Air Quenched

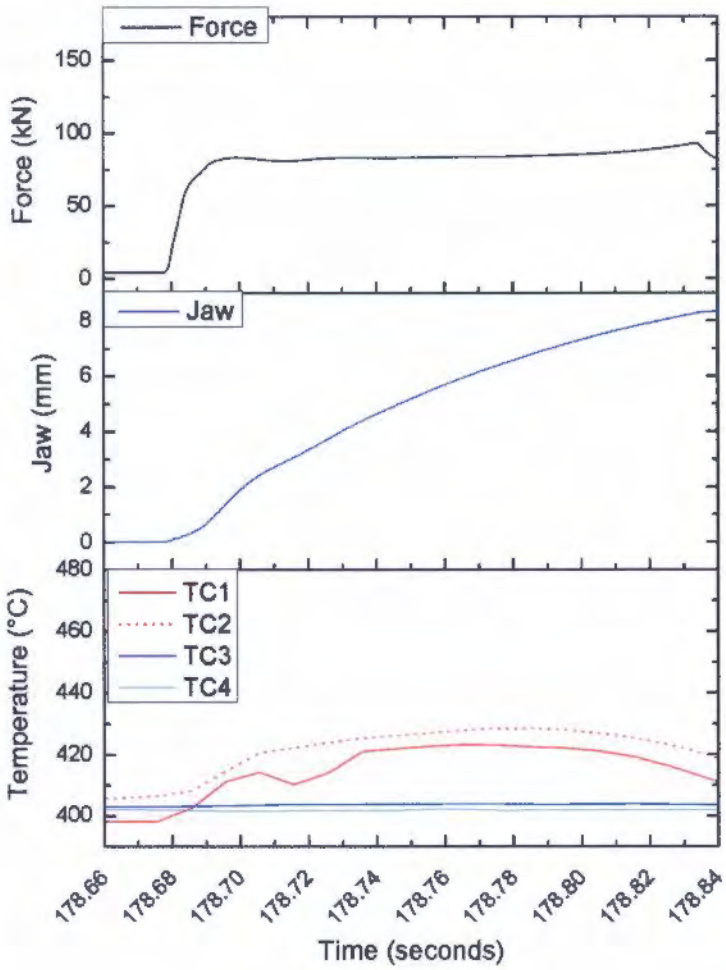

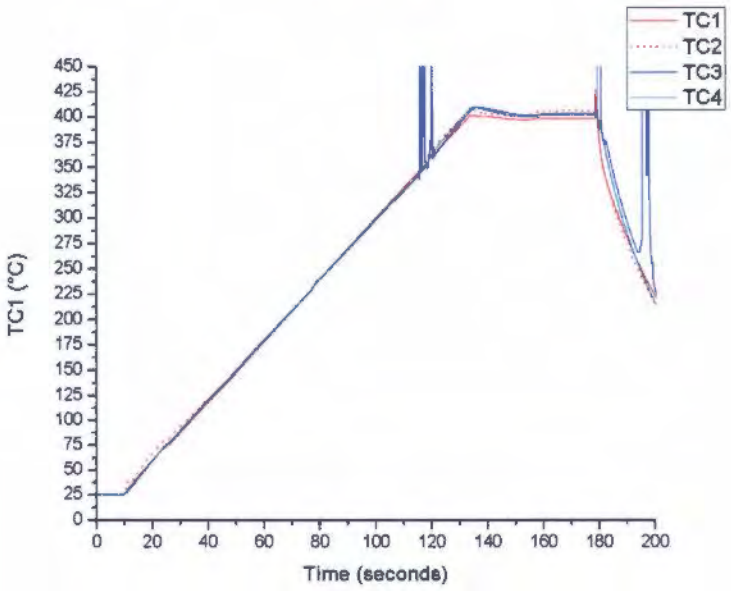

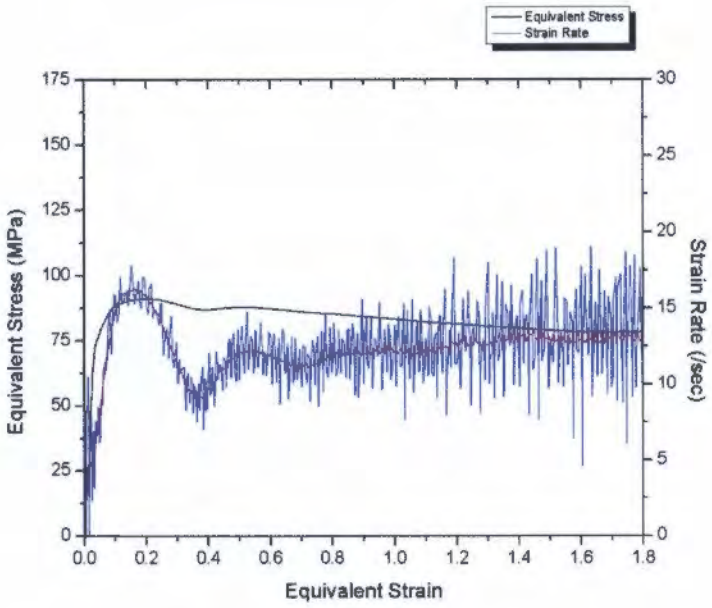

Summary:

	Value	Unit		Value	Unit
$TC1_{start}$	399.4	°C	$TC3_{start}$	403.1	°C
$TC2_{start}$	407.0	°C	$TC4_{start}$	402.0	°C
T_{grad}	7.6	°C	T_{start}	403.2	°C
$T_{0.8\text{-}0.9}$	424.8	°C	$\triangle T$	21.6	°C
$\dot{\varepsilon}_{whole}$	12.0	sec^{-1}	$\dot{\varepsilon}_{0.8-0.9}$	12.0	sec^{-1}
Flow Stress	84.81	MPa	$ln(Z)$	29.21	

Temperature: 400°C | Strain rate: 30 sec^{-1} | Strain 1.6 | Graphite Foil Lubrication

Test 1: Water Quenched

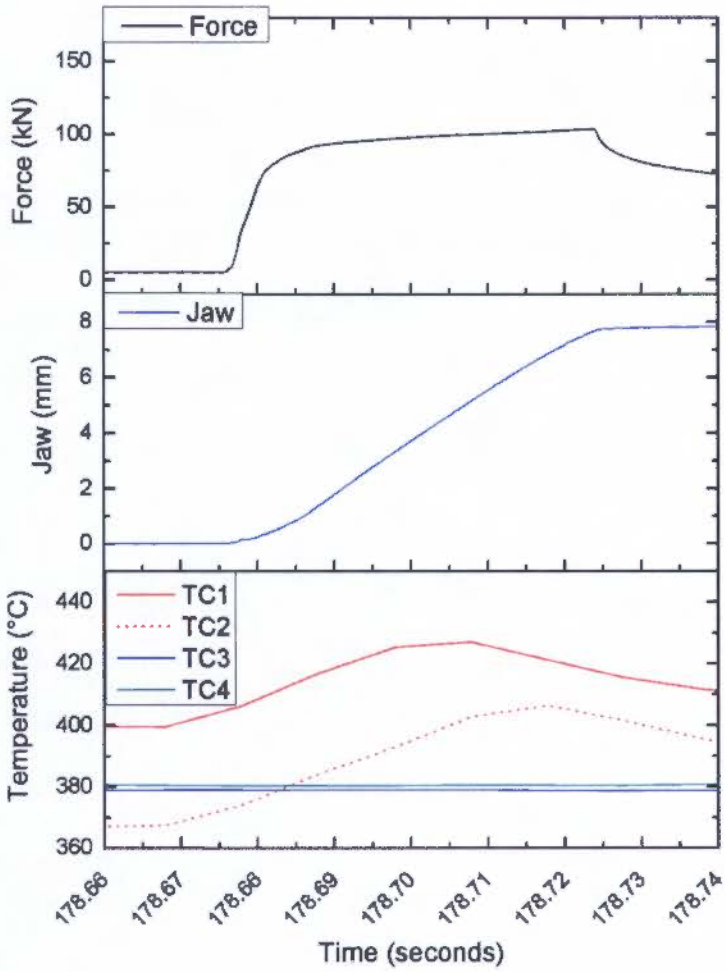

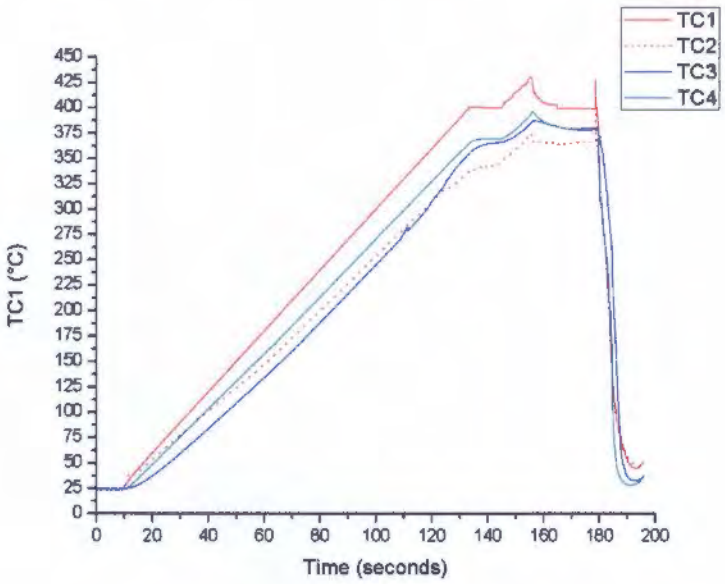

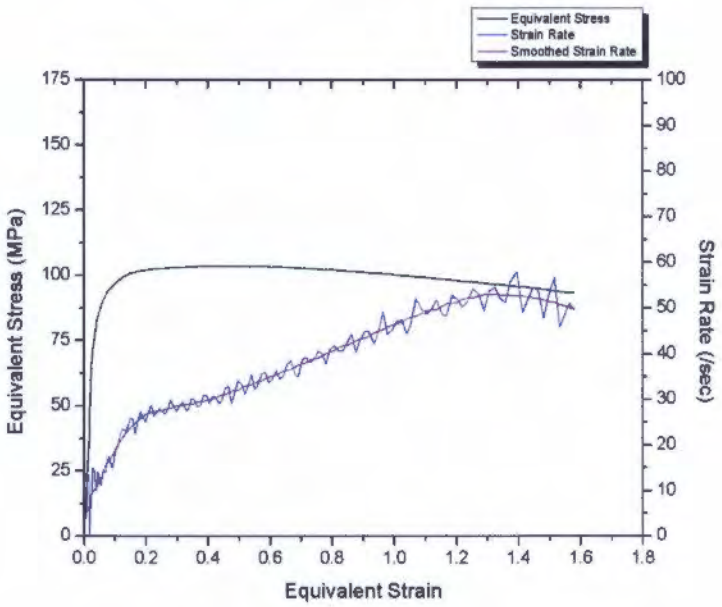

Summary:

	Value	Unit		Value	Unit
$TC1_{start}$	404.9	°C	$TC3_{start}$	379.0	°C
$TC2_{start}$	372.7	°C	$TC4_{start}$	380.4	°C
T_{grad}	32.2	°C	T_{start}	388.8	°C
$T_{0.8\text{-}0.9}$	414.8	°C	$\triangle T$	26.0	°C
$\dot{\varepsilon}_{whole}$	33.7	sec^{-1}	$\dot{\varepsilon}_{0.8-0.9}$	41.9	sec^{-1}
Flow Stress	101.6	MPa	$ln(Z)$	30.84	

Test 2: Air Quenched

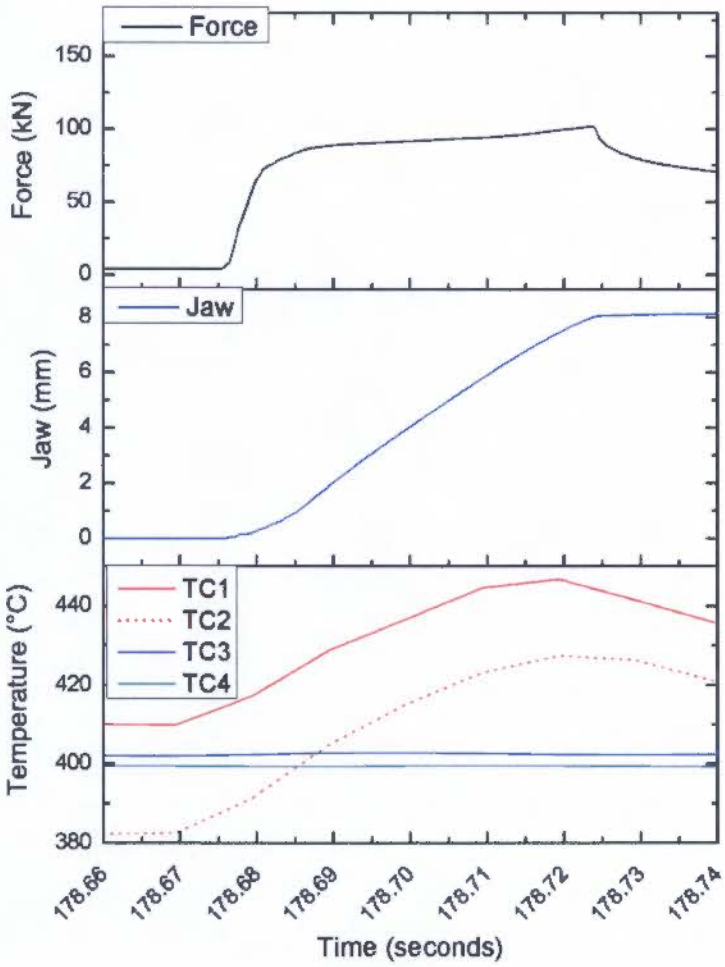

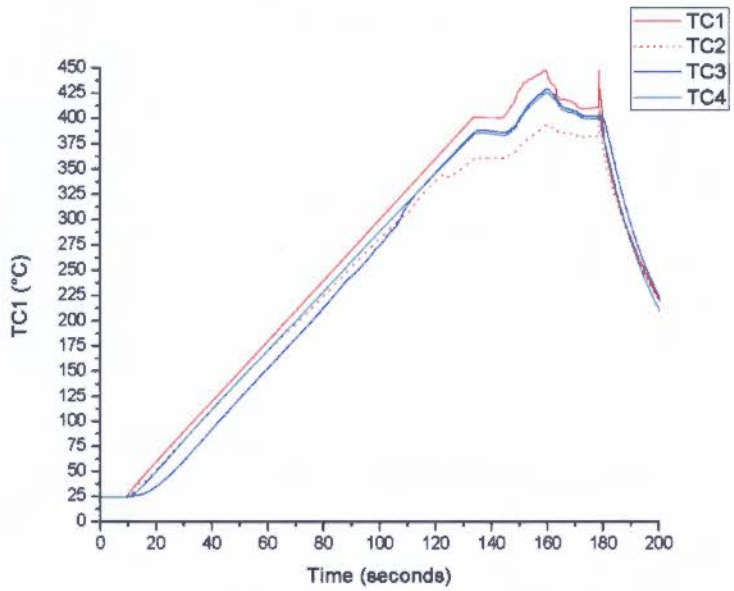

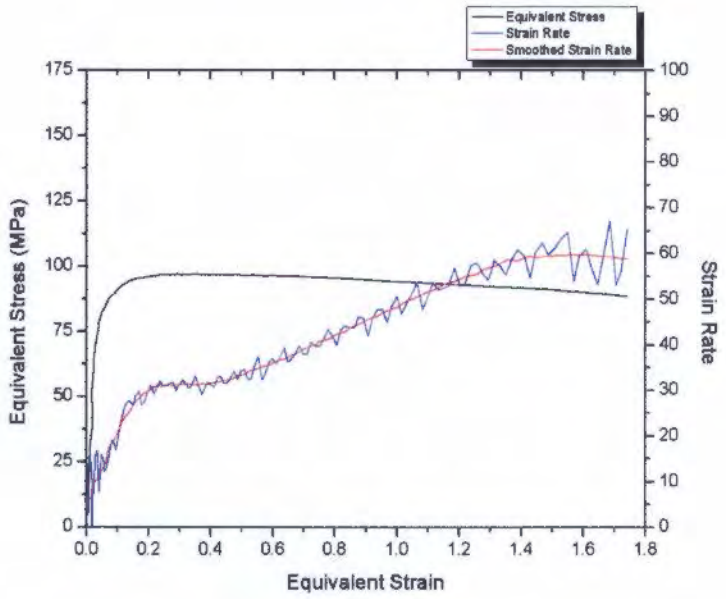

Summary:

	Value	Unit		Value	Unit
$TC1_{start}$	414.5	°C	$TC3_{start}$	402.2	°C
$TC2_{start}$	388.3	°C	$TC4_{start}$	399.4	°C
T_{grad}	26.2	°C	T_{start}	401.4	°C
$T_{0.8\text{-}0.9}$	432.0	°C	ΔT	30.6	°C
$\dot{\varepsilon}_{whole}$	37.5	sec^{-1}	$\dot{\varepsilon}_{0.8-0.9}$	43.5	sec^{-1}
Flow Stress	95.2	MPa	$ln(Z)$	30.22	

Temperature: 400°C | Strain rate: 100 sec^{-1} | Strain 1.6 | Graphite Foil Lubrication

Test 1: Water Quenched

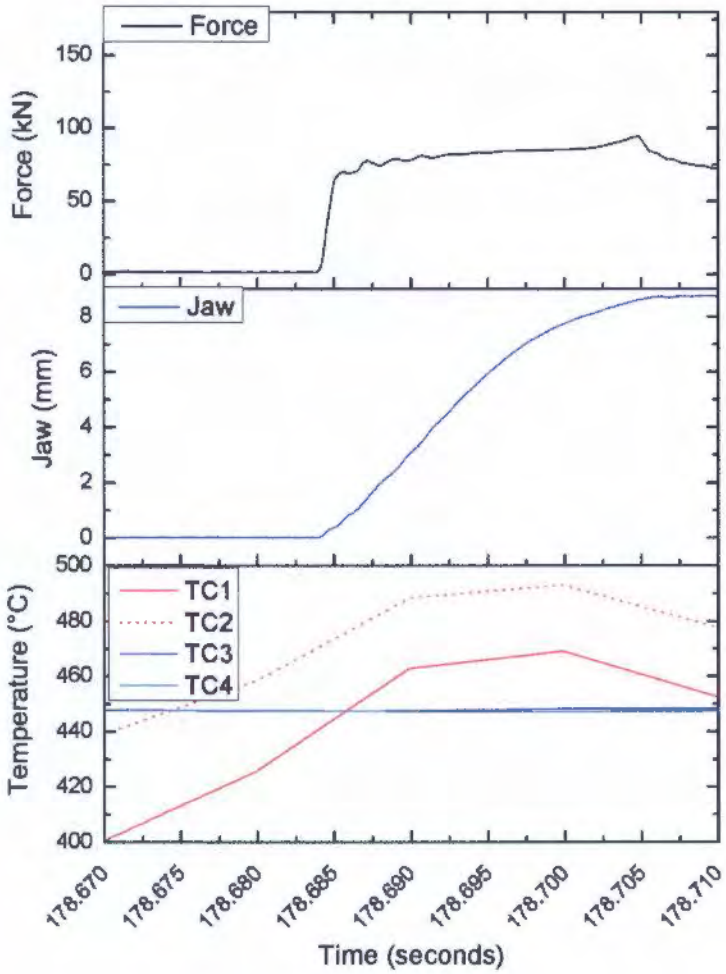

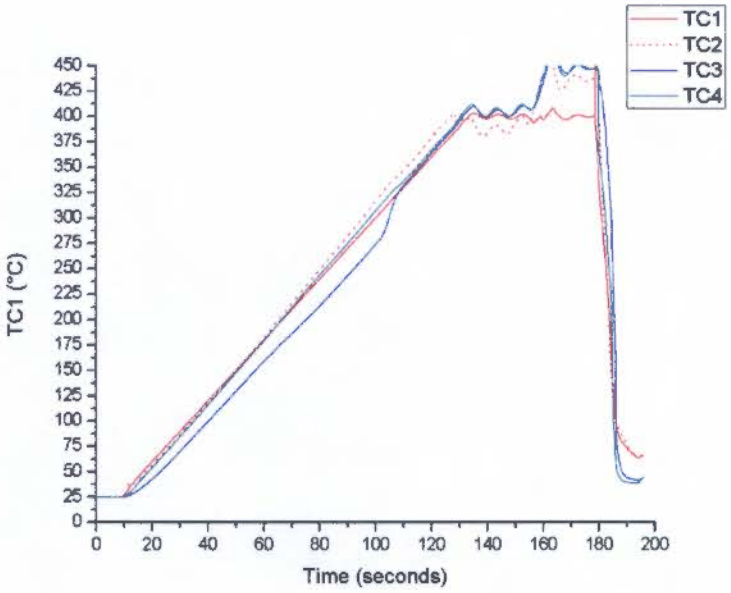

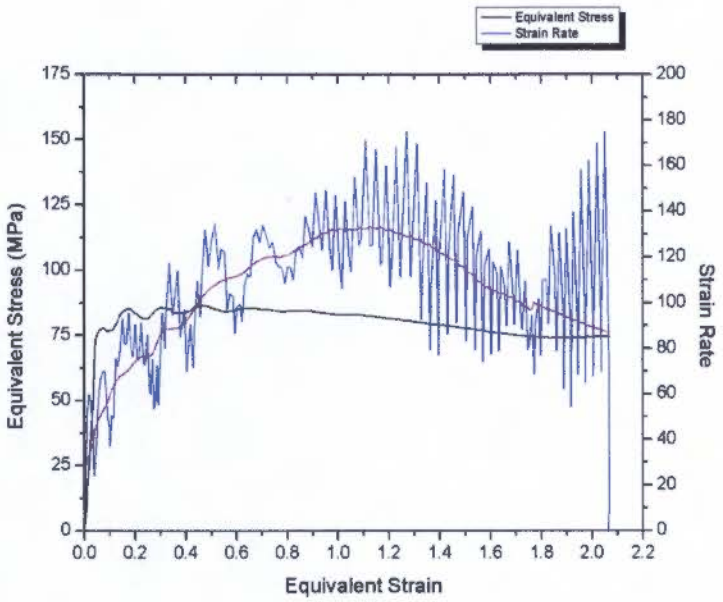

Summary:

	Value	Unit		Value	Unit
$TC1_{start}$	440.1	°C	$TC3_{start}$	447.5	°C
$TC2_{start}$	470.0	°C	$TC4_{start}$	447.5	°C
T_{grad}	29.9	°C	T_{start}	455.1	°C
$T_{0.8\text{-}0.9}$	477.8	°C	ΔT	22.8	°C
$\dot{\varepsilon}_{whole}$	99.5	sec^{-1}	$\dot{\varepsilon}_{0.8-0.9}$	124.3	sec^{-1}
Flow Stress	84.35	MPa	$ln(Z)$	29.65	

Test 2: Air Quenched

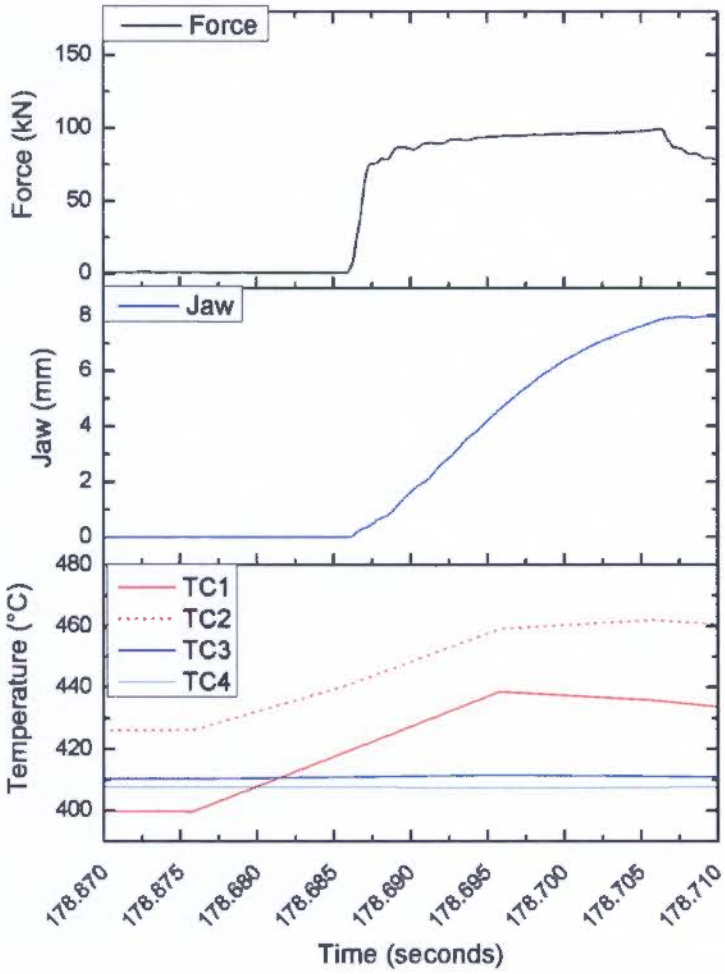

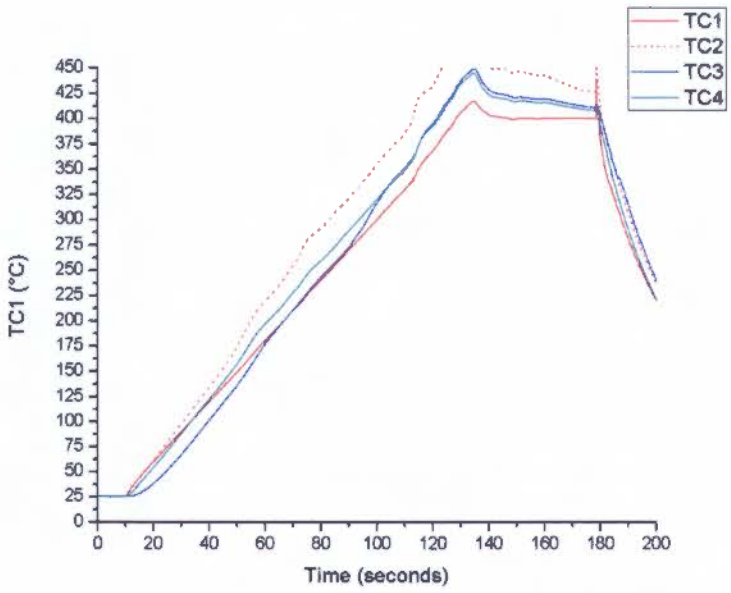

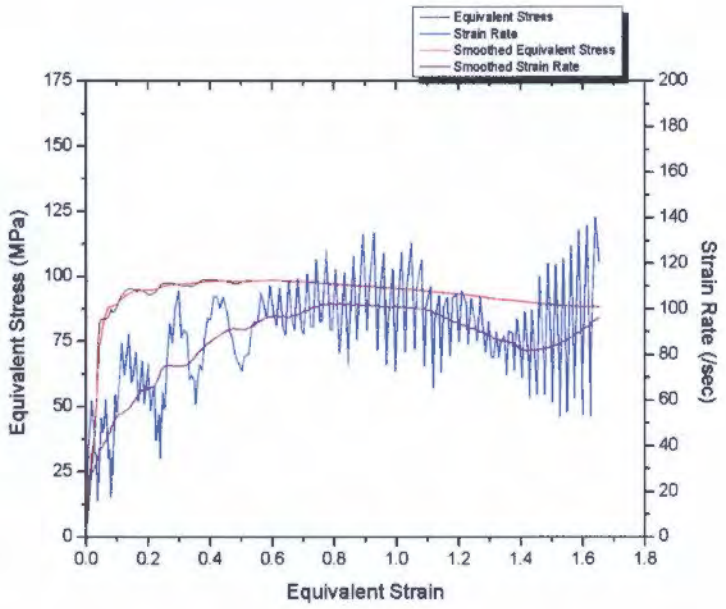

Summary:

	Value	Unit		Value	Unit
$TC1_{start}$	419.1	°C	$TC3_{start}$	410.9	°C
$TC2_{start}$	440.6	°C	$TC4_{start}$	407.7	°C
T_{grad}	21.5	°C	T_{start}	429.9	°C
$T_{0.8\text{-}0.9}$	448.9	°C	$\triangle T$	19.1	°C
$\dot{\varepsilon}_{whole}$	82.2	sec^{-1}	$\dot{\varepsilon}_{0.8-0.9}$	102.0	sec^{-1}
Flow Stress	96.62	MPa	$ln(Z)$	30.45	

Appendix I: PSC Overview of Evans and Ricks [49], DSI configuration and Modified Configuration

Nominal Temperature (°C)	Nominal Strain Rate (sec^{-1})	Evans and Ricks PSC Results			DSI PSC Configuration			Modified PSC Configuration		
		$T_{0.8\text{-}0.9}$ (°C)	Strain Rate, $\dot{\varepsilon}_{0.8\text{-}0.9}$ (sec^{-1})	Mean Flow Stress (MPa)	$T_{0.8\text{-}0.9}$ (°C)	Strain Rate, $\dot{\varepsilon}_{0.8\text{-}0.9}$ (sec^{-1})	Mean Flow Stress (MPa)	$T_{0.8\text{-}0.9}$ (°C)	Strain Rate, $\dot{\varepsilon}_{0.8\text{-}0.9}$ (sec^{-1})	Mean Flow Stress (MPa)
300	10	337.1	10.1	137.8	328.2 331	11.2 11.4	126.1 124.6	323.3 329.7	10.6 10.5	127.7 132.2
300	30	324.4	30.7	144	337.9 347.4	48.2 49.9	133.6 132	348.2 342.1	32.8 34.3	136.7 137.9
300	100	316.1	83.4	149.3	345.6 353.7	101.6 212	132.5 137.1	346 343.6	91.9 74.8	141.1 139.4
350	10	375	10.2	117.9	374.3 370.6	11.3 11	103.1 102.2	394.5 380.6	10.7 9.55	100.6 105.2
350	30	375.7	30.7	123.8	386 387.8	48.2 50.3	111.6 109	396.7 389.1	39.3 39.6	110.7 114.5
350	100	365.2	97.7	136.9	391.1 384.7	93.3 101.1	115 114.6	390.2 391.8	99.7 102.7	120.8 126
400	10	426.4	9.9	93.6	418.4 414.6	11.1 10.3	80.76 77.19	440.4 424.8	10.7 12	77.07 84.81
400	30	417.6	30.8	101.6	428.3 431.2	47.5 48	91.54 88.74	414.8 432	30.8 43.5	101.6 95.2
400	100	412.7	93	107.1	436.8 433.2	92.1 92.3	93.45 96.72	477.7 448.9	124 102	84.35 96.62

Appendix J: Rolling Simulation Results

Full Pass PSC Rolling Simulation Tests

Test 1:

1st Pass - Temperature

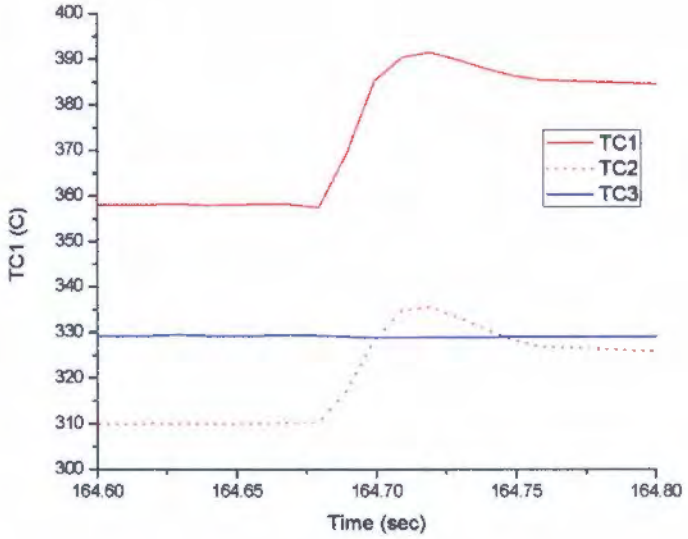

2nd Pass - Temperature

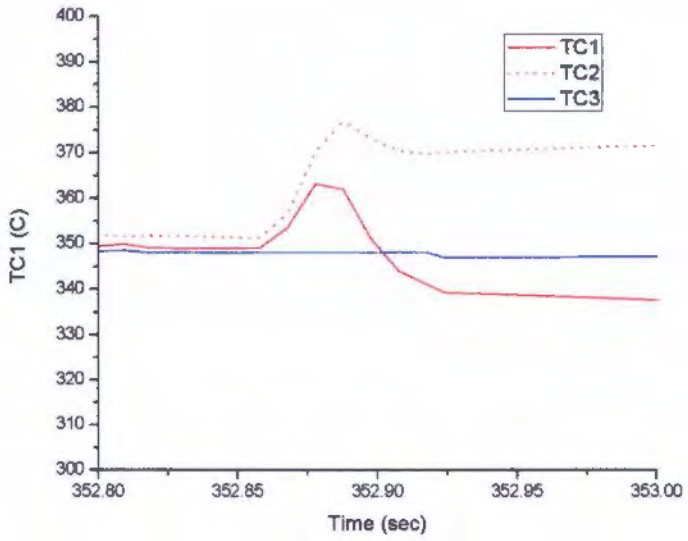

3rd Pass - Temperature

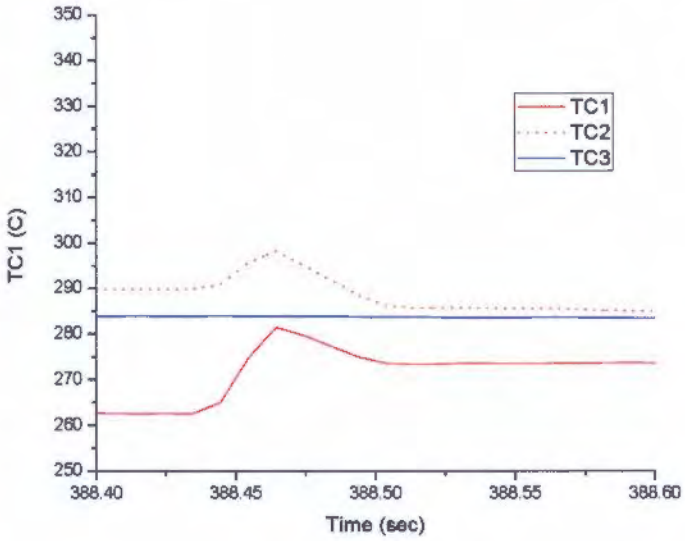

1st Pass - Strain Rate

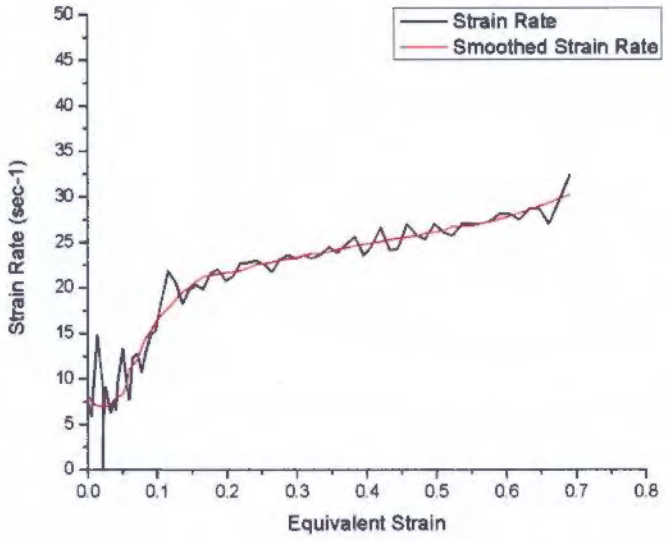

2nd Pass - Strain Rate

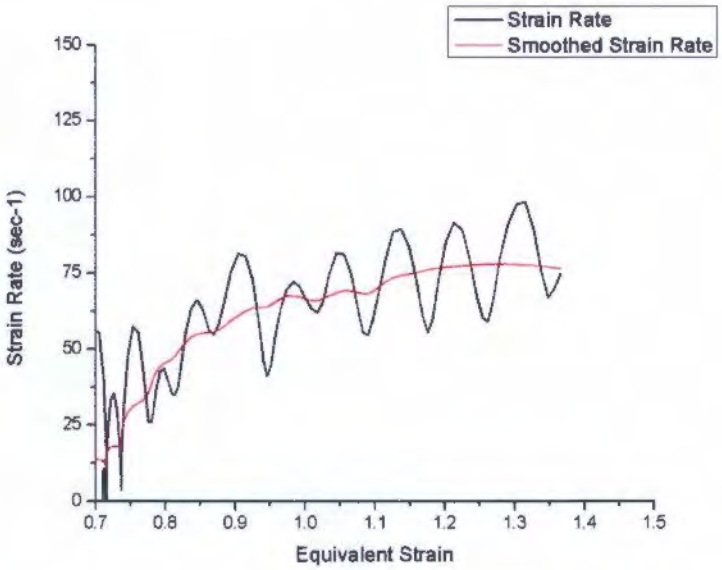

3rd Pass - Strain Rate

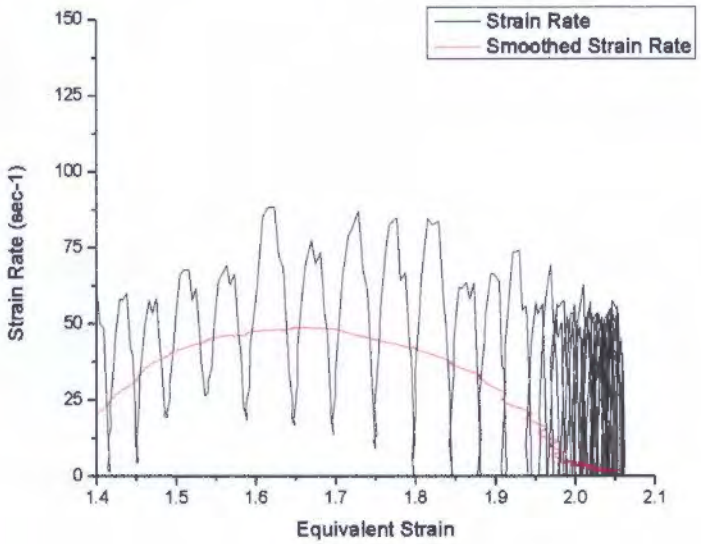

Test 2:

1st Pass - Temperature

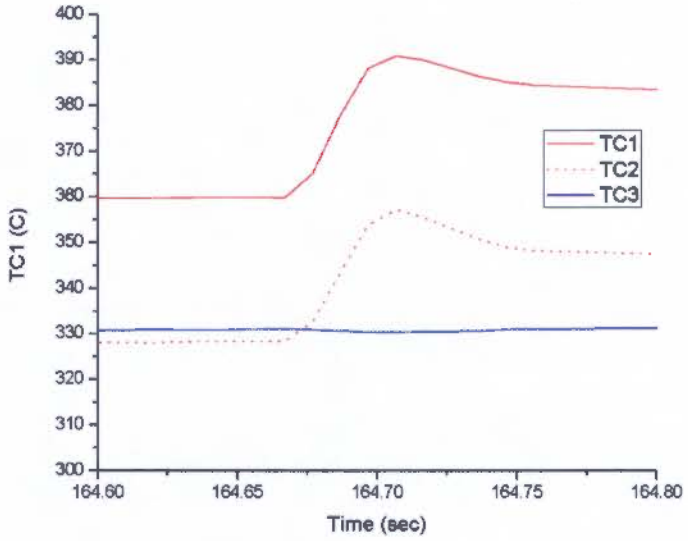

2nd Pass - Temperature

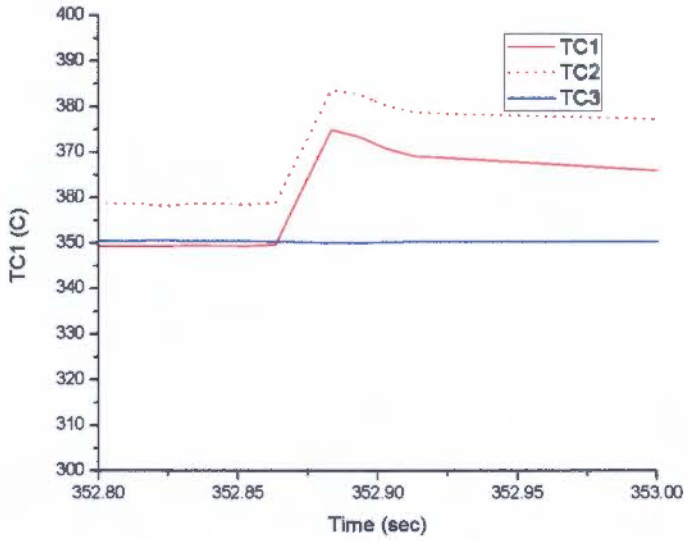

3rd Pass - Temperature

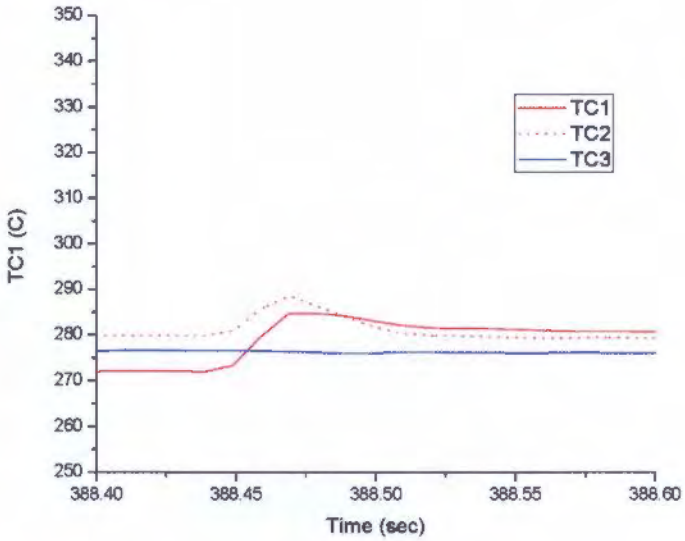

1st Pass - Strain Rate

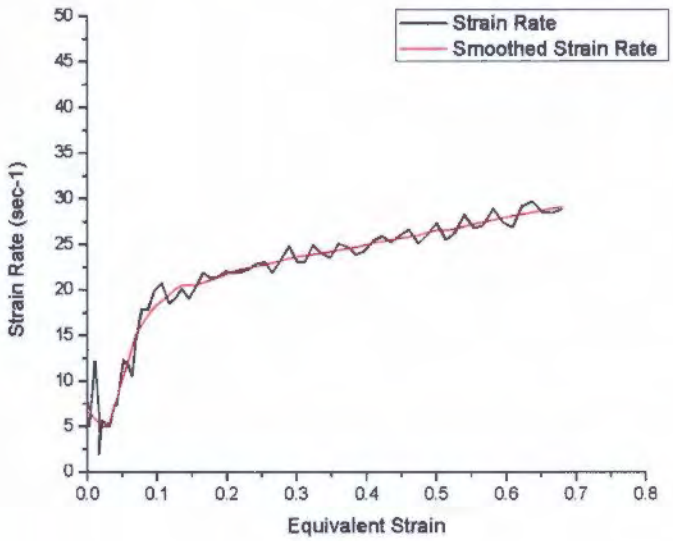

2nd Pass - Strain Rate

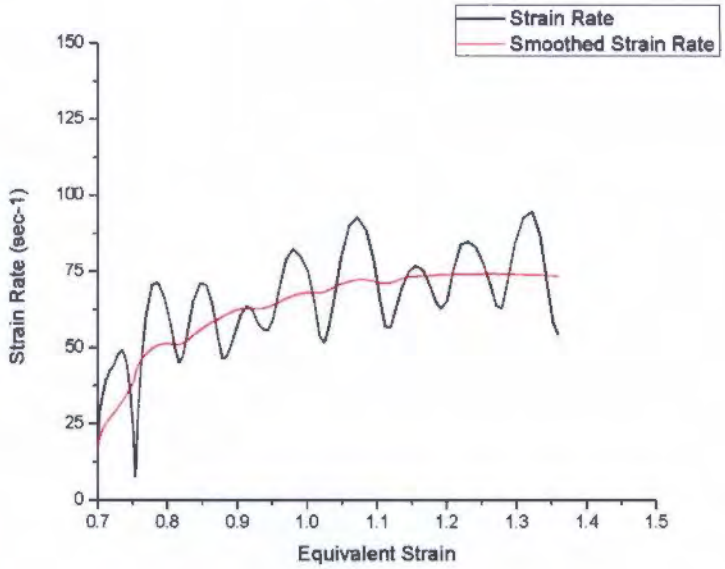

3rd Pass - Strain Rate

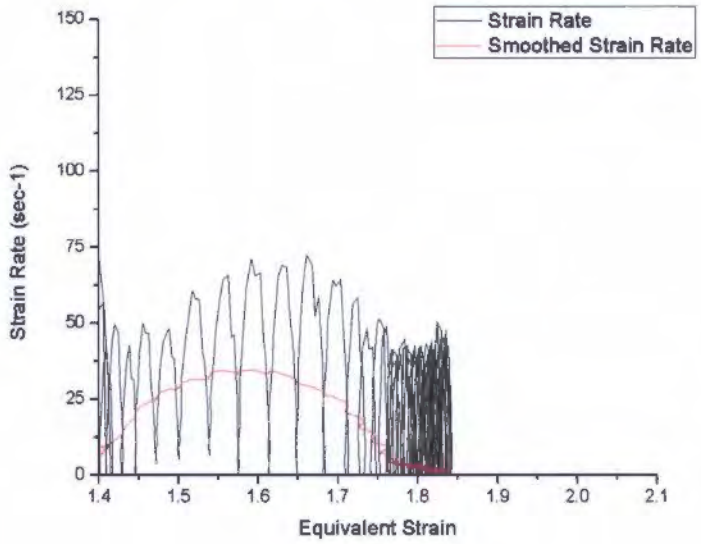

2nd and 3rd Pass PSC Rolling Simulation Tests

Test 1:

2nd Pass - Temperature

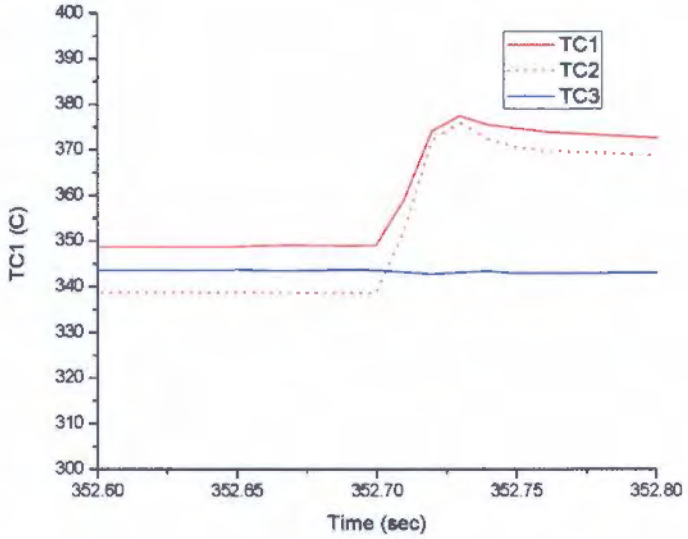

3rd Pass - Temperature

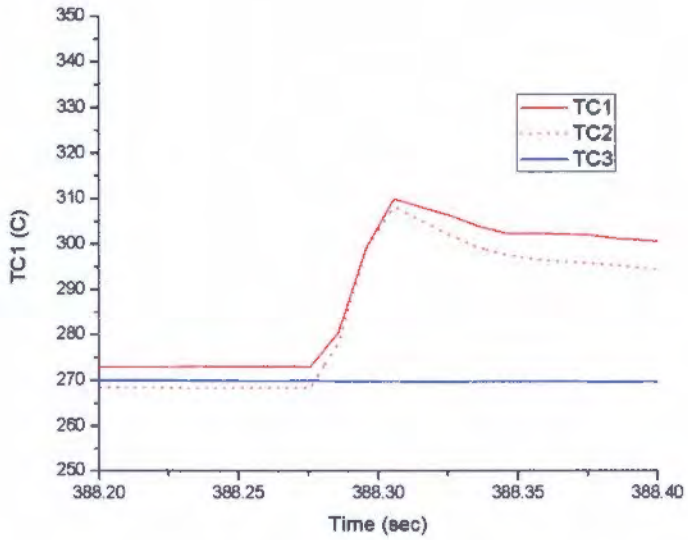

2nd Pass - Strain Rate

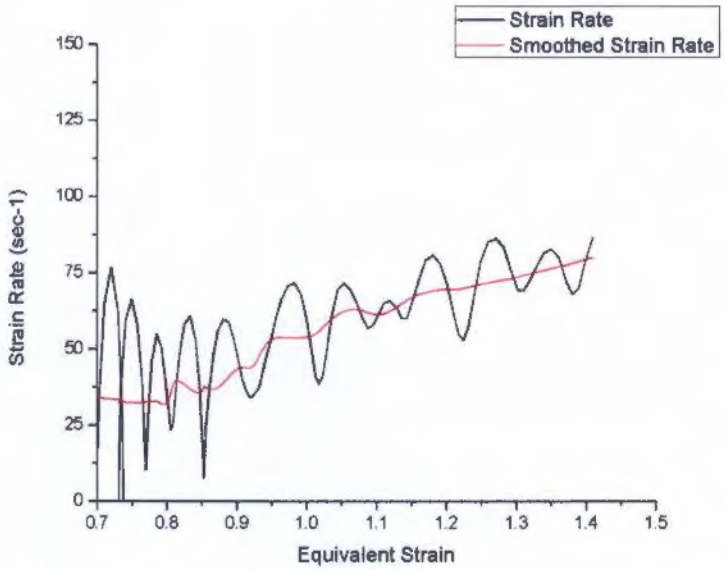

3rd Pass - Strain Rate

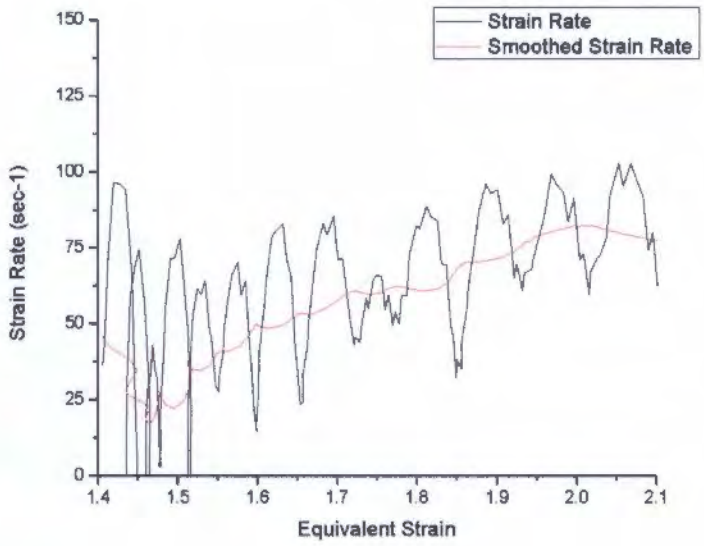

Test 2:

2nd Pass - Temperature

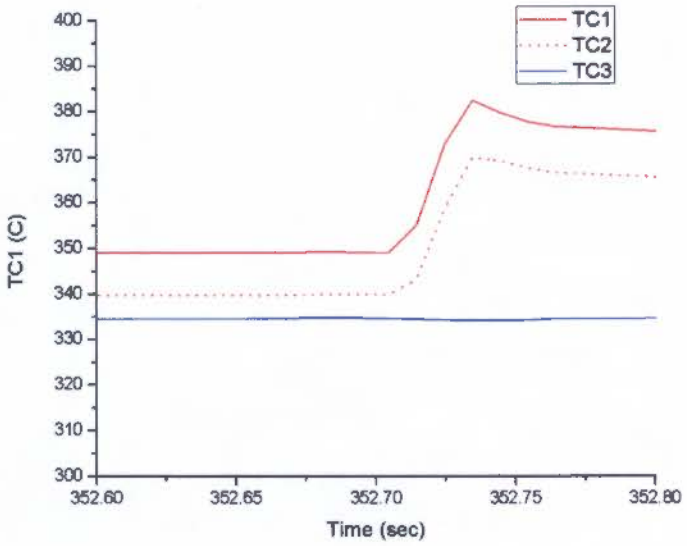

3rd Pass - Temperature

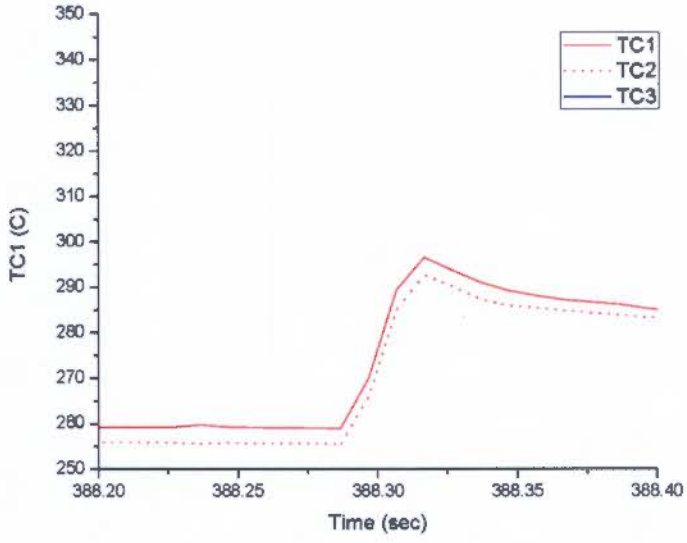

2nd Pass - Strain Rate

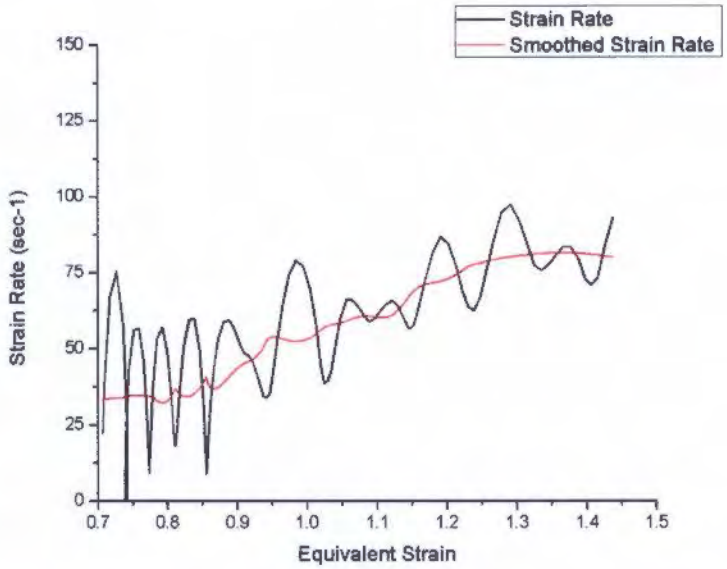

3rd Pass - Strain Rate

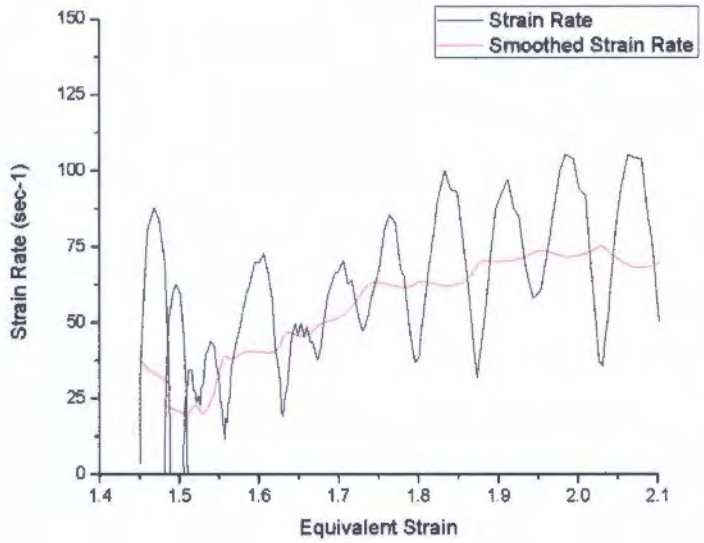

1st Pass PSC Rolling Simulation Tests

Test 1:

1st Pass - Temperature

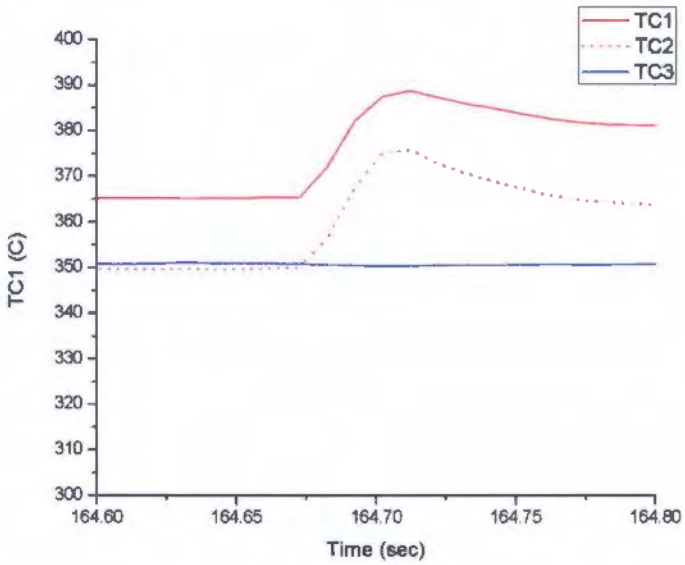

1st Pass - Strain Rate

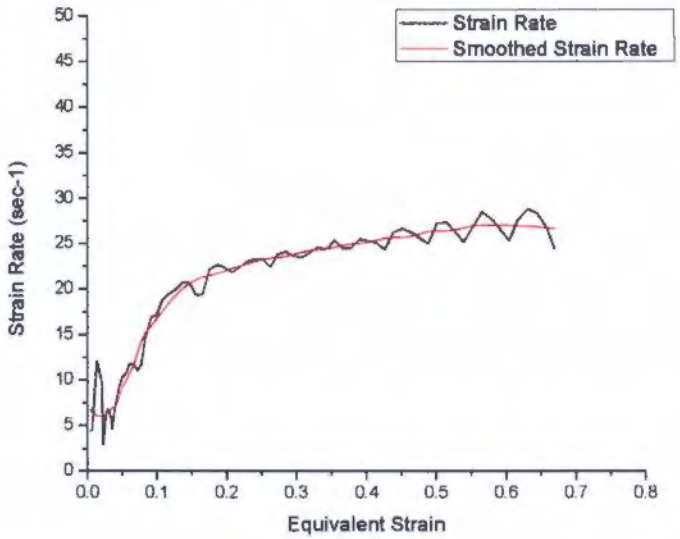

Test 2:

1st Pass - Temperature

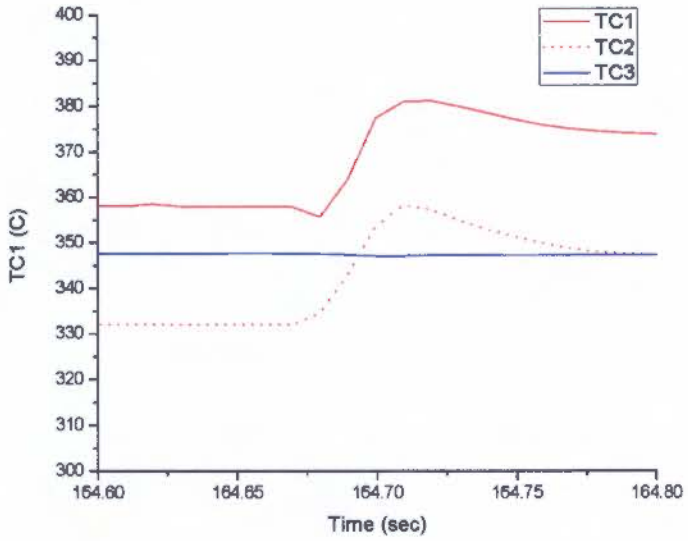

1st Pass - Strain Rate

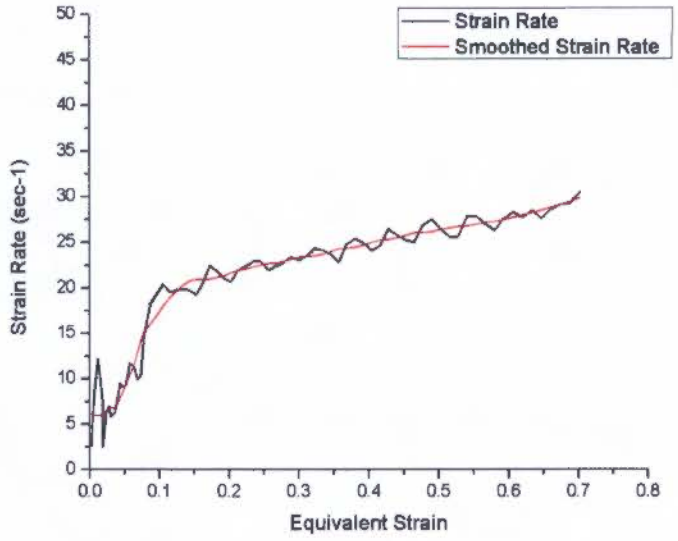

Appendix K: Polarized Light Optical Microscopy

Validation PSC Tests:

- 300°C | 10 sec-1 | DSI PSC Configuration Test 1
- 300°C | 10 sec-1 | Modified PSC Configuration Test 1
- 300°C | 100 sec-1 | DSI PSC Configuration Test 2

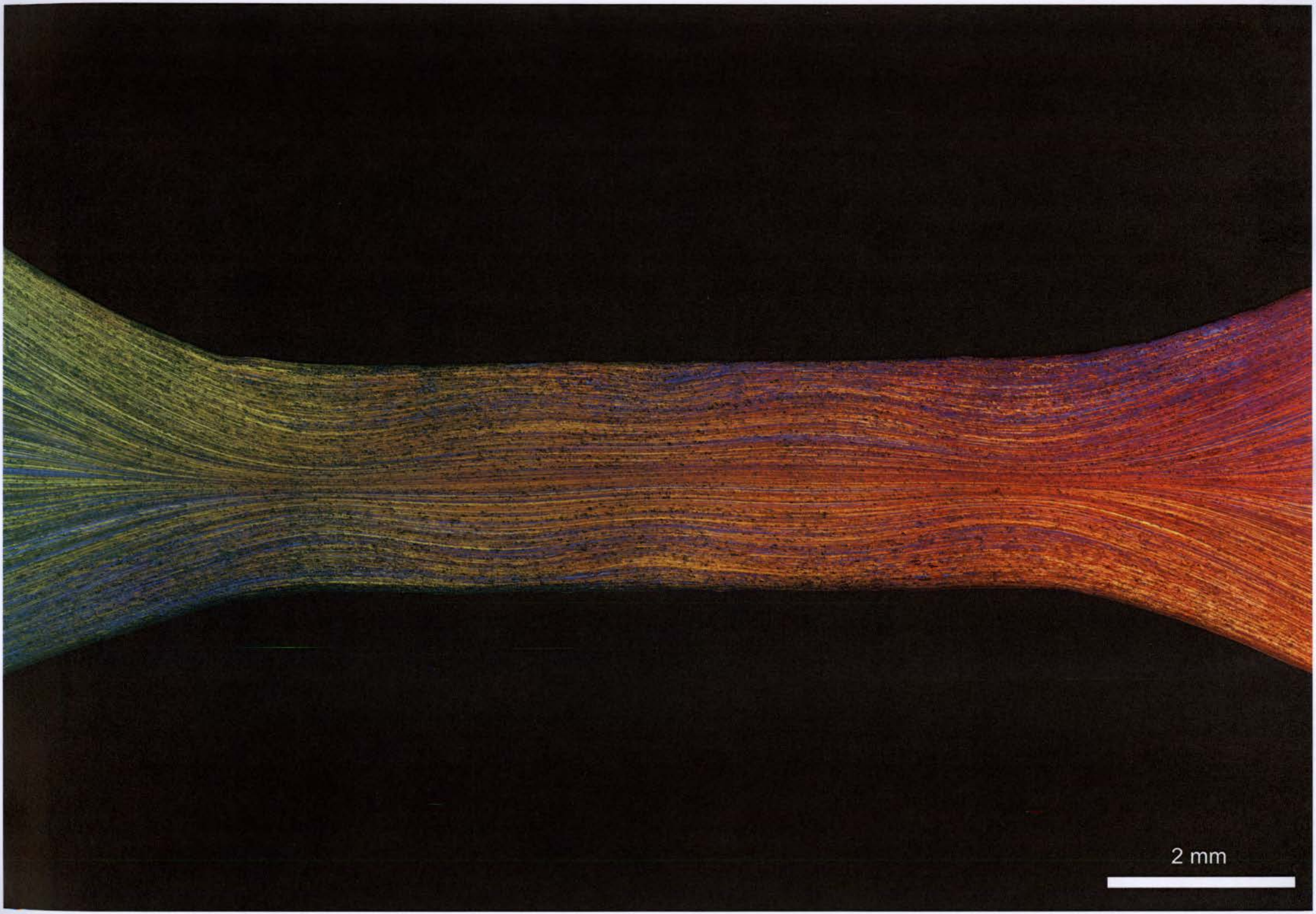
2 mm

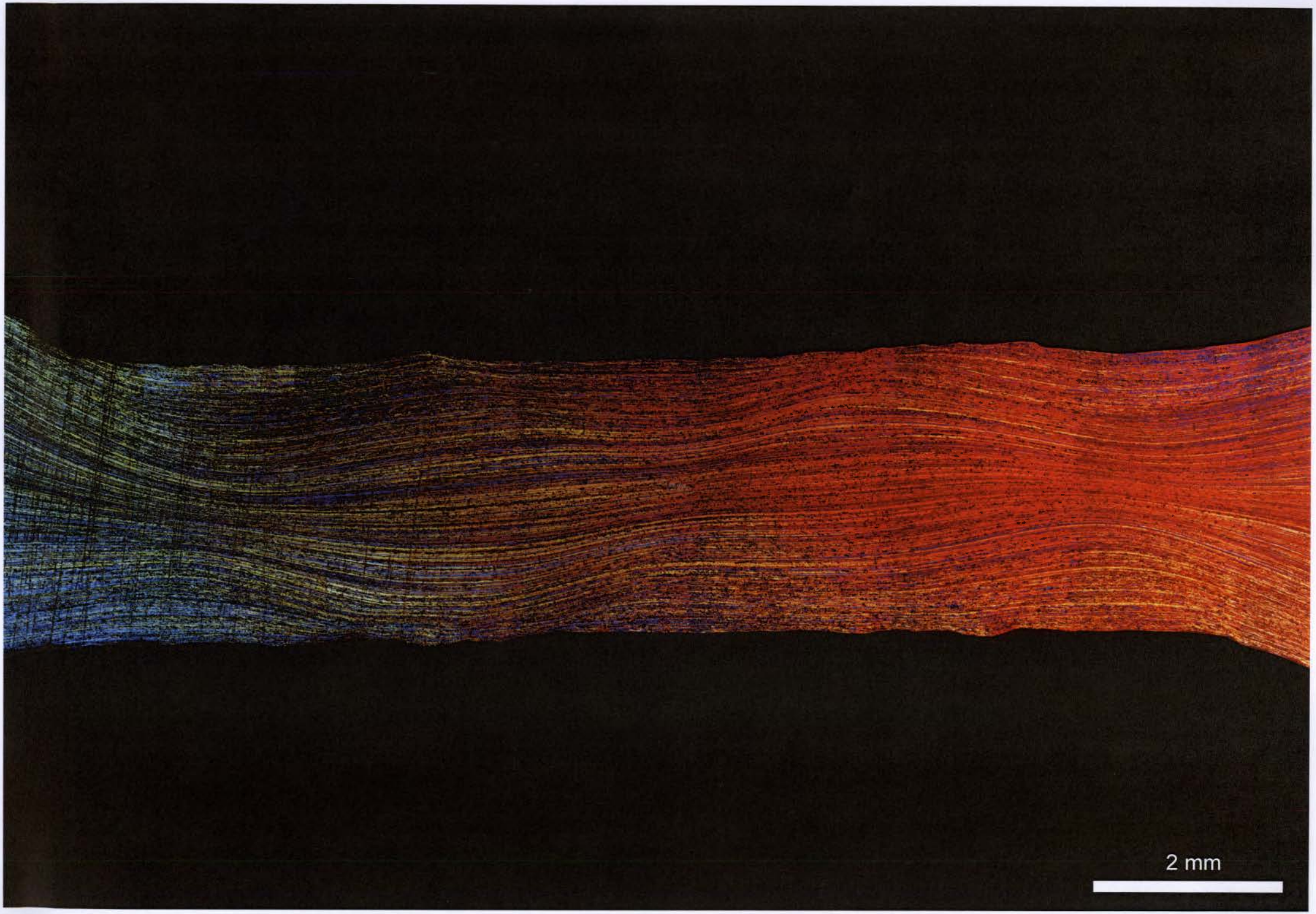
2 mm

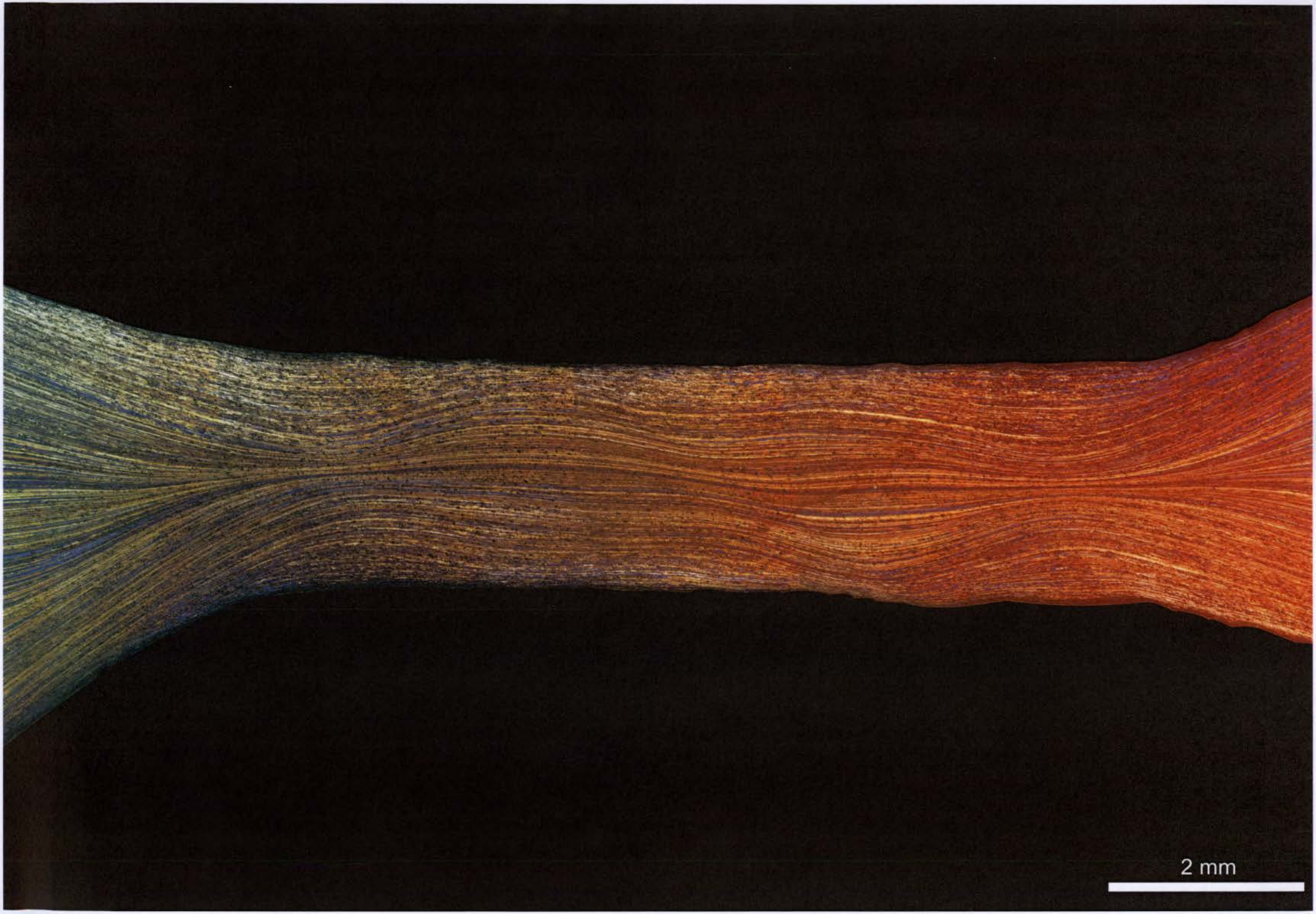
2 mm

Validation PSC Tests:

- 300°C | 100 sec-1 | Modified PSC Configuration Test 1
- 400°C | 10 sec-1 | DSI PSC Configuration Test 1
- 400°C | 100 sec-1 | Modified PSC Configuration Test 1

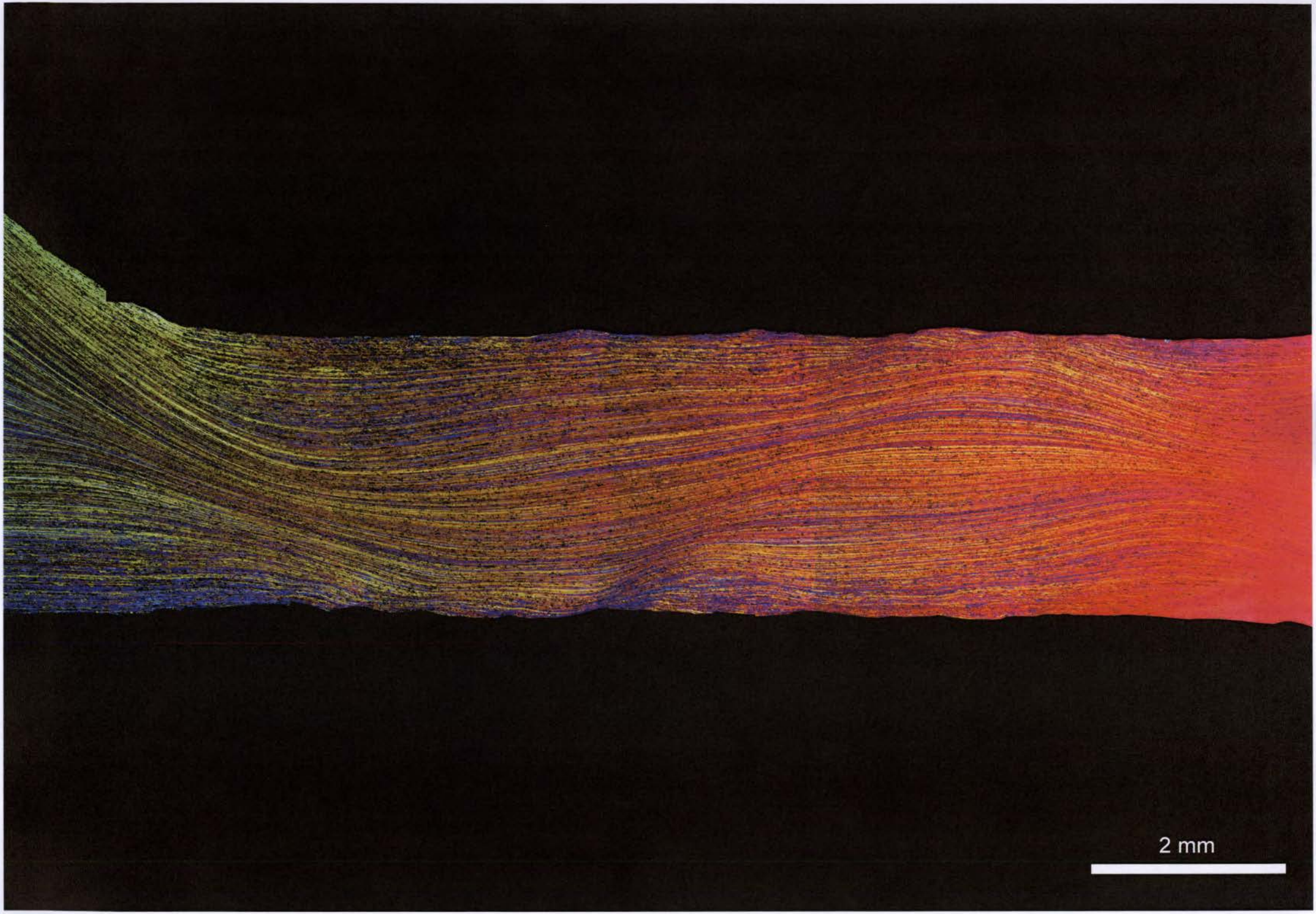
2 mm

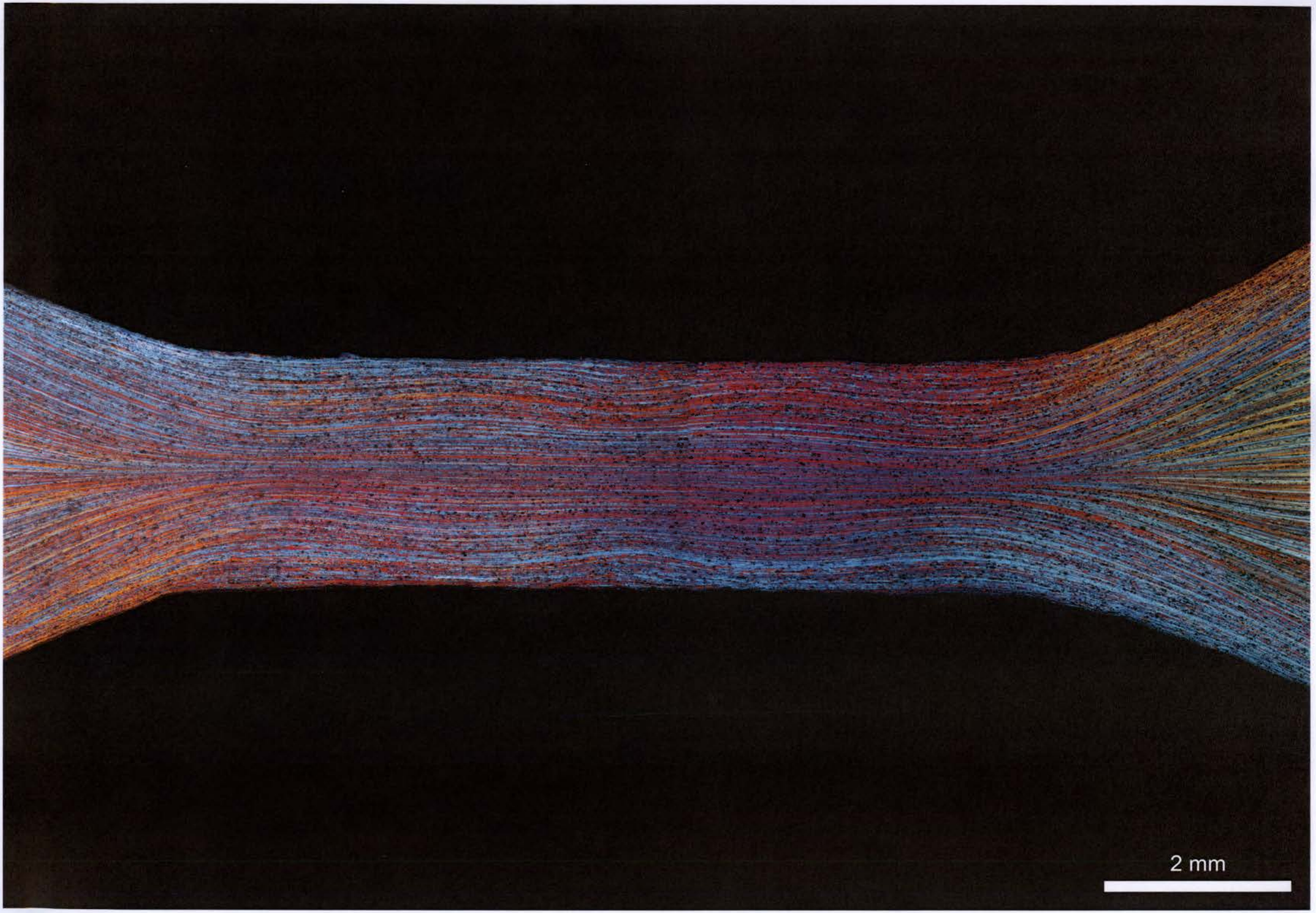
2 mm

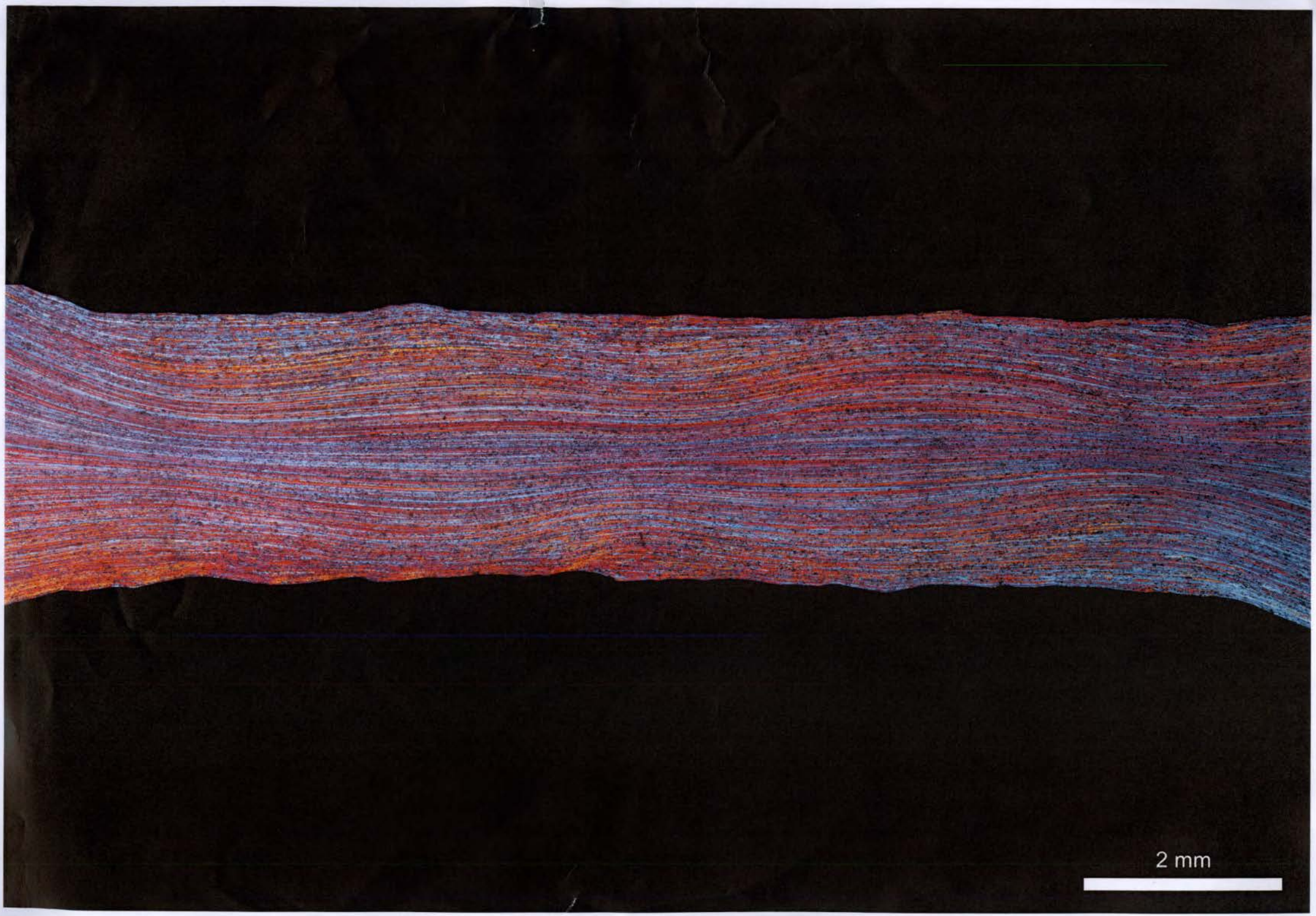
2 mm